Delft University of Technology

CH4llenger

Ultimate Energy Efficient Transatlantic Aircraft

AE3200: Design/Synthesis Exercise

Group 27

TUDelft

This page was intentionally left blank.

Final Report

Ultimate Energy Efficient Transatlantic Aircraft

by

Group 27

Student Name	Student Number
Robin Bos	5260566
Paul Mertens	5261406
Aurora Nieuwenhuis	5273552
Grégoire Dastros-Pitei	5282217
Paulina Dabrowska	5459281
Adam Wójciński	5483158
Daniil Zorzos	5484685
Thomas Claudel	5495393
Tibi Quinn	5551404
Jeroen Slagmolen	5576490

Document Version: 1.0

Changelog

Version	Changes	Date
0.5	Draft version	19-06-2024
1.0	Final version	25-06-2024

Tutor:	Paul Roling
Coaches:	Jan Groot and Nan Tao
Project Duration:	April 2024 - June 2024
Faculty:	Faculty of Aerospace Engineering, Delft

Cover: Designed by Tibi Quinn
Style: TU Delft Report Style

TU Delft

Nomenclature

Symbols

Symbol	Definition	Unit
A	Aspect Ratio	[−]
A_8	Engine nozzle cross-sectional area	[m^2]
A_{18}	Engine bypass cross-sectional area	[m^2]
AC	Aircraft Cost	[$]
A_{intake}	Engine intake area	[m^2]
A_m	Area wingbox	[m^2]
$A_{tanksurface}$	Tank surface area	[m^2]
b	Wingspan	[m]
b_y	Yehudi span	[m]
B_r	Stringer boom area	[m^2]
BPR	Bypass ratio	[−]
c	Chord length	[m]
Cam	Cost per mile	[$/mi]
$Cam_{airf_{lab}}$	Cost per mile for airframe labour	[$/mi]
$Cam_{airf_{mat}}$	Cost per mile for airframe materials	[$/mi]
$Cam_{eng_{lab}}$	Cost per mile for engine labour	[$/mi]
$Cam_{eng_{mat}}$	Cost per mile for engine materials	[$/mi]
Cam_{crew}	Cost per mile for crew	[$/mi]
Cam_{depr}	Cost per mile for depreciation	[$/mi]
Cam_{hull}	Cost per mile for hull insurance	[$/mi]
C_L	Lift coefficient	[−]
C_{L_α}	Lift curve derivative	[−]
C_{L_0}	Zero angle of attack lift coefficient	[−]
C_{L_d}	Design lift coefficient	[−]
$C_{l_{\delta a}}$	aileron control derivative	[−]
C_{l_p}	Roll damping	[−]
C_D	Drag coefficient	[−]
C_{D_0}	Zero-lift drag coefficient	[−]
C_e	Cost per engine	[$]
C_m	Moment coefficient	[−]
C_{m_0}	Zero-angle moment coefficient	[−]
C_N	Normal force coefficient	[−]
$c_{p_{gas}}$	Gas heat capacity at constant pressure	[J/K]

Symbol	Definition	Unit
$\dot{m}_{air_{turbine}}$	Air mass flow through turbine	[kg/s]
$\dot{m}_{bp}$	Air mass flow through bypass	[kg/s]
$\dot{m}_{core}$	Air mass flow through core	[kg/s]
$\dot{m}_{fuel}$	Fuel mass flow	[kg/s]
N_p	Number of seats available	[−]
n	Load factor	[−]
n_e	Number of engines	[−]
p_{amb}	Ambient pressure	[Pa]
p_8	Engine nozzle pressure	[Pa]
p_{18}	Engine bypass pressure	[Pa]
$P_{in,ambient}$	Ambient power into tank	[W]
Re	Reynolds number	[−]
r_L	Labour rate	[$h]
r_{rod}	Rod radius	[−]
S	Wing Surface Area	[m^2]
S_h	Tail Area	[m^2]
S_h/S	Tail-Wing Area ratio	[−]
S_{ref}	Wing Reference Area	[m^2]
T	Thrust	[kN]
T_{bp}	Thrust from bypass	[kN]
T_{core}	Thrust from core	[kN]
T/W	Thrust-to-weight ratio	[−]
t_b	Block time	[h]
TC	Total aircraft capital cost	[$]
t/c	Thickness-to-chord ratio	[−]
$t_{cylindrical}$	Cylindrical tank wall thickness	[mm]
t_{dep}	Depreciation period	[years]
t_f	Flight time	[h]
$t_{insulation}$	Insulation thickness	[mm]
t_{skin}	Skin thickness	[mm]
t_{spar}	Spar thickness	[mm]
t_{sphere}	Spherical tank wall thickness	[mm]
$t_{stringer}$	Stringer thickness	[mm]
$w_{stringer}$	Stringer width	[mm]
q_s	Shear flow	[N/m]
U	Utilisation factor	[h/year]
V	Velocity	[m/s]
V_{air}	Air volume	[m^3]
V_b	Block speed	[mi/h]

C_r	Root chord	[m]
C_{r_e}	Root chord extension	[m]
C_t	Tip chord	[m]
$\bar{c}$	Mean Aerodynamic Chord	[m]
E	Young's modulus	[GPa]
F_{axial}	Axial force	[N]
F_{to}	Takeoff force	[N]
G	Shear modulus	[GPa]
g	Average gravitational acceleration at Earth's surface	[m/s]
h	Height	[m]
$h_{stringer}$	Stringer height	[mm]
I_{xx}	Area moment of inertia around fuselage axis	[m^4]
I_{yy}	Area moment of inertia around wingspan axis	[m^4]
J	Torsional stiffness	[Nm]
k_a	Airfoil technology factor	[−]
k_c	Sheet buckling constant	[−]
k_s	Web buckling constant	[−]
L/D	Lift over Drag Ratio	[−]
LF	Load Factor	[%]
L_{mh_c}	Number of labour man-hours per flight cycle	[h]
L_{mh_f}	Number of labour man-hours per flight hour	[h]
l_m	Distance main wheel to C.G.	[m]
l_n	Distance nose wheel to C.G.	[m]
$l_{winglet}$	Length of winglet	[m]
M_{dd}	Drag divergence Mach number	[−]
M_{cruise}	Cruise Mach number	[−]
M_{cr}	Critical Mach number	[−]
MOS	Margin of safety	[−]
M_F	Mass of the Wing group	[kg]
M_W	Mass of the Fuselage group	[kg]
M_x	Moment around x-axis	[Nm]
$m_{insulation}$	Insulation mass	[kg]
$\dot{m}_{air}$	Air mass flow	[kg/s]
V_8	Engine core flow jet velocity	[m/s]
V_{18}	Engine bypass flow jet velocity	[m/s]
V_{stall}	Stall speed	[m/s]
V_z	Shear force in z-direction	[N]
W_{to}	Take-off weight	[kg]
W/S	Wing Loading	[−]
X_{FCG}	Long. location of the fuselage group C.G.	[m]
x_{LEMAC}	Long. location of the leading edge of the MAC	[m]
y_{mlg}	Lateral location of the main landing gear	[m]
y_{pos}	Lateral position of considered object	[m]
z	Height of C.G.	[m]
z_{pos}	Ground clearance of considered object	[m]

α	Angle of attack	[°]
ΔT	Temperature difference	[K]
δa	Aileron deflection	[°]
η_{cc}	Combustion chamber efficiency	[−]
θ	Wing twist angle	[°]
Λ	Sweep angle	[°]
$\Lambda_{0.25c}$	Quarter-chord sweep angle	[°]
λ	Taper ratio	[−]
ν	Poisson's ratio	[−]
ρ	Density	[kg/m^3]
$\rho_{insulation}$	Insulation density	[kg/m^3]
σ_{cr}	Critical bending stress	[MPa]
σ_y	Yield tensile stress	[MPa]
τ	Shear stress	[MPa]
τ_{cr}	Critical shear stress	[MPa]
τ_y	Yield shear stress	[MPa]
ϕ	Clearance angle object considered	[°]
Ψ	Overturn angle	[°]

Abbreviations

Abbreviation	Definition
A321neo	A321 new engine option
A/C	Air-conditioning
ACARS	Aircraft Communications Addressing and Reporting System
ACN	Aircraft Classification Number
ACP	Audio Control Panel
ADSEE	Aerospace Design & Systems Engineering Elements
AoA	Angle of Attack
APU	Auxiliary Power Unit
ATC	Air Traffic Control
CAGR	Compound Annual Growth Rate
CDU	Control Display Unit
CFD	Computational Fluid Dynamics
CFRP	Carbon Fibre Reinforced Polymer
CMU	Communication Management Unit
C.G.	Centre of Gravity
CH4	Methane
CO2	Carbon Dioxide
CVR	Cockpit Voice Recorder
CS	Certification Specifications
DAC	Direct Air Capture
DOC	Direct Operating Cost
DSE	Design/Synthesis Exercise
EASA	European Union Aviation Safety Agency
EBHA	Electric Backup Hydraulic Actuator
ECS	Environmental Control System
ELT	Emergency Locator Transmitter
FAA	Federal Aviation Authority
FEM	Finite Element Method
GFRP	Glass Fibre Reinforced Polymer
H2	Hydrogen
H2O	Water
HF	High Frequency
HLD	High Lift Device
HP	High Pressure
ICAO	International Civil Aviation Organisation
IOC	Indirect Operating Cost
IFALPA	International Federation of Air Line Pilots' Associations
IOC	Indirect Operation Cost
IP	Intermediate Pressure
ISA	International Standard Atmosphere
LCA	Life Cycle Assessment
LCN	Load Classification Number
LD	Load Device

Abbreviation	Definition
LHV	Lower Heating Value
LNG	Liquid Natural Gas
LF	Load Factor
LP	Low Pressure
MAC	Mean Aerodynamic Chord
MGC	Mean Geometric Chord
MTOW	Maximum Take-Off Weight
NACA	National Advisory Committee for Aeronautics
NASA	National Aeronautics and Space Administration
NGO	Non-governmental Organization
NLR	Royal Netherlands Aerospace Centre
NOx	Nitrous Oxides
NRCC	National Research Council Canada
OEW	Operating Empty Weight
PA	Passenger Address
PACK	Pressurisation & Air Conditioning Kit
PCN	Pavement Classification Number
PDDL	Project Design and Development Logic
PEMFC	Proton-Exchange Membrane Fuel Cell
PM	Particular Matter
PSEU	Proximity Switch Electronics Unit
PSHE	Plate and Shell Heat Exchanger
PSM	Program Switch Module
PV	Photovoltaic
RAMS	Reliability, Availability, Maintainability and Safety
RAT	Ram Air Turbine
RCP	Radio Control Panel
R&D	Research and Development
REU	Remote Electronic Unit
ROI	Return On Investment
RTP	Radio Tuning Panel
SATCOM	Sattelite Communication
SCM	SDU Configuration Module
SDU	Satellite Data Unit
SELCAL	Selective Calling System
SOFC	Solid Oxide Fuel Cell
TBC	Thermal Barrier Coating
TRL	Technology Readiness Level
ULD	Underwater Locating Device
UN	United Nations
VHF	Very High Frequency
VOC	Volatile Organic Compound
VR	Voice Recorder

Executive Overview

Aviation has a large environmental impact, accounting for about 2% of energy-related CO_2 emissions[1]. In the near future, this will have to be mitigated to reach global climate goals. In order to do so, aircraft will have to be able to fly on more sustainable and eventually CO_2 neutral fuels. The goal of this project was to design an aircraft for this purpose that can fly at transatlantic range. This, in turn, led to the mission need statement: "To reduce the environmental impact of aviation by designing a novel aircraft that is capable of transatlantic flights by 2030".

To fulfil this goal, a preliminary design for a methane-fuelled aircraft was developed, as this simple compound burns cleaner relative to kerosene-type jet fuel, and can be produced synthetically. The goal of this report is to present this design, called the CH4llenger, as well as the associated logistics of production, transportation, and refuelling processes.

Figure 1: The CH4llenger.

Requirements

In order to establish clear design objectives, a comprehensive set of requirements was compiled. The primary focus was placed on stakeholder requirements, a substantial portion of which was provided by the client. Furthermore, a stakeholder analysis was conducted to identify additional requirements coming from other stakeholders. This resulted in the 14 requirements presented in Table 1, which drove the design decisions made during the project.

[1] `https://www.iea.org/energy-system/transport/aviation`, [Cited on 19-June-2024]

Table 1: Subsystem requirements from the stakeholders.

ID	Name	Requirement
CH4-STK-01	Range	The aircraft shall have a range of 3500 nautical miles
CH4-STK-02	Capacity	The aircraft shall be able to accommodate 206 passengers in a 2-class configuration during transatlantic flight
CH4-STK-03	Payload Weight	The aircraft shall have a maximum payload weight of at least 25 tonnes
CH4-STK-04	Runway Length	The aircraft shall be able to operate from a 3000-meter runway at MTOW and 0m ISA
CH4-STK-05	Turn-around Time	The aircraft shall have a turn-around time of at most one hour
CH4-STK-06	Turn-around Procedures	The aircraft shall be able to perform standard turn-around procedures
CH4-STK-07	Net Zero Emissions	The aircraft shall have net zero CO2 emissions
CH4-STK-08	Lowest Energy	The aircraft shall fly with the lowest possible required energy
CH4-STK-09	Prototype Ready	A prototype of the aircraft shall be ready by 2030
CH4-STK-10	Costs	The aircraft shall have a maximum unit cost of $120 million
CH4-STK-11	Remote Airports	The aircraft shall be able to operate from remote airports
CH4-STK-12	Regulations	The aircraft shall comply with rules from regulating bodies
CH4-STK-13	Social Sustainability	The aircraft shall help the social sustainability of the aviation industry
CH4-STK-14	Sustainability	The aircraft shall be able to fly on sustainable fuels

Trade-Off Summary

To achieve the project goals and fulfil the stakeholder requirements, flying on kerosene-type fuel of fossil origin was determined to not be viable. Therefore, several alternative fuels were considered as potential substitutes for conventional aviation fuels. The primary candidates identified were methane, liquid hydrogen, and a combination of hydrogen and synthetically produced kerosene.

Regarding the aircraft design, emphasis was placed on decisions related to the selected fuel. Components not directly associated with the fuel were largely aligned with conventional aircraft designs currently in use. With this in mind, various design concepts were explored, focusing on different fuel tank placements. From these, 15 concepts were initially selected and a trade-off was conducted to narrow them down to 4: methane stored under wings, methane stored in an extended fuselage, hydrogen stored on top of the passenger cabin, and a hybrid design with hydrogen stored under the wing. A preliminary performance analysis was performed for each configuration, and the design that incorporated methane storage in removable tanks underneath the wings was selected for further development, due to its high L/D and advantages in logistics. This design used CH4-04-A as identifier code during the Midterm report [1] and will henceforth be referred to as CH4llenger.

Functions and Risks

To advance the aircraft design, a comprehensive analysis of its functions was required. For this, a functional flow diagram and functional breakdown structure were created. Among other things, this presents all the functions the aircraft needs to perform during its lifetime.

These functions impose another set of requirements on the aircraft system. While these are often more technical than stakeholder requirements, there is some overlap, as certain functions are mandated by governing bodies such as the European Union Aviation Safety Agency (EASA). These requirement are presented in Table 2.

Table 2: Subsystem requirements derived from the functional flow diagram.

ID	Name	Requirement
CH4-FUN-01	Communication	The aircraft shall allow the pilots to communicate with ATC
CH4-FUN-02	Engine Control	The aircraft's engines shall be controllable
CH4-FUN-03	Ground Control	The aircraft shall be controllable during taxi

Continued on next page

Table 2– continued from previous page

ID	Name	Requirement
CH4-FUN-04	Take-off	The aircraft shall be able to perform take-off
CH4-FUN-05	Climb	The aircraft shall be able to climb away from the airport
CH4-FUN-06	Stowing	The aircraft shall be able to stow its landing gear
CH4-FUN-07	In Air Control	The aircraft shall be controllable in the air
CH4-FUN-08	Cruise	The aircraft shall be able to enter cruise conditions
CH4-FUN-09	Trim	The aircraft shall be able to be trimmed
CH4-FUN-10	Clearance	The aircraft shall not touch the ground with anything other than the landing gear during operations
CH4-FUN-11	Receiving Fuel	The airports shall be able to receive the fuel for the aircraft
CH4-FUN-12	Storing Fuel	The airports shall have the infrastructure to store the fuel for the aircraft
CH4-FUN-13	Refuelling	The airports shall have the infrastructure to refuel the aircraft

Both the project and the product are subject to risks, related to the uncertainty of outcomes during the project's development and the product's operation. For this project, the technical risks were identified and assessed by ranking them on the basis of likelihood and severity of impact. This risk assessment facilitated the tracking and mitigation of risks. The identified risks were represented in a risk map, and mitigation strategies were developed, some of which led to additional system requirements. The most critical risks were identified as 'The use of a novel propulsion system' and 'The placement of the propulsion system'. These are provided with independent mitigation strategies including extensive testing, certification and communication with subcontractors, thus lowering their associated risk scores.

Aircraft Design Process

The aircraft design underwent a conventional iteration for the preliminary sizing of the main structural components. This began with a Class I investigation, resulting in an initial C.G. estimate of the aircraft by considering the OEW and fuel weights by using literature from Roskam. Thereafter, the wings, tail, empennage, fuselage and landing gear C.G.'s were sized, thus allowing for a Class II weight estimation to be performed.

Utilising a scissor plot of the unique characteristics of the aircraft, the stability and control characteristics of the aircraft were analysed and designed around. Iterating through the weight estimations and taking into account the fuel-less wings, and the external wing tanks implemented as point loads on the wings, the final sizing of wings was conceived. As such, Ch4llenger is presented in Figure 1, furthermore with the main systems sized, the interior is synthesised, including emergency access points, as depicted in Figure 2.

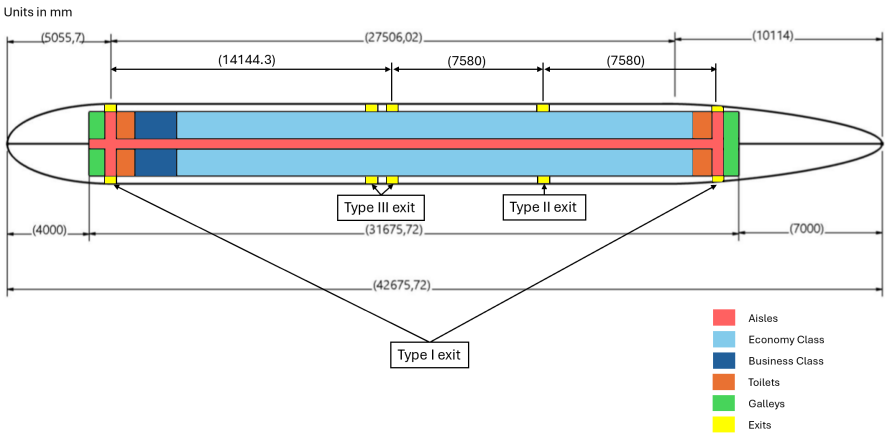

Figure 2: Top view of the fuselage and cabin.

Propulsion

As CH4llenger uses methane, rather than the conventional kerosene, large changes were made to the design of the aircraft, particularly to the propulsion system as this is most impacted by the fuel. The layout of the system is depicted in Figure 3, showing the layout of the propulsion system, with the engine connected to the liquid storage tank through various means. Firstly, the baseflow path follows the liquid methane that is pumped out of the tank and brought through a system with two vaporisers in series. The electric heater is powered by the auxiliary power unit (APU) and used when the engine-fed heater is too cold to gasify the liquid methane. When the engine is warm enough, the engine-fed heater provides the majority of gasification capability and sustains cruise flight. The second path commences from the venting of the liquid tank, continuing to a high-pressure 40-bar tank, that feeds into the combustion chamber of the engine, allowing for rapid throttling. Moreover, a feed line from the baseflow to the gaseous tank allows for a path of contingency in case there are issues in the plumbing. Finally, a crosslink path connects one side of the aircraft to the other, to allow for fuel transfer in the case of a one-engine operative scenario.

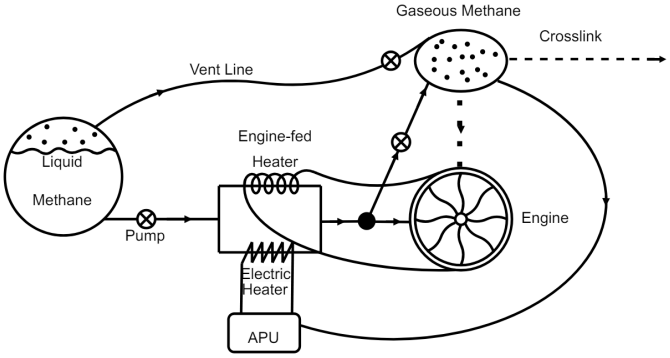

Figure 3: Concept for the layout of the propulsion system.

The CFM LEAP-1A engine was used as a benchmark due to its efficient and sustainable characteristics. From this, the mass flow of the fuel was investigated through assessing the efficiencies of the compressor, combustion chamber and turbine stages. This resulted in a mass flow of 0.53 kg/s per engine during cruise, which was used to adequately size the fuel tanks. Furthermore, with the flame temperature being 2200 K, a nickel-iron-chromium alloy called Discalloy[2] mixed with a thermal barrier coating and passive air cooling are used, which can sustain the flame temperature.

With the mass flow established, the storage of the liquid methane fuel was investigated. The actual tank was assumed to be a cylinder with spherical ends, with a volume of 30.000 litres, all enclosed by a fairing. In order to maintain the cryogenic temperatures, of around -160 ° C, a strong insulating layer of Polyvinylchloride was used, which optimised density and conductivity, whilst minimising the amount of mass necessary. Moreover, materials relating to the fairing were investigated, with the function to be aerodynamic but also to absorb impacts such as from a bird strike. A surface layer of CFRP was chosen, with an interior of polyurethane foam, thus allowing for shape and function. The tanks are to be mounted via three supporting rods, made of Al-2219, thus allowing the tanks to be easily removed when at the airport. The tanks also have the capability to be detached at any instance with releasable bolts. This means that in case of an emergency, the liquid storage tanks can be dropped and the aircraft can continue flying for a minimum time of 30 seconds before the fuel still stored in the gaseous tanks is depleted.

[2] https://nickelinstitute.org/media/8d93486143182f5/nickel_incopub393_updated-june-2021.pdf[Cited on 17-June-2024]

Each half wing contains three gaseous methane tanks in order to improve throttleability and to sustain thrust for 30 seconds should the mass flow from the liquid tanks be interrupted. These tanks slightly decrease in diameter as the wing decrease in thickness along the span. The first tank has a diameter of 42.2 cm, the next 39.9 cm and the gas tank closest to the wing tip has a diameter of 37.7 cm. These sizes are dependent on the thickness of the airfoil and therefore decrease per bay. Each tank is sized to withstand a pressure of 208.5 bar and is made of Al-2219. Figure 4 shows the placement of these tanks in the left half of the wing.

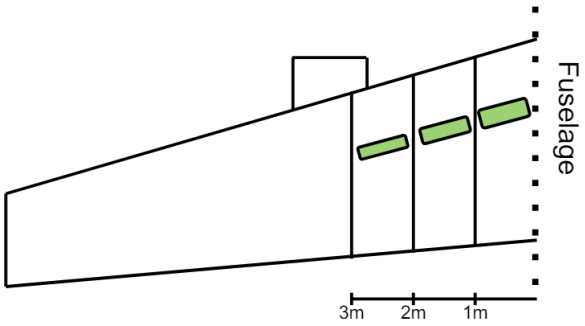

Figure 4: Placement of the gaseous methane tanks.

Structures and Materials

For the wingbox, a Solvey graphite fabric composite was used due to its excellent material properties. Modern wingboxes are often made of carbon fibre composites as they allow for weight saving when compared to aluminium alloys which are typically used For the fuselage the main structural elements such as the skin and stringers were made of Al-Li2198 as the skin of the fuselage is so thin that the weight saving aspects of composites can not be optimally utilised.

The loads on the wing were determined using the aerodynamic data from XFLR5 and the weights obtained from the Class II weight estimation. It was found that the wing-mounted fuel tanks provide a significant bending relief countering the aerodynamic loads in flight, but increase the overall weight of the wing group, where the point loading has a large effect when the aircraft is not producing lift. The most critical load case for bending was **LC03: 80% fuel 2.5g turbulence cruise** and for twist it was **LC01: MTOW taxi sea-level**. The maximum wingtip deflection for the most extreme load case was found to be 2.78 m upwards, with a maximum twist angle of 7.68 ° as seen in Figure 5. The wingbox was designed accordingly, such that it can carry the most extreme loads without failure. The calculations resulted in a wingbox skin thickness of 6 mm, reinforced by T-shaped stringers; the maximum number being 33 per side near the wing root. A similar analysis was performed for the fuselage, which has a 2 mm thickness and 128 stringers, spaced closer near the top and bottom and further away near the central axis. The wing and fuselage were designed with a margin of safety and for the most extreme loading, such that the aircraft can operate as safely as possible.

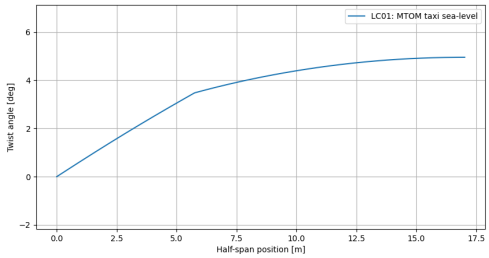

(a) Wing twist

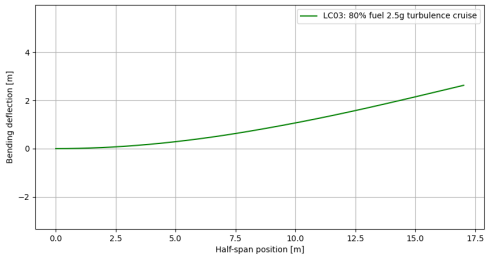

(b) Deflection of the wing

Figure 5: Effect of most critical wing loading cases.

Internal Systems

The pneumatic, hydraulic, electrical and communications systems have been designed for CH4llenger. The pneumatic system uses the bleed air from the engines to de-ice the wing and provide air to the cabin for pressurisation and passenger comfort. The hydraulic system is needed to move the mechanical parts of the aircraft, such as the flaps and slats. CH4llenger has two reservoir paths along with a backup electric hydraulic actuator. An electrical system, encompassing the different electrical components in the aircraft, was created. Furthermore, a communications system was designed to show how data flows from antennas to system elements. A hardware and a software block diagram are also created to show the flow of inputs and outputs to different systems.

Operations

Apart from the design of the aircraft, the designing of the operations and logistics that surround its functioning is critical. This describes how fuel is produced, transported and stored at the airport. Moreover, operations at the airport including refuelling and ground operations are expanded upon too.

Airports were divided into three groups: large, medium and small airports, with large having up to twelve transatlantic flights, medium up to four transatlantic flights and small with only one transatlantic flight a week. Furthermore, types of routes were described by identifying six initial airports that would start the methane revolution. From those, two were Large airports, two were medium and two small. All combinations of routes between the airports are considered apart from small to small due to the very low traffic that would occur between them and thus the limited need for infrastructure and investment necessary.

Moreover, the generation of fuel was considered, with two predominant means of synthesis: biomethane and synthetic methane. The basis of synthetic methane is the chemical process of methanation whereby hydrogen and carbon-dioxide react to produce methane and water. A key consideration in methanation is the utilisation of hydrogen, and in order to maintain an energy-efficient and sustainable aircraft operation, the hydrogen must be generated from green electricity. Furthermore, the carbon is to be captured, thus aiding in the push for carbon neutrality. Secondly, biomethane provides methane originating from biomass. It is a promising source of methane as there is a large push by European governments to implement its infrastructure throughout Europe, spurred by the ongoing Ukraine war. Furthermore, liquefaction infrastructure will be necessary at or close to the airports, as methane can only be stored for up to five days in liquid state.

Once produced, transportation options were assessed, with a focus on the capabilities of the different airports. For Large airports 660.000 litres of fuel would be necessary to supply the fuel for 12 flights per day, thus 20 trucks or 6 train wagons worth of fuel would be required per day to fuel the airport and allow for proper operations. Pipelines could also be used to support the influx of fuel during busy

periods at large airports. Medium airports would expect 165.000 litres of fuel a day, to supply up to 4 daily flights and would expect fuel to arrive via trucks or trains. Medium airports could also use pipelines depending on the infrastructure surrounding the airport. Both airport types would require liquefaction plants to have a liquid methane supply. As for small airports, only 55.000 litres of fuel would be necessary per week, assuming one weekly flight, this can be provided by two liquid methane trucks.

The refuelling operations at the airport are also discussed. Aircraft refuelling trucks shall carry the designed liquid methane tanks to the fuel depot at the airport. There the tanks will be filled with liquid methane. Subsequently, the trucks drive to the aircraft, remove the empty tanks and attach the filled tanks. Thereafter, the empty tanks are taken to the storage area and purged/vented, before either going to maintenance or being refuelled again. At Small airports, no infrastructure is in place to refuel the external tanks when detached from the aircraft, so the tanks will be fuelled when attached to the aircraft. This will increase the refuelling time as the time to fill the tanks is longer than the time to transport and detach/attach the tanks. Passengers will also not be allowed to board during that refuelling, thus the turn around time will increase.

RAMS

An additional consideration in the functioning of the aircraft design are the reliability, availability, maintenance and safety aspects. Reliability pertains to the ability of the systems to work according to their intended function without failure and Availability regards the readiness of the systems to operate when needed. Several failure modes were investigated, particularly on the refuelling system, which is novel and untested before this project. The likelihood of the failure is low, yet additional mitigation is performed to further reduce the likelihood of failure, such as having specific sensors to detect leaks, or additional strengthening of the tanks to reduce the chance of rupture. Moreover, maintainability aspects were discussed and categorised into Check Types, dictated by the number of flight hours necessary before the maintenance needs to occur. These are type A at 750 hours, C at 12,000 hours and D at 6 years. Finally, the safety of the system was considered and its continuous assurance. This was looked at from an airworthiness point of view and thus concluded that the project shall communicate and work closely with the FAA and EASA to generate certification and requirements to develop guidelines that will help guide safe operations of the aircraft.

Market and Cost Analysis

The expected amount of passengers is set to increase to 10 billion passengers, equivalent to 20 trillion kilometres per year by 2050. Sustaining the current rate of emissions would lead to a 260% increase in emissions compared to 2019. This presents a challenge in terms of providing enough aircraft to the commercial aviation market, but also preventing global CO_2 emissions from rising too much. Looking at the Sustainable Aviation Fuel (SAF) market, this is expected to grow significantly in the near-term, from 1.1 B$ to 16.8 B$. These projections hint at a growing demand and incentives for the sustainable aviation market, giving the CH4llenger aircraft a significant advantage.

To analyse the costs of the aircraft, the research & development (R&D), manufacturing, and operational costs were considered. Here, it was found that the main change to R&D costs would be due to a novel propulsion design. Nevertheless, they were kept low at about 30 M$. Manufacturing costs also do not change significantly, being at about 90 M$. This leads to an overall aircraft cost of about 120 M$, successfully achieving the design requirement. Operational costs have also been found to be similar to conventional aircraft, with estimated fuel price per mile being essentially the same in the long-term (2.22 $/mi vs 2.21 $/mi).

Sustainability

Sustainability was analysed from a social, economic and environmental point of view, with emphasis placed on the latter one. The various engineering departments accounted for environmental sustainability by including separate criteria during key design decisions. Additionally, a detailed analysis was performed on the use of methane, in comparison to Jet A/A-1 and hydrogen fuel. It was found that kerosene emits roughly 30 % more CO_2 and about ten times more NO_x emissions, compared to methane. Hence, methane, even when derived from natural gas, would lead to significant improvements in environmental sustainability. Nevertheless, from an economic sustainability perspective, synthetic methane production is currently much more expensive than Jet A/A-1 and Hydrogen, presenting a possible challenge. This cost, however, is expected to reduce significantly with scaled production and evolving methanation technology, leading to estimated synthetic methane costs of 31 cents per kilogram in 2050.

Compliance

After having created and analysed the aircraft design, the stakeholder and functional requirements were revisited. It was found that most requirements were fulfilled, with some exceptions to requirements which could not be evaluated at this stage of the design. One of those is the trimmability requirement, which will be analysed in detail only once the detailed analysis is concluded.

Future

After successfully concluding a preliminary design of the aircraft, several tasks are still to be performed. Firstly, the aircraft has to be designed in more detail, going into FEM and CFD analysis. Following this, prototypes have to be built, and real-life tests performed. Finally, the aircraft needs to be certified and manufactured. Regarding the latter, infrastructure has to be implemented to support the specific requirements that the aircraft needs to adhere to. While all of these tasks cannot be performed in much detail at the current stage, a general Project Design and Development Logic (PDDL) and Gantt chart were created. According to the conceived documents, a prototype will be created and flown by 2030, whereas the production of the aircraft will commence in 2034.

Contents

1. Introduction

With an increasing market in commercial flights coupled with raising concerns regarding the environmental impact of aviation, the industry must evolve. As such, novel ideas must be pushed for, tried and tested with the hope that a new sustainable era of aviation emerges, thus allowing passengers to continue flying around the globe, whilst ensuring industry standards like the IATA 2050 goal[1] come to fruition. Furthermore, change is needed, and as much as it can bring opportunity and revolution, public friction from the familiar ease of fossil fuels and political scepticism to untried methods are likely hurdles that are to be mitigated in the process.

This report introduces and presents the CH4llenger, a sustainable and energy-efficient aircraft that can support the growth of the aerospace industry in an environmentally friendly manner. The aircraft will fly on synthetically produced methane, addressing its mission need statement:

> "To reduce the environmental impact of aviation by designing a novel aircraft that is capable of transatlantic flights by 2030."

The project objective statement follows:

> "To design an aircraft with a similar payload, range and characteristics to the A321neo that is able to fly at transatlantic range on renewable energy."

Based on these goals, a methane-fuelled aircraft was designed, allowing for CO_2-neutral flying [1]. Building on this concept, the CH4llenger was designed to fly across the Atlantic Ocean as efficiently as possible. This report details the initial design stages, providing a preliminary overview of the characteristics and performance of the aircraft. Special attention has been given to the production of the fuel, the logistics associated with the aircraft, and the sustainability aspects, ensuring the feasibility of the concept.

The report starts with a summary of the design choices made that led to selecting synthetic methane as the sustainable fuel, presented in chapter 2. The functional aspects of the aircraft as well as the technical risks are subsequently outlined in chapter 3. Following that, in chapter 4, the aircraft requirements are laid out, while the initial sizing of the systems is shown in chapter 5. Subsequently, chapter 6 delves into the details of the propulsion system. In chapter 7, material research is presented and different options are proposed for the several subsystems. Afterwards, chapter 8 presents the iterative design process leading to the final aircraft characteristics. The report then continues with chapter 9, in which the selected material properties are described along with the analysis of the structural capabilities of the wing and fuselage. Chapter 10 then presents the different internal subsystems in the form of schematic diagrams, while chapter 11 discusses the safety and airworthiness of the aircraft. Afterwards, the typical operations, transportation and refuelling procedures of the novel aircraft are presented in chapter 12. Following that, chapter 13 explores the financial side of the project. The several sustainability aspects are then analysed in chapter 14, while chapter 15 evaluates the compliance of the final product with the previously defined requirements. Finally, chapter 16 introduces the future steps to be taken in order to finalise the design of the CH4llenger.

[1] https://www.iata.org/contentassets/b3783d24c5834634af59148c718472bb/net-zero-tracking-progress-methodology.pdf, [Cited on 17-June-2024]

2. Trade-Off Summary

The goal of this project is to design a carbon-neutral aircraft that flies on a sustainable fuel and can fly at transatlantic range. To do this the aircraft has to be designed such that it is optimised to energy efficient flight, as well as the operations around its functions. Furthermore, a fuel has to be chosen that can be produced and burned carbon neutrally. In order to optimise energy efficiency, an investigation into the logistics around the production, transport, handling, and refuelling of the fuel was performed.

The project began by researching a variety of possible fuel options. A design options tree, Figure 2.1, was made for the different fuel options, which were divided into carbon-based, non-carbon-based, and hybrids of the two. Many options were initially removed due to being unfeasible because of their high associated mass or not meeting requirements. Moreover, a fuel market analysis was performed leading to Table 2.1. This depicts the current market size and expected compound annual growth rate (CAGR) of each of the fuels, thus representing the support each fuel shall obtain in the near future. Moreover, the strength of each fuel's political agenda from green (strong) to red (weak) is represented, thus depicting how much aid each fuel could get from the local or EU governments. Finally, the Technology Readiness Level (TRL) is represented, showing how well the technology for each fuel is implemented in the industry, thus showing the level of friction each fuel could expect to get ahead of implementation. In conclusion, the design options tree in Figure 2.1 was synthesised, with disregarded options being marked in red. Subsequently, three fuel options were chosen: hydrogen, methane, and a hybrid of hydrogen and synthetic kerosene.

Table 2.1: Summary of fuel markets [2].

Fuel Type	Market Size (Billions $)	CAGR (%)	Political Agenda	TRL
Green Hydrogen	4.47	36.5	Green	6-9
Batteries	45.7	14.13	Orange	4-9
Bio/Synfuels	1.1	47.7	Green	2-9
Chemical Compounds/LNG	74.6	1.6	Orange	9
Ammonia	205.34	5.4	Orange	2

Based on these three fuel types different design options were made for the tank placement. Only conventional aircraft configurations were considered due to the short time to market and unit cost of under 120 M$ being stakeholder requirements [3]. Non-conventional aircraft will have a longer time to market and cost more, thus these designs were not considered. The different options for tank placement were synthesised in a design options tree, shown in Figure 2.2, describing locations considered for each fuel option. From these, the unfeasible options were removed, presented in red in the design options tree. This only left the 15 designs presented below.

- **HYB-01-A**: Hybrid with removable external tanks under the wing.
- **HYB-01-B**: Hybrid with fixed external tanks under the wing.
- **HYB-02**: Hybrid with the fuel tank on top at the back.
- **HYB-03**: Hybrid narrow-body with the fuel tank in the back of the fuselage.
- **HYB-04**: Hybrid wide-body with fuel tanks in the back of the fuselage.
- **LH2-01**: Hydrogen narrow-body with fuel tanks in the back of the fuselage.
- **LH2-02**: Hydrogen wide-body with fuel tanks in the back of the fuselage.
- **LH2-03-A**: Hydrogen with removable wing tip tanks.
- **LH2-03-B**: Hydrogen with fixed wing-tip tanks.
- **LH2-04**: Hydrogen with integrated upper fuel tank.

- **CH4-01**: Methane narrow-body with a fuel tank in the front cargo hold and in the back of the fuselage.
- **CH4-02**: Methane wide-body with a fuel tank in the front cargo hold and in the back of the fuselage.
- **CH4-03**: Methane with integrated upper fuel tank.
- **CH4-04-A**: Methane with removable external tanks under wing
- **CH4-04-B**: Methane with fixed external tanks under wing

A trade-off was performed on the final design options. All designs were assessed on performance, safety and risk, ground handling and airport operations, innovation, energy required, and sustainability. These aspects were thoroughly researched for each design. This led to four different designs that would be considered in greater detail: methane tanks under the wings, methane stored in the fuselage, hydrogen in a tank on the top of the fuselage, and a hybrid with hydrogen stored in tanks under the wings.

Preliminary sizing was done for each design configuration. A Class I weight estimation, payload range diagram, and wing loading diagram were made for each option. Subsequently, a fuselage, wing and performance analysis was synthesised. These designs were then compared based on various factors such as L/D, weight and ease of operations at the airport. Based on these factors the aircraft designs were ranked. This concluded with the methane under the wing tanks configuration being chosen, due to its high L/D and easy refuelling procedure.

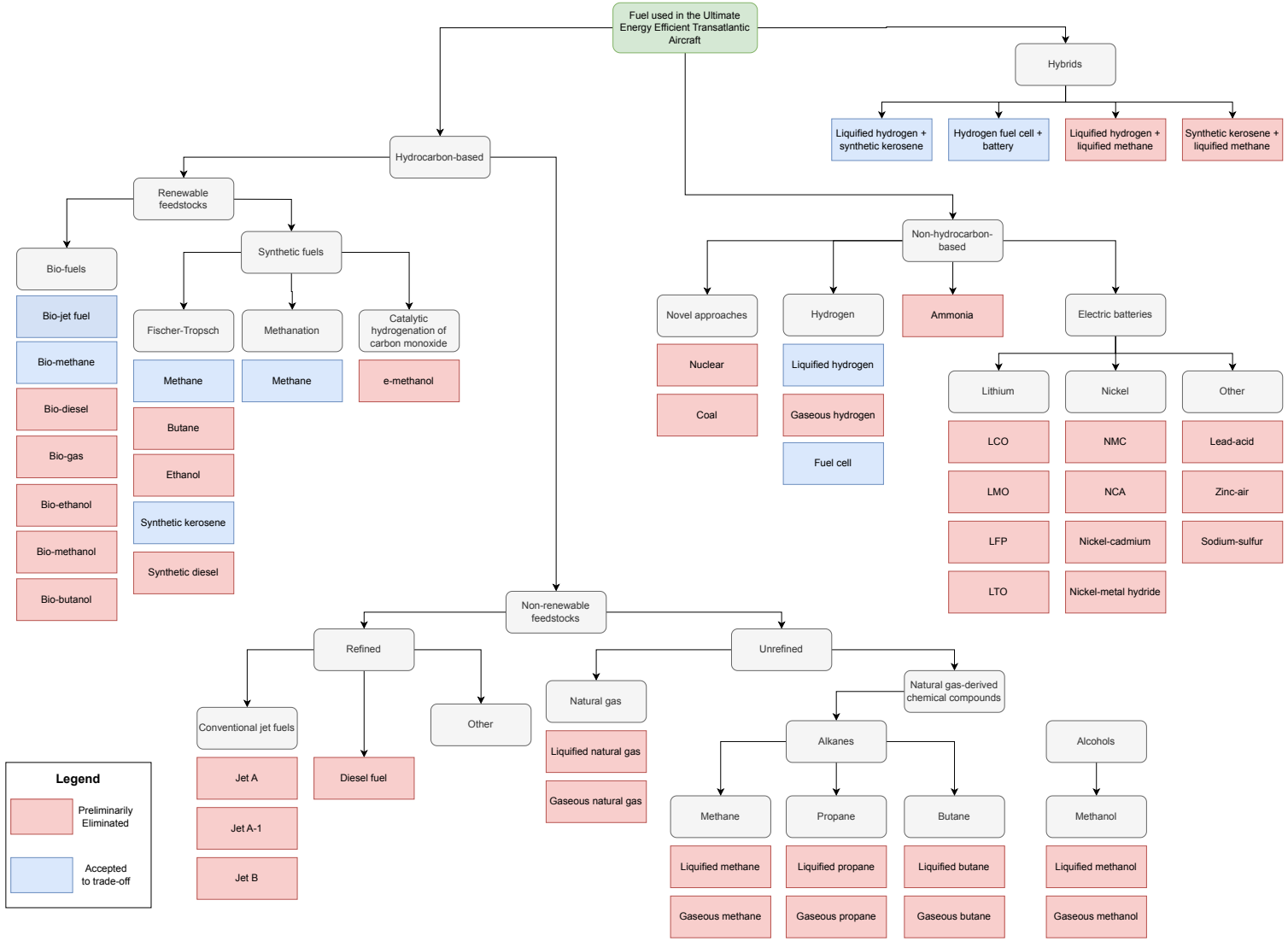

Figure 2.1: Design option tree presenting the different fuels considered.

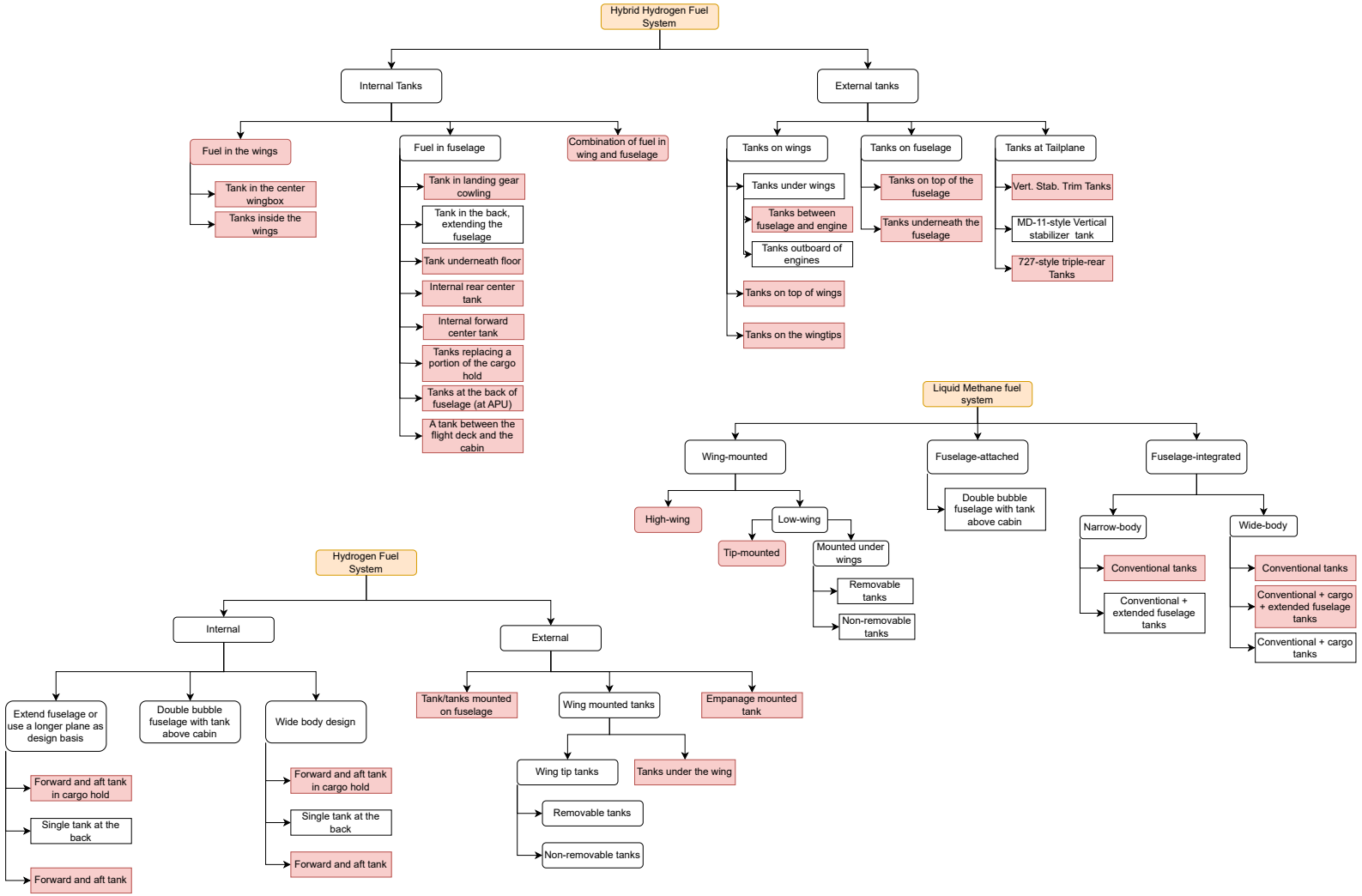

Figure 2.2: Design option tree presenting the different fuel tank placements.

3. Functions and Risks

Of massive importance to any engineering project are its functions and risks, which this chapter looks at. In section 3.1, the functions that the aircraft needs to perform are discussed to ensure the full picture of aircraft operations is considered. In section 3.2, the possible risks that pose a threat to the aircraft are assessed from a technical point of view. Lastly, section 3.3 contains the N^2 interface diagram, showing the relations between different aircraft systems.

3.1. Functional Flow Diagram and Breakdown Structure

In this section, all the functions the aircraft is expected to perform during operation are outlined. First, in subsection 3.1.1 a functional flow diagram is presented with all functions in chronological order. Then, in subsection 3.1.2, a functional breakdown structure presents all grouped (sub-)functions, with the associated systems.

3.1.1. Functional Flow Diagram

The functional flow diagram, presented in Figure 3.1 is utilised to identify the necessary capabilities and functions of the aircraft in its operation. This helps inspire any functional requirements necessary for the implementation of the aircraft post-design stage. These functions are divided into differing levels of detail where the red blocks have the lowest level of detail and the white blocks the highest. The "operate aircraft" function is given in the greatest detail, as this is the most important phase of an aircraft's lifetime.

In addition to regular operations, the diagram also considered cases like aborted take-offs or landings, and loitering. With red arrows, the procedures are indicated which are unexpected. Hence, a good overview of all functions which the aircraft is supposed to perform is given. These functions can then also serve to create the requirements for the final design. Such functional requirements are noted in Table 4.2, with critical requirements including; the airports shall have the infrastructure to refuel the aircraft and the aircraft shall be able to enter cruise conditions.

3.1.2. Functional Breakdown Structure

In order to achieve an overview of all the functions and sub-functions the aircraft has to perform to complete its purpose successfully, a functional breakdown structure is created and presented in Figure 3.2. This is broken down into corresponding phases with the functional flow diagram Figure 3.1, and details their functions. For each function, a corresponding identifier is specified as well as the particular system it relates to. Only Level 3 functional requirements are associated with systems as the levels above pertain to the whole aircraft and Level 4 are directly associated with a specific system. Furthermore, there are special functions added that do not correspond to normal aircraft operations. These look at specific cases, notably, situations when there is an emergency like an engine which is inoperative.

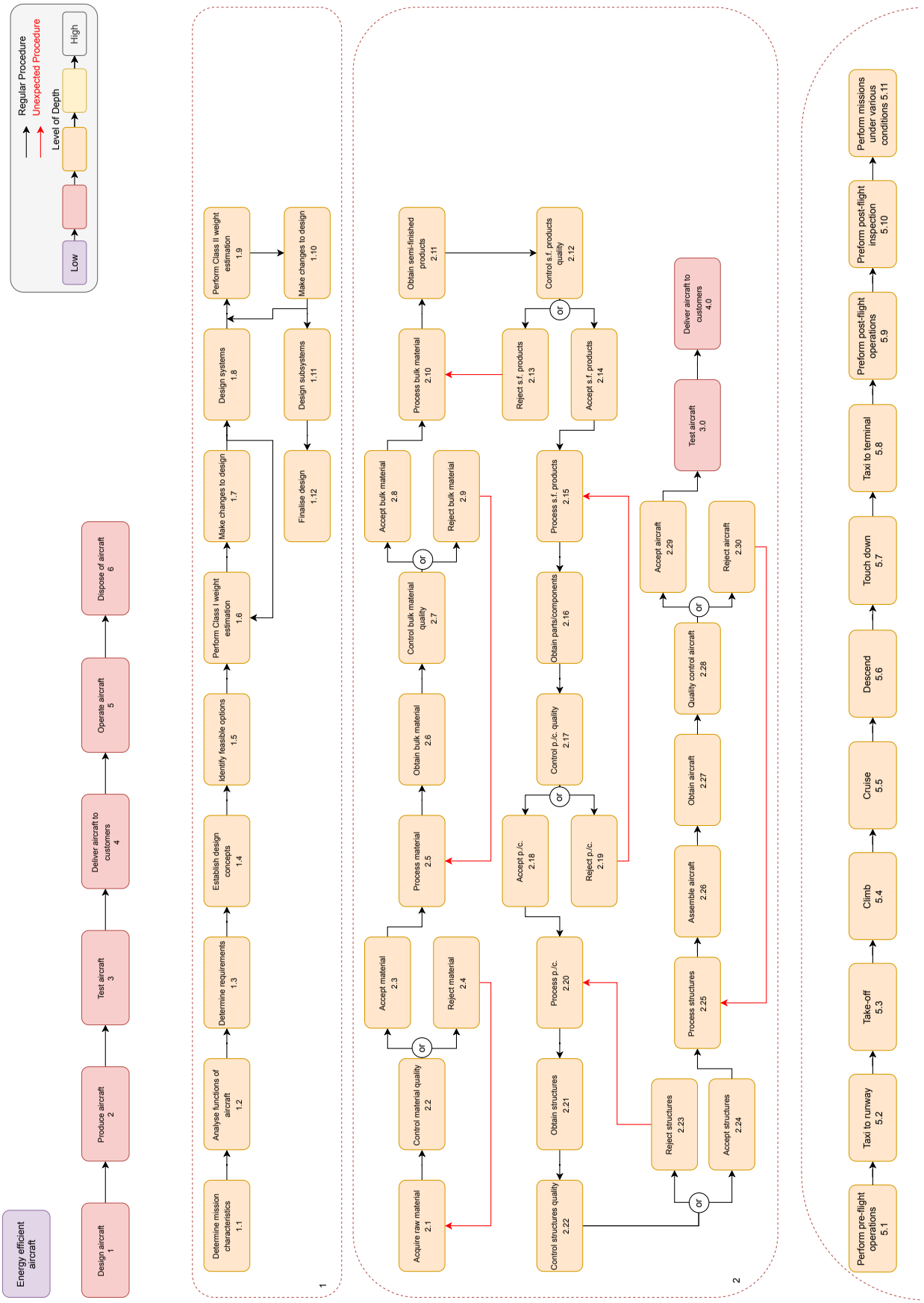
Regular Procedure
Unexpected Procedure
Level of Depth
Low
High
Energy efficient aircraft
Design aircraft 1
Produce aircraft 2
Test aircraft 3
Deliver aircraft to customers 4
Operate aircraft 5
Dispose of aircraft 6
Determine mission characteristics 1.1
Analyse functions of aircraft 1.2
Determine requirements 1.3
Establish design concepts 1.4
Identify feasible options 1.5
Perform Class I weight estimation 1.6
Make changes to design 1.7
Design systems 1.8
Perform Class II weight estimation 1.9
Make changes to design 1.10
Design subsystems 1.11
Finalise design 1.12
1
Acquire raw material 2.1
Control material quality 2.2
Accept material 2.3
Reject material 2.4
Process material 2.5
Obtain bulk material 2.6
Control bulk material quality 2.7
Accept bulk material 2.8
Reject bulk material 2.9
Process bulk material 2.10
Obtain semi-finished products 2.11
Control s.f. products quality 2.12
Reject s.f. products 2.13
Accept s.f. products 2.14
Process s.f. products 2.15
Obtain parts/components 2.16
Control p./c. quality 2.17
Accept p./c. 2.18
Reject p./c. 2.19
Process p./c. 2.20
Obtain structures 2.21
Control structures quality 2.22
Reject structures 2.23
Accept structures 2.24
Process structures 2.25
Assemble aircraft 2.26
Obtain aircraft 2.27
Quality control aircraft 2.28
Accept aircraft 2.29
Reject aircraft 2.30
Test aircraft 3.0
Deliver aircraft to customers 4.0
2
Perform pre-flight operations 5.1
Taxi to runway 5.2
Take-off 5.3
Climb 5.4
Cruise 5.5
Descend 5.6
Touch down 5.7
Taxi to terminal 5.8
Preform post-flight operations 5.9
Preform post-flight inspection 5.10
Perform missions under various conditions 5.11

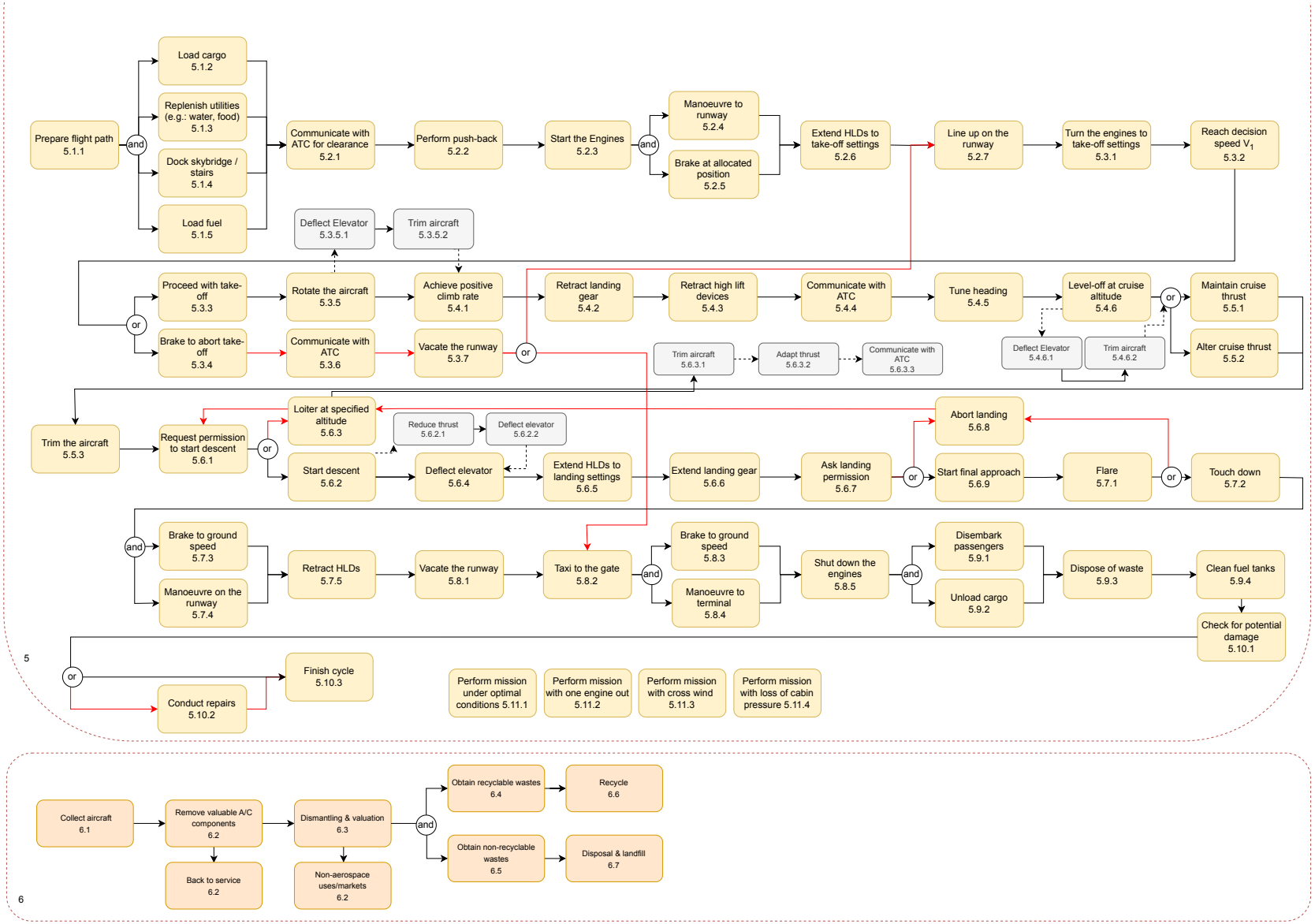

Figure 3.1: Functional flow diagram showing the flow of aircraft functions.

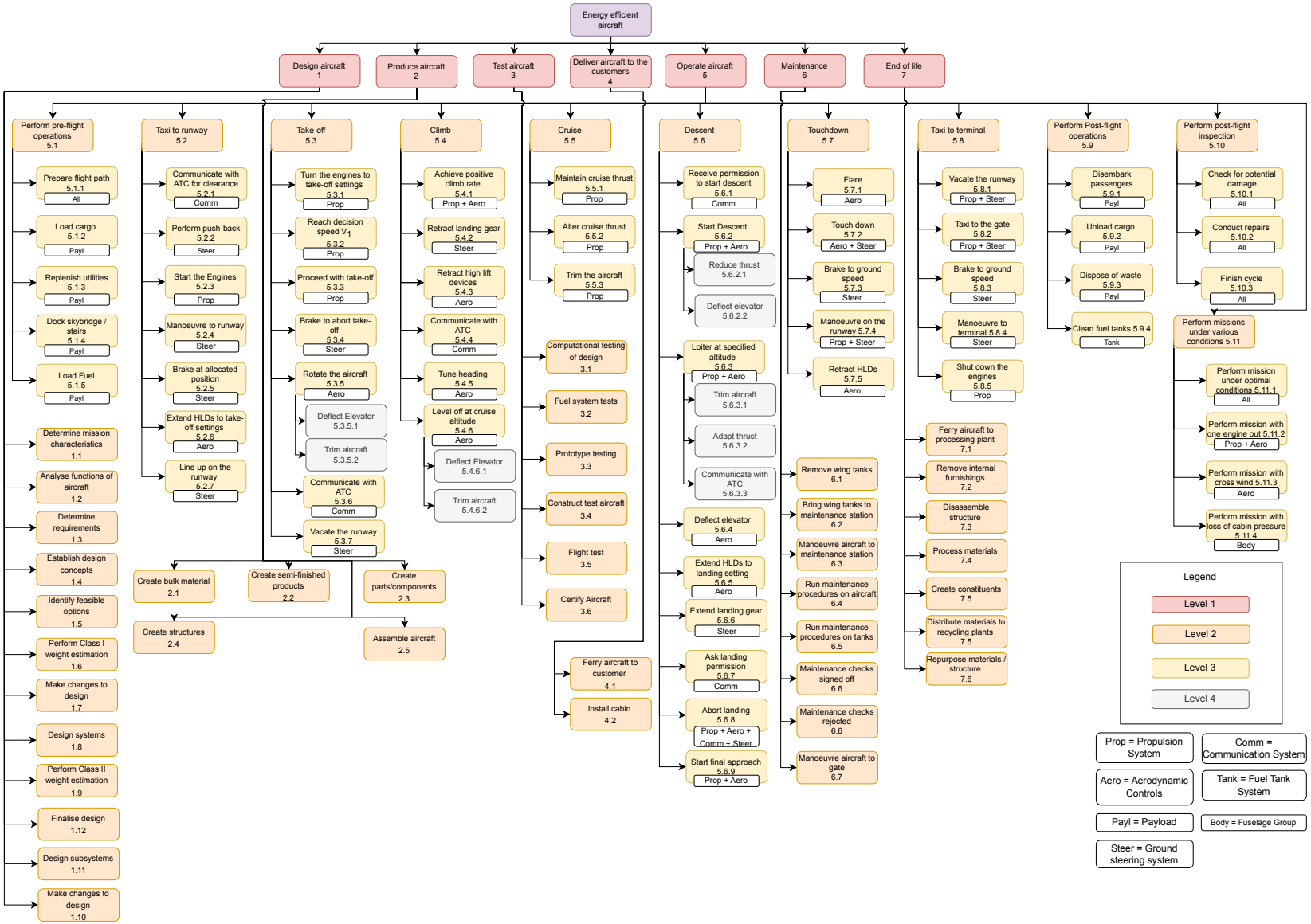

Figure 3.2: Functional breakdown structure showing the relations of aircraft functions.

3.2. Risk Analysis

Technical risk alludes to uncertainty of outcome during the operation of a process. During the operational lifespan of the aircraft, it can encounter a multitude of risks, many of which are critical to mission success. Therefore, all risks are unidentified and assessed to keep track of them. This is done in subsection 3.2.1 and subsection 3.2.2. Then in subsection 3.2.3, the risks are presented in a risk map and mitigation strategies are discussed. Lastly, in subsection 3.2.4, the most critical risks are discussed.

3.2.1. Risk Identification

From the WBS, the main technical risks are identified and elaborated in a risk analysis. Subsection 3.2.2 contains the process of determining the most relevant risks and the resulting list. Moreover, the risks included are split into Operational (O), purely Mission (M), and Budget (B) risks. To be more specific, operational risks are any risks that interfere with the flow of airport/ground operations and logistics. Mission risks attest to the aircraft itself and affect its attributes such as its system performance or its safety standards. Lastly, budget risks involve the disruption and violation of cost, timeline, etc. Risks are identified with a format of **Risk - Type - #**, abbreviated as **R - M - 01** for example.

3.2.2. Risk Assessment

Risks were developed by looking at the FBS and the WBS and determining several risks during each phase. Moreover, their likelihood, which is simply the chance of the risk occurring, and the impact level were also determined. On the one hand, the lowest level of likelihood (1) indicates an improbable chance of occurrence, while the highest level (10) indicates almost a certain risk, and it is highly likely to be already considered during the early stages of the design process. On the other hand, an impact level of 1 suggests the consequence of the risk would have minimal effect either operationally, the design, or the budget, while an impact level of 10 suggests a catastrophic result that would mean the project's complete failure.

To ensure the enforcement of the mitigation plans throughout the design process, a team member is responsible for each risk. All team members' names are abbreviated and initials are used. The complete list can be found in Table 3.1.
Primarily, Table 3.2 contains the current risks still being considered from the previous project milestone. Each one is split into a cause, event, and consequence. The severity of the overall consequence is described by the likelihood and impact levels, while a holistic total risk value is done by multiplying the two numbers. Additionally, a mitigation plan for each risk is included, along with a post-mitigation (PM) total risk value, which reflects its effect. If the risk has a total score of 36 or under, it is considered acceptable, yet obviously monitored. If higher, it is considered a critical risk.

Table 3.1: Initials of team members' names as used in the diagrams in alphabetical order of the first initial.

Team Member	Initials	Team Member	Initials
Aurora Nieuwenhuis	AN	Adam Wójciński	AW
Daniil Zorzos	DZ	Grégoire Dastros-Pitei	GDP
Jeroen Slagmolen	JS	Paulina Dabrowska	PD
Paul Mertens	PM	Robin Bos	RB
Thomas Claudel	TC	Tibi Quinn	TQ

Table 3.2: Risk table relating to CH_4 external tank configuration.

ID	Cause	Event	Consequence	Likelihood (1-10)	Impact (1-10)	Total Risk	Mitigation	PM Risk	Assignee
R-M-01	CH_4 gasifies faster than calculated	Fuel tank vents due to overpressure	Loss of fuel and lowered range of flight, potentially leading to critical loss	2	10	20	Use proven insulation methods, develop passive gasification prediction model and modify gaseous CH_4 storage system to store higher pressures, lowered impact	14	PD

Continued on next page

Table 3.2– continued from previous page

ID	Cause	Event	Consequence	Like-lihood (1-10)	Impact (1-10)	Total Risk	Mitigation	PM Risk	Assignee
R-M-02	Not proper pipe insulation	Liquid Oxygen forms on fuel pipes	If in contact with spark, could combust	3	9	27	Ensure sufficient insulation on pipes, lowered impact	15	AN
R-M-03	Vacuum/Insulation of CH_4 fuel storage not as effective as predicted	Fuel discharges more rapidly than expected	Larger heavier storage systems required	4	8	32	Implement pressure management systems and have backup/multi-layer insulation system, lowered likelihood	16	AW
R-M-04	Incorrect propulsion system C.G. calculations	Incorrect system placement	Incorrect stability analysis and mission failure due to unusable aircraft	4	10	40	Conduct thorough design reviews and utilise tools such as CAD during V&V and sensitivity analysis, lowered likelihood and impact	16	GDP
R-M-05	Using novel propulsion system	Thrust is lower than expected	The aircraft is unable to fly predetermined range leading to fatal loss	6	10	60	In-depth research, prototyping and modelling, efficient use of safety factors and test extensively, lowered likelihood	40	TC
R-M-06	Fuel purifying processes are not robustly tested	Fuel is not pure enough	Aircraft flies at lower efficiency/build-up of solid $N_2/O_2/H_2O$	6	8	48	Ask fuel producers to have a certification proving the purity of fuel and have quality control performed on the fuel per batch, lowered likelihood and impact	24	JS
R-M-07	Placement of novel fuel storage system	System explodes into engine and fuselage	Plane unable to maintain flight and crashes	6	10	60	Testing the strength of storage and engine cowlings in order to maintain any rare blasts, lowered likelihood and impact	27	DZ
R-M-08	Wing tanks create a different aerodynamic configuration	Flight characteristics are massively different to conventional	Aircraft becomes impractical and uncomfortable to fly from a pilot's perspective	6	8	48	Develop simulations to be tried and tested by humans, and have an active control system outer loop, lowered impact	36	RB
R-M-09	New vaporiser used	Methane not gasified fast enough	Lack of thrust and mission failure	2	8	16	Have vaporiser certified by subcontractor, allow electric vaporiser to be used in flight and design gaseous system to increase mass flow as backups, lowered likelihood and impact	6	RB
R-M-10	Tank connection rod fails	Tank falls off	Plane is severely unbalanced and half of fuel is lost	3	10	30	Allow for cross-linking capabilities of fuel to ensure two engine flight case. Ensure safety factors are implemented to avoid severe tank disaster cases, lowered likelihood	20	RB
R-M-11	Aircraft cannot take-off at MTOW in remote locations	Incorrect weight calculations	Aircraft stranded in hard to reach location	1	10	10	Include updated relevant calculations during crew training, lowered impact	8	DZ
R-M-12	No fuel in wings and point loads from wing tanks	Wing too heavy, bending moment on wing root is too great and point loads create excessive stress	Wing fails	2	10	20	Ensure structural rigidity through testing of a variety of alternative materials, lowered impact	16	DZ
R-M-13	Different gaseous/fluid dynamics of fuel compared to conventional	C.G. of aircraft changes unpredictably	Leads to instability and control of the aircraft and different component sizing needed	4	10	40	Run tests to simulate the change in aircraft properties using new fuel, lowered likelihood and impact	18	JS
R-M-14	Onboard emergency	Emergency landing must take place before planned landing	Aircraft cannot land due to being overweight with fuel	3	8	24	Develop systems and procedures for crew to safely execute fuel dumping to reach necessary weight, lowered impact	15	DZ
R-M-15	Loss of power, critical system failure	CH_4 under wings ignites upon crash landing/ditching	Explosive damage to wing, fuselage and severe limit in passenger survivability	2	10	20	Use tested detachable wing tank mechanism capable of being jettisoning prior to a crash landing or ditching, lowered impact	10	AW
R-M-16	Protruding CH_4 tanks	Excessive drag	Flight underperformance, efficiency decreases	3	6	18	Investigation in tank shapes, and potential use of special nose shape to increase aerodynamic efficiency, lowered impact	12	PM
R-M-17	Different internal structures compared to conventional due to lack of fuel in wings and new CH_4 propulsion system	Structural failure due to	Catastrophic mission failure	3	10	30	Use calculations/FEM to investigate potential structural weaknesses which might require reinforcements, lowered likelihood and impact	14	TQ
R-M-18	Gaseous CH_4 buildup	Malfunction of gaseous CH_4 venting system	Delays in external tank turnaround due to tanks needing to be replaced again	4	6	24	Make vent system be designed to avoid air intrusion, and unobstructed from weather, lowered likelihood	12	GDP
R-B-01	Increased national LNG demand	Local infrastructure cannot sustain big raise in demand and fails	Infrastructure fails and delays/limited number of flights ensue, dropping traffic at airports	2	8	16	Model the predicted increase in resource usage and plan accordingly with fuel parties, lowered likelihood and impact	6	PM
R-B-02	Use of novel fuel storage technologies in airports	Storage tank on such a large scales will need R&D, will have backlog and delays	Cost and time budgets are affected negatively	4	4	16	Budget margins to take it into account, lowered likelihood	8	PM
R-B-03	Novel fuel airport storage is very specific	Storage and distribution needs are more expensive	Cost requirements violated	4	6	24	Allow for margins in the cost budget, lowered likelihood	12	AW
R-O-01	Rigid safety requirements around refuelling with novel fuel	Refuelling takes longer than anticipated	Longer turnaround times and loss in profit	5	6	30	Train ground crew well in advance and ensure knowledge of refuelling requirements, lowered impact	25	TC
R-O-02	Demand of sustainable flights beat supply of fuels	Not enough fuel at airport to facilitate quick refuelling	Loss in operating time and lower profits	4	8	32	Develop realistic market plan with fuel providers, lowered likelihood	16	GDP

Continued on next page

Table 3.2– continued from previous page

ID	Cause	Event	Consequence	Like-li-hood (1-10)	Imp-act (1-10)	Total Risk	Mitigation	PM Risk	Assi-gnee
R-O-03	Improper manu-facturing of novel aircraft parts, es-pecially the CH_4 pump systems	Faults progressively found during lifetime of aircraft	Loss of trust and neg-ative public perception on sustainable aircraft designs	4	10	40	Use stringent certification process and con-tinuous compliance checks during produc-tion; have airline engagement and feedback mechanisms, lowered likelihood and im-pact	24	TC
R-O-04	Novel fuel system very specific	Specific set of skills nec-essary to operate/main-tain aircraft	Unskilled global work-force take longer on maintenance/turn-around	4	8	32	Develop a standardised training procedure, lowered likelihood	16	PD
R-O-05	Complicated struc-ture and shape of internal CH_4 tank(s)	Limited accessibility of the fuel tank parts	Inspection checks are more expensive and time-consuming	5	4	20	Implement maintenance scheduling and documentation; use predictive mainte-nance insights using data collected from the aircraft maintenance to focus on when issues are likely to arise, lowered impact	15	TQ

3.2.3. Risk Map

The risk map in Figure 3.3 depicts the relative significance of a specific risk. It is done by considering the numerically depicted impact and likelihood values, each on a scale of 1-10, with 1 representing a low likelihood or impact and 10 representing high likelihood or impact. For ease of analysis, the different sections are coloured in order to represent the combined severity of a risk, with red indicating detrimental risks and green being relatively tame. The risks of the risk table can be directly implemented into the risk map, with their risks before mitigation in black font and post-mitigation represented in white.

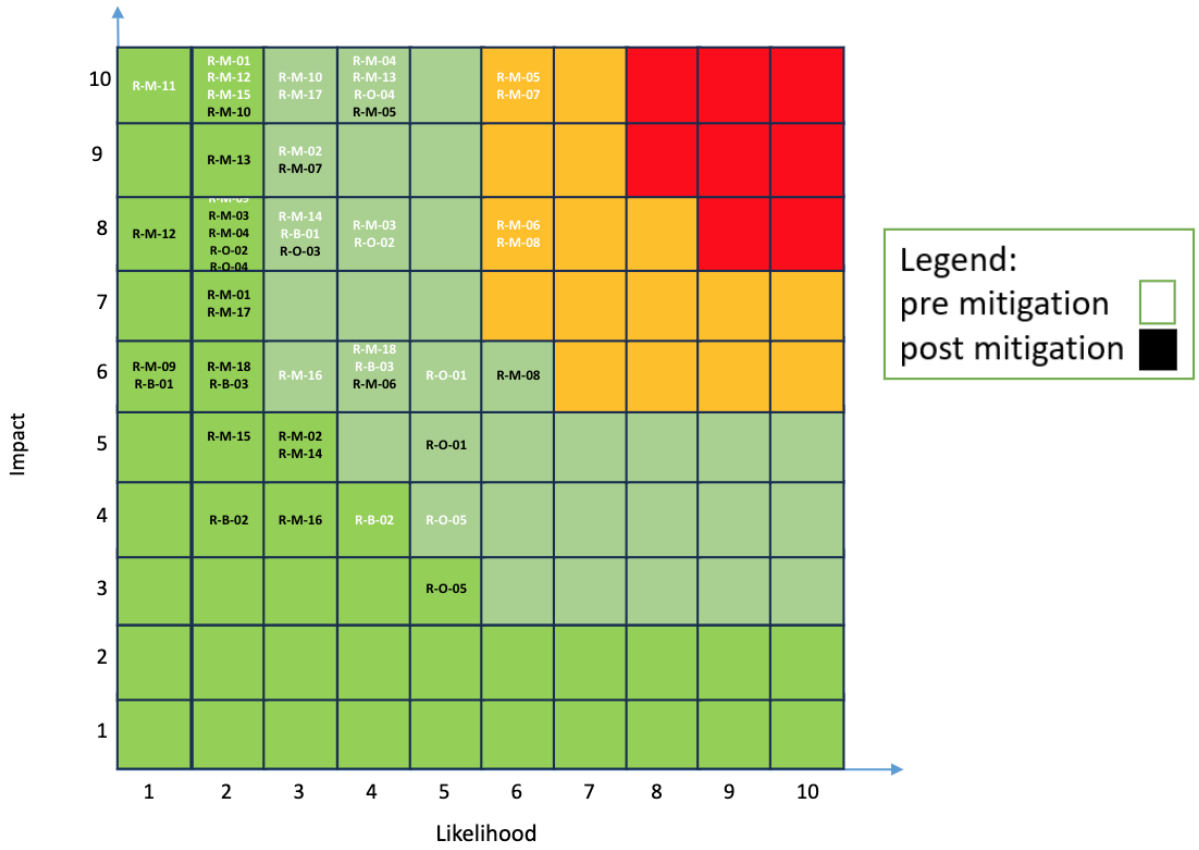

Figure 3.3: Risk map showing likelihood versus the impact of the pre-and post-mitigation cases.

3.2.4. Critical Risks

As evident by the high total risks seen in Table 3.2 and the relative placement in Figure 3.3, the most critical activities to be mitigated are mission risks associated with: 'the use of a novel propulsion system' (R-M-05) and 'the placement of the propulsion system' (R-M-07).

To mitigate the risks associated with (R-M-05), specifically relating to unexpectedly low thrust, mitigation to reduce the likelihood is implemented. Mitigation is in the form of performing in-depth research utilising strong safety factors and extensive testing. This will give a robust idea of how the system shall perform over specific use cases, ensuring the aircraft is capable of flying transatlantic as well as covering other propulsion-related requirements. This pertains to the creation of requirement CH4-STK-14-02 and CH4-OPS-04, which describe the production of the fuel. Moreover, mitigation of (R-M-07) concerning the safety of the passengers is analysed. This is done through verification and validation of the propulsion system to design to a confidence level within the limits of certification and passenger safety. As well as that, the strength of engine cowling will be specifically designed to control and contain any rare blasts. In summary, the propulsion system will have to be tested sufficiently to be certified by authorities, thus inspiring and adding to requirement **CH4-STK-12**.

Furthermore, regarding (R-M-06), this could lead to inefficiencies in thrust, damage in the storage system and damage in the propulsion system. Therefore, mitigation is important, specifically by requiring fuel producers to provide a certification proving the purity of fuel and performing quality control on each fuel batch. This ensures consistent high-quality fuel, which would keep the propulsion system working and reduce maintenance man-hours.

It would be prudent to pay attention to (R-M-08), as it could lead to the aircraft being impractical and uncomfortable to fly from a pilot's perspective. This is not ideal, particularly for long operations and emergencies. To mitigate this, pilots can test simulations depicting the dynamics of the aircraft, and their feedback be implemented. Moreover, an active control system outer loop essentially acts like a suspension, modifying the flight condition over time, easing the pilot's (and passenger's) comfort.

3.3. N2 Interface Diagram

In order to attain a better understanding of the aircraft's systems, the interfaces between them need to be identified. This provides insight into the relations between systems, thus acting as a guideline during subsequent design phases. For that reason an N^2 was created, which shall be the focus of this chapter. The full N^2 diagram can be found in Figure 3.4 located below, with outputs of a system extending to the right, and inputs being vertically on top.

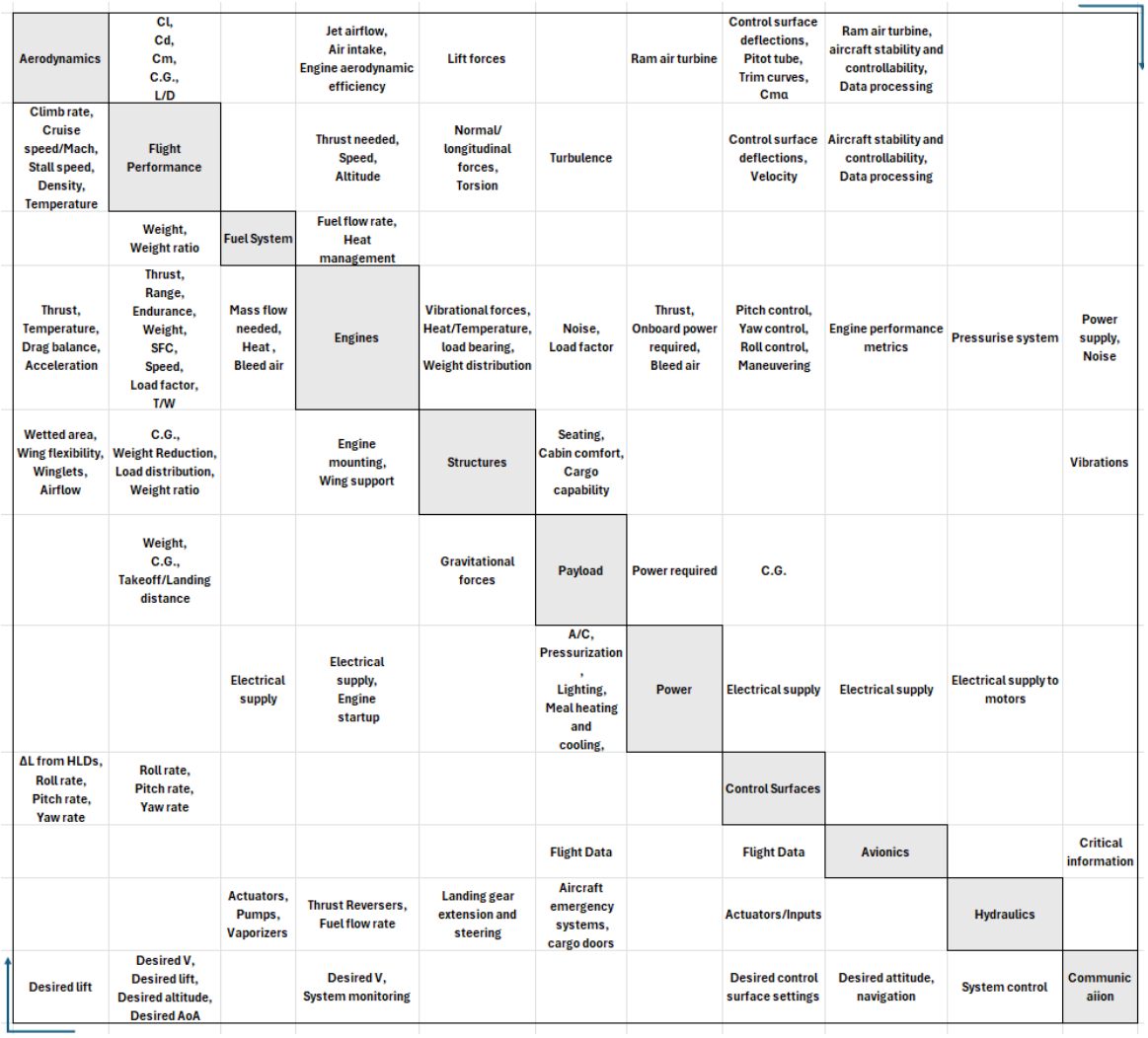

Figure 3.4: The N^2 interface diagram showing the inferences between the aircraft's systems.

As made clear, the different systems feed each other with information. This provides an easy method to iterate and converge to certain sizing, for example, during the Class II weight estimation to iterate to an OEW and accurate system weights. Moreover, the chart gives insight into which variables are critical in the design of the aircraft, such as the C.G. position, which dominates the initial stages of the design.

4. Requirements

Requirements are necessary to fulfil particular wants and needs of stake- and shareholders, but also to address functions and certifications that are imposed on the aircraft design. During the early stages of designing the aircraft, a general design was conceived as shown in chapter 2. These decisions led to a group of subsystems for each of which a new set of requirements had to be made. This chapter presents each of these requirements that the subsystems have to abide by in order for the aircraft to fulfil its system requirements.

Firstly, the market is explored in section 4.1, whereby the climate and growth of the specific methane and aircraft industries are explored. Moreover, in section 4.2, the stakeholders of the project are analysed. These two determine global requirements pertaining to the mission and need statements of the project. In sectionsection 4.3, the requirements originating from the stakeholders are analysed in section 4.4, the requirements arising from the functions of the aircraft are shown. Subsequently, in section 4.5, the requirements for the wing subsystem are presented to ensure the wing generates enough lift while withstanding the accompanying loads. In section 4.6, the requirements pertaining to the fuselage are given, to make sure it can house the required payload and sustain the pressure loads. Next, in section 4.7, the requirements imposed on the landing gear are discussed, and in section 4.8, the empennage requirements are presented. In section 4.9 the propulsion requirements are given, related to the fuel system requirements given in section 4.10. Lastly, ground operations are addressed in section 4.11.

4.1. Aircraft Market Analysis

In order to be able to position the product in the market and enable determining the pricing strategy, a market analysis is first conducted in which the state of the sector, the position of the aircraft product in this sector (market segment and competitor analysis), as well as the potential customers, are analysed. The aircraft sector as a whole is analysed, with a special focus on the growing sustainable aviation market. Firstly, current trends in the sector are laid out and the growth rate is determined. Afterwards, market segmentation is performed and the market share as well as cost projections are identified.

4.1.1. Current Trends

The commercial aviation industry is set to keep growing. By 2050, 10 billion passengers are expected to fly a cumulative 20 trillion kilometres, generating 2350 million tons of CO_2 in total, which is roughly 2.6 times the emissions from 2019. These emissions are set to keep growing, potentially reaching up to 3.6 times the emissions from 2005 and causing 22% of the total global emissions by 2050 if decarbonisation is not achieved[1].

In terms of the aircraft market size, this trend is clearly visible in the numbers. The global aircraft market size was estimated to be 400 B$ in 2022 and is expected to reach about 561.50 B$ by 2030, growing at a Compound Annual Growth Rate (CAGR) of 3.5% between 2023 and 2032[2].

Given the current increasing focus on sustainability policies and regulations enforcing environmental impact reduction, such as the 2050 net zero emissions commitment, the aviation industry is set to shift

[1] `https://www2.deloitte.com/us/en/insights/industry/aerospace-defense/decarbonizing-aerospace`, [Cited on 01-May-2024]

[2] `https://www.precedenceresearch.com/aircraft-market`, [Cited on 02-May-2024]

towards energy-efficient aviation. Thus, a rise in demand for sustainable options is to be expected and market growth predictions agree with this. For example, the Sustainable Aviation Fuel (SAF) market is projected to experience a 47.7 % CAGR due to a growth from 1.1 B$ in 2023 to 16.8 B$ by 2030[3].

4.1.2. SWOT Analysis

Furthermore, a SWOT analysis was performed, analysing several Strengths, Weaknesses, Opportunities and Threats that can be identified for the energy-efficient aircraft market. These are specified in Figure 4.1.

Figure 4.1: SWOT diagram for the energy efficient aircraft business.

In addition to more aviation general elements, such as growth in the tourism industry and increasing standard of living, some more sustainability-focused elements have been added to the SWOT analysis. One environmental impact-related opportunity is the increasing focus on sustainability that can currently be observed, stemming from regulations like the 2050 net zero emissions that are driving the aviation sector's innovations. This also allows aircraft manufacturers to capitalise on being the ones to create the world's first net zero energy efficient transatlantic passenger aircraft, gaining significant advantages over the competition. Furthermore, this focus on sustainability also induces some weaknesses, such as the high dependence on sustainable fuel suppliers and infrastructure, the high development cost of these new technologies and the slow adoption of new technologies.

4.1.3. Market Segmentation

The global sustainable aviation market can be segmented based on fuel type, aircraft type, platform and region. In terms of fuel type, the categories distinguished are biofuel, hydrogen fuel and power-to-liquid (synthetic) fuel. Aircraft types include among others fixed wings and rotorcraft. Moreover, the platform segmentation consists of commercial aviation, military aviation, business, & general aviation as well as unmanned aerial vehicles. When looking at the regions, North America, Europe, Asia-Pacific, Middle East and Latin America can be distinguished. From these, the biggest growth is expected in the sustainable aviation fuel market for the Asia-Pacific and North American market segments, with a CAGR of 53% and 42% respectively from 2023 to 2032. Furthermore, the other segments with the highest projected growth are the fixed-wing and commercial aviation sector [3].

Thus, this project's energy-efficient aircraft belongs to the segment that consists of fixed-winged, commercial long-haul aircraft, corresponding to the methane fuel type segment. Since there currently

[3] `https://www.acumenresearchandconsulting.com/sustainable-aviation-fuel-market`, [Cited on 01-May-2024]

is no product in this segment with net zero emissions, a first-mover advantage can be used to gain a high initial market share in this segment. When demand subsequently increases, the product can be adapted to the other market segments in order to gain market share there as well, by for example enabling other fuels, such as hydrogen, to be used in the CH4llenger. However, this would require substantial modifications to the aircraft.

As of now, the competition in the fixed-winged commercial long-haul aircraft segment consists of well-established EOMs, such as Boeing and Airbus, who are currently developing net zero transatlantic alternatives. One notable sustainable aircraft in the pipeline for example, is Airbus' ZEROe, the world's first hydrogen-powered commercial aircraft[4].

4.1.4. Expected Market Share

Given the competition, it is important to identify the prospective customer group and the expected sales of the aircraft, in order to make an estimate of the expected market share. In the upcoming years, major airlines are expected to make big investments in their fleet in order to keep up with the growth in air traffic and climate regulations.

According to NLR's report on the Route to Net Zero, it is stated that: "by 2050, improvements in aircraft and engine technology and subsequent fleet replacement hold the largest promise for decarbonising European aviation" [5]. Thus, the potential of the CH4llenger arises: providing a transatlantic net-zero aircraft capable of meeting the 2050 European Green Deal and Paris Agreement goals of net-zero carbon emissions.

According to Clean Aviation, 75% of the total 23 513 active aircraft fleet will be renewed by 2050 [6] [7], implying a market gap of 17 635 aircraft. In addition, to keep up with the aviation demand, approximately an additional 24 000 aircraft are expected until 2042 [8]. Combined, this led to 41 700 aircraft being delivered. Assuming transatlantic narrow-body fixed-wing aircraft constitute 10 % of the total aircraft fleet, this would lead to about 4170 aircraft to be replaced[9]. Furthermore, it is projected that a share of 50% of net-zero fuelled single-aisle aircraft will be used to renew the fleet of the major airlines in the base case and 90% in the optimistic case, based on a market study for net-zero aircraft fleet size compared to for example carbon offsets [4]. Assuming the methane fuel will co-exist with hydrogen-powered and aircraft, an expected share of 20% of these is expected to be for the methane plane.

Thus, for the base case, $4170 * 0.5 * 0.2 = 417$ CH4llenger aircraft are expected and for the optimistic case $4170 * 0.9 * 0.2 = 751$ aircraft. For the rest of the cost calculations, the base case of 417 aircraft will be taken as it establishes the bottom line of expected demand.

4.2. Stakeholder Analysis

The key stakeholders include not only the direct project stakeholders, namely the client or tutor in this case, but also the parties the final aircraft will impact. These include private customers, fuel producers,

[4] https://www.airbus.com/en/innovation/low-carbon-aviation/hydrogen/zeroe, [cited 19-June-24]

[5] https://reports.nlr.nl/server/api/core/bitstreams/c9002b7e-224f-420c-b6da-ab6aecd48ea2/content, [Cited on 17-June-2024]

[6] https://www.clean-aviation.eu/media/executive-directors-blog/our-2050-is-now-pioneering-greener-aircraft, [Cited on 17-June-2024]

[7] https://about.ch-aviation.com/blog/2022/06/30/june-2022-global-fleet-size-analysis-by-ch-aviation/, [Cited on 17-June-2024]

[8] https://www.statista.com/statistics/262971/aircraft-fleets-by-region-worldwide/, [Cited on 17-June-2024]

[9] https://www.reuters.com/business/aerospace-defense/demand-transatlantic-flights-soars-americans-cant-get-enough-europe-2023-03-21/, [Cited on 17-June-2024]

airlines, airports, regulators and corporate & cargo providers, as shown in the stakeholder map in Figure 4.2[10].

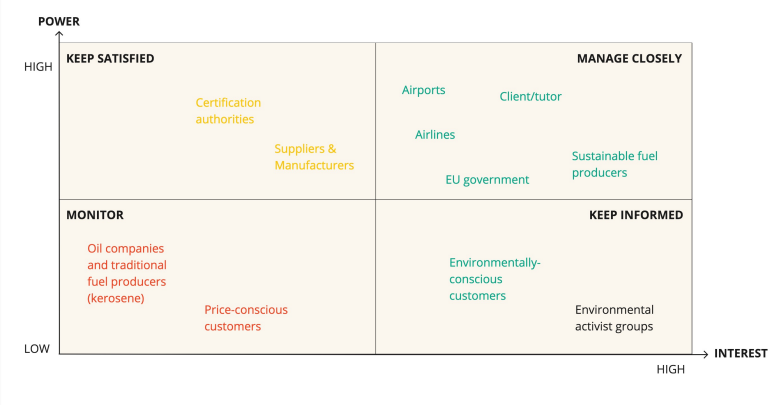

Figure 4.2: Map showing the power and interest of stakeholders.

As can be seen in Figure 4.2, the different stakeholders are organised in terms of their interests and power. A colour scheme is applied to identify the stakeholders with a positive interest or stake (green), a relatively neutral stake; having neither high nor low interest (orange), and lastly a negative one (red). Shown in black are the environmental activist groups, which can have both positive or negative stakes depending on the beliefs of the group; while some may champion making the aviation sector more sustainable, while some might believe it is not enough and continue protesting against aviation altogether.

Resulting from the stakeholder map, it can be concluded that the key stakeholders are the ones in the upper right quadrant, as they have both a high influence on the project (power) as well as the stake (interest). These key stakeholders consist of the client/tutor, sustainable fuel producers, airports, airlines and the government.

4.3. Stakeholder Requirements

Table 4.1 lists all requirements obtained from the client and found through the stakeholder analysis in section 4.2. Some requirements contain sub-requirements, denoted by the same ID number.

Table 4.1: Subsystem requirements from the stakeholders.

ID	Name	Requirement
CH4-MNS	Mission Need Statement	To reduce the environmental impact of aviation by designing a novel aircraft that is capable of transatlantic flights by 2030
CH4-STK-01	Range	The aircraft shall have a range of 3500 nautical miles
CH4-STK-02	Capacity	The aircraft shall be able to accommodate 206 passengers in a 2-class configuration during transatlantic flight
CH4-STK-02-01	Seats	The aircraft shall be able to accommodate 206 passenger seats
CH4-STK-02-02	Food	The aircraft shall be able to carry enough food for 206 passengers during a transatlantic flight
CH4-STK-02-03	Toilets	The aircraft shall have enough toilets to allow 206 passengers to use the toilets during a transatlantic flight
CH4-STK-03	Payload Weight	The aircraft shall have a maximum payload weight of at least 25 tonnes
CH4-STK-04	Runway Length	The aircraft shall be able to operate from a 3000-meter runway at MTOW and 0m ISA
CH4-STK-05	Turn-around Time	The aircraft shall have a turn-around time of at most one hour
CH4-STK-06	Turn-around Procedures	The aircraft shall be able to perform standard turn-around procedures
CH4-STK-06-01	Cargo	The aircraft shall allow for loading and unloading of the cargo
CH4-STK-06-02	Passengers	The aircraft shall allow for loading and unloading of the passengers

Continued on next page

[10] https://www.strategyand.pwc.com/de/en/industries/aerospace-defense/sustainable-aviation-fuel.html, [Cited on 1-May-2024]

Table 4.1– continued from previous page

ID	Name	Requirement
CH4-STK-06-03	Utilities	The aircraft shall allow for servicing the utilities
CH4-STK-06-04	Fuel	The aircraft shall allow for it to be refuelled
CH4-STK-07	Net Zero Emissions	The aircraft shall have net zero CO_2 emissions
CH4-STK-08	Lowest Energy	The aircraft shall fly with the lowest possible required energy
CH4-STK-09	Prototype Ready	A prototype of the aircraft shall be ready by 2030
CH4-STK-10	Costs	The aircraft shall have a maximum unit cost of $120 million
CH4-STK-11	Remote Airports	The aircraft shall be able to operate from remote airports
CH4-STK-12	Regulations	The aircraft shall comply with rules from regulating bodies
CH4-STK-13	Social Sustainability	The aircraft shall help the social sustainability of the aviation industry
CH4-STK-14	Sustainability	The aircraft shall be able to fly on sustainable fuels
CH4-STK-14-01	Fuel Type	The aircraft shall be able to fly on a fuel possible to be sustainably produced
CH4-STK-14-02	Fuel Production	The fuel shall be produced sustainably
CH4-STK-14-03	Fuel Transport	The fuel shall be transported sustainably

4.4. Functional Requirements

Table 4.2 lists all functional requirements. Those were derived from the functional analysis of the aircraft.

Table 4.2: Subsystem requirements derived from the functional flow diagram.

ID	Name	Requirement
CH4-FUN-01	Communication	The aircraft shall allow the pilots to communicate with ATC
CH4-FUN-02	Engine Control	The aircraft's engines shall be controllable
CH4-FUN-02-01	Engine Start	The aircraft's engines shall be able to be started
CH4-FUN-02-02	Engine Throttle	The aircraft's engines shall be able to be throttled
CH4-FUN-03	Ground Control	The aircraft shall be controllable during taxi
CH4-FUN-04	Take-off	The aircraft shall be able to perform take-off
CH4-FUN-05	Climb	The aircraft shall be able to climb away from the airport
CH4-FUN-06	Stowing	The aircraft shall be able to stow its landing gear
CH4-FUN-07	In Air Control	The aircraft shall be controllable in the air
CH4-FUN-07-01	Roll	The aircraft shall have roll control
CH4-FUN-07-02	Yaw	The aircraft shall have yaw control
CH4-FUN-07-03	Pitch	The aircraft shall have pitch control
CH4-FUN-08	Cruise	The aircraft shall be able to enter cruise conditions
CH4-FUN-09	Trim	The aircraft shall be able to be trimmed
CH4-FUN-10	Clearance	The aircraft shall not touch the ground with anything other than the landing gear during operations
CH4-FUN-11	Receiving Fuel	The airports shall be able to receive the fuel for the aircraft
CH4-FUN-12	Storing Fuel	The airports shall have the infrastructure to store the fuel for the aircraft
CH4-FUN-13	Refuelling	The airports shall have the infrastructure to refuel the aircraft

4.5. Wing

Table 4.3 lists all subsystem requirements for the wing. They ensure that the wing remains functional even in extreme conditions.

Table 4.3: Subsystem requirements for the wing.

ID	Name	Requirement
CH4-WING-01	Lift Cruise	The wing shall be able to generate enough lift to support the aircraft during cruise
CH4-WING-01-01	C_L Cruise	The wing shall be able to generate a maximum lift coefficient of at least 1.5 in cruise configuration
CH4-WING-02	Lift Take-off	The wing shall be able to generate enough lift to support the aircraft in taking off from a 3000 m runway
CH4-WING-02-01	C_L Take-off	The wing shall be able to generate a maximum lift coefficient of at least 2.6 in take-off configuration
CH4-WING-02-01-01	C_L Increase 1	The wing's high lift devices shall increase the C_L at least by 0.5
CH4-WING-03	Lift Landing	The wing shall be able to generate enough lift to support the aircraft during landing
CH4-WING-03-01	C_L Landing	The wing should be able to generate a maximum lift coefficient of at least 2.5 in Landing configuration
CH4-WING-03-01-01	C_L Increase 2	The wing's high lift devices will increase the C_L at least by 0.5
CH4-WING-04	Structural	The wing shall withstand the loads it is subjected to during operations
CH4-WING-04-01	Deflection	The wing shall not deflect more than 15% of its length during normal operations
CH4-WING-04-02	Twist	The wing shall not twist more than 10% during normal operations
CH4-WING-05	Engines	The wing shall have space to attach the engines

Continued on next page

Table 4.3– continued from previous page

ID	Name	Requirement
CH4-WING-06	Tanks	The wing shall have space to attach the fuel tanks
CH4-WING-07	Landing Gear	The wing shall have space to store the landing gear
CH4-WING-08	Drag Divergence	The wing shall not have drag divergence at cruise mach number
CH4-WING-09	Controllability	The wing shall allow for the installation of the ailerons
CH4-WING-09-01	Roll Rate	The ailerons shall ensure a roll rate of 32 degrees per second

4.6. Fuselage

Table 4.4 lists all subsystem requirements for the fuselage. Those pertain to all subsystems accommodated in the fuselage structure.

Table 4.4: Subsystem requirements for the fuselage.

ID	Name	Requirement
CH4-FUS-01	Flight deck	The fuselage shall accommodate a space separated from the cabin from which the pilots can pilot the aircraft
CH4-FUS-01-01	Pilot Seating	The flight deck shall have seating to accommodate 2 pilots
CH4-FUS-01-02	Instrumentation	The flight deck shall have all instruments needed to control the aircraft
CH4-FUS-01-03	Communication	The flight deck shall have a radio to facilitate communication with ATC
CH4-FUS-01-04	View Angle	The flight deck windows shall allow for an over-the-nose angle of at least 11 degrees
CH4-FUS-01-05	Access	The flight deck door shall ensure access only to authorised personnel
CH4-FUS-02	Capacity	The fuselage shall be able to accommodate 206 passengers in a 2-class configuration during transatlantic flight
CH4-FUS-02-01	Seats	The fuselage shall be able to accommodate 206 passenger seats
CH4-STK-02-02	Food	The fuselage shall be able to prepare enough food for 206 passengers during a transatlantic flight
CH4-STK-02-03	Toilets	The fuselage shall have enough toilets to allow 206 passengers to use the toilets during a transatlantic flight
CH4-FUS-03	Loading/ Unloading	The fuselage shall allow for passengers to be loaded and unloaded in reasonable time
CH4-FUS-03-01	Loading Doors	The fuselage shall have enough access doors to load passengers in at most 17.2 minutes
CH4-FUS-03-02	Unloading Doors	The fuselage shall have enough access doors to unload passengers in at most 10.3 minutes
CH4-FUS-03-03	Loading Aisles	The fuselage shall have enough aisle space to load passengers in at most 17.2 minutes
CH4-FUS-03-04	Unloading Aisles	The fuselage shall have enough aisle space to unload passengers in at most 10.3 minutes
CH4-FUS-04	Overhead Lockers	The fuselage shall allow for passenger carry-on luggage to be stored in overhead lockers
CH4-FUS-05	Cargo	The fuselage shall be able to store all passenger check-in luggage in the cargo hold
CH4-FUS-06	Emergency Exits	The fuselage shall have enough emergency exits to comply with CS-25.807
CH4-FUS-06-01	Emergency Doors	The fuselage shall have 2 type I doors and 3 type II doors on either side
CH4-FUS-06-02	Accessibility	The emergency doors shall be easily accessible
CH4-FUS-07	Cargo Doors	The fuselage shall allow the cargo bay to be loaded and unloaded in reasonable time
CH4-FUS-07-01	Cargo Loading	The fuselage shall have enough cargo doors to allow the cargo to be loaded in at most 10 minutes
CH4-FUS-07-02	Cargo Unloading	The fuselage shall have enough cargo doors to allow the cargo to be unloaded in at most 10 minutes
CH4-FUS-08	Nose Gear	The fuselage shall allow the nose landing gear to be stored
CH4-FUS-09	Strike	The fuselage shall not strike the runway on take-off or landing
CH4-FUS-10	Pressurisation	The fuselage shall be able to be pressurised to 0.75 bar
CH4-FUS-11	Structure	The fuselage shall be able to withstand loads experienced during operations
CH-FUS-11-01	Pressure Loads	The fuselage shall be able to withstand repeated pressurisation
CH-FUS-11-02	Wing Loads	The fuselage shall be able to withstand the loads from the wing during normal operations
CH-FUS-12	APU	The fuselage shall have space to house the APU

4.7. Landing Gear

Table 4.5 lists all subsystem requirements for the landing gear. Those ensure that the landing gear can function as intended and support other subsystems.

Table 4.5: Subsystem requirements for the landing gear.

ID	Name	Requirement
CH4-LAND-01	Retraction	The landing gear shall be able to retract
CH4-LAND-02	Support	The landing gear shall be able to support the weight of the aircraft on the ramp
CH4-LAND-03	Damage	The landing gear shall not damage the pavement of the airfield on landing
CH4-LAND-04	Tip-over	The landing dear position shall ensure the aircraft does not tip over
CH4-LAND-04-01	Longitudinal Tip-over	The landing gear position shall ensure a tip-over angle of 16 degrees
CH4-LAND-04-02	Lateral Tip-over	The landing gear position shall ensure a lateral tip-over angle of 55 degrees
CH4-LAND-05	Scrape Angle	The landing gear shall ensure the aircraft has a scrape angle of at least 14 degrees
CH4-LAND-06	Landing	The landing gear shall support the aircraft during landing
CH4-LAND-07	Steering	The landing gear shall allow for the aircraft to be steered on the ground
CH4-LAND-07-01	Steering Weight	The nose landing gear shall carry at least 8% of the aircraft weight
CH4-LAND-08	Rotation	The landing gear position shall allow for easy rotation of the aircraft
CH4-LAND-08-01	Rotation Weight	The nose landing gear shall carry at most 15% of the aircraft weight
CH4-LAND-09	Engine strike	The landing gear shall ensure that the engine doesn't strike at a 5° bank angle
CH4-LAND-10	Tank strike	The landing gear shall ensure that the tank doesn't strike at a 5 ° bank angle
CH4-LAND-11	Wing strike	The landing gear shall ensure that the wing tip doesn't strike at a 5 ° bank angle

4.8. Empennage

Table 4.6 lists all subsystem requirements for the empennage. Those primarily concern the stability of the aircraft.

Table 4.6: Subsystem requirements for the empennage.

ID	Name	Requirement
CH4-EMP-01	stability	The empennage shall ensure static stability for the aircraft
CH4-EMP-01-01	Longitudinal Stability	The horizontal stabiliser shall ensure that the aircraft is statically stable longitudinally
CH4-EMP-01-02	Lateral Stability	The vertical stabiliser shall ensure that the aircraft is statically stable laterally
CH4-EMP-02	Lateral Control	The vertical stabiliser shall house a rudder to provide the aircraft with yawing capability
CH4-EMP-03	Longitudinal Control	The horizontal stabiliser shall house an elevator to provide the aircraft with pitching capability
CH4-EMP-04	Trim	The horizontal stabiliser shall allow for the aircraft to be trimmed
CH4-EMP-05	Structure	The empennage shall be able to withstand the loads it is subjected to during normal operations

4.9. Propulsion

Table 4.7 lists all subsystem requirements for the propulsion system. Those primarily ensure that the aircraft can generate sufficient thrust in various conditions.

Table 4.7: Subsystem requirements for the propulsion.

ID	Name	Requirement
CH4-PROP-01	Start	The engine shall be able to be started
CH4-PROP-02	Throttle	The engine shall be able to be throttled up and down
CH4-PROP-03	Thrust	The engines shall provide enough thrust to propel the aircraft in normal operations
CH-PROP-03-01	Thrust Force	A single-engine shall provide at least 23.87 kN of thrust
CH4-PROP-04	Cruise Fuel Mass Flow	The engines shall be able to accommodate sufficient amounts of fuel during cruise
CH4-PROP-05	Take-Off Fuel Mass Flow	The engines shall be able to accommodate sufficient amounts of fuel during take-off
CH4-PROP-06	Idle	The engines shall be able to run an idle mode

4.10. Fuel System

Table 4.8 lists all subsystem requirements for the fuel system. Those are largely related to the propulsion system requirements.

Table 4.8: Subsystem requirements for the fuel system.

ID	Name	Requirement
CH4-FSYS-01	Range	The fuel system shall provide the aircraft with enough fuel to fly 3500 Nm
CH4-FSYS-01-01	Volume	The fuel tanks shall be able to hold enough fuel to fly 3500 Nm

Continued on next page

Table 4.8– continued from previous page

ID	Name	Requirement
CH4-FSYS-01-02	Fuel Provided	The fuel system shall be able to provide the engines with continuous fuel for 3500 Nm
CH4-FSYS-02	Throttle	The fuel system shall provide the engines with enough fuel to be able to throttle up
CH4-FSYS-03	Strikes	The fuel tanks shall be able to withstand bird strikes
CH4-FSYS-04	Over-pressure	The fuel system shall be able to vent methane in case of over-pressure
CH4-FSYS-05	LOX	The fuel system shall prevent the forming of liquid oxygen on the outside
CH4-FSYS-06	Tank Loss	The fuel system shall ensure both engines are operable in case of losing one tank
CH4-FSYS-07	Landing weight	The fuel system shall be able to dump fuel in case of overweight landing
CH4-FSYS-01-03	Fuel Mass Flow	The fuel system shall be able to gasify sufficient amounts of fuel continuously during operations
CH4-FSYS-08	Gas Tank	The gas tank shall maintain a higher pressure than the combustion chamber
CH4-FSYS-09	APU	The APU shall provide enough energy to power all associated systems

4.11. Operations

Table 4.9 lists all requirements for the ground operations of the aircraft. Those are largely dictated by the fuel.

Table 4.9: Subsystem requirements for the operations.

ID	Name	Requirement
CH4-OPS-01	Receiving Fuel	The airports shall be able to receive the fuel for the aircraft
CH4-OPS-02	Storing Fuel	The airports shall have the infrastructure to store the fuel for the aircraft
CH4-OPS-03	Refuelling	The airports shall have the infrastructure to refuel the aircraft
CH4-OPS-04	Production	The fuel shall be produced sustainably
CH4-OPS-05	Transport	The fuel shall be transported sustainably
CH4-OPS-06	Refuelling Time	The airport infrastructure shall allow the aircraft to be refuelled in 50 min
CH4-OPS-07	Routes	Flight routes shall be connected with other airports capable of using methane
CH4-OPS-08	Energy	The airports shall be able to generate electricity and be heated from the fuel

5. Preliminary System Design

After having selected the CH4-04-A design configuration presented in the Midterm report [1], also known as the CH4llenger, its initial design had to be created. Doing so allows for a preliminary starting point before the subsequent iterations and improvements of the aircraft can take place. For that purpose, a Class I C.G. estimation was first performed with the aim of preliminarily locating the most forward and the most aft centre of gravity as described in section 5.1. Afterwards, as explained in section 5.2, the process of sizing the wing took place, which included the selection of the airfoil for the aircraft, the initial design of the wing planform as well as the design of high-lift devices and integration of the fuel tank into the wing group. Following that, section 5.4 and section 5.5 present a preliminary design of the fuselage and landing gear, respectively. This is, in turn, followed by an initial sizing of the empennage, as presented in section 5.6.

5.1. Class I C.G. Estimation

For the initial sizing of the landing gear and the empennage, a first estimation of the centre of gravity has to be made. For the estimation, methods from the Aerospace Design & Systems Engineering Elements (ADSEE) course were used alongside data from Roskam [5, 6]. First, the Operational Empty Weight (OEW) of 54 815 kg, fuel weight of 23 529 kg and payload weight of 25 000 kg were used, stemming from the Class I weight estimation [1]. The weights of individual parts were estimated using statistical data from Roskam. Initial estimations for the weight of the tanks were used. These weights were combined with estimations for their individual centre of gravity locations, leading to an estimation for the OEW centre of gravity. Combined with the payload and the fuel this leads to the centre of gravity excursion depicted in Table 5.1.

Table 5.1: Class I estimation of the centre of gravity for different load cases.

Load case	Centre of gravity distance from nose [m]
OEW	20.13
OEW+payload	19.98
OEW + Fuel	20.62
All	20.38

5.2. Wing Sizing

The wing subsystem sizing is heavily dependent on the airfoil aerodynamic characteristics. This section begins with an airfoil analysis, where different 3D wing models are assembled and tested in XFLR5 [1]. Subsequently, a choice is made and the wing geometry is further iterated. Once the planform geometry is known, the control surfaces and high-lift devices are sized and integrated.

5.2.1. Airfoil Selection

The initial aerodynamic analysis was concluded by selecting the NACA 23015 airfoil as a basis for the initial wing design [1]. It was chosen due to being similar to the customised airfoil used in the Airbus A320 family [7]. However, unlike the A320 family and other conventional aircraft, regular fuel tanks are not present inside the wing of the methane aircraft. This creates an opportunity to potentially use a thinner or more cambered airfoil since large fuel tanks do not need to be accommodated inside.

[1] `https://www.xflr5.tech/xflr5.htm`, [Cited on 31-May-2024]

In order to compare the airfoils to one another, the XFLR5 program, which allows the user to generate the NACA series airfoils and perform an aerodynamic analysis was used. Varying the thickness-to-chord ratio of the NACA 23015 using XFLR5 resulted in promising improvements in terms of the aerodynamic performance of NACA 23010, i.e. 10 % thickness-to-chord ratio. As a result, the airfoil was also selected as a potential candidate for further analysis. On the other hand, the aircraft is to be operating on the verge of the transonic regime. Consequently, a supercritical airfoil is also a favourable option. After an initial analysis, the SC(2)-0010[2] profile has been recognised, as it performed especially well in terms of drag. That created a shortlist of three potential airfoils, which have been selected for further analysis.

Having identified three promising candidates, a 3D wing model was created in XFLR5. The initial performance analysis and sizing yielded the wing area and wing span of 160.26 m^2 and 39.02 m respectively [1]. The initial estimate of the taper ratio of 0.4 was used. However, the sweep angle, which depends on the technology factor of the airfoil, varies between the options. The technology factor for supercritical airfoils is generally higher than for the NACA series and was assumed to be 0.935 [8]. For the NACA 23015 and NACA 23010 airfoils, however, it was taken to be 0.87 [9]. This results in a 30.03 ° quarter-chord sweep angle for the supercritical airfoil and 36.34 ° for the remaining two. A first estimate for the dihedral angle is 3 °, based on the general guidelines [8]. Lastly, blended winglets were also added to improve the performance by reducing the effects of wingtip vortices[3]. Based on statistics of similar sized airliners[4], the length of the winglet can be modelled as a linear function:

$$l_{winglet} \approx 0.013b + 1.15, \tag{5.1}$$

with a wingspan b of 39.02 m, the length of the winglet is 1.66 m. For the chord sizing, the tip chord of the winglet to the tip chord of the wing is 0.30[5]. With a wing tip chord of 1.87 m, a winglet tip chord length of 0.56 m was calculated. Finally, a winglet angle of 70° was decided upon while the sweep of the trailing edge of the winglet was determined to be equal to the sweep of the trailing edge of the wing.

Subsequently, the aerodynamic characteristics of the three wings were plotted and evaluated. To facilitate the analysis, the Reynolds number had to be calculated by means of Equation 5.2:

$$Re = \frac{\rho V \bar{c}}{\mu}, \tag{5.2}$$

where μ is the dynamic viscosity of air, taken as 1.42×10^{-5} Pas [6]. Moreover, the mean aerodynamic chord (MAC) was substituted for $\bar{c}$, at that stage assumed to be equal to the mean geometric chord:

$$\bar{c} = \frac{2}{3} c_r \frac{1+\lambda+\lambda^2}{1+\lambda}, \tag{5.3}$$

where λ is the taper ratio and c_r is the root chord, as calculated in the initial performance analysis [1]. This gives an MGC≈MAC equal to 4.51 m. Finally, with a cruise speed of 230 $ms^{-}1$ and altitude of 38 000 ft [1], this yields a Reynolds number of $2.425 \cdot 10^7$.

Subsequently, the wing twist had to be selected. Given that it is generally desired for the wing root to stall first, it is to exhibit the most positive twist compared to the rest of the wing. This will result in the root reaching its stall angle first, in which case the outer portion of the wing would be allowed to be

[2] http://airfoiltools.com/airfoil/details?airfoil=sc20010-il, [Cited on 31-May-2024]

[3] https://www1.grc.nasa.gov/beginners-guide-to-aeronautics/winglets/, [Cited on 31-May-2024]

[4] https://www.fzt.haw-hamburg.de/pers/Scholz/arbeiten/DataMorichon.xls, [Cited on 31-May-2024]

[5] https://cms.education.gov.il/NR/rdonlyres/D9F6FC7B-A508-43C8-BB34-5C6D8AE0346D/178686/Understanding_Winglets_Technology.pdf, [Cited on 3-June-2024]

[6] https://www.engineeringtoolbox.com/air-absolute-kinematic-viscosity-d_601.html, [Cited on 4-June-2024]

used for recovery from the stall condition, thanks to the control surfaces placed there [7]. Based on that, a range of twist of 6.5 ° has preliminarily been chosen, resulting in the twist of the wing being 4.5 ° at the root and −2.0 ° at the wing tip. Finally, a linear relation between the twist angle and the lateral position of the wing has been assumed so as to streamline the future production of the structure.

The results of the analysis are visualised in Figure 5.1 and compared in Table 5.2. The metrics used to compare the performance are drag coefficient, maximum lift coefficient, lift-to-drag ratio, moment coefficient, as well as the required sweep angle. The performance metrics were evaluated quantitatively, with deviations from the initial NACA 23015 wing expressed as percentages to highlight the differences in performance across the analysed parameters.

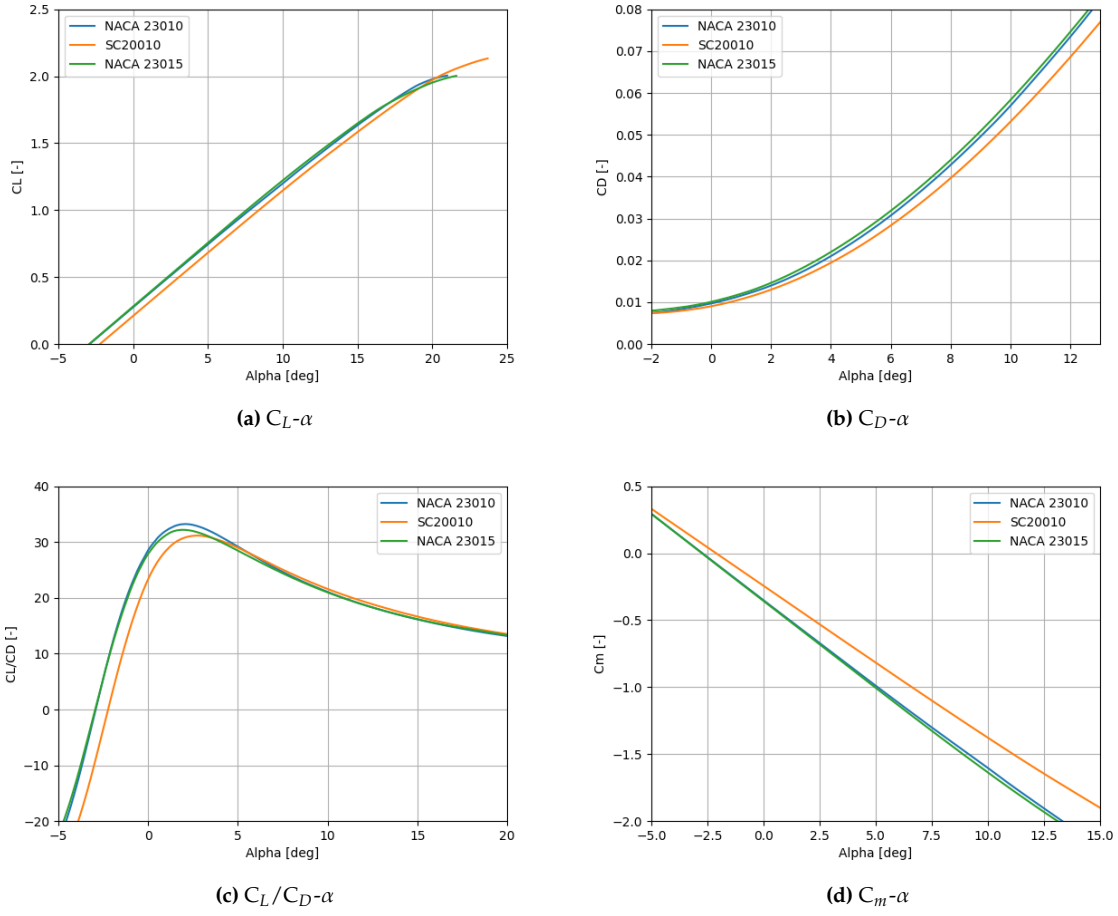

(a) C_L-α **(b)** C_D-α

(c) C_L/C_D-α **(d)** C_m-α

Figure 5.1: Aerodynamic characteristics of the 3D wings with different airfoils obtained from an XFLR5 analysis.

As can be seen in Figure 5.1a, the $C_L - \alpha$ wing behaviour of the three options is quite similar. The SC(2)-0010 has a lower lift at zero angle of attack due to symmetry, but it is non-zero because of the applied twist. However, it offers the highest stall angle and $C_{L,max}$, which would likely allow for reducing the size of the wing the most, due to its effects on the wing loading diagram. A smaller wing would be greatly beneficial, as currently, the wingspan is almost 4 m larger than that of the reference A321neo.

Importantly, the drag of the SC(2)-0010 wing is the lowest, as shown in Figure 5.1b. However, its L/D is inferior to the NACA 23015 and 23010 for angles of attack lower than 5 °, i.e. in cruise (see: Figure 5.1c). On the other hand, it is superior for higher angles of attack.

[7] `https://simpleflying.com/aircraft-wing-twist/`, [Cited on 17-June-2024]

The pitching moment coefficient is plotted in Figure 5.1d. The $C_m - \alpha$ slope is the least negative for the SC(2)-0010 airfoil. Most importantly, all configurations show a negative slope, which is stabilising.

Notably, the required sweep is quite high for all configurations, as can be seen in Table 5.2. This can be attributed to the inaccuracies in the initial estimation, but it is already clear that the supercritical airfoil allows for a lower sweep. While beneficial in delaying the onset of shockwaves [8], swept wings are more susceptible to higher torsional loads as well as twist bend-coupling, resulting in a structure that would likely have to be additionally reinforced and thus heavier [10].

Table 5.2: Comparison of the wing designs based on the airfoil options.

Parameter	NACA 23015	NACA 23010	SC(2)-0010
$\Lambda_{0.25c}$	36.34 °	36.34 °	30.03 °
C_D	Benchmark	4% lower	10% lower
$C_{L,max}$	C_L max 2.0, stall angle 21°	Same C_L max as the 23015, stall occurs 1° earlier	Higher C_L max, 2.1, bigger stall angle (24°)
C_L/C_D	Lowest	Highest before alpha = 5°	Highest after alpha = 5°
C_m	Benchmark	2% smaller	16% smaller

Considering Table 5.2, the NACA 23015 can be discarded, as it does not offer any major benefits, except slightly thicker wing does offer more structural benefits, requiring fewer reinforcements. The supercritical SC(2)-0010 and the NACA 23010 are both viable options that offer different advantages, therefore it was decided to iterate both designs further, allowing for a holistic overview of the entire wing planform, before making a final choice.

5.2.2. Planform Design

The planform geometry was reevaluated for both wing options selected in subsection 5.2.1. The new maximum lift coefficient of a clean configuration; $C_{L,max}$, has increased from 1.7 to 2.1 for the SC(2)-0010 and to 2.0 for the NACA 23010 [1]. While the C_L at landing cannot be calculated at this stage due to the high-lift devices not having been designed yet, it is approximated to be 2.7 and 2.6 respectively [8] for the two wings. $C_{L,max}$ affects the aircraft's wing loading, which corresponds to a new thrust-to-weight ratio, which are obtained from the $W/S - T/W$ diagram created earlier [1]. This has an effect on the required wing surface area S and the wingspan b. The updated parameters were calculated as before [1], and are tabulated in Table 5.3.

Table 5.3: Comparison of the wing design using the two airfoils; SC(2)-0010 and NACA 23010.

Parameter	Unit	SC(2)-0010	NACA 23010
$C_{L,max_{clean}}$	[-]	2.1	2.0
$C_{L,land}$	[-]	2.7	2.6
W/S	[Nm^{-2}]	7443.09	7167.42
S	[m^2]	136.30	141.54
b	[m]	35.98	36.67

The SC(2)-0010 design allows for a smaller wing, notably placing the aircraft in the C category (<36.00 m)[8]. It also offers a larger C_L both for clean and landing configurations. It was also found earlier that the sweep can be decreased due to its supercritical properties. Therefore, the wing design proceeds with the SC(2)-0010 airfoil. First, the planform geometry is iterated for the smaller wing.

The quarter-chord sweep angle follows from the cruise condition; the drag-divergence Mach number, and the technology factor of the airfoil. The cruise Mach number is taken to be 0.78, as this corresponds

[8] `https://www.icao.int/safety/fsix/Library/Manual%20Aerodrome%20Stds.pdf`, [Cited on 3-June-2024]

to the cruise speed of the A321neo, which the CFM LEAP-1A engine is optimised for. The wing is designed such that the following relation holds [8]:

$$M_{dd} = M_{cruise} + 0.03, \tag{5.4}$$

The drag-divergence Mach number is also related to the sweep angle [11]:

$$M_{dd} = \frac{k_a - t/c}{\cos \Lambda_{0.25c}} - \frac{C_L}{10\left(\cos \Lambda_{0.25c}\right)^3} \tag{5.5}$$

where k_a is the technology factor, 0.95 in the case of supercritical airfoils and 0.87 in the case of NACA ones [12]. Setting M_{dd} to 0.81 according to Equation 5.4 allows for optimising the sweep angle. Solving Equation 5.5 for $M_{dd} = 0.81$ yields a quarter-chord sweep of $\Lambda_{0.25c} = 23.62°$, much improved with respect to the initial estimation and in the same range as the A321[9].

A new sweep angle results in a new taper ratio, related as:

$$\lambda = 0.2\left(2 - \Lambda_{0.25c}\frac{\pi}{180}\right), \tag{5.6}$$

which gives 0.318. The root chord can be obtained from the following relation:

$$c_r = \frac{2S}{(1+\lambda)\,b}, \tag{5.7}$$

which is now 5.75 m, and the tip chord, following from the taper ratio, is 1.83 m. The dihedral angle can be decreased to 2 °, based on the general guidelines [8].

The updated geometry is summarised in Table 5.4, while the design cruise parameters can be found in Table 5.5. As mentioned before, the cruise parameters largely follow from the characteristics of the A321neo, since the CFM LEAP-1A engine was tailored to optimise its fuel efficiency[10].

Table 5.4: Initial sizing for the wing geometry.

Parameter	Value	Unit
Quarter-chord sweep angle	23.62	[°]
Taper ratio	0.318	[-]
Root chord	5.75	[m]
Tip chord	1.83	[m]
Dihedral angle	+2.0	[°]
Twist angle at the root	+4.5	[°]
Twist angle at the tip	-2.0	[°]

Table 5.5: Design cruise condition parameters.

Parameter	Value	Unit
Altitude	38 000	[ft]
Mach number	0.78	[-]
Airspeed	230.15	[ms^{-1}]
Drag-divergence Mach number	0.81	[-]
Reynolds number	$2.525{\cdot}10^7$	[-]

5.2.3. High Lift Devices and Control Surfaces

Having completed a preliminary wing platform sizing, an initial design of the high-lift devices (HLDs), as well as the control surfaces, may follow. Before that occurs, however, the spar locations have to be determined, which in the case of CH4-04-A have preliminarily been chosen to be at 20% of the local chord for the front spar and 75% for the aft spar [6].

Ailerons

For aileron sizing, it has been determined that they are to be placed towards the outermost edge of the wing, ending at 0.25 m from the wing tip. They are to also occupy the last 25% of the local chord length, starting just behind the aft spar. Using data for Class II aircraft, which necessitate a roll performance of 45 ° in 1.4 s, the aileron control ($C_{l_{\delta a}}$) and roll damping (C_{l_p}) derivatives are calculated by means of Equation 5.8 and Equation 5.9 respectively.

[9] https://booksite.elsevier.com/9780340741528/appendices/data-a/table-1/table.htm, [Cited on 17-June-2024]

[10] https://web.archive.org/web/20160403132507/http://www.airbus.com/aircraftfamilies/passengeraircraft/a320family/technology-and-innovation/, [Cited on 17-June-2024]

$$C_{l\delta a} = \frac{2c_{l\alpha}\tau}{S_{\text{ref}}b}\int_{b_1}^{b_2} c(y)y\,dy \qquad (5.8) \qquad C_{l_P} = -\frac{4(c_{l\alpha}+c_{d_0})}{S_{\text{ref}}b^2}\int_0^{\frac{b}{2}} y^2c(y)\,dy \qquad (5.9)$$

where τ is the aileron effectiveness, $c(y)$ the local chord length and y the lateral coordinate. The resultant values of the derivatives are subsequently used to calculate the aircraft roll rate given a maximum aileron deflection (P), chosen to be 25 °, through Equation 5.10.

$$P = -\frac{C_{l_{\delta a}}}{C_{l_P}}\delta a\left(\frac{2V}{b}\right) \qquad (5.10)$$

where δa is the aileron deflection. Finally, the resultant roll rate has to be equivalent to the Class II roll performance as specified earlier, for which the aileron geometry is continuously updated. The process results in an initial aileron span of 2.07 m, corresponding to an initial area of 1.08 m^2, with the initial values presented in Table 5.6. Those values are to be iterated upon, however, as shall be described in section 8.1.

Table 5.6: Initial sizing of the aileron.

Variable	Value	Unit
Front spar	20	% MAC
Rear spar	75	% MAC
Aileron_end	17.74	[m]
Aileron_start	15.67	[m]
Aileron_chord	15	[% local chord]
Aileron_deflection	25	[deg]
Aileron_span	2.07	[m]
Aileron_area	1.08	[m^2]

Flaps

After a comparison between slotted and Fowler flap types, a Fowler flap was chosen due to its increased efficiency despite its more complex system. Specifically, the double-slotted Fowler flaps provide more lift compared to the single-slotted ones. Although it was briefly considered to utilise the triple-slotted Fowler flaps, which provide even more lift than the double-slotted ones, its mechanism would require more space sacrificing flap area. For this wing size, the benefits are negligible, as such configuration is more optimal for larger wings which fit the system more easily. As for their placement, just like in the case of the A321neo, they start at the wing-fuselage connection and continuously extend outwards until 0.1 m away from the beginning of the ailerons. Furthermore, the flaps are also interrupted by the fuel tank placed underneath the wing. This, in turn, results in a 2.13 m gap in between the flaps between 7.43 m and 9.56 m of the lateral span. Although this will affect the local lift generation upon take-off and landing, it will not have an overall effect on the aircraft performance due to a greater area covered by the flaps.

The flaps do not cover the entire wing chord, however, occupying the last 15% of the chord, instead. This is due to the aft spar being located at 75% of the chord, preventing the location of the spars further forward. On top of that, 10% of the chord length has been left to accommodate the control system elements [13]. This results in the flaps having a total initial surface area of 6.33 m^2 and a reference area of 38.73 m^2, for each half-wing, respectively, as presented in Table 5.7. Those values, just like in the case of the ailerons, are subject to changes as caused by the iterative process. Furthermore, the flaps have been designed for a deflection of 20° on take-off and 50° upon landing [13], resulting in the extension of the local chord by 9% at take-off and 13% at landing. Based on that, it has been concluded that the double-slotted Fowler flaps will result in an increase in $C_{L_{max}}$, 0.83 upon take-off and 0.86 upon landing.

Table 5.7: Initial sizing of the flaps.

Variable	Value	Unit
Flaps_deflection, TO	20	[deg]
Flaps_deflection, land	50	[deg]
Flaps_end	15.57	[m]
Flaps_area	6.33	[m^2]
Flaps_reference_area	38.73	[m^2]
Flaps_chord	15	[% local chord]

Slats

Subsequently, for the leading edge HLDs, slats have been determined to be suitable for the CH4-04-A aircraft. As with the flaps, the slats also start at the fuselage and are interrupted by the fuel tank. On top of that the slats are interrupted by the engine pylon for which the gap was estimated to be 0.5 m on either side of the engine centre-line. Furthermore, the slats end at 0.5 m from the wingtip and do not extend in the winglet. The slats extend the chord by 12 % [14]. From this, a $C_{l,max}$ of 0.448 was obtained. With this, a reference wing area of 43.6 m^2 and the $\Lambda_{hingeline}$ of 26.18 °, a $\Delta C_{L,max}$ of 0.23 was obtained using Equation 5.12. This is equal for both take-off and landing as the slats extend with the same length in these configurations.

$$S_{ref} = \int_{b1}^{b2} C_r + \frac{C_t - C_r}{0.5 \cdot b} y dy \qquad (5.11) \qquad \Delta C_{L,max} = 0.9 \Delta C_{l,max} \frac{S_{ref}}{S} cos(\Lambda_{hingeline}) \qquad (5.12)$$

Table 5.8: Initial sizing of the slats.

Variable	Value	Unit
Slats_reference_area	43.6	[m^2]
Slats_end	14.362	[m]
$\Delta C_{L,max,TO}$	1.06	[-]
$\Delta C_{L,max,landing}$	1.094	[-]

Based on the above formulas the total $\Delta C_{L,max}$ of the flaps and slats has been calculated. For the take-off condition, both types of HLDs provide a combined $\Delta C_{L,max}$ of 1.06 for take-off and 1.094 for the landing condition, as summarised in Table 5.8.

5.3. Preliminary Engine and Methane Tank Integration

While no conventional tanks are placed in the wing, the detachable fuel tank concept incorporates two external liquid methane tanks mounted underneath the wing. As estimated before, the liquid methane volume that has to be accommodated in one of the two tanks equals 30.69 m^3 [1]. The maximum external diameter of the CFM LEAP-1A engine nacelle is taken to be 2.7 m[11], mounted at the horizontal distance of 5.75 m from the fuselage centreline on the A321neo, which is to be kept the same for CH4llenger [15]. Although placing the engines further inboard was considered, doing so would significantly hinder the landing gear placement. A simplified representation of the current wing half-span, dihedral, and engine are shown in Figure 5.2 in black. It should be noted that, due to a lack of information at this stage, the tank pylon is neglected, and merely the overall maximum diameter is included. The coordinate system used is centred at the wing root, with a $y-$axis extending spanwise, and a $z-$axis positive up.

[11] `https://www.safran-group.com/products-services/airbus-a320neo-nacelles`, [Cited on 5-June-2024]

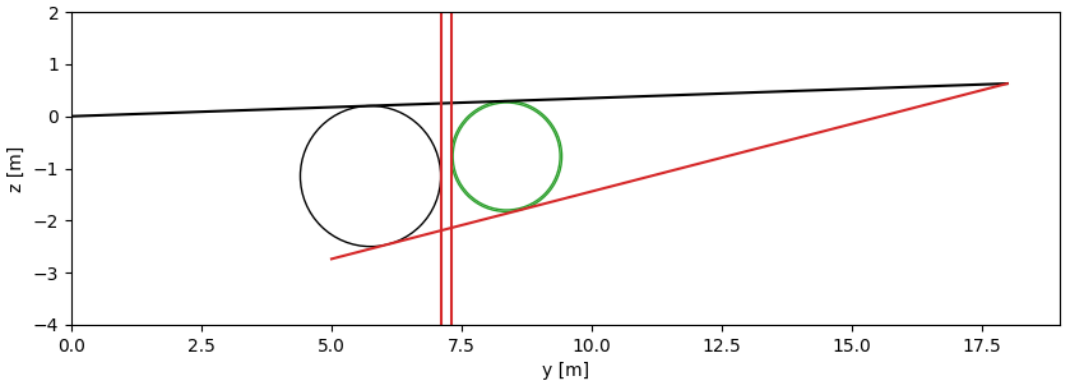

Figure 5.2: The general approach to the lateral sizing of the methane tank.

The red lines show the clearances that were established for a safe operation. Based on the known fuel volume, it was deemed unfeasible to place the tank inboard of the engine, due to the presence of main landing gear. While no formal regulations concerning wing-mounted methane tanks have been found, the following set of constraints has been formulated, largely following from engine clearances:

1. The vertical distance from the ground to the tank surface should not be smaller than 0.46 m, which is the engine clearance found on the A321neo [15].
2. The outer edge of the tank should not exceed the 5 ° clearance measured from the outer edge of the main landing gear [5].
3. The horizontal distance between the engine outer edge and the tank inner edge should not be smaller than 0.2 m due to the risk of excessive interference drag[12].
4. The outer edge of the tank should not exceed the line between the wingtip and tangent to the outer edge of the engine. This is done to minimise the damage to the tank in case the aircraft tips over.

As calculated and drawn using Python, conditions 3. and 4. are found to be limiting, already satisfying the remaining two. It was also found that maximising the tank diameter should be prioritised, since a tank too long could strike the ground on take-off, and the tank itself requires an additional aerodynamic fairing. Therefore, as shown in green in Figure 5.2, the diameter was maximised such that it fits between the wing and the two clearance lines. The resulting spanwise mounting point is 8.491 m, and the corresponding diameter is 2.128 m. It should be noted that this is the maximum *outer* diameter that should not be exceeded, including the thickness of the fairing, the insulation, and the tank thickness itself. Those findings are to serve as an input for a more detailed tank sizing which is to be described in subsection 6.4.1.

5.4. Fuselage Sizing

The fuselage was sized based on the requirements for cargo, passenger capacity, and some of the stakeholder requirements such as **CH4-STK-06-02**, **CH4-STK-02**, and its sub-requirements. The fuselage is a narrow-body, that needs to house 206 passengers in a two-class configuration. Furthermore, it needs to house lavatories, galleys, and the flight deck. It was also decided to use LD3-45 containers to store the cargo for easier loading and unloading. They are the smallest type of LD containers and fit best in a narrow-body.

[12]Such distance would be comparable to the engine-fuselage clearance as found on commercial aircraft such as Boeing 717 [16].

The aircraft is a narrow-body, so 6 seats can be fitted abreast, combined with the LD3-45 containers a width of 3.889 m is needed for a circular cross-section. This leads to the drawing shown in Figure 5.3.

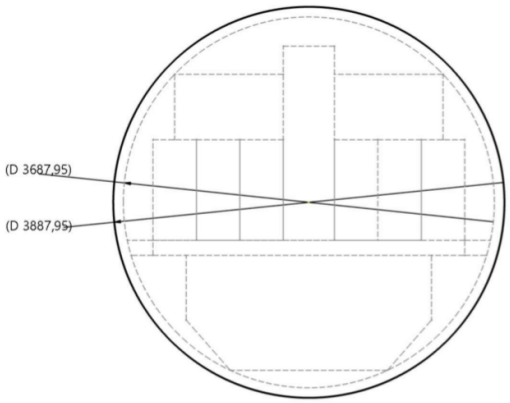

Figure 5.3: Cross-sectional view of the fuselage and cabin.

CH4-FUS-06-01 dictates that enough emergency exits need to be present to evacuate the aircraft in case of an emergency. To comply with these requirements for an aircraft with 206 passengers two type I doors and three type III doors need to be installed on either side of the fuselage. It was decided to place the two type I doors at the back and front of the aircraft with hallways leading to both. Two type III doors were placed over the wing and as the other door was not over the wing this type III door was replaced by a type II door, which was installed between the wing and rear doors.

The seat pitch was chosen to be thirty inches in economy, to keep the aircraft short, and forty inches for business. It was decided to put 198 passengers in economy, making 33 six abreast rows, and 8 in business making two 4 abreast rows. This was chosen because it would fit all required passengers precisely in two classes. For 3 rows an extra 6 inches were added to ensure easy access to the emergency exits to satisfy **CH4-FUS-06-02**. The length of the plane is further driven by amenities such as the 4 toilets and the 2 galleys that need to be added to accommodate the passengers in accordance with **CH4-FUS-02** and sub-requirements. All of these combined with hallways for loading and unloading lead to a total cabin length of 31.7 m. A 2.5 m long flight deck is installed as for the flight distance of the aircraft having 2 pilots is enough, this means that 4 meters is added at the nose to also have space for the radar. Additionally, seven meters were added at the back for the empennage. This leads to a total length of 42.7 m.

To prevent drag divergence at our maximum Mach number the nose has a fineness ratio of 1.3 leading to a nosecone length of 5.06 m [17]. For aerodynamic reasons, the tail cone has a fineness ratio of 2.6 leading to a tail cone length of 10.1 m. This means that the length of the cylindrical section is 27.5 m. The top view of the fuselage is shown in Figure 5.4.

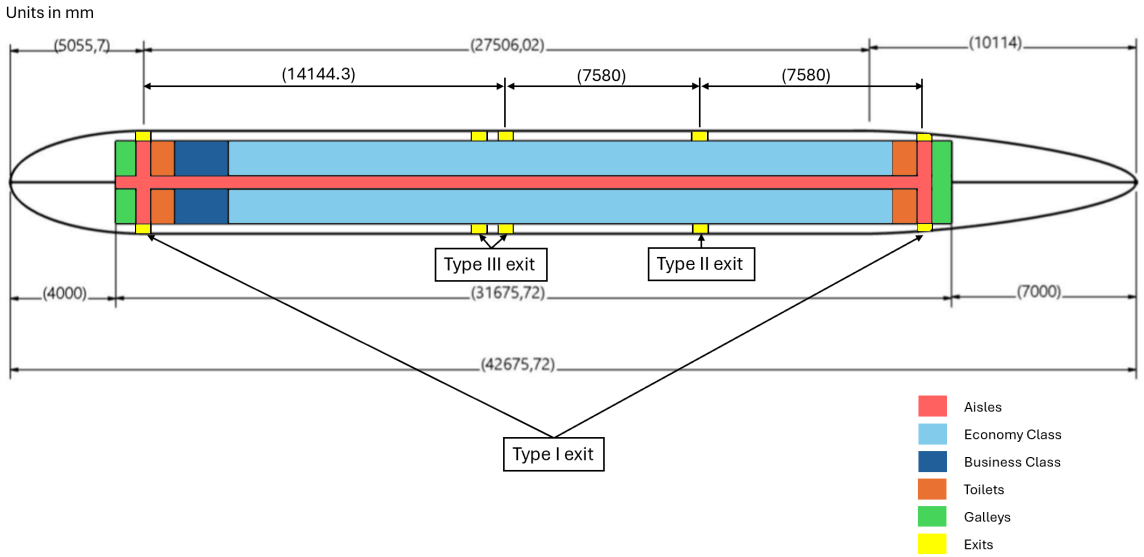

Figure 5.4: Top view of the fuselage and cabin.

To ensure that the pilots would have a good view of the runway and other essential things during operations the placement and sizing of the tail flight deck and its windscreen took into account a large enough view angle. From the position of the pilot a 15 ° over nose angle and a 30 ° upwards angle in accordance with **CH4-FUS-01-04**. Furthermore, the tail cone has a 10 ° upsweep to prevent striking the tail in case of rotation. This is shown in Figure 5.5.

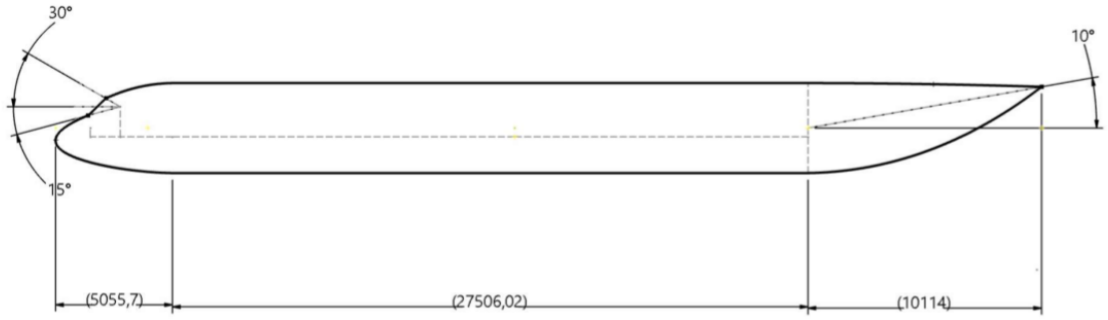

Figure 5.5: Side view of the fuselage and cabin.

5.5. Landing Gear Sizing

The main goal of the landing gear is to support the aircraft on the ground, allow for steering during taxiing, and make sure the aircraft stays clear of the ground during rotation as specified in requirements **CH4-FUN-03** and **CH4-FUN-10**. Furthermore, The wheels need to be designed to carry the weight of the aircraft without damaging the pavement of the runway.

5.5.1. Wheel Design

For the design of the wheel, it was first estimated how many wheels the aircraft would need to have, for which the weight on each wheel needed to be estimated. For a first estimate, 8 % of the weight will be carried by the nose wheel, to ensure it can be used to steer the aircraft. The rest of the weight is carried by the main wheels. During landing, each main wheel can carry up to 210 000 N, which means that based on the Class I weight estimation, 4 main wheels would be needed. An LCN of 50 was chosen as this is also used on aircraft of similar size and this leads to a pressure of 10 kg/cm^2. Based on this landing gear loading and tyre pressure, it can be seen that a main wheel size of 127 cm in diameter by

40 cm wide wheel and a 74 cm in diameter by 21 cm wide nose wheel needs to be installed [5].

5.5.2. Landing gear placement

As it was decided to place the tank after the landing gear this had to be designed before the tanks were placed. This placement was decided upon as it would avoid over-extending the landing gear just to get a slightly more optimal tank position. To ensure the landing gear could do its work its placement in a longitudinal position and lateral position had to be determined.

In order to make sure that the aircraft will not tip over backwards or strike the tail, a maximum rotation angle had to be determined. For the first sizing, a maximum rotation angle of 14 ° was chosen. This means that a relatively large angle will be beneficial for the tanks. A tip-over angle of 16 ° was chosen to ensure that the aircraft would always lean on its tail before tipping over. From this, the main landing gear was placed 21.97 m behind the nose to comply with these requirements. The length of the landing gear for this is 2.76 m without collapsing.

To make sure that the aircraft is steerable, 8 % of the weight of the aircraft needs to be carried by the nose landing gear. In order to do this, the nose wheel is initially placed 5.1 m from the nose based on Equation 5.13. l_n is the distance between the nose wheel and the most aft C.G. and l_m is the distance between the main gear and the most aft C.G. This placement also leaves enough room to store the wheel forwards in the nose.

$$l_n \cdot 0.08MTOW = l_m \cdot 0.92MTOW \tag{5.13}$$

For the lateral positioning of the landing gear the tip-over angle was determined to be the most critical. In order to prevent tip over at all conditions the landing gear has to comply with Equation 5.14. With Ψ being 55° and z being the height of the centre of gravity. Based on this the wheel needs to be placed 3.7 m outwards, leading to a track of 7.4 m. Finally, Equation 5.15 was used to analyse the position of the engine tank and wing tip, but none were as critical for the positioning. ϕ being taken as 5° [5].

$$y_{mlg} > \frac{l_n + l_m}{\sqrt{\frac{l_n^2 tan^2\Psi}{z^2} - 1}} \tag{5.14}$$

$$y_{mlg} > y_{pos} - \frac{z_{pos}}{tan\phi} \tag{5.15}$$

5.6. Empennage Sizing

For an initial estimate of the empennage size, the data from the A321 was taken as a baseline[13]. Combined with data from the fuselage and wing sizing done earlier a rough estimate of the tail size can be made using formulas for the tail volume [5]. Furthermore, a sizing of the elevator and rudder was also made. For that, it has been determined that both control surfaces are to occupy the last 25 % of the respective chords and extend the entire length of the horizontal and vertical tail, respectively. The reason for that is that by placing it at such a chord location, the highest efficiencies of the entire empennage can be attained [5], tying into the overall goal of the project of creating the most energy-efficient aircraft possible. Finally, both the horizontal and the vertical tail utilise the NACA 0012 airfoil, given its utilisation onboard several commercial aircraft [18]. The results of such analysis can be found in Table 5.9 and Table 5.10. These values will serve as an initial estimate of the empennage design to continue with the Class II weight estimation.

[13] https://booksite.elsevier.com/9780340741528/appendices/data-a/table-1/table.htm, [Cited on 5-June-2024]

Table 5.9: Initial sizing of the horizontal tail.

Parameter	Value	Unit	Source
Horizontal tail volume V_h	0.957	-	A321
tail length l_h	18	m	Fuselage sizing
Horizontal tail area S_h	29.5	m^2	[5]
Horizontal aspect ratio A_h	5	-	A321
Horizontal sweep Λ_h	29	deg	A321
Horizontal taper ratio λ_h	0.256	-	A321
Horizontal span b_h	12.15	m	[5]
Horizontal root chord Cr_h	3.87	m	[5]
Horizontal tip chord Ct_h	0.99	m	[5]
Elevator root chord Cr_e	0.97	m	[5]
Elevator tip chord Ct_e	0.25	m	[5]

Table 5.10: Initial sizing of the vertical tail.

Parameter	Value	Unit	Source
Vertical tail volume V_v	0.079	-	A321
tail length l_v	19	m	Fuselage sizing
Vertical tail area S_v	20.00	m^2	[5]
Vertical aspect ratio A_v	1.82	-	A321
Vertical sweep Λ_v	34	deg	A321
Vertical taper ratio λ_v	0.303	-	A321
Vertical height h_v	6.03	m	[5]
Vertical root chord Cr_v	5.09	m	[5]
Vertical tip chord Ct_v	1.54	m	[5]
Rudder root chord Cr_r	1.27	m	[5]
Rudder tip chord Ct_r	0.39	m	[5]

5.7. Verification and Validation

Throughout the preliminary sizing process, the design team performed numerous calculations by means of the Microsoft Excel program. In order to verify the correct functioning of the program, its outputs were compared to the numerical calculations performed by hand. Furthermore, the functions themselves were also verified by inserting dummy values into the program and analysing the logicality of the outputs. Following the verification process, several outputs were validated by comparing them to the A321neo. The parameters selected for comparison were the MTOW, OEW, wing surface area, wingspan, tail area and wing sweep. The reason behind selecting those parameters is twofold. The first two parameters correspond to the weight of the aircraft, one of the most relevant parameters concerning aircraft performance. The remaining parameters, however, correspond to the sizing and dimensions of the aircraft wing and empennage. An increase in those would increase the aircraft drag, hindering its performance. The results of such comparison have been presented below in Table 5.11.

Table 5.11: Comparison of A321neo and CH4llenger.

Variable	A321neo	CH4llenger	Relative difference [%]
MTOW [kg]	93 500	103 344	10.53
OEW [kg]	48 725	54 815	12.50
S [m^2]	122.4	136.3	11.36
b [m]	32.58	35.98	10.44
S_h/S [-]	0.253	0.216	-14.62
$\Lambda_{0.25}$ [deg]	25.0	23.6	-5.60

When looking at the table, it can be observed that most values are around 10 % greater than the ones found onboard the A321neo. Although this would initially indicate a potentially worse aircraft performance, the values obtained for the CH4llenger aircraft are somewhat conservative and are bound to be optimised at the later stage of the design as will be explained in chapter 8. As a result, the values can be considered validated. Looking at the last two variables, however, the obtained values are considerably lower than the ones found aboard the neo. Both of those differences can be explained, though. Firstly, the lower horizontal tail size can be attributed to a larger moment arm of the tail, caused by a greater distance between the main wing and the empennage. This, in turn, results in a smaller required surface area of the horizontal tail. Finally, the quarter-chord sweep value is also slightly smaller than the one found on the A321neo. The main reason for that, however, is the different airfoil used, based on which the planform design was optimised such that the sweep of the wing is minimised. As a result, the values can be considered to be validated, allowing the team to proceed further with the design.

5.8. Recommendations

Before continuing with the design process, several points of improvement have been identified, which would allow for the enhanced performance of the under-design aircraft.

First of all, the value of twist has been preliminary selected based on initial research such that the aircraft performance is satisfactory by implementing a potential stall recovery mechanism. It could, however, be further improved to optimise the required twist.

The current shape of the fuselage is a preliminary idea. Although the sizing needs for the cabin and flight deck are final, the shape of the tail cone can still be iterated upon to optimise the fuselage aerodynamically. As the focus of the project is more on the tanks and fuel system, this has not yet been taken into account. The exact shape could still be optimised to possibly reduce drag and the chance of a tail strike.

Currently, the wheels are sized based on LCN. According to Airbus, this method is outdated and the ACN-PCN method should be used [15]. This is not done in this report, as not much information on this is freely available. In the future, this could be updated. Finally, the loading of cargo has not yet been considered in detail. For later phases of the design, it is recommended to also consider the cargo doors for the aircraft to be able to be loaded in a timely manner.

6. Propulsion System Design

The propulsion system of the CH4llenger is quite different when compared to a typical aircraft. As the CH4llenger will be flying on synthetic methane the fuel flow system will completely change as seen in section 6.1. Ultimately the only thing that requires relatively few modifications from typical aircraft is the engine, and even there multiple changes are made as seen in section 6.2. Furthermore, a heat exchange system was designed in section 6.3 to gasify the liquid methane before its being fed into the engine. As liquid methane is much more difficult to store than kerosene the fuel is stored in tanks under the wing rather than inside the wing. These tanks are sized in section 6.4. Furthermore, section 6.5 and section 6.6 discuss the sizing of the gaseous methane tanks and off the APU. section 6.7 discusses the weight estimation of the fuel system. section 6.8 and section 6.9 will discuss the verification, validation and sensitivity analysis procedures. Finally recommendations are represented in section 6.10.

6.1. Layout

A schematic layout of the propulsion system per wing is shown in Figure 6.1. The fuel systems in each wing are symmetrical with respect to the centre line of the fuselage. The flow of fuel starts in the large external tank, which holds liquid methane. From there, the liquid methane is pumped through a pipeline connecting the tank to the wing and engine. The pipeline is split in a parallel configuration. One line is fed through an electric heater, which gasifies the methane, utilising electricity from the APU. This heater is activated during start-up ahead of the engines being warmed up and during take-off to help facilitate the increased mass flow of gaseous methane needed. Alternatively, the pipeline runs through a shell in plate vaporiser. This vaporiser uses a warm heating fluid from the engine, to gasify liquid methane during take-off, cruise and landing. The electric heat exchanger needs to be used first in order to start the main engines so that the heating fluid has a high enough temperature that there is no risk of the heating fluid freezing when interacting with the liquid methane pipes. Once the engine has reached a sufficient temperature and the shell in plate heat exchanger can supply enough energy for vaporisation the electric vaporisation unit can be switched off. It is to be noted that when a station is mentioned, this is done in bold to get a clearer overview.

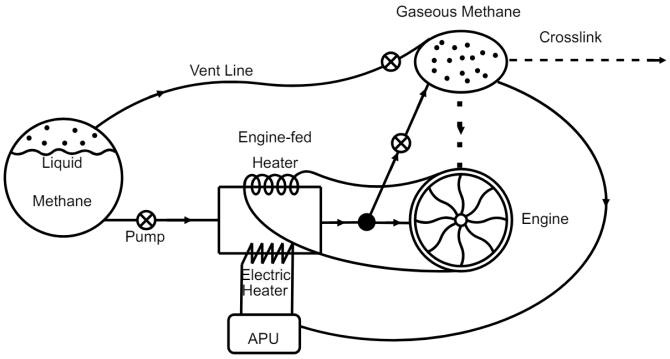

Figure 6.1: Concept for the layout of the propulsion system.

Once the methane is in its gaseous state, the two paths join and the main flow goes through a junction, with one path into the first of the three gaseous methane tanks and another straight to the engine. Going straight to the engine allows for continuous mass flow from the liquid tank, which is the main store of fuel. In the gaseous tanks, the stored methane can be used for instantaneous throttle responses,

as the heating of liquid methane may cause lag responses in the control of the aircraft in the main flow. The gaseous tank is also fed by the venting of the liquid tank, as to relieve over pressure and maximise fuel efficiency. Furthermore, a crossfeed link connects the tank to the second external wing tank, thus allowing for the transfer of fuel during a one-engine-operative scenario. The external fuel tank also includes a vent with a flame in case of over-pressure. The three tanks are held at a high pressure, thus allowing the tanks to feed directly into the high pressure combustion chambers, allowing for instantaneous throttle responses. The gaseous methane from the tank is then fed into each engine.

Finally, gaseous methane from the three tanks are used to fuel the APU, for powering the electric heater, but also to run other environmental control and startup processes that the APU oversees. The start-up of the APU is done with the boiled off methane that is stored in these gaseous tanks. Once the APU is started, the electricity generated by the APU is used to heat up the liquid methane through the electric vaporiser allowing for an increase in fuel flow which can then be used to start up the main engines. Stemming from Figure 6.1, a detailed layout is synthesised and is presented in Figure 6.2.

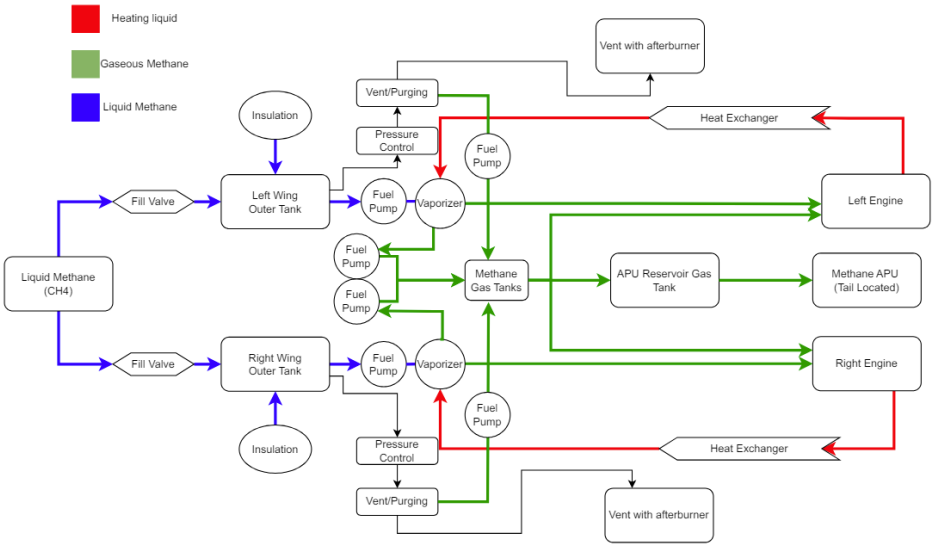

Figure 6.2: Layout of the fuel system.

6.2. Engine

This section entails the engine sizing of the propulsion system. Key variables such as mass flow and thrust are evaluated at cruise flight, which allows for a further evaluated idea of the characteristics of the aircraft, but also help size other systems, such as the tanks.

The engine underwent a pressure and temperature analysis through the different stations. As such, different efficiencies were explored, enabling an in-depth mass flow and thrust evaluation to be synthesised. The stations are positioned at important locations where the temperature and/or pressure change due to internal processes imposed by the fan, compressors, combustion chamber, turbines and exit. Moreover, this evaluation helps understand if methane can be simply substituted in, or if major modifications are needed to be implemented.

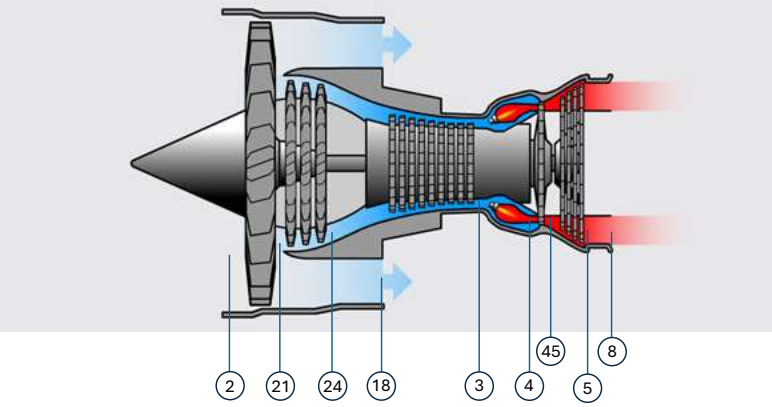

Figure 6.3: Schematic of the LEAP-1A with the engine stations.

The journey of the airflow is depicted in Figure 6.3[1], which commences by calculating ambient temperature, pressure and velocity conditions at cruise and slight perturbations to such conditions within the cowling at **Station 2**. Subsequently, the fan slightly pressurises and heats up the flow, thus spelling the conditions at **Station 21**.

Furthermore, the bypass ratio is used here to evaluate the mass flows of hot and cold air, the ratio between how much air passes outside the jet engine versus air going through the core of the engine.

Within the jet engine, the flow encounters the compressor system, formulated by a high and low compressor. The flow first meets a low-pressure compressor which is responsible for the precompression of the flow coming from the ambient conditions, thus at **Station 24** the pressure increases two-fold. The temperature rises too, but not by such a large magnitude. Having been precompressed, the flow is ready to enter the high pressure compressor, where a 20-fold increase in pressure occurs. This also raises the temperature too, but again by not the same magnitude.

With the air extremely pressurised, it is ready to enter the combustion chamber of the aircraft at **Station 3**. Here the pressurised air is mixed with vapour of the fuel and sparked to ignite. Thus, the flame temperature of the fuel is reached at **Station 4** and huge amounts of force are achieved to subsequently drive the turbine system. The turbine system's role is to use the force generated through the fuel combustion to drive the compressors, but more importantly, the fan which accelerates the quieter bypass air, which provides the majority of the aircraft thrust.

The turbine system is formed of a high-pressure and low-pressure compressor, whose roles are to reduce the conditions in the jet engine back to the ambient by transforming the energy into thrust. At **Station 4**, the flow encounters the high-pressure compressor, where the majority of pressure decrease occurs, along with some temperature decrease.

Subsequently, at **Station 45**, the flow encounters the low-pressure turbine, which finishes off the pressure reduction, and as much of the temperature too, based on efficiencies, exiting at **Station 5**. Subsequently, there's room for the flow to be channelled, and the flow reaches **Station 8** at the nozzle, at the end of its journey through the jet. Simultaneously, the bypass air has been accelerated and flows freely through the interior of the nacelle up to **Station 18**.

An important aspect to consider for both bypass and jet flows is to analyse whether or not they are

[1] `https://www.sphaera.co.uk/aircraftEngines.htm`, [Cited on 24-June-2024]

choked. Choked flow looks at the ratio of pressure between **Station 5** and ambient conditions versus the ratio of pressure between **Station 5** and the critical pressure of the flow. If the ratio with the critical pressure is lower than that with the ambient pressure, the flow is choked and thrust calculations need to include an additional term taking into account the difference in pressure at the exit of the nacelle/nozzle (**Stations 8 and 18**).

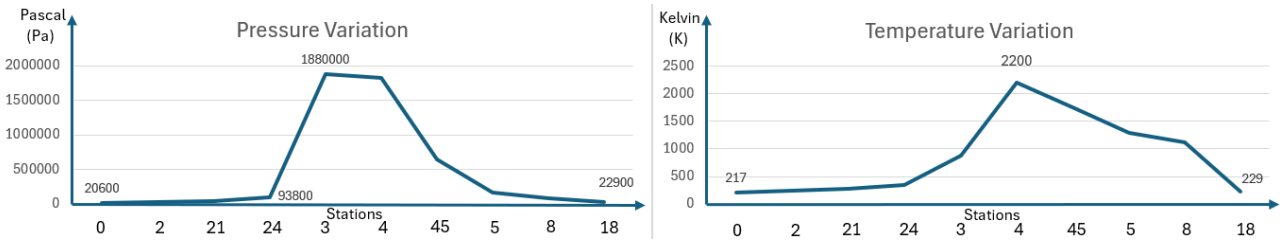

Figure 6.4: Pressure and Temperature variation through engine stations at cruise.

To summarise, Figure 6.3 and Figure 6.4 depict that at cruise conditions, the engine works efficiently by having entry and exit temperatures and pressures of similar values, within 11% and 6% of each other respectively. As such, a relatively high amount of energy is focused on propelling the air in order to create thrust, and minimal amounts are lost to the environment through unused pressure and temperature differences. Moreover, until station 24 there are low pressures. This is explained by the fact that the pressure ratio of the compressor stage is 40:1 in total, yet the high pressure station has a ratio of 20:1, thus the low pressure compressor has a ratio of 2:1, explaining the low increase in pressure over that section. Finally, the peak temperature of 2200 K occurs just after the combustion chamber and represents the flame temperature of methane.

6.2.1. Material Structure

In the analysis of the engine design, an investigation into substituting methane as opposed to kerosene in the LEAP-1A engines was performed. This was done by researching the materials in the engine and testing their heat properties against the expected heat conditions found during operations with Methane. As per the maintenance handbook of the LEAP-1A engine, the high-pressure turbine in the 'hot-section' of the engine is formed of a Nickel Alloy. As per [19, 20], Nickel by itself has a melting point of 1723 K, with alloys having values around it [21]. This includes a Nickel-Iron-Chromium alloy called Discalloy [2], whose melting point can reach 1738 K. Furthermore, thermal coatings are used to increase the temperature resistance of the component, utilising industry proven materials like yttria-stabilized zirconia, which can reach melting point temperatures of 3000 K [22, 23].

Methane has a flame temperature when burnt in air of around 2273 K [24]. This seems incredibly high, however utilising innovative cooling techniques such as pores visible to the outside flow and Thermal Barrier Coatings (TBCs), this can be mitigated. Moreover, active cooling options such as allowing bypass air to perforate through compressor and turbine blades allow the air around the metal to remain cool.

Computational analysis has been performed on the temperature profile of burning methane in comparison to kerosene. The results suggest that methane burns faster than kerosene, meaning the high temperatures are concentrated in the combustion primary zone. This is beneficial to the turbine as a more desirable temperature profile is created towards the exit [25].

[2] `https://nickelinstitute.org/media/8d93486143182f5/nickel_incopub393_updated-june-2021.pdf`, [Cited on 17-June-2024]

6.2.2. Mass Flow Calculations

An important value to consider is the mass flow of the methane during cruise and take-off. Knowing the mass flow determines whether the initial mass of the fuel and, consequently, the sizing of the tank, is sufficient. Preliminary, it is expected that less mass of methane will be needed during cruise, in comparison to kerosene. This is due to their Lower Heating Values (LHV) in MJ/kg, which specify the quantity of heat released given a kilogram of the absolute quantity of heat released after burning a kilogram of fuel. The LHV of methane and kerosene is 50 MJ/kg, and 43 MJ/kg, respectively. This implies that the burning methane expels more energy than its kerosene counterpart, given the same mass.

For cruise, the aircraft will be flying at 38 000 ft, with a Mach number of 0.78. The Leap-1A has a bypass ratio of 11:1 and a total compression ratio of 40:1. The calculation consisted of calculating the temperature and pressure values at each stage of the engine, including after the compressor, combustor, turbine, and exit of the fan nozzle.

The mass flow of the fuel largely depends on the intake of air. Given the intake area of the LEAP, we can calculate the mass flow rate of air at the entry of the engine using Equation 6.1 [26]. The hot mass flow will actually be one-twelfth of the mass flow that enters. (Equation 6.2)

$$\dot{m}_{air} = \rho V A_{intake} \tag{6.1}$$

$$\dot{m}_{air_{turbine}} = \dot{m}_{air} \cdot \frac{1}{1+BPR} \tag{6.2}$$

The mass flow of the methane is calculated using Equation 6.3. It depends on the air mass flow rate through the core, the temperature difference between the air before and after the combustor, the combusting efficiency, and the lower heating value of methane. This gave an approximate value of 0.53 kg/s in cruise conditions.

$$\dot{m}_{fuel} = \frac{\dot{m}_{air_{turbine}} \cdot c_{p_{gas}} \cdot \Delta T}{\eta_{cc} \cdot LHV} \tag{6.3}$$

This result makes sense given the amount of methane used in the preliminary weight sizing. Using values for kerosene yields a mass flow of 0.65 kg/s, which confirms the expectations earlier, as it is more than methane. It is also important to note that the isentropic efficiencies were approximated to be 0.9 [27]. Lowering the efficiency values decreases the fuel mass flow rate but also reduces the SFC and the thrust, as will be explained in subsection 6.2.3.

6.2.3. Thrust Calculations

Moving on, it is vital to determine whether enough energy will be provided by the engine. To begin with, the power needed to drive the fan, the low-pressure combustor, and the high-pressure combustor was calculated. This allowed for the calculation of the temperatures and pressures at the exit of the turbine, which determines whether the flow in the core is choked. It turned out that the core flow was choked, meaning the thrust from each flow is represented by Equation 6.4, where V_8 is the jet velocity of the core flow, p_8 is the static temperature at the exit of the nozzle of the core, and A_8 is the cross-sectional area of the nozzle flow.

$$T_{core} = (\dot{m}_{core} + \dot{m}_{fuel}) \cdot V_8 + A_8 \cdot (p_8 - p_{amb}) \tag{6.4}$$

Moreover, a large proportion of the thrust is provided from the bypass. This is where the majority of the air goes through and is not affected by the pressure and temperature changes the core does. The thrust of the bypass is calculated using Equation 6.5, where the variables of the equation are the same but for the bypass flow. A synopsis of the thrusts are included in Table 6.1. Lastly, the specific fuel consumption can be determined from the thrust and mass flow [28].

Table 6.1: Results showing thrust of the engines.

	Thrust [kN]
Core	12.99
Bypass	27.61
Total	40.60

$$T_{bp} = \dot{m}_{bp} \cdot V_{18} + A_{18} \cdot (p_{18} - p_{amb}) \qquad (6.5)$$

$$SFC = \frac{\dot{m}_f}{T_{bp} + T_{core}} = 13.16 \frac{g}{kNs} \qquad (6.6)$$

It is important to note that the efficiencies chosen affect the fuel mass flow and the resulting thrust. For instance, for the above calculations, isentropic efficiencies of 0.85 were chosen. This was done as a sort of lower, worst case scenario in terms of efficiencies, given the efficiencies of the LEAP are not known to the public. Additionally, in order to visualise the temperature and pressure values calculated for the engine.

6.3. Electric and Engine-Fed Heat Exchange

As already mentioned, in order to gasify the liquid methane, two heat exchanges are used. The electric heater, run from electricity provided by the APU, will be made out of metal coils going around the liquid methane piping. Such heaters can easily be controlled by their power input. When going into a more detailed design, either an available or custom-made heater can be used. The sizing of such a heater will mainly depend on its efficiency and power needed to sustain certain mass flows. In order to find the power required to obtain a certain mass flow Equation 6.7 is used.

$$P_r = \dot{m} \cdot SLH_v \qquad (6.7)$$

Where P_r is the power required, SLH_v is the specific latent heat of vaporization, which is 510 kJ/kg [29] for methane, and $\dot{m}$ is the mass flow needed by the engine.The electric heater should be able to provide a thermal capacity of around 100 kW to each wing. This gasifies roughly 0.2 kg of methane per second from each liquid tank. A total mass flow of 0.4 kg/s of methane gas is enough to power the APU and start the main engines. Once the engines are burning the engine heated vaporiser, which uses a glycol fluid, as heating fluid can start up. In order to take off, a mass flow off 1.1 kg/s is required. To do this, each wing propulsion group requires an input off 562 kW. With an electric heater that can provide 100 kW to each wing group and a shell in plate heater that has a thermal capacity of 500 kW, this requirement is met.

The shell in plate heating system uses glycol which circulates around the engine and then transfers this heat to the liquid methane through a shell and plate vaporiser. The workings of such a vaporiser are quite complex, as it is dependent on the turbulence of the flow in the hot liquid and the circulation within this flow. In order to further understand the working properties of a shell and plate vaporiser Guillaume Salomons, an engineer working at Cryonorm Systems, was contacted. Salomons explained that a plate and shell heat exchanger (PSHE) works better than a shell-in-shell heat exchanger for systems where the weight is of importance, such as in an aircraft. Ideally, the electric heater does not need to be used during the cruise so this shell and plate vaporiser should be able to gasify 0.55 kg/s of methane as this is the mass flow needed for the cruise in each engine. The thermal capacity of the heat exchange should thus be at least, 280 kW assuming it perfectly conducts the heat and all energy is used for vaporisation. The PSHE partial 2-phase heat exchanger from Vahterus can vaporise 0.5 kg/s of natural gas from LNG [30]. As LNG contains upwards of 90 % methane, this vaporiser would also work for pure methane. This plate and shell vaporiser from Vahterus has a thermal capacity of 504 kW and is designed to gasify 0.5 kg/s [30].

The PSHE not only vaporises the LNG but also heats up the gas to 15 °C [30]. As this higher temperature is not necessary for the combustion of methane if the LNG inflow is increased then the same thermal capacity would, theoretically, increase the gaseous output of the vaporiser. If the majority of this energy goes to vaporisation rather than heating of the gas, the outflow of the gas should reach around 0.98 kg/s when using Equation 6.7. Furthermore, the temperature of the hot fluid in the Vahterus heat exchange is only at 30 °C when it enters the heat exchange. Using the heat from the engine, the warm fluid circuit can be heated up to 100 °C, which would greatly increase the thermal capacity. As the temperature in the combustion chamber reaches up to 2200 K, great care would be needed to select the proper location to heat the fluid in order to avoid boiling of the liquid. Ultimately, a company such as Cryonorm or Vahterus would need to be contacted to design a vaporiser specifically for the aircraft. However, based on the technology of this Plate and Shell heat exchanger from Vahterus, the vaporisation of the required mass flow of liquid methane is certainly possible. For the current design stage, a weight estimation of this Vahterus heat exchanger can be used. The Partial 2 phase exchanger has a dry mass of 88 kg, taking a conservative assumption for wet mass we can assume each vaporiser will weigh around 120 kg, as this includes about 25 kg for the glycol circuit [30].

Further design of the heat transfer mechanisms has been omitted due to the complicated nature of heat convection. Nevertheless, a specific heating fluid was selected. The main criteria used in the selection of the liquid were the boiling-point and freezing-point temperatures, the specific heat and thermal conductivity. Companies such as Cryonorm or Vahterus typically use a glycol water mixture. It was found that a 50-50 mixture of propylene glycol with water has the most fitting properties. Nevertheless, its minimum temperature of about −50 °C and maximum temperature of about 150 °C will require careful tuning such that the fluid does not freeze or boil [3].

6.4. Liquid Methane Fuel Tank

As observed in section 6.1, a two-tank configuration is utilised in the implementation of liquid methane. Each tank serves a different function, with the external tank storing the majority of the fuel and the gaseous tank acting as a pressure buffer and fuel flow regulator into the engine.

6.4.1. Liquid Methane Fuel Tank Structure and Materials

In terms of the liquid methane fuel tanks, both being cylindrical tanks with spherical end-caps and localised in pods under the wings enclosed by a fairing, several considerations need to be taken into account in order to determine the suitable materials for the inner layer, insulation and outer layer of the tank.

In terms of the inner layer of the tanks, the most promising material suggested for such a cryogenic fuel tank by among others NASA [31], Brewer [32] and Winnefield [33] is the aluminium alloy Al-2219. This alloy performs well at cryogenic conditions, is easy to manufacture and capable of maintaining the structural integrity of the tank [34].

When it comes to the insulation layer of the tank, three possible types of insulation can be considered for cryogenic tanks. These types are vacuum, multi-layer and rigid foam insulation. The first type, vacuum insulation, has the lowest thermal conductivity of the three, which leads to near-zero boil-off rates. However, heavy external walls are required in order to resist the high external pressure that can cause buckling. On the other hand, multi-layer insulation not only has a higher thermal conductivity than the vacuum option, leading to more boil-off, but it also is heavier. Lastly, polymer foam insulation does have a higher thermal conductivity, it has the lowest density out of the three, and could therefore offer weight savings, along with potential lower costs. Regarding the various types of polymer foam insulation available, four have been considered. These are Polymethacrylimide, Polyurethane, Polyvinylchloride, and Polyurethane (with chopped glass fibre) [34]. In order to find the

[3] `https://www.engineeringtoolbox.com/propylene-glycol-d_363.html` [Cited on 05-June-2024]

best combination between density and conductivity, it was calculated how much mass is needed for the same amount of insulation. In the end, Polyvinylchloride was found to be the best-performing in this aspect and subsequently chosen.

Now, looking at the outer layer, a fairing is to be added in order to improve the aerodynamic characteristics of the tank. The design of the fairing is modelled according to the description of a streamlined body by Torenbeek [35]. Taking into account the 1.75 fineness ratio mentioned for the nose and the 2.75 fineness ratio for the tail, a 17.5 m tank would be needed. This creates problems with striking the tank during rotation, so the aerodynamic sections were shortened to account for this, leading to a length of 16.55 m. Additionally, an upsweep was added to the tail to further prevent strikes. The final fairing dimensions are shown in Figure 6.5. Furthermore, the surface area of the tank was determined to be 93.85 m^2. This value was found by summing the areas of the 16.24 m^2 ellipsoid nose, 53.11 m^2 cylindrical body and 24.50 m^2 paraboloid tail, computed with their respective area formulas.

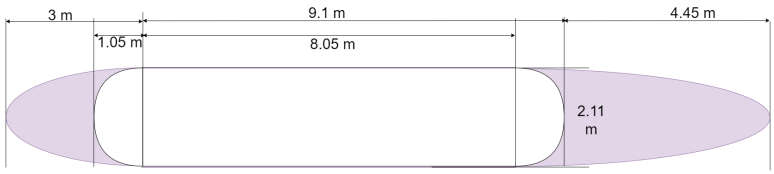

Figure 6.5: Concept for the under-wing fuel tanks.

Several factors then can be taken into account in order to select the appropriate material for this fairing. The materials that were compared are Kevlar, Carbon Fibre Reinforced Polymer (CFRP), aluminium, Glass Fibre Reinforced Polymer (GFRP), titanium and steel due to their application potential in aerospace structures. For this trade-off, the factors considered are the ability of the material to absorb impacts, the weight of the structure, cost, temperature behaviour and sustainability Table 6.2.

Looking at similar aircraft structures, existing nose cones and leading edge designs were considered. Regarding existing nose cone, materials, these were mostly GFRP. However, this is not because of structural reasons, but because of radar-transparency reasons [4]. Given that no radar system will be placed within the fuel tank fairings, this does not provide a good reason to use GFRP. The leading edges of wings usually consist of aluminium. However, the reason for this is mostly for deicing purposes [5]. De-icing is not a major priority for the fuel tank fairing, given that it does not act as a lifting surface. Therefore, is also not a valid justification to use aluminium.

Revisiting the properties of the different materials in the trade-off table Table 6.2, and combining the scores dependent on how important certain criteria are, it is found that CFRP slightly outperforms all the other materials. This choice is further reinforced by considering other special properties of CFRP. Despite CFRP having to be shielded from lightning strikes, it seems to have a good burn-through resistance, and corrosion resistance [6]. Given that the CFRP will surround a highly flammable and very cold liquid, which may catch fire and/or cause ice formation on the surface, these two properties are likely beneficial.

Furthermore, it was considered that due to CFRP's relatively lower toughness, extra reinforcements need to be added to the inside of the fairing in order to be able to absorb energy to protect from impacts, such as bird strikes. For this reason, an extra layer of shock-absorbing material should be added to the nose cone of the external fuel tank. From research conducted on highly impact-resistant materials, it

[4] `http://www.grahamhague.com/nosecones.shtml`, [Cited on 12-June-2024]

[5] https://aircrafttechnic.com/aviation_technology/why-are-the-b787-leading-edges-made-from-aluminum/, [Cited on 12-June-2024]

[6] `https://safetyfirst.airbus.com/safe-operations-with-composite-aircraft/`, [Cited on 12-June-2024]

has been found that a moderately thick layer of polyurethane foam is able to resist high velocity of impact [36]. More specifically, considering a bird strike velocity of 107.3 m/s, experiments conducted by the National Research Council Canada (NRCC) have proven three 127 mm thick polyurethane foams to be capable of withstanding bird strike impacts in the tail cone [37]. Following this result, it is expected that a 400 mm layer of foam inside the nose of the wing tank is able to absorb the required force generated by such a collision. Given the foam's density of 0.062 kg/m^3, the ellipsoid nose's area of 16.24 m^2 subsection 6.4.1 and the foam thickness of 400 mm, the total mass of this foam layer is then calculated to be 406 g. Although this material is able to resist extensive damage by a bird strike, future research needs to be conducted regarding the load transfer to the pylon, which was marked by the NRCC as a potential flaw, in order to ensure no excessive forces do not occur due to the tank's foam layer absorption of the impact.

Table 6.2: Trade-off of the fairing materials.

	Toughness	Weight	Cost	Temperature Properties	Sustainability	Total Score
Criteria Weight	3	5	1	3	3	
CFRP	2	5	1	5	2	3.53
Aluminium	3	3	4	5	3	3.47
GFRP	4	4	3	3	1	3.13
Titanium	4	2	3	4	4	3.27
Steel	2	1	5	2	3	2.07

6.4.2. Fuel Tank Wall Thickness Calculations

Sizing the thicknesses of the various tank wall materials involves looking at what task they are supposed to perform. Starting with the aluminium inner layer, it bears the loads of the tank pressure. This pressure difference has been set to a reasonable 3 bars. Below, there are the formulas given for the required thickness of the cylindrical tank walls, given the pressure requirements, material properties and tank size [34].

$$t_{cylindrical} = \frac{D_0 \cdot \Delta p \cdot FoS}{2 \cdot \sigma_a \cdot e_w - 1.2 \cdot \Delta p \cdot FoS} \tag{6.8}$$

$$t_{sphere} = \frac{D_0 \cdot \Delta p \cdot FoS}{4 \cdot \sigma_a \cdot e_w - 0.4 \cdot \Delta p \cdot FoS} \tag{6.9}$$

Assuming the inner lining to consist of Al-2219, a weld-efficiency of 0.8 (e_w), and taking a factor of safety (FoS) of 2, it is found that this layer will have a cylindrical thickness of 2.76 mm, and a spherical thickness of 1.38 mm. This leads to an inner lining mass per tank of 477 kg.

Next up, several polymers have been considered for the insulation of the tank walls. These were also found from [34] and, in the end, the one which has the lowest mass for a given ambient power into the tank, was considered, being Polyvinyl Chloride.

$$t_{insulation} = \frac{\sigma \cdot A_{tanksurface} \cdot \Delta T}{P_{in,ambient}} \tag{6.10}$$

$$m_{insulation} = \rho_{insulation} \cdot A_{tanksurface} \cdot t_{insulation} \tag{6.11}$$

$P_{in,ambient}$ is the ambient power into the tank. This has been set to a value of 2000 W, enough power to gasify 0.004 kg/second. After engine startup, such a value is negligible when considering that the engine uses about 0.5 kg/second. This value is more important when considering filling up the methane tank and looking at the pressure build-up. Given that about 5 m^3 of each fuel tank is empty, at the given rate of fuel gasification, it would take about two hours for the tanks to obtain the design pressure of 3 bars. This seems like an appropriate amount of time for the handling of the fuel tanks, accounting for possible delays.

The power input calculations assume that there is perfect heat transfer between the ambient air to the tank fairing, between the tank fairing and insulation layer, between the insulation layer and the inner aluminium, and between the aluminium and the liquid inside the tank. So essentially, the only place where heat transfer is not considered perfect is within the insulation layer. These are not assumptions which can usually be made, especially the one with the transfer from ambient air and the tank fairing surface. Nevertheless, a more detailed approach is not possible unless detailed simulations are performed. Finally, it is calculated that an insulation thickness of 3 cm is required, corresponding to an insulation mass of 102 kg.

Lastly, the thickness of the fairing needs to be sized. It has been decided that the outer fairing material will not be absorbing the majority of the energy from potential strikes from birds or hail. On the contrary, it mainly acts to keep an aerodynamic shape and prevent the fuel tank from scraping on the ground during impact. Another material to absorb the shocks is discussed in more depth in subsection 6.4.1. Given that CFRP is selected and the structure is not expected to sustain large structural loads, it has been decided that the outer thickness will be approximated to the minimum thicknesses used in CFRP applications. It is said that typical composite materials in aerospace applications are between 1.25 mm and 20 mm thick [7].

The lower boundary will be used to size the fairing, given that it is related to skin thicknesses, as opposed to the upper boundary. While this value is very rough, this is a point which can be improved in future iterations of the design. Looking at the density of typical CFRP structures, this corresponds to about 1550 kg/m^3 [8]. Revisiting the total surface area of the fairing, this was found to be 93.85 m^2 subsection 6.4.1. Following, the weight of each fuel tank fairing is found to be roughly 182 kg.

6.4.3. Liquid Methane Tank Mounting Mechanism

In order to carry the liquid methane tank, a strong mounting mechanism is necessary. The majority of the loads present will be axial, due to the weight of the tank. This is unlike engine pylons, where a large bending moment is created due to the thrust. In the axial direction, the largest force will be present during turbulence or hard landings, where an acceleration of about 2.5G, however, industry-standard certification requires tolerance of 3.8G in loading [38] due to gusts or turbulence that can occur during flight. Another key loading case is during take-off when the aircraft is set to experience 2G (with safety margin) at a critically maximum pitch angle of 20°. The placement of the rods shall coincide with the spars at 0.2 and 0.75 chord length of the airfoil. This helps as it allows the wingbox spars to carry the loads of the tank.

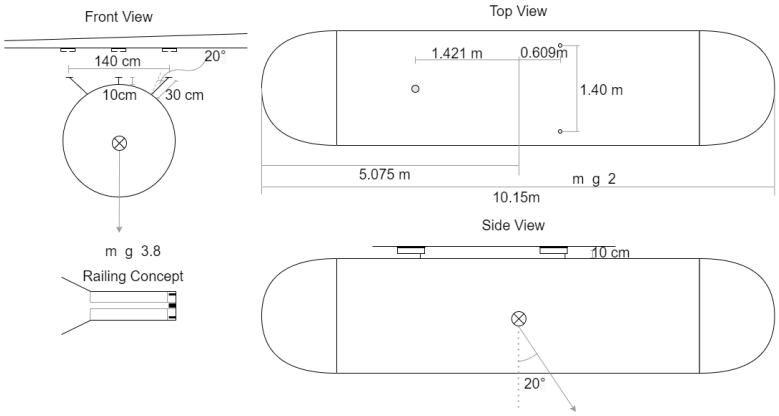

Figure 6.6: Schematic depicting tank mounting method and associated loads.

[7] https://www.olympus-ims.com/en/applications/aerospace-composites/, [Cited on 12-June-2024]
[8] https://www.avient.com/idea/carbon-fiber-composites, [Cited on 12-June-2024]

The schematics in Figure 6.6 depict the general idea of how the tank could feasibly be mounted. The top left image shows a front view of the tank under the wing, with its Al-2219 rods extending out of the tank structure and the receiving railings directly above, connected to the wing. Furthermore, the turbulent load of 3.8Gs in the axial direction is shown. The bottom right depicts a side view of the tank, depicting specifically the short length of the railings, accommodating the attachment of the tanks. Moreover, it shows the angled take-off loads that will be experienced on the tank (at a maximum of 20°). The top right image shows a top view of the tank and depicts the locations where the rods could be placed on the tank, thus allowing for sufficient structural support and spacing between railings. Lastly, the bottom right image shows the railing concept. The funnel acts as a guide for the rods to enter the railing, and then the rod follows the track up to the locking mechanism at the right-hand side of the railing.

One rod would be placed at the front while two at the back. Hence, the two rods at the back would carry the same amount of horizontal and vertical loads as the one at the front. The loading cases are displayed in Figure 6.6. The way these rods are designed is by determining the necessary surface area to sustain axial/shear loads. Then the radii for all rods are determined such that they sustain the same amount of bending stress. Firstly, an analysis of whether the axial or shear stress is more significant is performed. The equations necessary are seen below in Equation 6.12 and Equation 6.13.

The tanks are attached to the wings by means of railings. This is a traditional method of mounting probes to aircraft of varying mass and size. As such, this method is redesigned to carry the liquid methane wing tanks necessary to operate this aircraft. The rails shall be rather short, only needing to be long enough to aid the mounting and detachment of the tank on the ground, as seen in Figure 6.6. The rear rods are mounted at an angle of 30°, which allows for sufficient spacing between the rails and facilitates easier inspection and repairability of the mounting structure.

$$\tau = \frac{F_{lateral}}{A_{total}} \tag{6.12}$$

$$\sigma = \frac{F_{axial}}{A_{total}} \tag{6.13}$$

It was taken that the material used is made out of Al-2219. This would benefit from weight savings but could be readjusted to a stronger alloy if necessary. As the yield shear strength for this material is not publicly provided, the Mises yield criterion was taken as an approximation [9], found in Equation 6.14.

$$\tau_y = \frac{\sigma_y}{\sqrt{3}} \tag{6.14}$$

$$\frac{2F_{horizontal}}{r_{rod1}^3} = \frac{F_{horizontal}}{r_{rod2}^3} \tag{6.15}$$

From this, it was found that the axial stress is the most constraining load. Therefore, the surface area was calculated from this value. Then, the radius of the rods was calculated in such a way that all rods carry the same load. The equality, after having simplified terms, can be seen in Equation 6.15, where rod1 indicates the front rods and rod2 indicates one of the rear rods.

This equality can then be transformed into a relation of radii, seen in Equation 6.16. Finally, the radii can be determined with Equation 6.16 such that the sum of the rod cross-sectional areas is equal to the necessary area for axial stresses.

$$r_{rod1} = 2^{1/3} \cdot r_{rod2} \tag{6.16}$$

$$h = \frac{\sigma \cdot \pi \cdot r^3}{F \cdot 4} \tag{6.17}$$

[9] https://www.engineersedge.com/material_science/von_mises.htm, [Cited on 02-May-2024]

After obtaining radii, the bending stress equation [39] can be reformulated to Equation 6.17 such that it indicates what the maximum height is, in order not to exceed maximum stresses.

Taking a safety factor of 2, this results in a maximum vertical height of 5 cm, a frontal rod radius of about 2.2 cm, and a rear rod radius of about 1.7 cm. These numbers are significantly lower than expected and results in a vertical rod height which seems too low to fit any attachment mechanism. Hence, the surface area of the rods was increased by changing the safety factor of the axial stress to 7. This leads to a maximum height of 35 cm, a number high enough for a mounting mechanism of the rear rods. Now the front rod has a radius of 4 cm, and the rear rods have a radius of 3.2 cm. If the rear rods are banked at a 30° angle with the maximum height, and the front rod is vertical with a length of about 5 cm, this leads to a total rod mass of about 8 kg per tank. Such a mass is insignificant in the larger scheme of the aircraft and does not need to be optimised. Additionally, due to the high safety factor for the axial stresses, this accounts for additional unaccounted stresses.

6.4.4. Tank Removal Operations

With the defining feature of this aircraft being the external fuel tanks, an explanation of their removal in normal operations as well as emergencies is elaborated.

The aircraft utilises rails that line the width of the airfoil. As seen in Figure 6.6, such rails are long enough to facilitate the alignment of the tanks whilst being off-loaded from the trucks on the ground. This means that the trucks can align themselves under the wing without being absolutely accurate. Then they are raised and guided through the rails until attached via a hooking mechanism, which stays engaged during flight. Loads are transferred between the tank and wing via rods fabricated of Al-2219. Once landed, the hooking mechanism disengages, allowing for the tanks to be rolled off the railings onto the truck beds, thus completing the cycle.

In order to be able to jettison the fuel tanks in the air or during a hard landing, explosive bolts and electrical hinges can be used, as is the case for military drop-tanks [10]. The procedure of this jettisoning would be as follows: first, the pilot presses a release button in the cockpit with the correct switch selection. Following from this, a pyro-electric charge is sent, ensuring the explosive bolts connecting the rails to the tank are activated. The tanks subsequently are pushed away from the plane under high pressure, causing a nose dive trajectory due to their front C.G. position.

6.4.5. Liquid Methane Fuel Tank Connections

When it comes to connecting the liquid methane tank to the aircraft propulsion system, a fuel line and pressure line will extend from the tank and run through the wing box to be ultimately connected to the gas tanks in the fuselage. Moreover, a filler cap is present on the bottom of the tank in order to enable refuelling without detaching the tanks, as well as a top opening providing the possibility for venting.

In order to be able to control the fuel flow from the external fuel tank to the internal gas tanks, the liquid methane fuel flow is controlled by fuel level control valves that automatically regulate the fuel flow from the fuel tanks to the vaporiser and ultimately the internal gas tanks. Furthermore, a fuel shutoff valve, controlled by the engine switch, enables fuel to enter the fuel pumps [40]. Moreover, to enable the pressure control of the tank, the pressurised air is controlled by a two-position fuel tank pressure relief valve connected to the pressure line. Additionally, a thermal relief valve on the pressure line is installed to prevent pipeline over-pressure. However, condensation drains will likely not be necessary due to the outside air temperature never getting past −160 °C, as the lowest temperature expected during flight is −90 °C, thus no condensing of the gaseous methane is predicted.

[10] https://pyroalliance.ariane.group/en/defence-activities/missile/explosive-bolts/, [Cited on 17-June-2024]

To allow the pilot to control the available fuel left in the tank, a fuel quantity gauge is to be used on the instrument panel, indicating the total fuel supply as measured by the densitometer.

6.4.6. Fuel Tank Sloshing

When in flight, fuel will be continuously burnt off. Throughout this process, the tank will gradually get emptier and the liquid methane will start to slosh around. Manoeuvre-induced transient as well as steady-state sloshing can thus be expected in the partly-filled tank. These dynamic load shifts act in the roll and pitch planes, thus potentially adversely affecting the roll and pitch of the aircraft as a whole. An effective method to limit the magnitude of fuel sloshing in the tank, is by sectioning the inside of the tank by means of baffles. These not only suppress the intensity of the sloshing, but also enhance the fuel tank structural integrity [41]. The baffles themselves feature a large central orifice and a semicircular opening at the bottom that serves as an equaliser.

According to [41], the baffles should be mounted at specific intervals within the tank. Scaling the baffle spacing as proposed by this study and adapting it for usage in the external fuel tank, the baffle positions as shown in Figure 6.7 are found.

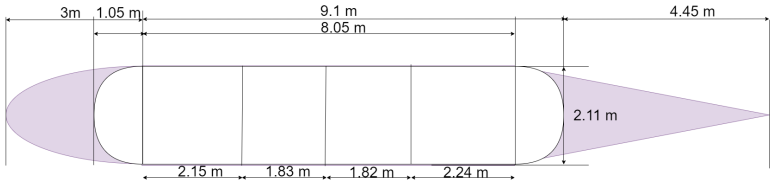

Figure 6.7: Layout of the external fuel tank with baffles.

6.4.7. Dump-and-Burn Methane Fuel System

In the event that the aircraft has taken off and needs to perform an emergency landing, there is a need to dump a large proportion of the fuel, in the range of tens of thousand of litres. If left unburned, methane released to the atmosphere will lead to a much more devastating impact compared to carbon dioxide [11]. Therefore, it seems appropriate to burn the dumped fuel in what is called a 'dump-and-burn'. It is known that usual fuel dump systems on commercial aircraft sometimes placed on the tip of the wing [42]. However, in order to assure the reliability of such a vital system, it is preferred to have it be placed right at the fuel tank. Reliability will be increased due to the small line of fuel, and few connections necessary. Hence, a nozzle will be placed at the back of the tank fairing, alongside with burners to ignite the fuel. To ensure that the fuel is being continuously ejected at a desired fuel flow, a valve and pumping system will be put into place. The location of this fuel system can be visualised in Figure 6.8.

6.4.8. Fuel Tank Skid-Pad

In the unlikely event that the back of the fuel tank strikes the ground, precautions have been set in place. Precautions are necessary due to the highly explosive nature of pressurised methane fuel tanks. In some existing commercial aircraft, the back of the plane is protected from tailstrikes by having a skid-pad placed where impact is most likely to occur [12]. Seeing as there is sufficient place inside the rear fairing of the fuel tank, this option is viable for our design too. In Figure 6.8 a skid-pad can be seen in its engaged position. Notably, the skid-pad will only be in its engaged position during take-off and landing, due to aerodynamic reasons.

[11] https://www.unep.org/news-and-stories/story/methane-emissions-are-driving-climate-change-heres-how-reduce-them, [Cited on 12-June-2024]

[12] https://www.atsb.gov.au/publications/investigation_reports/2016/aair/ao-2016-131, [Cited on 05-july-2024]

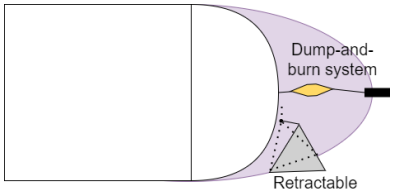

Figure 6.8: Close-up of the systems in the back of the fuel fairing, shown in purple (tank drawing not to scale).

6.5. Gaseous Methane Tank Sizing

Gaseous methane tanks are required to have a suitable throttleability, and shortly sustain thrust in emergency situations. These are placed within the wing in order to ensure the shortest feed lines possible, thus reducing pressure losses and improving safety. For these tanks, there are two requirements. Firstly, they have to store enough fuel to power the engines at maximum power for 30 seconds, and secondly, they have to store pressures larger than the combustion chamber pressure. The second requirement ensures that there is no pump required between the gas tanks and the engine. Given that each engine has a cruise mass flow of about 0.53 kg/s section 6.2, it is assumed that the maximum thrust is twice this mass flow. This would result in about 32 kg of mass required per engine. Additionally, the Leap-A engines have a total pressure ratio of about 40:1 [13], leading to a combustion chamber pressure of 40 bars at sea level. Due to such high pressures, it is necessary to design gaseous tanks which are in the shape of a cylinder. The end caps of these tanks are taken to be half-spheres. Looking at the wing, it has been found that three tanks with each a length of 1 meter can fit. The tank closest to the root can have an outer diameter of 42.2 cm, the next tank a diameter of 39.9 cm, and the last tank a diameter of 37.7 cm. These dimensions were determined looking at the airfoil and accounting for a margin of 3 cm at the top and bottom due to the stringers which are present. A visualisation of the location can be seen in Figure 6.9. The pressure within the tanks necessary to hold the required mass, can be determined using Equation 6.18.

$$P = \frac{n \cdot R \cdot T}{V_{air}} = \frac{m \cdot R \cdot T}{V_{air} \cdot M} \tag{6.18}$$

Here, it is assumed that all tanks are kept at the same pressure, as this helps with the pumping system. Additionally, the temperature has been taken to be −50 °C, as this is the temperature to which the heater heats up the liquid methane. Taking the equations Equation 6.8 and Equation 6.9, and combining these with the previous equations, assuming constant pressure and the total volume provided in the wings (which includes the structural thickness), a required pressure of 208.5 bars was found. Additionally, looking at all the various wall thicknesses for the three tanks, and taking the density of Al-2219, a total tank weight per wing of 434 kg was found.

6.5.1. Gaseous tank placement

As is seen in Figure 6.9, the general placement of the gaseous tanks is denoted, spanning from the fuselage. The tanks are positioned in the wing, close to the engine, to allow for direct feeding into the combustion chamber at high pressures. They are positioned at around 38 % of the chord, as this is the part of the wing where the airfoil is the thickest. With the gaseous tanks in the wings, space is also cleared from the central fuselage, which maximises space for cargo and other systems. A limitation preventing a single continuous tank are the ribs that span the airfoil. As such, three tanks are conceived, each fitting between the ribs (which have a spacing of 1 metre). They are fitted at the thickest part of the airfoil, however as the wing gets thinner as it extends, the tanks have a smaller diameter as they progress along the wing. The tanks have the same pressure in each, thus allowing for direct injection of the gases into the combustion chamber without need for excessive plumbing. That being said, the tanks will hold different masses of gaseous methane, respective to their size.

[13] `https://www.mtu.de/engines/commercial-aircraft-engines/narrowbody-and-regional-jets/leap-1a/-1b/`, [Cited on 12-June-2024]

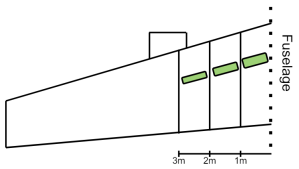

Figure 6.9: Placement of the gaseous methane tanks (Green Elements).

6.6. Auxiliary Power Unit

During on-ground operations, the Auxiliary Power Unit (APU) delivers bleed-air and electrical power to the aircraft. Furthermore, it is able to deliver in-flight backup power in case of an emergency. Different types of APUs are available, consisting of both combustion type and fuel cell type APUs. Passenger transatlantic aircraft, such as the A321neo, typically use combustion type APUs located in the tail of the aircraft. More recently, however, advances are being made in fuel cell APUs, and research is showing its benefits in reducing local emissions at the airport. A comparison between both type of APUs is provided in Table 6.3.

Table 6.3: Comparison between conventional combustion APU and fuel cell APU.

Characteristic	A321neo APU	Fuel Cell APU	Comments
Fuel Type	Kerosene	SOFC	Combustion APUs have commonly been fuelled by kerosene, however methane as APU fuel is possible.
Efficiency	20-30%	32-48%	SOFC efficiency in cruise is 45-48 % and during on-ground operations 32-36%.
Weight	164 kg	221-522 kg	The fuel cell APU will be 2-4x as heavy as the combustion type
Location	Tail cone A/C	Distributed on A/C	To reduce energy losses for fuel cell APUs, the lines between the electrical source and loads should be minimised.
Noise	High	Low	However, muffler is installed on combustion APU to limit noise pollution.
Emissions	High	Low	Fuel cell offers a 0.4-1.6% NO_x reduction of total aircraft fuel burn in cruise and 100% reduction at gate. During landing and take-off it offers a 15% NO_x reduction.
TRL	High	Low	Combustion type APUs are readily available. Fuel cell APUs have not yet been used on commercial aircraft.

Different types of fuel cell APUs are considered, specifically the Solid Oxide Fuel Cell (SOFC) and Proton-Exchange Membrane Fuel Cell (PEMFC). The SOFC fuel cell type APU was selected for this comparison, as SOFCs are more suitable for longer mission aircraft with large energy consumption compared to the lower power draw provided by PEMFCs. Furthermore, the PEMFC type fuel cell APUs offer issues with regard to water management and is less tolerating to impurities in the fuel compared to SOFCS. Thus, SOFCs are considered the most promising option for the APU [43].

Considering the requirements for the APU on board, a total power requirement of 460 kW was found. This auxiliary power estimate was based on the power draw from the Environmental Control System (50-100kW), the electrical system (cabin lighting of 2 kW, avionics of 5-10kW, galleys of 5-10kW and in-flight entertainment of 3 kW) and pneumatic systems (engine start of 150-200kW and anti-icing of 30-50kW) [44]. Taking the upper limits and adding a safety margin of 1.3, a peak power draw of 460 kW was found. It was then validated by comparing the power draw to that of similar aircraft, such as the A320-200, with a power draw of 450 kW [45].

As it is operative during a very small portion of the flight, namely roughly 10 minutes before and 10 minutes after landing compared to the 9.25 h block time subsection 13.6.1, the increase in mass was determined to outweigh the fuel savings/emission reductions. Furthermore, the TRL was deemed a critical factor to meeting the 2030 timeline as set by CH4-STK-09. However, a recommendation is to explore the use of the fuel cells further, especially when they are in a higher TRL level, in order to reduce emissions further. According to [46], in order to use methane as the fuel to power the fuel

cells, a fuel processor is needed to convert it to hydrogen first. After it is transformed to hydrogen, it can enter the fuel cell. A challenge that should be addressed is the maximum output work of this methane-supplied system is estimated at 250 kW. Since the total power estimate during peak load was found to be 460 kW, one such system would not be sufficient. Thus, developing such a methane fuel cell system capable of delivering the required peak power is proposed as a future recommendation.

6.7. Fuel System Weight Estimation

In order to estimate the mass of the entire fuel system, all components have to be looked at individually. The fuel system is composed out of the liquid and gaseous methane tanks, the pumps, the piping, and engine-fed and electric heaters.

Regarding the liquid methane tank, this mainly consists out of the aluminium inner lining, the polymer foam insulation, the outer CFRP fairing, the foam impact absorbent, the skid-pad, the dump-and-burn system, and the supporting structure. The first three have been found for each tank to be 477 kg, 102 kg, and 182 kg, respectively subsection 6.4.2. While there is no data available for existing skid-pad weights, or dump-and-burn systems, the latter three components have been set to 50 kg per tank. Lastly, the foam impact absorbent is negligible as observed in the fuel tank section subsection 6.4.1. Going on to the gaseous methane tanks, their combined weight per engine has been found to be 434 kg.

As is shown in Figure 6.1, there will be a total of 3 pumps needed for the entire fuel system. While the two pumps going into the gaseous methane tank will need to provide about 200 bars of pressure (pressure of the gas tanks), the other pump which leads directly from the liquid methane tank to the engine, will require only 40 bars of pressure (Max pressure of the combustion chamber). As it is difficult to find an approximate mass for these pumps, it has been assumed that the 200 bars pumps are 100 kg each and the 40 bars pump is 50 kg. The same way of estimation was taken for the fuel piping, as it was not possible to find existing pipes, which are able to sustain the same conditions as necessary. Therefore, a piping mass of about 100 kg per wing is given. It is to be noted that pressure valves are included as well. Lastly, while the engine-fed heater was found to be 120 kg each in section 6.3, an electric heater could not be found and its mass was taken to be 30 kg. Finally, after having estimated all the individual fuel system components, they are combined to reach a total estimate. This estimate is 3490 kg for the entire fuel system, or 1745 kg per wing. The removable part of the fuel system is 1922 kg in total or 961 kg per wing.

6.8. Verification and Validation

Verification and validation techniques were adopted to ensure proper calculation of mass flows and characteristics pertaining to the propulsion system. This was specifically focused on the mass flow of the fuel as this was a driving requirement for sizing the engine, gaseous methane tanks and propulsion system plumbing. The mass flow was driven by the efficiency of the engine, and thus was the focus of the verification and validation. Unit tests were performed on all the formulas used to verify the calculations performed for the engine fuel mass flow.

6.8.1. Verification

Verification of the code was performed by implementing unit tests. Each unit test looked at the output of temperature and pressure between stations within the engine. The output of the unit tests was compared to reasonable values to assess if the calculations were returning results of the correct magnitude. Furthermore, extreme value testing was implemented. Here, physical values were changed to 0 representing an extreme case that should theoretically change the mass flow to 0 kg/s. Values changed were: intake area, velocity, Lower Heating Value and bypass ratio. All of them resulted in 0 kg/s mass flow, apart from the bypass ratio, which increased it massively. This is to be expected, as all the air flow would go through the jet engine, thus requiring a lot more fuel to maintain the same air-fuel ratio.

6.8.2. Validation

Validation was performed by comparing the code to as close of a real life scenario as possible. As such, mass flows and efficiency ratios used in kerosene engines were observed and compared to the methane alternative engine. As close as this validates the engine, the data would have to be validated more rigorously before being brought to market. This should be done by developing a prototype engine and physically running it to assess real efficiencies, mass flows and thrusts generated.

6.9. Sensitivity Analysis

A sensitivity test was performed, reviewing how different variables relating to the mass flow of fuel in the engine would impact the results. Inputs were increased and decreased by 10 % of the value used for the final set of results, with the idea that a decreased mass flow (indicated in green)is more beneficial for the design of the aircraft.

Table 6.4: Results of sensitivity test performed on the engine.

Variable	Variation (%)	Fuel Mass Flow (% change)
Mach Number	+10	+10.90
Mach Number	-10	-9.09
Intake size	+10	+10.90
Intake size	-10	-9.09
Bypass Ratio	+10	-7.27
Bypass Ratio	-10	+10.90
Lower Heating Value	+10	-9.09
Lower Heating Value	-10	+12.72

To summarise Table 6.4, the mass flow relates more or less directly to the inputs involved in sizing the engine. Some elements such as editing the Lower Heating Value allow for increases in efficiency, but in reality would be very hard to implement. Several design recommendations can be concluded: the bypass could be increased to allow for more efficient thrust and thus further improve the overall efficiency of the aircraft. However, this is restricted by requirements of the aircraft, such as the maximum height under the wing, which restricts the diameter of the engine.

6.10. Recommendations

With future scope for research and development past the synthesis of this report, some recommendations on the propulsion system are suggested. Additionally, some recommendations are given to improve the design of the external wing tank.

With the goal of the aircraft needing to be energy efficient, a critical issue could be the release of Nitrous Oxide (NO_x) through the combustion of methane. A possible mitigation to this could be the recuperation of the emission back into the combustion chamber. This would work by having the NO_x heat above 300 ° C, thus splitting into Oxygen and Nitrogen[14]. This allows for more oxidiser in the combustion chamber, allowing for more fuel to be injected, thus producing more thrust. This could be implemented as a throttleability contingency in case the high pressure gaseous tanks fail. Moreover, it could be used to increase the maximum thrust of the aircraft in case it needs to go faster.

Furthermore, for the external wing tanks, experiments are to be done to quantify the load transfer to the pylons in the case of a strengthened tank for the bird strike case. Moreover, it is suggested to further investigate a system to recover the wing tanks in case of an emergency jettison, by for example adding a parachute system or drag flaps to prevent damage upon touchdown.

[14] https://auto.howstuffworks.com/question259.htm, [Cited on 06-June-2024]

7. Materials and Manufacturing

The material that is selected for a subsystem dictates many characteristics of its design. The density and strength properties determine the shape, thickness, and weight of components. For this reason, it is important to carefully consider the material chosen for specific subsystems so that it can optimally complete the task it must be designed for. In section 7.1 several materials are discussed, including more traditional and modern materials. Then in section 7.2 a material for the main structure of the fuselage is selected. In section 7.3 the same is done for the wing and empennage. The chapter concludes with section 7.4 in which the materials for several smaller subsystems are selected.

7.1. Material Properties and Selection

A vital aircraft design point focuses on the materials that make up the entire aircraft. Material selection drives the structural performance as well as the overall weight, which in turn influences the aircraft's performance. The critical components in terms of structural design, for which a material selection must be carefully assessed are the airframe and skin. The fuselage of the aircraft, both wings, and the empennage are some of the heaviest components on the aircraft, and although it is desirable to reduce their weights, it is important to select materials strong enough to support the frequent loads they will experience. In order to get a better idea of which materials are being considered for the main aircraft parts, the main options are listed and described.

Aluminium: The most commonly used aircraft material. A number of its alloys, such as Al-2024, are commonly used in the aerospace industry. Relative to other metals, it has a high strength to weight ratio, is resistant to corrosion and fatigue, and is also cost-effective. Additional benefits include ease of manufacturing, recycling, heat conductivity, etc. [1].

Modern Composites: Modern aerospace composites include Carbon-Fibre Reinforced Polymers (CFRP) as well as Fibreglass/GFRP. For CFRP, a carbon-fibre filament is generally bonded with layers of thermoset resins to create an applicable material[2]. It has superior weight saving and strength qualities at the cost of being expensive and difficult to mould. Many new jets such as the A350 and 787 apply these materials wherever feasible because the benefits and modernity make it very appealing [47].

Aluminium-Lithium Alloy: These are alloys consisting of namely, aluminium and lithium, however, they often also contain copper and zirconium. While still metals, the benefit is lower weight and improved strength relative to classic aerospace aluminium alloys. These properties come by way of the lithium added to the alloy blend, which lowers density while increasing stiffness [48].

Except for certain components such as the engine pylon, landing gear structure, windshield/windows, and nose cones, commercial aircraft do not have standard material layouts. It varies greatly in size, shape, availability, cost, etc. Just because a material has the best numbers does not mean it will be the best option. Many non-performance-related criteria also have the potential to drive a material selection decision.

[1] `https://www.thyssenkrupp-materials.co.uk/aerospace-grade-aluminum`, [Cited on 04-June-2024]
[2] `https://www.sglcarbon.com/en/carbon-fibers-and-cfrp/`, [Cited on 10-June-24]

7.2. Fuselage Selection

The fuselage is the largest part of the aircraft, however, its skin is very thin, supported by an internal structure, and needs to be pressurised during flight. Newer aircraft like the Boeing 787 and Airbus A350 have moved to use composites for their fuselage skin and structure, but classic aluminium alloys have been the typical backbone in the manufacturing of airliners for decades.

After consultation with Professor Calvin Rans PhD, various design paths were made clear. A driving reason why not to use composites for the fuselage skin is that it can be difficult to reach the desired skin thickness in the manufacturing process without having to exceed it. This is especially critical for a smaller airliner, especially in comparison to A350 and 787 wide-bodies, which have thicker skins[3]. In fact, the 787 is over-designed in thickness due to this manufacturing reason. As carbon-fibre laminates can only be placed in plys of a certain thickness, for very thin sheets the desired thickness is often overshot due to manufacturing reasons. This can negate the weight-saving benefits of CFRP entirely, thereby removing the reason for using it. Additionally, as the design is centred around sustainability, having to build large and complex facilities for manufacturing as well as committing to the very energy-intensive production process of CFRP for the aircraft fuselage seems sub-optimal [49].
The aforementioned reasons meant that CFRP was eliminated from consideration for the fuselage material, despite its expected and desirable weight-saving benefits. The fuselage material trade-off then remained between either a classic aerospace aluminium alloy, such as Al-2024-T3, or a modern third-generation aluminium-lithium alloy such as Al-Li 2198.

The decision between the two options boils down to an objective comparison of material properties, considering similar manufacturing processes and neglecting relative cost. Al-Li 2198, in comparison to Al 2024-T3, is simply a better performer. It has been seen in research that its Tensile Yield Strength is roughly 10 % to 20 % higher than its baseline counterpart [50]. This can be seen in Figure 7.1.

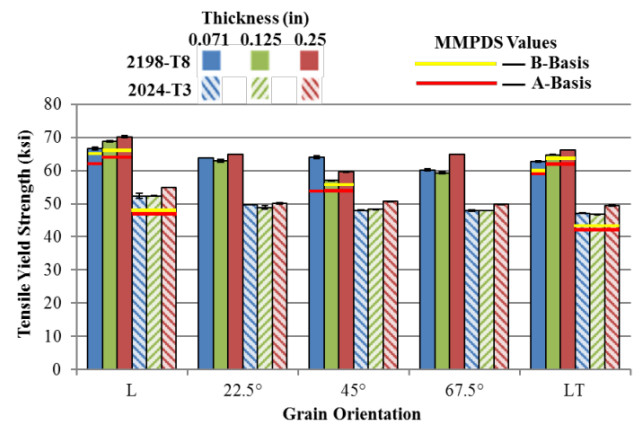

Figure 7.1: Comparison of average yield strength for Al-Li 2198-T8 versus Al 2024-T3 [50].

Considering Al-Li 2195 and Al-Cu-Li, for example, these each have tensile strengths of roughly 550 MPa relative to the Al 2024-T3 strength of 440 MPa [4] [5] [6]. Additionally Al-Li has a density in the range of 1.56 g/cm^3 to 2.69 g/cm^3 which is lower than the classic aluminium density of 2.78 g/cm^3 [6] [7]. In the consideration of fatigue, Al-Li has been proven to have a high fatigue crack growth resistance

[3] http://www.lb.boeing.com/commercial/aeromagazine/articles/qtr_4_06/article_04_2.html, [Cited on 04-June-2024]
[4] https://www.samaterials.com/aluminium/1774-2195-aluminum-lithium-alloy.html, [Cited on 04-June-2024]
[5] https://www.americanelements.com/aluminum-copper-lithium-alloy, [Cited on 04-June-2024]
[6] https://www.matweb.com/search/datasheet.aspx?MatGUID=57483b4d782940faaf12964a1821fb61&ckck=1, [Cited on 04-June-2024]
[7] https://www.matweb.com/search/datasheet.aspx?matguid=a242cc507a044923a3c3f5f0cb9f03c9, [Cited on 04-June-2024]

and superior overall qualities [8]. The following Table 7.1 displays the differing material properties of Al-2024-T3 and Al-Li 2198 in a bar form with a thickness below 6.3 mm, as seen on MatWeb and Wixsteel[9].

Table 7.1: Comparison between material properties of Al 2024-T3 vs. Al-Li 2198.

Material	Tensile Strength (Ultimate)	Yield Strength	E Modulus	Density
Al 2024-T3	395 MPa	290 MPa	73.1 GPa	2.78 g/cm^3
Al-Li 2198	476 MPa	427 MPa	76.5 GPa	2.69 g/cm^3

These considerations lead to the ultimate decision of going with an Al-Li alloy for the fuselage skin. The superior properties drive this decision. Additionally, the interior support structure, namely the stringers and spars will consist of the same material as the skin. This simplifies the number of required aircraft materials and is logistically beneficial for the manufacturing process. Additionally, Al-Li alloys are manufacturable in conventional methods, similar to conventional aluminium alloys. Ultimately as such Al-Li 2198 was chosen as the most suitable of the aluminium alloys and will therefore be used for the fuselage.

7.3. Wing & Empennage Selection

In general, the wing skin and wingbox structure are significantly thicker than the fuselage skin. This is due to the fact that it must provide similar stiffness but has a far smaller cross-sectional area. Additionally, it is non-pressurised and needs to provide support for two-point loads below the wing namely, the engine and the cryogenic methane tank. This material selection includes the wings sheets, the wingbox, high-lift devices, and control surfaces like the ailerons and speedbrakes. The same design choices can be made in the empennage, this includes the horizontal stabiliser, the vertical stabiliser, and respective control surfaces like the rudder and elevators.

Due to this higher sheet thickness, the reasoning that eliminated CFRP for the fuselage is void for the wing. CFRP is superior for weight and strength purposes in comparison to both Aluminium and Aluminium-Lithium. Additionally, the parts that will be constructed with it are significantly smaller and would improve the manufacturing energy.

In the case of CFRP, there are two main construction methods. A laminate is produced with ply layers stacked at varying angles, and various properties can be customised as desired. The result is a very strong material that is still lightweight. Alternatively, a sandwich is an especially lightweight construction where a low-density core is "sandwiched" between two skins. This core could be a honeycomb or foam. It is not as strong as a laminate but proves useful in areas that experience less loading and lead to weight saving [10].

The entire wingbox will be made of a CFRP laminate, as this provides the structural requirements needed and has multiple weight-saving benefits when compared to an aluminium alloy. All the aspects of the wingbox such as the spars, stringers and sheets will be made of the same laminate. The vertical and horizontal stabilisers will also have their wingbox made of a CFRP laminate, however, these two tail wingboxes are not designed at this stage. The leading edge of the wing, vertical stabiliser, and horizontal stabilisers are however made of aluminium. This is due to its superior and necessary heat conductivity relative to composites, which aids in de-icing and spreading warmth from the bleed air system used for de-icing. It also aids with erosion/bird-strike protection, as impacts from rain/hail

[8] https://www.totalmateria.com/en-us/articles/aluminum-lithium-alloys-1/, [Cited on 04-June-2024]

[9] https://www.wixsteel.com/products/aluminum-alloy/2000-series-aluminum-alloy/2198, [Cited on 04-June-2024]

[10] https://www.oxyblack.com/index.php/en/composites/laminates-sandwiches, [Cited on 04-June-2024]

can cause the delamination of a composite over time[11]. A design choice was made to use the classic and proven Al-2024-T3 alloy for the leading edges of the wing and empennage.

The selected material was ultimately Solvay CYCOM® 381 Epoxy Prepreg with AS4 Graphite Fabric and 195FAW Epoxy. The material properties were found from the MatWeb material database, which further gave a description that the material was suitable for, among other things, primary and secondary aircraft structures such as a wingbox [12].

Most material properties were given by MatWeb, and these are listed in Table 7.2. The shear modulus and the density were not listed on the MatWeb site. As these properties are needed for weight calculations and to find the twist angle due to torsion, they were estimated based of typical values for comparable carbon fibres. Density was estimated assuming a mix of 40 % resin and 60 % fibres, where the graphite fabric has a density of roughly 1.79 g/cm^3 and the resin has a density of 1.2 g/cm^3 [51]. The shear modulus was estimated based on typical carbon fibres. While this is not ideal, it allows for initial estimations of the wingbox weight.

Table 7.2: Material properties Solvay CYCOM® 381 Epoxy Prepreg with AS4 Graphite Fabric and 195FAW Epoxy.

Property	Value
Tensile strength	758 [MPa][13]
E Modulus	74 [GPa][14]
Shear strength	80 [MPa][15]
Shear Modulus	3.14 [GPa]*
Density	1.554 [g/cm^3]*

7.4. Miscellaneous Selections

There are two main parts of the aircraft that require stronger metals than any aluminium alloy can provide. The pylon, supporting the engine on the wing, is vital and must endure many kilonewtons worth of thrust produced, as well as forces from varying angles due to turbulence. It is commonly titanium, high-strength steel, an aluminium alloy or a mix. Each wing will have two pylon structures as another one is needed for the fuel tank. Then the landing gear must support the entire weight of the plane and transfer the load efficiently into the wheels and ground. Here, high-strength steel and titanium are commonplace. Lastly, the nose-cone section of the aircraft contains the radar system but is subjected to the largest frontal surface area of the aircraft. Therefore, it needs a material which is both strong and lets radio waves through it [16]. For this reason, glass-fibre is conventionally used and will be used in this design too.

An exact glass-fibre is not selected due to the limitations of detail for this report. Nevertheless, the selected material for the engine and tank pylons is Al-2219. Finally, a combination of Ti-6Al-4V and a High-strength AISI 4340 Steel will be used for the landing gear struts[17] [18]. These are laid out in Table 7.3.

Table 7.3: Display of titanium and steel for aerospace applications.

Material	Tensile Strength (Ultimate)	Yield Strength	E Modulus	Density
Steel 4130	1282 MPa	862 MPa	200 GPa	7.85 g/cm^3
Ti-6Al-4V	950 MPa	880 MPa	113 GPa	4.43 g/cm^3

[11] https://aircrafttechnic.com/aviation_technology/why-are-the-b787-leading-edges-made-from-aluminum/, [Cited on 04-June-2024]

[12] https://www.matweb.com/search/DataSheet.aspx?MatGUID=a556be59bfdb47609263a3b763790a11, [Cited on 11-June-2024]

[16] http://www.grahamhague.com/nosecones.shtml, [Cited on 18-June-2024]

[17] https://www.matweb.com/search/DataSheet.aspx?MatGUID=fd2df45bffa54018b54989bc14092d9f&ckck=1, [Cited on 04-June-2024]

[18] https://www.matweb.com/search/datasheet_print.aspx?matguid=a0655d261898456b958e5f825ae85390, [Cited on 04-June-2024]

8. Synthesis and Analysis

Having concluded the preliminary design of the main subsystems of the aircraft, they need to be synthesised into a coherent design. However, several concessions have to be made to integrate the separate (sub)systems effectively. An iterative process is employed, where the design is continuously optimised to enhance its performance. This process is introduced in section 8.1, outlining all the undertaken steps. Each step is elaborated upon in dedicated sections, with section 8.2 focusing on a Class II weight estimation. Subsequently, section 8.3 covers the procedures behind the centre of gravity analysis. Building on that, section 8.4 introduces a ground loading diagram, which is then utilised in the creation of a scissor plot as explained in section 8.5. Afterwards, the design aspect of the landing gear storage is presented in section 8.6. The synthesis concludes with the presentation of the final aircraft dimensions in section 8.8, followed by an analysis of the aircraft's performance in section 8.9. Verification and validation in section 8.10 and the sensitivity analysis in section 8.11 verify, validate and prove the design is the most at this stage. Finally, the entire process is briefly reviewed, along with recommendations for further enhancements in section 8.12. Once the Synthesis is completed a CAD model of the aircraft was made, which is depicted in Figure 8.1.

Figure 8.1: The CH4llenger

8.1. Iterative Process

The design was iterated using Python until a converged MTOW was produced by the tool. The process started with the initial weight of 103 000 kg; an output of the Class I weight estimation [1]. The next step was to recreate a previously constructed wing loading diagram. With the initial Class I weight and the maximum thrust of the two CFM LEAP-1A engines, a thrust-to-weight ratio constraint was implemented to ensure that the design point is located below it, otherwise necessitating more powerful engines. This can be seen as the red horizontal line in Figure 8.2. The white area in the middle of the diagram shows all the design points where the wing and thrust loading are sufficient to comply with the requirements. In this area, the right-most design point was chosen, as it gives the highest wing loading and thus the lowest wing area. This is highlighted by the black point.

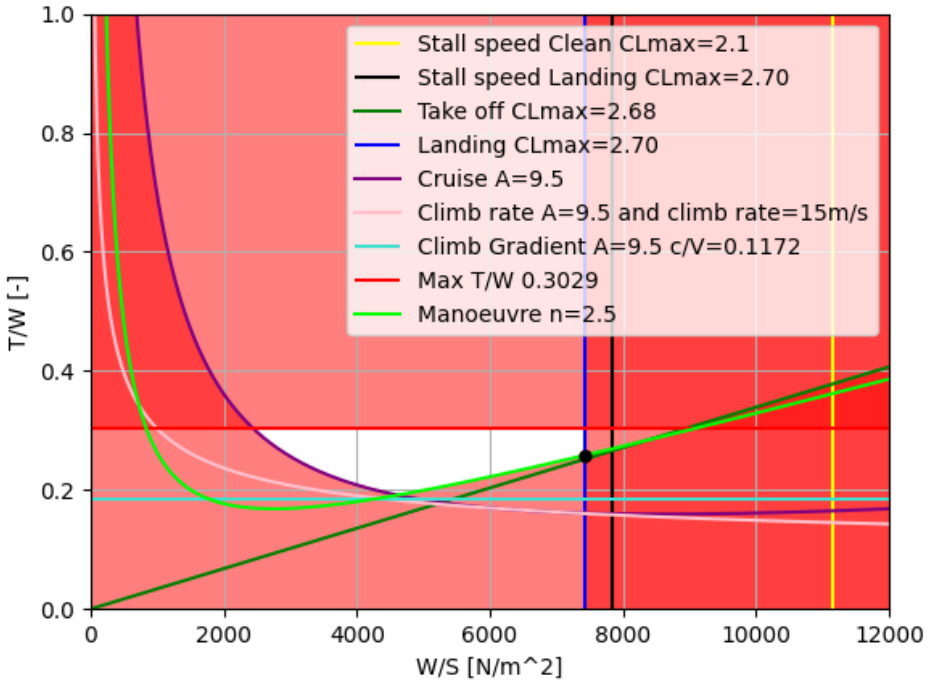

Figure 8.2: Wing and thrust loading diagram showing design point for the aircraft.

With the wing loading obtained, the wing was sized using the methods described in section 5.2 along with the ailerons and high lift devices. After computing the wing planform dimensions, a Class II weight estimation was performed which produced the weights of the individual subsystems, as described in section 8.2. The next step was empennage sizing, which was an iterative process by itself and was performed as a sub-iteration inside the overall process.

An initial sizing of the empennage was first performed, where the starting values were taken from section 5.6. With the size and placement of the empennage known, the wing was placed at a position complying with the constraints described in section 8.6. Then, a C.G. analysis was performed as described in section 8.3. Then, a ground loading diagram was created as described in section 8.4. With the C.G. range and scissor plot created in section 8.5, it was solved for the smallest tail area required. After doing so, the new weights of the empennage were calculated, which, along with the updated location of the main wing, was inserted into the beginning of this inner loop for the tail sizing. This process was repeated ten times, to ensure a converged solution, with the final values subsequently returned to the outer/main loop of the iterative process.

Finally, with the obtained empennage weights, a new wing loading diagram was created, concluding the outer loop, which was to be iterated upon until the MTOW converged within 1 % of its previous run. Had the MTOW started to diverge in the first five cycles, the iteration would have been stopped, and the code revisited to discover any potential faults needing addressing. To visualise the complete iterative process, a detailed layout of the undertaken steps was created and can be found below.

1. Use the weights from the Class I weight estimation as inputs to the iterative process.
2. Create a wing Loading diagram.
3. Compute the wing planform dimensions.
4. Perform a Class II weight estimation using the Raymer method.
5. Perform the inner loop.

(a) Size the empennage initially.
(b) Place the wing according to the constraints of the landing gear placement.
(c) Perform a C.G. analysis.
(d) Create a ground loading diagram.
(e) Create a scissor plot and solve it for the smallest horizontal tail area .
(f) Update the tail sizing and weight.
(g) Update the location of the main wing.

6. Iterate by going back to step 2.

8.2. Class II Weight Estimation

In order to obtain a Class II weight estimation, several methods were considered. While some of them envisioned more straightforward calculations, they would be lacking in accuracy. Simultaneously, one of the considered methods, FLOPS [52], promised higher levels of accuracy, as it is based on more recent statistical data. However, after initial attempts, it was determined to be too extensive and elaborate for the time and resources available. As a result, the Class II weight estimation was executed using the method found in Raymer [53], given its overall well-rounded trade-off between accuracy and complexity.

Having selected the method, the equations corresponding to it were converted into a Python code to allow for future iterations of the design. Based on that, the weights of separate aircraft groups, as specified by the Raymer method [53], were computed. The final, post-iteration values of the analysis can be observed in Table 8.1, found below. Notably, the weight of the fuel system has been omitted from the Raymer calculations as, given the novel fuel implemented, the Raymer method would not yield reliable values. Instead, the system weight was manually calculated as explained in section 6.7, resulting in the weight of the entire system of 3490 kg, of which 1922 kg can be attributed the fuel tanks, with the remaining values contributing to the weight of the miscellaneous group; 'misc'. This group consists of the passenger seats, lavatories, and the weight of the crew.

Table 8.1: Masses of the main aircraft subsystems.

Variable	Value [kg]	C.G. location [m]
Wing	6 347.36	20.40
Horizontal Tail	781.70	39.47
Vertical Tail	650.28	39.58
Fuselage	9 636.95	19.20
Main Landing Gear	3 506.07	21.17
Nose Landing Gear	681.76	6.75
Nacelle	1 824.26	15.94
Handling Equipment	27.72	19.20
Anti-Ice	184.82	20.40
A/C	1 095.36	19.20
Furnish	1330.14	19.20
Avionics	834.73	19.20
Electric	541.82	19.20
Hydraulics	106.73	19.20
Instruments	142.27	19.20
APU	374.00	39.58
Controls	551.94	19.20
Starter	92.67	15.94
Engine_controls	44.34	19.20
Engine	7 882.50	15.94
Misc	3 797.27	19.20
Fuel system	3 456.84	19.20
OEW	43 881.54	19.31
Fuel tank	*1 922.00*	*21.41*
Fuel	23 529.52	21.41
MTOW	94 333.06	19.94

8.3. Centre of Gravity Analysis

Having obtained the weights of the aircraft subsystems, the new operational empty weight and the maximum take-off weight were computed. The obtained values, along with the component group weights stemming from the Class II weight estimation, have subsequently been used in the centre of gravity analysis, which involved calculating the local C.G. of each subsystem before obtaining a final centre of gravity of the entire aircraft as presented in Table 8.1. In the table, however, only the final, post-iteration, C.G. locations are presented allowing for a straightforward analysis of the final values.

In order to compute the centre of gravity of the component groups, it was assumed that the weights of the handling group, air conditioning, furnishing, avionics, electric group, hydraulics, instrument group, flight controls, engine controls and miscellaneous are to be used jointly with the fuselage of the aircraft, resulting in a joint centre of gravity located at $0.45\,l_f$ [5]. Furthermore, to finalise the centre of gravity of the fuselage group, the centres of gravity of the horizontal and vertical tail and the APU were computed using methods found in [5]. Finally, the weights and centres of gravity of the nose and main landing gear were also included, with their positioning assumed using a geometrical method as presented in [5]. Based on that, the final weight of the fuselage group has been calculated to be about 27 500 kg with the centre of gravity corresponding to approximately 20.5 m.

A similar approach was conducted for the wing group, where several component groups had their centres of gravity assumed to be the same. The C.G. of the wing of the CH4llenger as well as the anti-ice system was calculated to be located at 0.47 of the MAC. The engines, the nacelle group as well as the pneumatic starters, though, have been grouped into the propulsion group with a C.G. located at -0.667 of the MAC. The obtained values were subsequently used to calculate the C.G. of the entire wing group, which resulted in a final C.G. value of -0.212 of the MAC and a corresponding weight of about 16 300 kg.

Subsequently, the tank placement needed to be considered. For that, it has been decided to place it such that the C.G. of the filled tank is located at 70 % of the length between the front and back spar of its longitudinal position. This would lead to the same C.G. location as the plane wing itself, when expressed as a fraction of the local chord [8], minimising the torsional moment generated by the fuel tank. This, in turn, would result in the spars carrying the same fractions of the total weight throughout the wing length.

Finally, an initial placement of the wing with respect to the fuselage had to be performed. For that Equation 8.1 was used [5], concluding the preliminary centre of gravity analysis, the final overview of which can be found in Table 8.1.

$$X_{\text{LEMAC}} = X_{\text{FC.G.}} + \bar{c}\left[\left(\frac{x}{c}\right)_{\text{WC.G.}} \frac{M_W}{M_F} - \left(\frac{x}{c}\right)_{\text{OEWC.G.}} \left(1 + \frac{M_W}{M_F}\right)\right] \tag{8.1}$$

where $\left(\frac{x}{c}\right)_{\text{OEWC.G.}}$ is the C.G. of the OEW, assumed to be located at 0.25 of the MAC [54]. It is important to note, however, that the position of the wing was required to undergo significant changes before obtaining a final value due to the necessity of combining the aerodynamically optimal wing location with the placement of the landing gear as described in section 8.6.

8.4. Loading Diagram

Having calculated the centre of gravity of the aircraft groups as well as the placement of the wing with respect to the fuselage, the next step is to obtain a loading diagram. This will allow for the calculation of the shift in the centre of gravity when the aircraft is stationary and subject to the loading of cargo, passengers and fuel. The resultant values will later serve as input for the scissor plot, as presented in section 8.5. Furthermore, the obtained C.G. range is to serve a different purpose. It will pose an additional requirement on the landing gear placement, as it must always be located behind the most

backwards C.G. to prevent the tip-over of the aircraft. Finally, based on the compiled diagram, a C.G. value for the aircraft at its MTOW will be obtained.

The loading diagram incorporates several steps. First, the cargo of the aircraft is loaded. In the case of CH4llenger, it has been determined that 45 % of the cargo is to be stored in the front cargo hold and the remaining 55 % in the one located at the back of the plane. Finally, given that the cargo may be first loaded only in the front or only in the back, both scenarios have to be considered in the loading diagram. After the cargo has been loaded onto the plane, the passengers are to follow. For the loading diagram, it has been assumed that they are to follow the window-aisle-middle rule, in which, first, the window seat passengers are boarding the plane, followed by the ones seated by the aisle, with the middle-seat passengers entering the aircraft at the very last. Given that, the loading may occur either front-to-back or back-two-front, once again, both cases are being considered in the loading diagram. After the passenger boarding has concluded, the fuel may finally be loaded onto the aircraft. This is depicted by a straight, single line in the figure, as there is only one scenario in which the fuel can be loaded onto the CH4-04-A aircraft. The entire diagram has been compiled and presented in Figure 8.3, which can be found below.

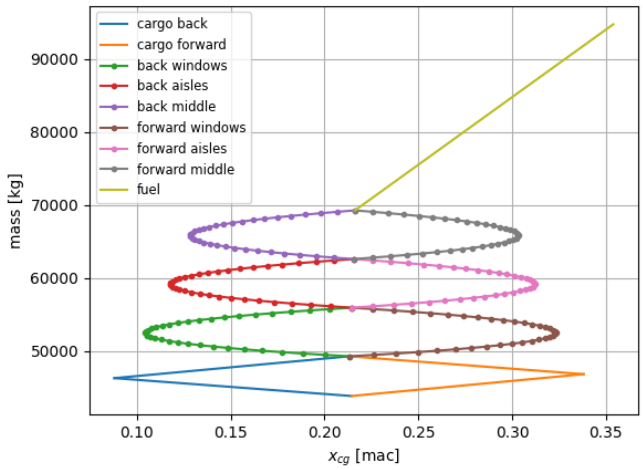

Figure 8.3: Loading diagram showing C.G. shift for different loading cases.

As can be observed in the above figure, the resultant range of the centres of gravity during aircraft loading is 0.074 to 0.372 when expressed as a percentage of the MAC. Furthermore, those values include a safety margin of 2 % on each side, ensuring that no tip-over occurs.

8.5. Scissor Plot

After obtaining the range in the centre of gravity of the aircraft, the next step in the design process is to re-assess the horizontal tail area with a scissor plot [55, 56]. With the scissor plot, the stability and controllability characteristics of the aircraft are plotted to find the required S_h/S for the aircraft. The tank is the main object of consideration for the scissor plots as it is what separates the aircraft from other conventional aircraft. This means that some additions to the scissor plot and loading diagram need to be made. Furthermore, for these plots, three aspects of the tank need to be considered.

Firstly, the tank has an influence on the C.G. of the aircraft. For that, it was decided to include the tanks as part of the fuel group rather than the OEW, given that the tanks will be removed during ground operations which needs to be considered in the resulting C.G. shifts.

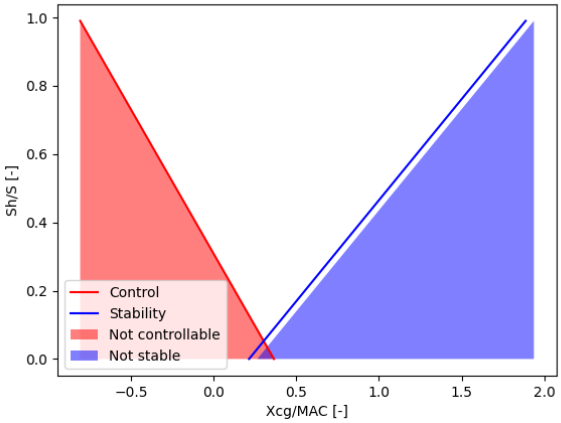

Figure 8.4: Scissor plot showing control and stability requirements on aircraft horizontal stabiliser.

Secondly, the influence on the aerodynamic centre needs to be considered. The position of the aerodynamic centre is important for the stability of the aircraft so the shift needs to be considered carefully. The aerodynamic centre of the tank itself is at 17% of the length of the tank according to Hoerner [57]. Taking the weighted average of the aerodynamic centre of the tank and of the wing, where the weight is based on how much lift each generates, the new a.c. location of the tanks and the wing can be located. Although, the aerodynamic centre of the tanks is located far in front when compared to the wing, it does not cause a substantial shift, given that the tanks do not create considerable lift.

Lastly, the tank generates an aerodynamic moment that needs to be taken into account for controllability, the most critical case for which is landing. As the tank is roughly symmetrical, it is assumed that its own aerodynamic moment at the aerodynamic centre is zero. As a result, the only moment that is to be generated around the wing is due to its lift and drag. For the lift, the resultant lift coefficient at landing is taken which at an angle of attack of 13° was found to be 0.12 [57]. This was subsequently multiplied by the distance between the aerodynamic centre of the tank and the aerodynamic centre of the wing and also normalised so that it is based on the wing area and not the diameter of the tank [57]. The drag coefficient, on the other hand, was found to be 0.066 which was also normalised to the wing area and multiplied by the height difference between the aerodynamic centre of the tank and the aerodynamic centre of the wing [58]. The obtained shift was then finally added to the overall aerodynamic moment for each tank.

With the controllability and stability curves plotted in Figure 8.4, the width between the control and stability curves must be able to fit the C.G. range of that aircraft. A wider C.G. range leads to a higher S_h/S to fit that range in between the curves. As a result, an interpolation is made to have a relation between the width of the 'scissor' and the front longitudinal C.G. position of the control curve. This interpolation is then used with the relation of the C.G. ranges for the wing placement as computed in section 8.4 to see what C.G. ranges lead to a stable and controllable aircraft regardless of the tail area. After that, the S_h/S ratio is calculated for the valid C.G. ranges, resulting in a tail area ratio, front C.G. position and C.G. range. Finally, the tail area is updated based on the wing area, from which the new weight of the empennage is calculated leading to an updated OEW and MTOW.

8.6. Wing Yehudi

For the main landing gear, it is desirable to store it in the wing as written in requirement **CH4-FUN-06**. When the landing gear is stored in the wing, it will result in a lower drag than putting it in large fairings which extend from the fuselage. Storing the gear in the wing also allows for a larger track-width which will prevent lateral tip-over. When initially sizing the wing, it was placed in front of the main

landing gear, however, if the gear needs to be stored in the wing, this approach has to be revisited. Moving the wing backwards to accommodate the gear or adding a so-called 'Yehudi' and shifting the wing backwards by a smaller distance. The first option is less feasible as initial iterations showed that the wing needed to be moved more than two meters backwards. This created problems on its own, one of which was the horizontal tail sizing. A preliminary stability and control analysis showed a big increase in the required horizontal tail area, leading to an increase in weight at the back of the aircraft, necessitating the placement of the wing even further aft. Based on that, it was decided to include the Yehudi. To make it a viable option, however, two constraints were imposed on it. First, the landing gear must be at most one meter behind the trailing edge. Secondly, the span of the Yehudi is to be limited to six meters, so as to limit the additional structural considerations required, while also making it comparable to the A321neo. Those constraints were subsequently used to find the optimal wing position in the iteration loop. The final values of the iteration can be found in Table 8.2, with the sketch of the yehudi presented below in Figure 8.5.

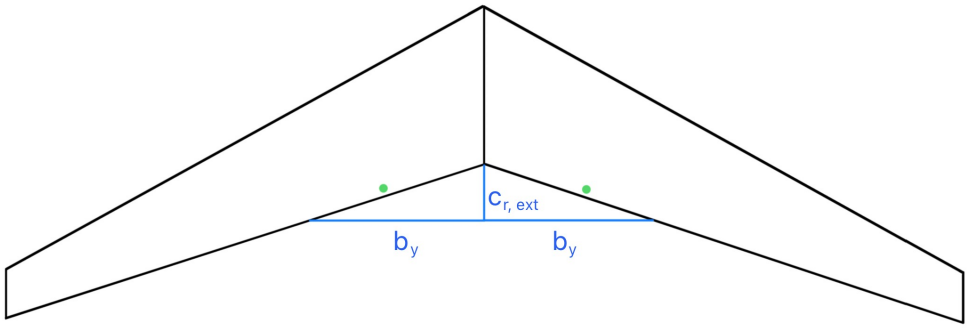

Figure 8.5: Sketch showing the initial concept for wing Yehudi.

As can be observed in the figure, the Yehudi (blue) extends the chord length of the wing planform (black) by having a 0° sweep until it intersects with the wing. The green dot represents the landing gear. Finally, an auxiliary spar was placed on top of the landing gear at the location of one meter in front of the trailing edge of the Yehudi. Its main purpose is to transfer the loads from the fuselage to the landing gear.

8.7. Landing Gear

The values in section 5.5 served as an initial estimate for the location and sizing of the landing gear, which was subsequently used for the calculation of the C.G. of the aircraft. Based on the analysis, it was found that the C.G. would end up much further forward than the C.G. obtained by means of the Class I estimation. It was also found that based on the scissor plot the wing was placed far in front of the main landing gear, making its storage problematic as described in section 8.6.

For the iteration described in section 8.6 it was decided to first set the landing gear length at 3.05 m as an average between the original length and a new length needed if the wing was placed in the forward position. This meant that the landing gear needed to be placed at least 20.8 m behind the nose to ensure the aircraft still had a scrape angle of at least 14 °. This also meant that the C.G. had to be at least 1.15 m in front of the main landing gear to ensure the tip-over angle of 16 °. The wing was then moved back to ensure that the landing gear could reasonably be stored in the wing. Equation 5.13 was then used to determine the position of the nose landing gear still having 8 % of the weight on the nose, leading to a nose landing gear position at least 13.3 m in front of the C.G. This iteration and a new look at the height of the C.G. led to a new idea for the track of the main landing gear, however, it was chosen not to move forward with this to ensure the tank does not strike during bank and pitch. This then leads to placement values described in Table 8.2 - Table 8.5.

8.8. CH4llenger Characteristics

Table 8.1 as well as Table 8.2 - Table 8.5 display the values returned after 10 iterations. While Table 8.1 focused on the final weights of the component groups, summing towards the final value of the OEW and, subsequently, MTOW as well as the corresponding centres of gravity, in Table 8.2 - Table 8.5, the most important dimensions of the respective components are presented. Table 8.2 focuses on the main systems of the CH4llenger aircraft, while Table 8.3 presents the data for the HLDs and control surfaces located on the wing. Afterwards, Table 8.4 summarises the characteristics of the empennage, while, finally, Table 8.5 includes the physical flight characteristics of the CH4llenger aircraft.

Table 8.2: Final Characteristics of the CH4llenger systems.

Group	Variable	Value	Unit
Wing	A	9.500	[-]
	S	122.01	[m^2]
	b	34.05	[m]
	sweep	26.36	[deg]
	dihedral	2	[deg]
	taper	0.31	[-]
	cr	5.48	[m]
	ct	1.69	[m]
	c_mac	3.92	[m]
	y_mac	7.01	[m]
	x_lemac	18.55	[m]
	sweep_LE	28.84	[deg]
	sweep_TE	18.16	[deg]
	winglet_ct	0.51	[m]
	winglet_b	1.59	[m]
	front_spar	20	[% MAC]
	aft_spar	75	[% MAC]
Yehudi	b_yehudi	6.00	[m]
	cr_extension	1.99	[m]
Fuselage	l_fuselage	42.68	[m]
	d_fuselage	3.89	[m]
Engine	l_engine	3.20	[m]
	d_engine_max	2.70	[m]
	y_engine	5.75	[m]
Landing Gear	x_mlg	21.17	[m]
	y_mlg	3.70	[m]
	x_nlg	6.75	[m]
	l_mlg	3.05	[m]
	l_nlg	2.95	[m]

Table 8.3: Final Characteristics of the HLDs and control surfaces.

Group	Variable	Value	Unit
Ailerons	aileron_start	14.94	[m]
	aileron_end	16.77	[m]
	aileron_b	1.83	[m]
	aileron_area	0.89	[m^2]
	aileron_deflection	25	[deg]
	aileron_chord	25	[% local chord]
Flaps	flaps_deflection, TO	25	[deg]
	flaps_deflection, land	50	[deg]
	flaps_chord	15	[% local chord]
	flaps_ref_area	39.49	[m^2]
	flaps_end	14.84	[m]
Slats	slats_ref_area	38.66	[m^2]
	slats_end	16.52	[m]

Table 8.4: Final Characteristics of the Empennage.

Group	Variable	Value	Unit
Horizontal Tail	x_htail	39.00	[m]
	V_h	0.96	[-]
	l_h	18.38	[m]
	A_h	5.00	[-]
	S_h	30.64	[m^2]
	Sweep_h	29.00	[deg]
	taper_h	0.26	[-]
	b_h	12.38	[m]
	cr_h	3.94	[m]
	ct_h	1.01	[m]
	cr_elevator	0.99	[m]
	ct_elevator	0.25	[m]
Vertical Tail	x_vtail	39.00	[m]
	V_v	0.08	[-]
	l_v	18.38	[m]
	A_v	1.82	[-]
	S_v	17.86	[m^2]
	Sweep_v	34.00	[deg]
	taper_v	0.30	[-]
	b_v	5.70	[m]
	cr_v	4.81	[m]
	ct_v	1.46	[m]
	cr_rudder	1.20	[m]
	ct_rudder	0.37	[m]

Table 8.5: Other Final Characteristics.

Group	Variable	Value	Unit
Other	C_L, cruise	0.73	[-]
	C_L_max	2.10	[-]
	$\Delta C_{L,max,TO}$	0.58	[-]
	$\Delta C_{L,max,land}$	0.60	[-]
	C_L_max, TO	2.68	[-]
	C_L_max, land	2.70	[-]
	CD_0	0.03	[-]
	e	0.78	[-]
	V_s	93.12	[m/s]
	V_s, land	68.89	[m/s]
	M_cruise	0.78	[-]
	M_dd	0.83	[-]
	cruise_altitude	38 000	[ft]
	Re	$2.53 \cdot 10^7$	[-]
	n_max	2.50	[g]
	D_tank	2.13	[m]
	thrust_max	281.92	[kN]
	T/W_max	0.31	[-]
	T/W	0.26	[-]
	W/S	7430.01	[N/m^2]

8.9. Performance Analysis

With the design of the aircraft concluded, its performance had to be analysed. For that, a payload-range diagram was created, as presented in Figure 8.6. In the diagram, two different curves can be observed. The first one is the original performance of the CH4llenger as presented in [1], while the second one

presents the updated design, encompassing the final iteration of the design.

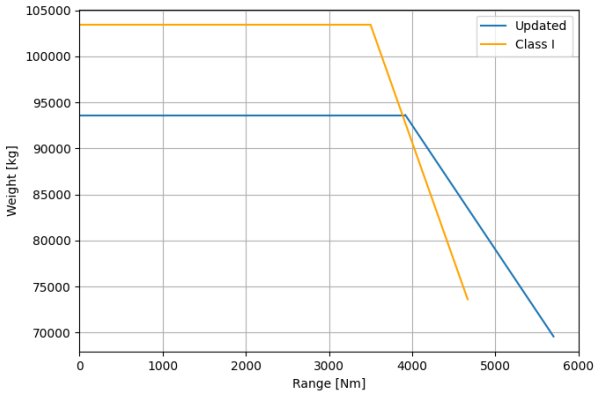

Figure 8.6: Payload-range diagram showing aircraft range for different loading cases.

When looking at the figure, two things can be observed. Firstly, the updated MTOW is considerably lower than previously. The reason for that is that the Class I version of the design encompassed preliminary assumptions and weights obtained from statistics, without considering the utilised materials and the actual design of the aircraft. As a result, the obtained weight was somewhat conservative, which became more accurate, as the design progressed. Secondly, the updated design range of the CH4llenger is 12 % higher than the one of the original estimate, standing at 3917 nm. This can be attributed to the unchanged weight of the fuel being carried. Over the course of the design process, it has been decided not to change it unless absolutely necessary, aiming for an extended range instead, allowing for additional routes to become available to the aircraft.

8.10. Verification & Validation

In order to verify the code, functions were tested individually upon implementation. With certain inputs, the outputs of the functions were compared with the results calculated by hand. Once a class was finished, it was run with dummy inputs and the results were checked as well before implementing the class in the main code. These unit tests verify individual components of the code. Finally, once all the code was implemented, system tests were performed to verify if a feasible design was returned by the iteration code. One of the tests was to check if the MTOW converges in the iterations to a final solution. In between the unit test and system test levels, more tests were performed to ensure the classes and functions were correctly connected. One of the encountered faults was that if the horizontal tail area was updated, the span and chord lengths were not updated. Another fault was discovered when calculating the length between the spars. It was found that the code was subtracting the front spar location from the rear spar, whereas, in reality, it should be in reversed order. As a result, it was changed in the code to function correctly.

The validation process compares the design parameters to a real-life aircraft, ensuring the aircraft parameters are of the correct value. Subsequently, the design is validated by means of the compliance matrix if the design fulfils the requirements, as will be elaborated upon in chapter 15. In terms of comparing the design parameters to a real-life aircraft, however, there is no methane-powered aircraft in production at this moment. As a result, a similar-sized conventional aircraft, the A321neo [15], will be used to compare the design parameters. This is done in Table 8.6 as can be observed below.

Table 8.6: Comparison of A321neo and CH4llenger.

Variable	A321neo	CH4llenger	Relative difference [%]
MTOW [kg]	93 500	94 333	0.9
OEW [kg]	48 725	43 882	-9.9
S [m^2]	122.4	122.0	-0.3
b [m]	32.58	34.05	4.5
S_h/S [-]	0.253	0.251	-0.7
$\Lambda_{0.25}$ [deg]	25.0	26.4	5.6

The OEW of the CH4llenger presents a noticeable difference by being almost 10 % lower than the one of the A321neo. This was expected, however, as the weight of the fuel tank is already included in the OEW of the A321neo, unlike in the case of the CH4llenger aircraft, where the fuel tank is a removable item and not fixed to the aircraft. Furthermore, the difference in wingspan (without winglets) was expected, as the CH4llenger has a higher wing aspect ratio compared to the A321neo. The difference in sweep could be explained by the fact that Airbus has more time and resources to develop a wing that is more optimised for aerodynamic performance. Based on this, it can be concluded that the CH4llenger is comparable to the A321neo. At the same time, however, there are still major differences due to the external tank, necessitating the testing of the prototype in order to validate this design.

8.11. Sensitivity Analysis

The sensitivity analysis assesses how the design would react to a variation of inputs. If a different set of inputs leads to a better design, the inputs need to be reconsidered to find the most optimal design. In this analysis, the following inputs were changed by ± 10% one at a time (with the rest of the parameters remaining constant): Landing runway length (S_land, C_L_{max}, CD0, A, stall speed (V_{stall}), Thrust, and Fuel mass (M_fuel). With the rest of the inputs set by requirements, changing them would result in a design which does not comply with the requirements. Furthermore, a change of 10% was chosen as that difference would clearly show the changes in parameters whilst not drastically affecting the design. These changes in variables compared the relative differences among the outputs such as MTOW, Wing area and range. Finally, to identify a more optimum design, the new aircraft would have a larger range while presenting a lower MTOW. This is highlighted with cell colours.

Table 8.7: Change in design parameters based on change in inputs.

Variable	Variation	MTOW [%]	Wing area [%]	Range [%]
S_land	-10%	+1.022674	+13.78576	+2.771509
	+10%	+0.372584	-2.57356	-1.65646
C_L_{max}	-10%	+0.866441	+10.9991	+2.36521
	+10%	+0.352316	-4.64716	-2.66499
CD0	-10%	0	0	+5.571825
	+10%	0	0	-5.07734
A	-10%	0.11657	+2.188345	-3.50204
	+10%	+1.363244	+3.130891	+2.165008
V_{stall}	-10%	0	0	0
	+10%	0	0	0
Thrust	-10%	0	0	0
	+10%	0	0	0
M_fuel	-10%	-2.56042	-0.47537	-8.76803
	+10%	+3,692428	+5.647078	+8.374341

From Table 8.7, it can be concluded that there is no case where a difference in variable input would lead to both a decrease in MTOW and an increase in range. The variations in the V_{stall} and Thrust variables lead to no changes in the design. This can be explained by Figure 8.2, in which the stall speed constraint lines do not influence the design point as the landing and take-off constraints are much more limiting. The thrust also does not affect the design point as the change in thrust would change the vertical line constraint for the max T/W. With there being a margin between the design point and

this constraint the thrust shift would not lead to a different design point, meaning that the current design can be considered to be the most optimal from the perspective of the analysed parameters.

8.12. Recommendations

Having concluded the design process, the team looked into the potential ways of further enhancing it. Based on that, several recommendations have been created, which will be described in this section.

In Figure 8.2, there is space between the horizontal T/W constraint and the design point. Based on that, two future recommendations can be drawn. Firstly, a less powerful engine could be used, hence allowing for a smaller powerplant to be utilised in order to save weight. Alternatively, the take-off and/or manoeuvre requirements could be increased to land on a shorter runway or be able to sustain a higher load factor for manoeuvring.

Furthermore, due to time constraints, the sizing of the vertical tail was simplified to fit within limitations. As a result, its sizing is still extremely preliminary compared to the rest of the design. This, in turn, means that its size can be further optimised to enhance the vertical tail's performance and ensure compliance with requirements and regulations.

When researching tail configurations, the 'dorsal fin' was discovered which adds directional stability to the aircraft at a high angle of sideslip [59]. This can be looked at in more detail in a future design process.

Finally, when considering the final design after the iteration, the fuel weight of 23 529 kg and the Breguet Range equation used in Class I weight estimation, a range of 3900 nm was found to be attainable. A more precise range can be determined by testing a scale model in a wind tunnel to obtain more accurate lift and drag coefficients. From this, the fuel weight and tank size can be optimised, enhancing the performance of the aircraft. On top of that, a family of aircraft could be conceived, allowing for different types of routes to be traversed using various aircraft.

9. Structural Analysis and Design

The structural analysis of the wing was performed using the aerodynamic data of the selected wing described in section 5.2 obtained from XFLR5[1]. Additionally, the distributed weight of the wing and the point loading due to the engine and the methane tank were incorporated as span-wise functions. Subsequently, the shear force, bending moment, and torsion were obtained as functions of a point on the half-span, as shown in the diagrams in section 9.2. The wingbox was preliminarily designed such that it does not fail under the most extreme load case in section 9.3. The stiffness properties of the wingbox allowed for determining the deflections of the wing, as discussed in section 9.4. Then, the internal shear and moment distributions based on the subsystem weight and C.G. positions were derived as presented in section 9.5. Lastly, the fuselage was sized for similar failure modes as for the wingbox in section 9.6.

Due to the time and resource constraints, certain simplifying assumptions were made in order to efficiently determine the stiffness requirements of the wing. They can be found in Table 9.1. In case the analysis yields unexpected results, the assumptions made can be easily traced and the potential causes of the errors can be identified.

Table 9.1: Assumptions made in the structural analysis of the wing.

Identifier	Assumption
SA-01	The total lift force of the aircraft is produced by the wing.
SA-02	The wing is of a trapezoidal shape, i.e. the yehudi is neglected and the chord varies linearly with half-span.
SA-03	The normal aerodynamic force acts along the quarter-chord of the wing.
SA-04	The total drag of the wing is composed of the parasitic drag and the lift-induced drag.
SA-05	The normal force on the wing can be approximated as the resultant aerodynamic force.
SA-06	The effect of the fuselage can be neglected.
SA-07	The shear centre of the wingbox aligns with its geometric centre
SA-08	The gas tanks inside the wings have a negligible effect on the load distribution.

9.1. Aerodynamic Force Distribution

The available XFLR5 data consisted of a limited number of data points; C_L, C_D, C_m values at certain points along the span. The missing data points were approximated via an interpolation, such that the force distributions could be represented with a smooth function. Additionally, in order to make the aerodynamic force analysis more efficient, the XFLR5 simulation was only run once, for a typical cruise condition, as described in section 5.2. Therefore, in order to simulate different load cases, the following approximation was used:

$$C_L(y) = C_{L_0}(y) + \frac{C_{L_d} - C_{L_0}}{C_{L_{15}} - C_{L_0}} \left(C_{L_{15}}(y) - C_{L_0}(y)\right), \tag{9.1}$$

where the subscripts 0 and 15 indicate the angle of attack in degrees, chosen arbitrarily from the linear region of the $C_L - \alpha$ graph. Additionally, (y) indicates a local value of C_L along the span, and lack thereof indicates the total lift coefficient of the wing. C_{L_d} is the design lift coefficient, which accounts for different flight conditions. For a given load case, it is obtained from:

$$C_{L_d} = \frac{nmg}{0.5\rho V^2 S}, \tag{9.2}$$

[1] `https://www.xflr5.tech/xflr5.htm`, [Cited on 12-June-2024]

where the desired conditions; airspeed, air density, load factor, and mass, can be filled in. At this stage of the design, it is assumed to be an accurate enough approximation of the lift coefficient distribution for arbitrary load cases. Eight load cases were defined, covering all major phases of flight, in order to determine what the critical flight condition is in terms of structural loading. They can be found in Table 9.2.

Table 9.2: Load cases analysed in terms of structural loading on the wing.

Identifier	Description
LC01	MTOW, taxi, sea-level, 10 m/s
LC02	MTOW, 1.15 g take-off (flaps extended), sea-level, 82 m/s
LC03	Max. payload, 80 % fuel, 2.5 g turbulence, cruise, 230 m/s
LC04	Max. payload, 80 % fuel, cruise, 230 m/s
LC05	Max. payload, 80 % fuel, −1.0 g nose-dive, cruise, 230 m/s
LC06	Max. payload, 10 % fuel, approach, sea-level, 72 m/s
LC07	Max. payload, 10 % fuel, landing (flaps extended), sea-level, 72 m/s
LC08	Max. payload, 10 % fuel, touch-down (flaps extended), sea-level, 72 m/s

Moreover, as discussed in subsection 5.2.3, the high lift devices; flaps and slats, locally increase the lift coefficient, resulting in an overall increased total lift of the wing. During takeoff and landing, i.e. LC02, LC07, and LC08, the flaps are extended and the lift coefficient is higher. A good comparison is the LC06 approach and the LC07 landing, for which the other flight parameters are the same. This allows for investigating the effects of extending flaps on the shear force, bending moment, and torsion in section 9.2. The exact location of the high lift devices is shown in Figure 9.1, according to subsection 5.2.3.

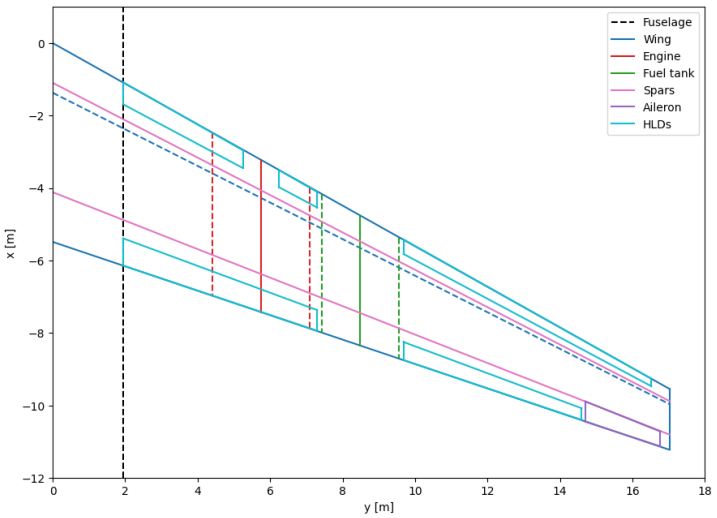

Figure 9.1: Top view of the simplified wing planform showing the location of the spars, HLDs, control surfaces, engine and fuel tank.

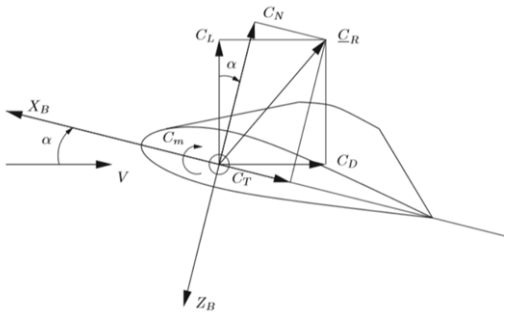

Figure 9.2: Body-centred coordinate system used in the structural analysis [60].

The drag coefficient was analysed in a similar manner, with the parasitic drag being interpolated as the lift coefficient before, and the lift-induced drag calculated from the already available local C_L, as per SA-04. Subsequently, the normal force coefficient is obtained according to:

$$C_N = C_L \cos\alpha + C_D \sin\alpha. \tag{9.3}$$

It should be noted that a Equation 9.3 is merely an approximation, and does not exactly reflect the force decomposition in Figure 9.2. However, it was assumed that, especially for small α, this is a valid approximation; see: SA-05. Additionally, the normal force is assumed to act along the quarter-chord line, as stated in SA-03.

9.2. Wing Loading

Three types of loading were analysed; the shear force along the $z-$axis, the bending moment of the wing around the $x-$axis, and the torsion around the $y-$axis. Subsequently, the most critical loading case was identified and the wingbox could be designed accordingly. The orientation of all plots is aligned with the coordinate system depicted in Figure 9.2.

9.2.1. Shear Force

The shear force along the body $z-$axis was obtained by integrating the distributed loading along the half-span; $q(y)$ [61]:

$$\frac{dS}{dy} = q(y), \tag{9.4}$$

where $q(y)$ is the sum of the distributed normal force and weight of the wing multiplied with the load factor:

$$q(y) = n\left(-N'(y) + w(y)\cos\alpha\right), \tag{9.5}$$

$$w(y) = \frac{W}{S}c(y). \tag{9.6}$$

$c(y)$ is the chord length at a point y, and $\frac{W}{S}$ is the previously obtained wing loading in section 8.1. Since the wing is effectively modelled as a cantilever beam of variable shape, the sole reaction force in the $z-$direction is acting at the root chord, i.e. the shear force at the wingtip must equal zero. The integral form of Equation 9.4 can therefore be written as:

$$\int_y^L \frac{dS}{dy} = S(L) - S(y) = \int_y^L q(y)dy \tag{9.7}$$

$$S(y) = -\int_y^L q(y)dy.$$

Lastly, integrating and adding unit step functions representing the point loading of the engine and the tank yields:

$$S(y) = -\int_y^L q(y)dy - nW_{eng}\left(1 - u_{y_{eng}}(y)\right) - nW_{tank}\left(1 - u_{y_{tank}}(y)\right). \tag{9.8}$$

In case of LC01; taxiing, and LC08; touch-down, an additional unit step function is imposed, namely

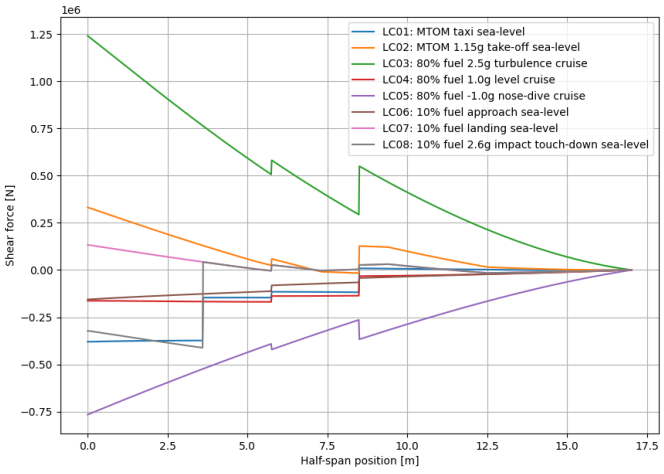

Figure 9.3: Shear force as a function of position along the wing half-span for the different load cases.

the reaction force on the main landing gear. All load cases are plotted in Figure 9.3.
It is immediately clear in Figure 9.3 that the two critical cases are the limits of the flight envelope; the 2.5 g and the −1.0 g manoeuvres at cruise speed. The "jumps" in the graph can be attributed to the two point loads, with the tank having a bigger impact on the shear force distribution than the engine due to its higher weight. The "jumps" are also scaled with the load factor, as can be seen when comparing LC03 to LC05. Additionally, in case of taxiing and touch-down, there is a relatively large "jump" associated with the reaction force on the MLG, which suggests that this point could benefit from additional reinforcements.

It should be noted that in case of LC04; level cruise, and LC06; approach at a point when the flaps have not been deployed yet, the shear force at the root has an unexpected negative sign. This is likely due to the $q(y)$ values being relatively small in those phases of flight, and the imperfect approximation of the normal force. Additionally, contrary to conventional aircraft, the weight of the tank produces a significant shear force. However, those cases are some of the least limiting, and adequate recommendations are made in section 9.9, suggesting a more in-depth aerodynamic analysis. To conclude, since LC03 results in the highest magnitude of the shear loading, it is taken as the most critical case in the next stages of the analysis. The safety margins are imposed later on in section 9.3.

9.2.2. Bending Moment

The bending moment around the aircraft body $x-$axis largely follows from the previously obtained shear force. It is calculated as follows [61]:

$$\frac{dM}{dy} = S(y). \tag{9.9}$$

Much like in Equation 9.7, the moment at the wingtip must equal zero, yielding the integral form:

$$M(y) = -\int_{y}^{L} S(y)dy. \tag{9.10}$$

Additionally, because of the sweep angle, there is a small contribution to the bending moment caused by the engine thrust, i.e.:

$$M_{eng} = T \sin \Lambda_{0.25c} z_{eng}, \tag{9.11}$$

resulting in:

$$M(y) = -\int_{y}^{L} S(y)dy + M_{eng}\left(1 - u_{y_{eng}}(y)\right). \tag{9.12}$$

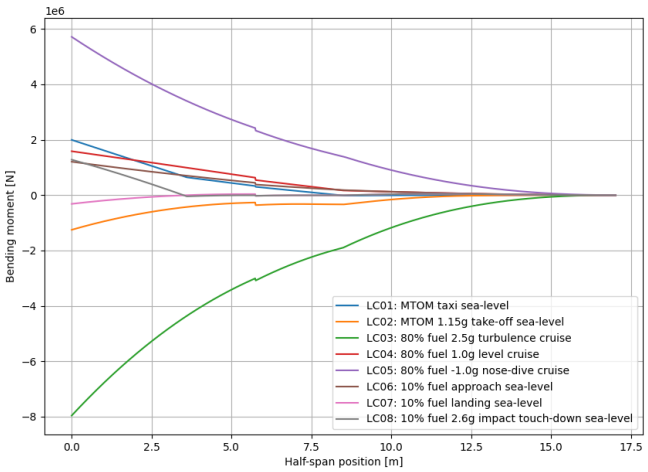

Figure 9.4: Bending moment as a function of position along the wing half-span for the different load cases.

As can be seen in Figure 9.4, the bending moment plots are of the opposite sign compared to the shear force plot, which follows from Equation 9.12. Thrust contributed to the bending moment in the same direction. Clearly, the two most critical loading cases identified in subsection 9.2.1 are once again the most limiting. It should also be noted that the bending moment is almost an order of magnitude larger than the shear force, due to integration.

9.2.3. Torsion

Torsion was the last loading mode considered, necessary to investigate the twist angle of the wing later on in section 9.4. The contributions to the total torque that were analysed are the normal force distribution, the pitching moment distribution, and the thrust component. As per assumption SA-07, the weight of the wing itself acts in the shear centre, therefore it does not contribute to torsion. The rate of change of torque was calculated using [61]:

$$\frac{d\tau}{dy} = N'(y)d_{s.c.}(y) + M'(y), \tag{9.13}$$

where $d_{s.c.}$ is the distance to the shear centre. After integrating and adding the thrust contribution as a unit step function, becomes:

$$T(y) = \int_y^L \left(N'(y)d_{s.c.}(y) + M'(y)\right) dy + T_{eng}(1 - u_{y_{eng}}(y)), \tag{9.14}$$

$$T_{eng} = T\cos\Lambda_{0.25c} z_{eng}, \tag{9.15}$$

$$M'(y) = C_m(y)0.5\rho V^2 c(y). \tag{9.16}$$

The moment coefficient was approximated for different conditions much like the lift earlier in Equation 9.1:

$$C_m(y) = C_{m_0}(y) + \frac{C_{m_d} - C_{m_0}}{C_{m_{15}} - C_{m_0}} \left(C_{m_{15}}(y) - C_{m_0}(y)\right). \tag{9.17}$$

Torsion for all load cases is shown in Figure 9.5. While the LC03 2.5 g pull-up case is once again among the critical cases, the take-off case; LC02, reaches marginally larger torque magnitudes between the root and the engine. This is due to the fact that the thrust required during take-off is typically higher than that in level cruise. The exact engine settings used in the analysis for each load case were approximated based on an example Quick Reference Handbook in a Flight Crew Operating Manual [62]. Additionally, it can be seen in Figure 9.5 that the torque produced by the engine is the largest contributor to the overall torque. This is because, coincidentally, the shear centre was found to be merely $0.03c(y)$ away from the quarter-chord line; the contribution of aerodynamic forces happens to be relatively small due to the short moment arm.

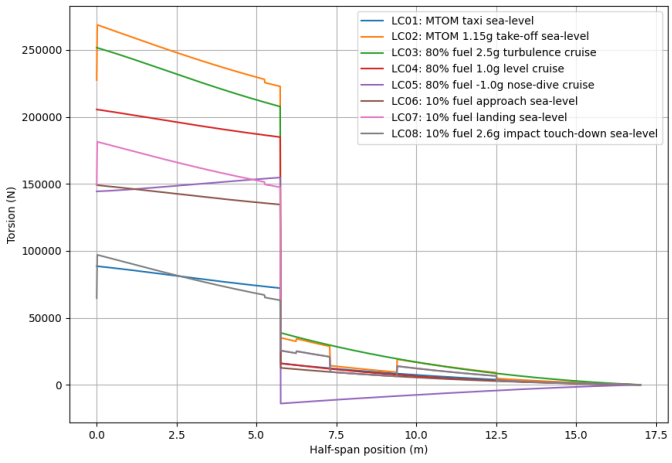

Figure 9.5: Torsion as a function of position along the wing half-span for the different load cases.

9.3. Wingbox Design

The wingbox is designed to withstand the wing loading forces, moments, and torsion, which were specified insection 9.2. Three main failure modes were considered: bending, shear, and buckling. In order to fit the gaseous methane tanks in the wingbox it was decided that the wingbox would only have a front and rear spar. The wingbox will thus consist of a front spar located at 20 % chord and a rear spar located at 75% chord as seen in Figure 9.6. In order to prevent buckling ribs will be added at every meter to split the wingbox up into multiple bays. These ribs limit the aspect ratio of the spars and sheets, which increases the k factor for buckling. Stringers are also added to increase the moment of inertia. At this stage, only the parallel axis term of the stringers was calculated, as this is much higher than the moment of inertia around the stringers own axis.

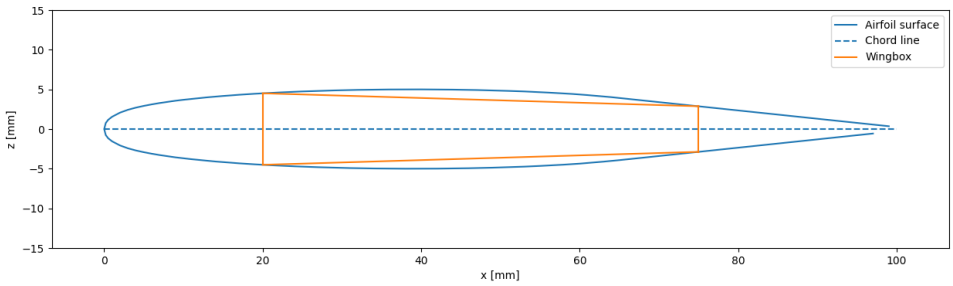

Figure 9.6: A simplified wingbox geometry inside the SC(2)-0010 airfoil.

9.3.1. Idealisation

For the purpose of simplifying the complex nature of structural analysis, structural idealisation was applied to the wingbox. The idealisation method chosen involved the following changes:

1. Placed stringers are changed to point areas, referred to as booms.
2. Skin and spar thickness between each boom is zero, and its contribution to bending is compensated by adding area to the booms.
3. Shear flow is constant between booms
4. Shear stress is calculated by mapping the shear flow to original geometry.

The assumption was made that the stringers act as booms with the contribution of the skin added to the booms using Equation 9.18. For this assumption the difference in stress used is simply the difference from the neutral axis which is just the height of the stringers.

$$B_1 = \frac{t_{skin} \cdot b}{6} \cdot \left(2 + \frac{\sigma_2}{\sigma_1}\right) \tag{9.18}$$

The effect of the idealisation to the geometry of the wingbox can be seen from the example in Figure 9.7. Note that the figures are not up to scale, but rather the areas are exaggerated for demonstration purposes.

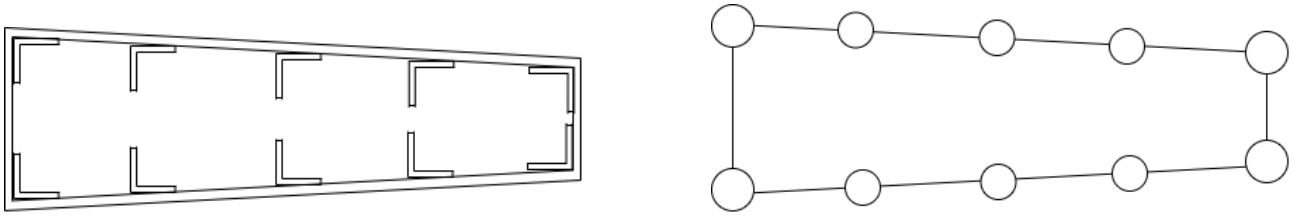

(a) Example wingbox.

(b) Example idealised wingbox.

Figure 9.7: Effect of idealisation on a wingbox with ten stringers.

9.3.2. Bending

In order to design the wingbox the first step was to check that the area moment of inertia was high enough to prevent tensile failure due to bending. Following this, the deflection under the bending and the twist angles were computed. For deflection and twist requirements were set as taken from chapter 4.

- **CH4-WING-04-01**: The wing tips shall have a maximum deflection of 15 % of the total wingspan.
- **CH4-WING-04-02**: The wing twist shall be less than ± 10°.

In order to calculate if the material fails, Equation 9.19 is used. The moment used is from the 2.5g turbulence load case at 80 % MTOW, as this is the most critical load case. The location where the stress is highest is at the top or bottom of the airfoil.

$$\sigma = \frac{MOS \cdot M_z \cdot 0.05 \cdot c}{I_{xx}} < \sigma_y \tag{9.19}$$

As the selected material has a tensile strength of 758 MPa the required $I_x x$ with a MOS of 1.5 was found for each span wise instance. Following this, the I_{xx} at each span wise position was calculated to check that this was above the limiting I_{xx}.

Stringer Selection

The next step was to select a stringer. Typical aerospace stringers come in multiple designs as seen in Figure 9.8. For the wing box simple T-stringers were sufficient. The spar caps are L-shaped and have a length and width of 25 mm and a thickness of 3 mm. The remaining stringers have a the same width and thickness however the length is 35 mm. After iterating the design and checking the failure modes the first 6 bays have 33 stringers on both the top and bottom sheet. Bays 6 through 10 have 17 stringers on each sheet. The remaining bays have 9 stringers on each sheet. This large difference is that after the fifth bay the engine weight significantly reduces the internal bending. In a typical aircraft the fuel tank is contained in the wingbox. This distributes the fuel load along the wing which can counteract the bending moment caused by the lift. As the CH4llenger has it's fuel in an external tank the fuel weight and engine weight act as point loads rather than distributed loads. This causes very high internal bending moments until the point where the engine and the tank are attached and can relieve this internal bending.

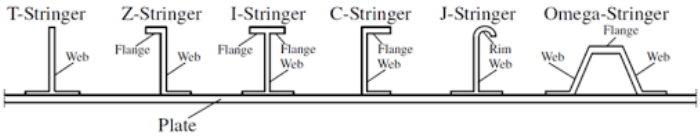

Figure 9.8: Typical aerospace stringers [63].

The final dimensions of the stringers and spar caps is displayed in Table 9.3. The number of stringers vary along the span of the wing, as the needed area moment of inertia is higher towards the root of the wing, meaning less stringers are needed towards the end. Hence, the number of stringers (including the two spar caps) are shown in Table 9.4.

Table 9.3: Skin, T-shaped stringer geometries and L-shaped spar caps.

	w (mm)	h (mm)	t (mm)	Area (mm^2)
Skin	[−]	[−]	6	[−]
Stringer	45	40	6	474
Spar Cap	40	40	6	444

Table 9.4: Number of stringers per wingbox section.

Wingspan %	Stringers per side
0-35	33
35-60	17
60-100	9

Final Bending Stresses

The idealisation of the wingbox essentially deems the choice of the stringer shape somewhat unnecessary. Nevertheless, using the equations mentioned before, the geometries of the reinforcements (Table 9.3 and their distribution (Table 9.4), a distribution of the maximum normal stresses is portrayed in Figure 9.9a. For both Figure 9.9a and Figure 9.9b the margin of safety (MOS) of 1.5 is already multiplied by the internal forces in the wing. So as the maximum bending stress shown in Figure 9.9a is 724 MPa which is below the tensile strength of 758 MPa.

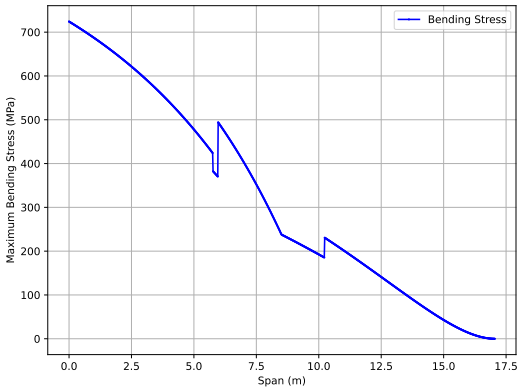

(a) Maximum bending stress along the span.

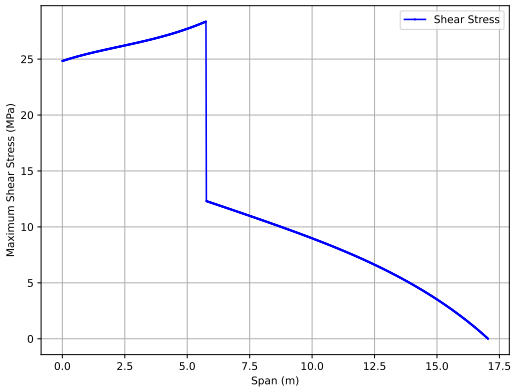

(b) Maximum shear stress along the span.

Figure 9.9: Internal force diagrams of the wing.

9.3.3. Shear

While shear is not typically constraining for a wingbox, it is still necessary to calculate the maximum shear stress in a bay of the wingbox. For shear stress in a bay Equation 9.20 is used. Where q_s is the shear flow and $T/(2tA_m)$ is the torsion contribution.

$$\tau_{cr} = \frac{q_s}{t} + \frac{T}{2 \cdot t \cdot A_m} \qquad q_s = \frac{-V_z}{I_{xx}} \cdot \sum B_r \cdot z + q_{s_0} \tag{9.20}$$

As the shear in the z-direction was considered to be perpendicular to the horizontal axis of the airfoil cross-section, there were not shear forces in the x-direction considered. The resultant maximum wing shear stress at each wingbox cross-section along the half-span of the wing is shown in Figure 9.9b.

9.3.4. Buckling

To design for buckling the spar web buckling and the sheet buckling was analysed. Spars buckle due to shear and torsion while the sheet buckle due to bending. Buckling is dependent on the thickness of the plate and the aspect ratio of the plate. Equation 9.21 is used to calculate the critical shear which causes buckling in the front and rear spar. Equation 9.22 is used to calculate the stress that causes buckling in either the bottom or top sheet.

$$\tau_{cr} = \frac{\pi^2 \cdot k_s \cdot E}{12 \cdot (1 - \nu^2))} \frac{t}{b}^2 \tag{9.21}$$

$$\sigma_{cr} = \frac{\pi^2 \cdot k_c \cdot E}{12 \cdot (1 - \nu^2))} \frac{t}{b}^2 \tag{9.22}$$

In these equations most parameters are the same. E is the Young's modulus of the material and v is the Poisson's ratio. Ks and Kc are constants that are taken from graphs dependent on the clamping and the aspect ratio of the plates. For spar buckling t is the thickness of the spar which was found to be 6 mm and for the webs the thickness was also 6 mm. As the shear stress was so low the spar buckling will not be critical and from the calculations it was found that the minimum thickness of the

spars was not dependent on the spar buckling but rather the minimum I$_x x$ value. For sheet buckling the b value is the distance between stringers. As the wing box experiences much higher internal loads up to the engine a design with 33 stringers on each sheet was chosen for the first five bays. This gave sufficient margins of safety. The margins of safety kept increasing in these first bays as seen in Figure 9.10. Hence, multiple stringers were removed after 35 % of the wing, resulting in 17 stringers. The middle part of the wing still seemed to be susceptible to buckling, so 17 stringers were kept up to 60 % of the wing, where then nine stringers were left. This decreases the stress at which the sheet buckles significantly, however as the stress that occurs in these bays is significantly smaller, the bays still have a minimum safety factor of 3. A graph displaying the bays and their buckling margin of safety is shown in Figure 9.10.

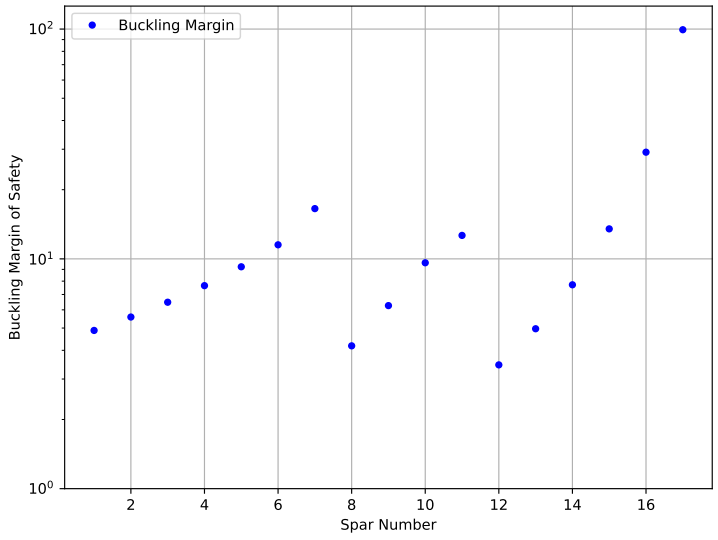

Figure 9.10: Wingbox sheet buckling safety margin.

Using the final design derived from the buckling analysis, an estimation of the wingbox weight was done using the density of the material. The final mass of the wingbox for one side of the wing was estimated to be around 1137 kg, and so 2274 kg in total.

9.4. Deflections

The two types of wing deflections that were deemed most important were the bending deflection due to the bending moment calculated in subsection 9.2.2, and the twist angle due to torsion around the wingbox shear centre, as determined in subsection 9.2.3. The preliminary wingbox design yielded the moment of inertia $I_{xx}(y)$, the wingbox enclosed area $A(y)$, $\oint \frac{ds}{t}$, and the material properties: the Young's and shear moduli E and G. The stiffness characteristics of the wingbox, together with the known loading, allowed for determining the deflections.

9.4.1. Bending Deflection

Bending deflection was obtained from:

$$M(y) = -EI_{xx}(y)\frac{d^2v}{dy^2}(y), \tag{9.23}$$

where $M(y)$ is the span-wise bending moment as calculated in subsection 9.2.2, and $\frac{d^2v}{dy^2}$ is the second-order derivative of the deflection at a point y. Integrating once and setting the deflection rate at the

root to zero:

$$\int_0^y \frac{d^2v}{dy^2}(y) = \int_0^y \frac{M(y)}{-EI_{xx}} \qquad \frac{dv}{dy}(y) - \frac{dv}{dy}(0) = \int_0^y \frac{M(y)}{-EI_{xx}} \qquad \frac{dv}{dy}(y) = \int_0^y \frac{M(y)}{-EI_{xx}}. \tag{9.24}$$

Integrating again and setting the deflection to zero at the root:

$$v(y) = \int_0^y \frac{dv}{dy}(y)dy. \tag{9.25}$$

As can be seen in Figure 9.11, the maximum deflection at the wingtip for the most critical load case is 2.78 m; 8.17 % of the total wingspan. This means that the requirement **CH4-WING-04-01** is satisfied. Despite the coordinate system established before, the plot was scaled and the axes realigned such that it best visually represents the wing deflection; positive upwards.

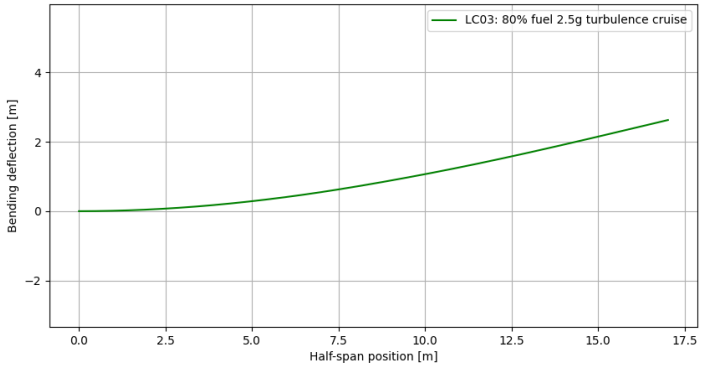

Figure 9.11: Deflection due to bending moment as function of position along the wing half-span for the most critical load case.

9.4.2. Twist Angle

Subsequently, the twist angle can be obtained from Equation 9.26:

$$\frac{d\theta}{dy} = \frac{T(y)}{GJ(y)}, \tag{9.26}$$

$$J(y) = \frac{4A(y)^2}{\oint \frac{ds(y)}{dt}}. \tag{9.27}$$

where $J(y)$ in Equation 9.27 is the torsional stiffness, which is a function of position along the span and calculated as: Since the wingbox is a thin-walled structure; the dimensions are much larger than the thicknesses, and it has a trapezoidal shape, the calculation of the enclosed area $A(y)$ is trivial and only dependent on the position along the half-span. For a given y, the thicknesses of the four "walls" enclosing the wingbox are constant per spar or skin, therefore $\oint \frac{ds(y)}{dt}$ is also straightforward. The twist can then be easily obtained, as depicted in Figure 9.12 The value at the wingtip, relative to the already applied twist, is 7.68 °, below the 10 ° requirement specified in **CH4-WING-04-02**. As mentioned in subsection 9.2.3, the torque due to thrust is by far the largest contributor. This is why, up until 5.75 m where the engine is mounted, the magnitude grows linearly. After that, the plot approaches a plateau; the aerodynamic forces contribution is small.

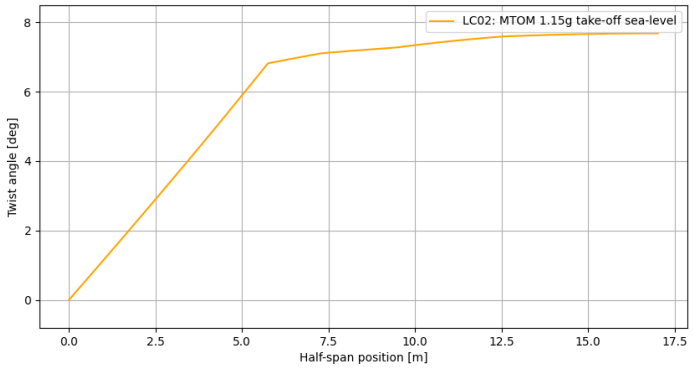

Figure 9.12: Twist angle due to torsion as function of position along the wing half-span for the most critical load case.

9.5. Fuselage Loading

For the fuselage two loading types were analysed. The shear force along the z-axis and the bending moment around the y-axis. As the fuselage has the same design from the start of the cylindrical section the structure only needs to be analysed for the most critical internal load. As the fuselage is not clamped the internal bending and internal shear should equal to zero at the start and end of the fuselage. Figure 9.13 shows the free-body diagram of the fuselage during flight. The two sets of orange arrows show the distributed fuselage weight and the payload weight. The first downwards blue arrows show the weight of the nose landing gear. Following this the next larger arrow is the weight of the engines and nacelles. The lift is depicted as point load acting at the leading edge of the mean aerodynamic chord and is depicted in green. The small blue arrow that follows this is the main landing gear and the large blue arrow is the weight of the fuel tanks and the weight of the fuel acting as a point load at the centre of gravity of the fuel. Finally, the two arrows at the empennage show the weight of the the horizontal and vertical tails, along with the lift produced by the horizontal tail.

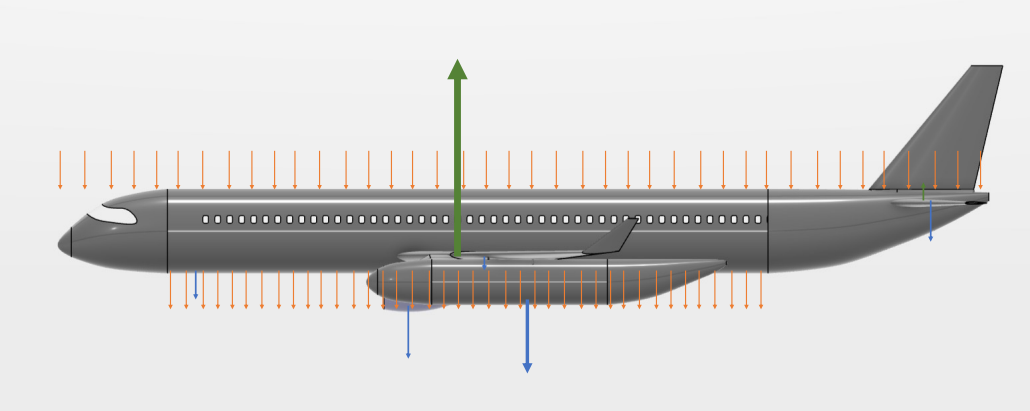

Figure 9.13: FBD of the fuselage during flight

9.5.1. Shear Force

Obtaining the shear force followed the same method as for the wing loading, however this time the loading was distributed along the centre line of the fuselage. Due to time constraints only the most limiting load case as previously found was looked at. This is the 2.5g turbulence load at 80 % fuel weight and max payload. The weights and C.G. values from the Class II estimations in section 8.2. Figure 9.14a shows the distribution of the internal shear from the front to the rear of the aircraft. At this point the shear force was equal to 826 000 N acting upwards.

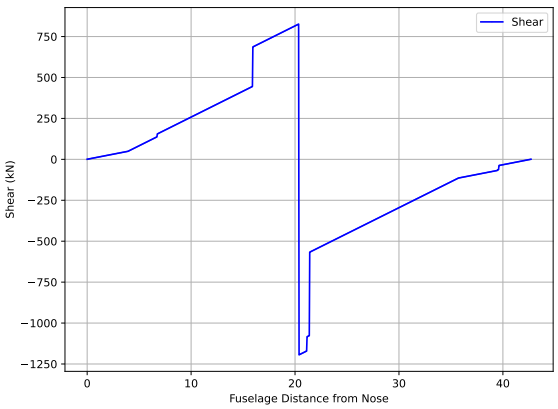

(a) Shear distribution of the fuselage.

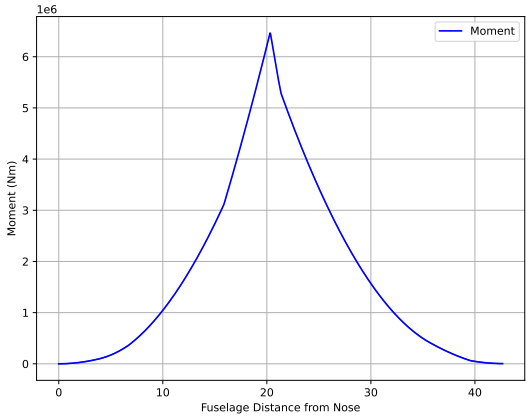

(b) Internal moment distribution of the fuselage.

9.5.2. Bending Moment

The bending moment along the y-axis is found by integrating the shear along the length of the fuselage. The most critical bending occurs at the leading edge of the mean aerodynamic chord, as this is where the lift is assumed to act. The most critical bending moment is 6 460 000 Nm as shown in Figure 9.14b.

9.6. Fuselage Structure

The first step in calculating the fuselage structure was checking the required thickness for the pressure difference at cruise altitude and the altitude at which the cabin is pressurised. In order to provide more comfort for the passengers, the cabin will be pressurised at 2000 m. From the pressurisation the skin thickness of the fuselage must be a minimum of 0.36 mm, as this is a thickness can cause manufacture deformities a fuselage thickness of 1 mm was initially assumed. The final fuselage structure is shown in Figure 9.15 and consists of a skin thickness of 2 mm and 128 stringers. Ultimately, buckling was the most critical and therefore the thickness was increased to 2 mm and the required number of stringers was used. This design allowed for fewer stringers to be used, which ultimately saved weight. The fuselage needs to be designed to withstand the following system requirements:

- **CH4-FUS-10**: The fuselage shall be able to be pressurised to 0.75 bar.
- **CH4-FUS-11**: The fuselage shall be able to withstand loads experience during operations.
- **CH4-FUS-11-01**: The fuselage shall be able to withstand repeated pressurisation.
- **CH4-FUS-11-02**: The fuselage shall be able to withstand the loads from the wing during normal operations.

9.6.1. Fuselage Minimum Skin Thickness

Primarily, the fuselage skin is undergoes internal stresses as a result of the pressure differences within the fuselage. The fuselage is pressurised to the ambient pressure at 2000 m, for comfort, as this pressure also adheres to the CS regulations. At this altitude there is an atmospheric pressure of 80 kPa compared to the cruise pressure of 24 kPa. The longitudinal and circumferential stress equations are Equation 9.28 and Equation 9.29, respectively.

$$\sigma_{long} = \frac{\Delta p R}{2t} \tag{9.28}$$

$$\sigma_{circ} = \frac{\Delta p R}{t} \tag{9.29}$$

.

From these, the limiting minimum thickness can be calculated, using a yield stress of 427 MPa. The thickness required for the pressure stresses was calculated to be 0.356 mm. This value provided a

lower limit to the fuselage thickness. Moreover, this level of precision for the thickness is unreasonable regarding manufacturing, and so an initial usage of 1 mm was used. This value was changed to 2 mm subsection 9.6.2, which concerns normal stress requirements.

9.6.2. Fuselage Design for Failure Modes

For the fuselage the same idealisation is made as for the wingbox. Once again Equation 9.18 is used in order to size the stringers to include the contribution of the string. Using this assumption allows for the booms to assume all the bending while the skin takes the shear. Using Equation 9.19 allows for the calculation of the bending stress at each boom. The most critical bending stress is in the top boom and is 103 MPa which is far below the yield strength of 427 MPa, even when a MOS of 1.5 is added.

In a similar fashion, the internal shear stresses were analysed using Equation 9.20. Once again, the vertical forces in the z-direction were considered; moreover, given the circular nature of the fuselage, the cut was made at the top to make the shear distribution calculations symmetric. The torsion contribution due to the rudder were neglected, as that is a higher level calculation done at a more advanced stage of the design process.

Lastly, the buckling of the fuselage needed to be calculated, as this tends to constrain the amount and the placement of the stringers. Equation 9.21 was used to size the stringer distance needed near the central axis, while Equation 9.22 was used to size the stringer distance needed near the top of the fuselage. To alleviate the amount of stringers required, it was eventually chosen to use a skin thickness of 2 mm. The final fuselage structure consists 128 stringers. The stringer layout is more concentrated near the top ends of the fuselage, which was a decision made after one round of weight optimisation, and is displayed in Figure 9.15.

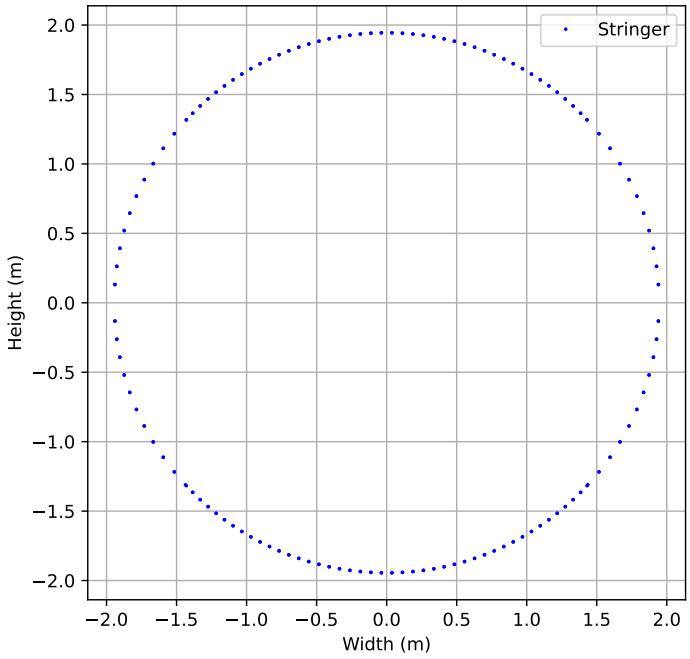

Figure 9.15: Diagram showing positions of fuselage stringers.

Lastly, it is important to include the consideration of windows. The design of the windows is a higher level analysis that can be done at a later design stage, but is still important in terms of the overall

fuselage weight calculation. Due to the stress concentrations around the windows, there will be structural reinforcements in place; as a rough estimation, the original fuselage mass of 7301 kg was increased by 25 %, to account for the windows. Hence, the final mass of the fuselage was estimated to be around 9126 kg.

9.6.3. Compliance with Fuselage Requirements

The skin thickness of 2 mm is greater than the minimum skin thickness needed to satisfy the 0.75 bars pressurisation requirement. The aircraft can even be pressurised to 0.8 bars. **CH4-FUS-11-02** is also met as the aircraft withstands the pressure loads and the wing loads for all failure mode. **CH4-FUS-11-01** has not been met at this stage, as a fatigue analysis has not yet been done.

9.7. Verification and Validation

In order to ensure proper verification and validation of the structural analysis multiple unit and system tests were conducted. Validation for the structural analysis mainly checked if the requirements were met.

9.7.1. Unit Tests

Every function in the load calculation tool was tested individually against manual calculations for a simple case, with positive results. Subsequently, it was investigated whether changing the sign of the load factor did indeed produce a shear force and moment plots mirrored against the $y-$axis. Print statements were added to functions that consisted of multiple mathematical operations, such that the result can be traced back and verified.

For the wingbox calculations the code was mainly written to calculate parameters as a function of span. In order to unit test the code the calculations were manually completed at the first spanwise instance, to then be checked with the python outputs for zero span. The $I_x x$ and Izz calculations were done manually, with the assumption that the stringers only have a parallel axis contribution. The shear calculations were also done by hand in order to calculate the sheer flow when assuming an open section and then to add qs0.

The deflection calculations mostly consisted of integrating the loads, therefore the unit test checked every step of the calculation against manual calculations. Specifically, the twist and bending deflection were calculated at the wingtip. These manual calculations matched the output of the graphs that were plotted so the unit tests for the deflection and wing twist were passed.

9.7.2. System Tests

System tests checked whether the interfaces between the functions and the overall results produced were aligned with the expectations. It was visually inspected whether the plots had the desired characteristics; the loads at the root are the largest and decrease to zero at the tip, the "jumps" are in the expected places. Additionally, in order to check whether the point loading due to the engine and the tank serve as a bending moment relief as anticipated, their sign was reversed and the total moment at the root was indeed larger than previously. Lastly, it was verified whether the most extreme cases were indeed the same as anticipated, i.e. larger load factor imposes proportionally higher loads, HLDs produce more lift and therefore more loading.

In order to test the system once the wingbox parameters were calculated, a code was written that checked the bending and sheer stress throughout the wingbox. If the wingbox fails at any point than a failure alert is given, while as long as the shear and bending stress are below the allowable shear and bending stress an all is well output is returned. This gives an immediate indication if changing any wingbox parameter such as number of stringers or a thickness is allowable or if a failure mode is

found. Furthermore, extreme value tests were conducted to verify that if the thickness doubled the stress was massively decrease and a zero stringer test was done to ensure that the stringers correctly add I_{xx}.

In addition to the unit tests, the deflection plots as a whole were also inspected. As expected, the bending deflection has the highest rate between the root and the engine, with a slower rate near the tip, where the loading has a smaller magnitude. Twist increases the most due to the thrust torque, and levels-off after that point.

9.7.3. Validation

Due to the unavailability of structural data of reference aircraft, validation mostly consisted of evaluating the results against the requirements. The weight of the wingbox and the fuselage were compared with the weights from the Class II estimation (section 8.2); the weight of the fuselage was within an acceptable difference, while the wingbox was a third of the wing weight, which is reasonable. The maximum magnitudes of bending deflection and twist were both below the requirements set.

9.8. Sensitivity Analysis

Sensitivity analyses are performed in this chapter to assess the reaction of the wingbox and fuselage characteristics to a variation in their corresponding inputs. The analyses are designed to provide an overview of whether the code performs as expected, as well as in indication of how optimal the selected design choices are. If a variation produces all positive effects, then a new design should be considered. A wingbox sensitivity analysis is performed in subsection 9.8.1, and a fuselage sensitivity analysis is performed in subsection 9.8.2.

9.8.1. Wingbox Sensitivity Analysis

Firstly, a sensitivity analysis is performed on the wingbox. The most important characteristics are the wingbox mass, wing tip deflection, as well as the wing twist, given that those constrains are derived from requirements.

Table 9.5: Results of sensitivity tests performed on the wingbox.

Variable	Variation	$I_{xx_{root}}$ [%]	$I_{xx_{35\%}}$ [%]	Deflection [%]	Twist [%]	Half Wingbox Mass [%]	Aircraft Range [%]	Failure
Number of Stringers	+3	+4.10	+4.73	-2.92	0	+2.31	-0.06	No
(0-35% wingspan)	-3	-4.10	-4.73	+3.19	0	-2.31	+0.06	No
Skin Thickness	+10%	+5.23	+4.58	-5.03	-8.02	+5.51	-0.16	No
	-10%	-5.23	-4.58	+5.60	+9.80	-5.51	+0.16	Yes
Spar Thickness	+10%	+0.26	+0.23	-0.27	-1.08	+0.25	0	No
	-10%	-0.26	-0.23	+0.27	+1.31	-0.25	0	No

As can be seen from Table 9.5, the number of stringers in the first part of the wingspan was varied by three, while the skin thickness and the spar thickness were varied by 10 %. The table shows a positive (green) outcome and a negative (red) outcome, as well as no change from the actual design (yellow). The situations in which there are positives in some changes results in sub-optimal changes in other sections, and so it is safe to conclude that the design choices of the wingbox are within an optimal range.

9.8.2. Fuselage Sensitivity Analysis

Similarly, a sensitivity analysis is also performed for the internal structure design of the fuselage. In this case, the fuselage thickness is uniform around its circumference.

Table 9.6: Results of sensitivity test performed on the fuselage.

Variable	Variation	[%]	I_{yy} [%]	Fuselage Weight [%]	Aircraft Range [%]	Failure
Number of Stringers	+12	+9.38	+5.72	+5.77	-0.75	No
	-12	-9.38	-5.72	-5.77	+0.75	Yes
Skin Thickness	+0.5	+25	+9.51	+9.60	-1.25	No
	-0.5	-25	-9.51	-9.60	+1.25	Yes

Table 9.6 shows the results of the fuselage cross-section input variations on the most important parameters of the fuselage. Firstly, the thickness of the fuselage was changed by 0.5 mm as more precise changes are not possible manufacturing-wise, deeming the sensitivity analysis useless. It is evident how the variations that make the fuselage stiffer also increase the weight, providing no benefit given that all those designs do not fail. On the other hand, the weight-saving variations actually result in fuselage failure, as there is too much change in the area moment of inertia. Hence, once again, the fuselage parameters seem to be within an optimal range.

9.9. Recommendations

Several recommendations can be made that would improve the quality of the structural analysis and design; following from the simplifications stated in Table 9.1. First, a more detailed and accurate aerodynamic analysis should be performed; the lift and drag distribution should be obtained from XFLR5 for every individual load case, rather than adjusting one set of data based on a given C_{L_d}. Additionally, it is recommended to obtain more data points along the half-span of the wing. If possible, a complete model of the aircraft should be analysed in XFLR5 or a similar software, such that the effects of the fuselage and other aircraft systems on the drag and force can be investigated. The model of the wing itself should resemble the actual wing better; for instance, the yehudi should be added to the wingbox structure, meaning an additional rib would likely be placed towards the end of the wing cross-section near the root.

Moreover, improvements can be made on the wingbox cross-sectional properties used. Firstly, the shear centre of the wingbox likely does not exactly coincide with its geometric centre, therefore it is recommended to perform adequate calculations, which are notably extensive for a closed section such as a trapezoid. The shape of the wingbox should be revisited; the upper and lower skin elements can be arched to fit inside the airfoil better, rather than having two straight elements. Not only would this increase the area of the wingbox and its I_{xx}, circular or curved sections would also be more torsion-resistant. In addition, while the idealisation is ideal for time purposes, using the actual shape of the cross-section would be more accurate.

Additionally, the actual designed wing would likely bend less from to external forces, due the extra spar placed along the yehudi and the increased chord length at the root. Moreover, the usage of formers within the fuselage should be considered during further design, as those help with the aircraft structure and create the equivalent of bays in wings. To add to that, further iterations of the wing and aircraft designs will change actual values of the wingbox and fuselage, meaning the values obtained are somewhat preliminary. However, this analysis was optimised for the limited time and resources and nonetheless yielded meaningful results.

10. Internal Aircraft Systems

A modern aircraft has a plethora of subsystems that are needed in order to be able to fly. This chapter contains schematic diagrams and descriptions of the key internal systems. First, the hardware and software interfaces are discussed in section 10.1. Next, the electric system is discussed, together with the dependencies of other systems in section 10.2. Following this, the hydraulic and pneumatic schematics are shown in section 10.3 and section 10.4. Lastly, the voice and data communication flow is discussed in section 10.5. The fuel management system has already been tackled in chapter 6.

10.1. Hardware and Software System

The hardware and software systems are two very interconnected systems. The hardware system is depicted in Figure 10.2 and shows all hardware components within the aircraft along with the flow of fuel, data, electricity or any other inputs or outputs. The legend describes which hardware components are part of which larger system. The circular blocks, containing the management system link the hardware to the software as they are guided by the software groups shown in Figure 10.1. The electric hardware consists of batteries, the APU and the engine generator. As this is a rather important system that needs to provide power to all other systems this system is further explained in section 10.2. The communications along with the data handling are also explained in more detail in section 10.5. Figure 10.1 shows the four main software groups depicted split into communications, navigational, control and cabin control software. These groups send data between each other and to the flight computer from which the pilot can act on the information. The software groups also provide the corresponding hardware with the correct settings that the hardware needs to be set at. Ultimately there are two main external inputs to the entire system, namely external communications input and pilot inputs into the flight computer, either directly or through the pilot controls.

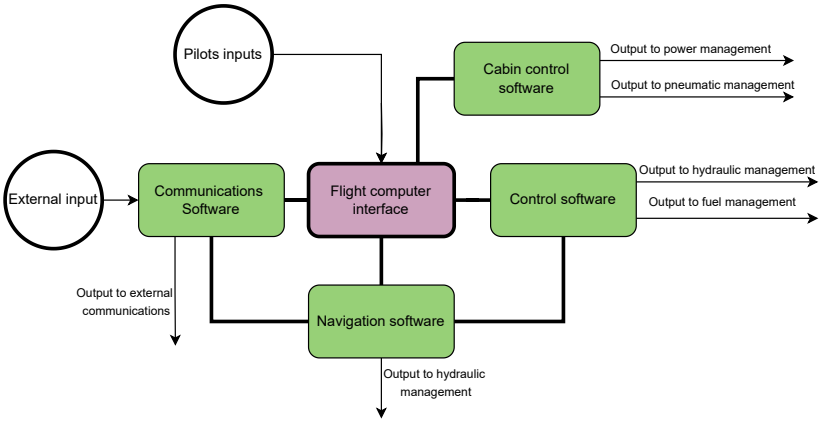

Figure 10.1: Schematic diagram showing the software interfaces of the aircraft.

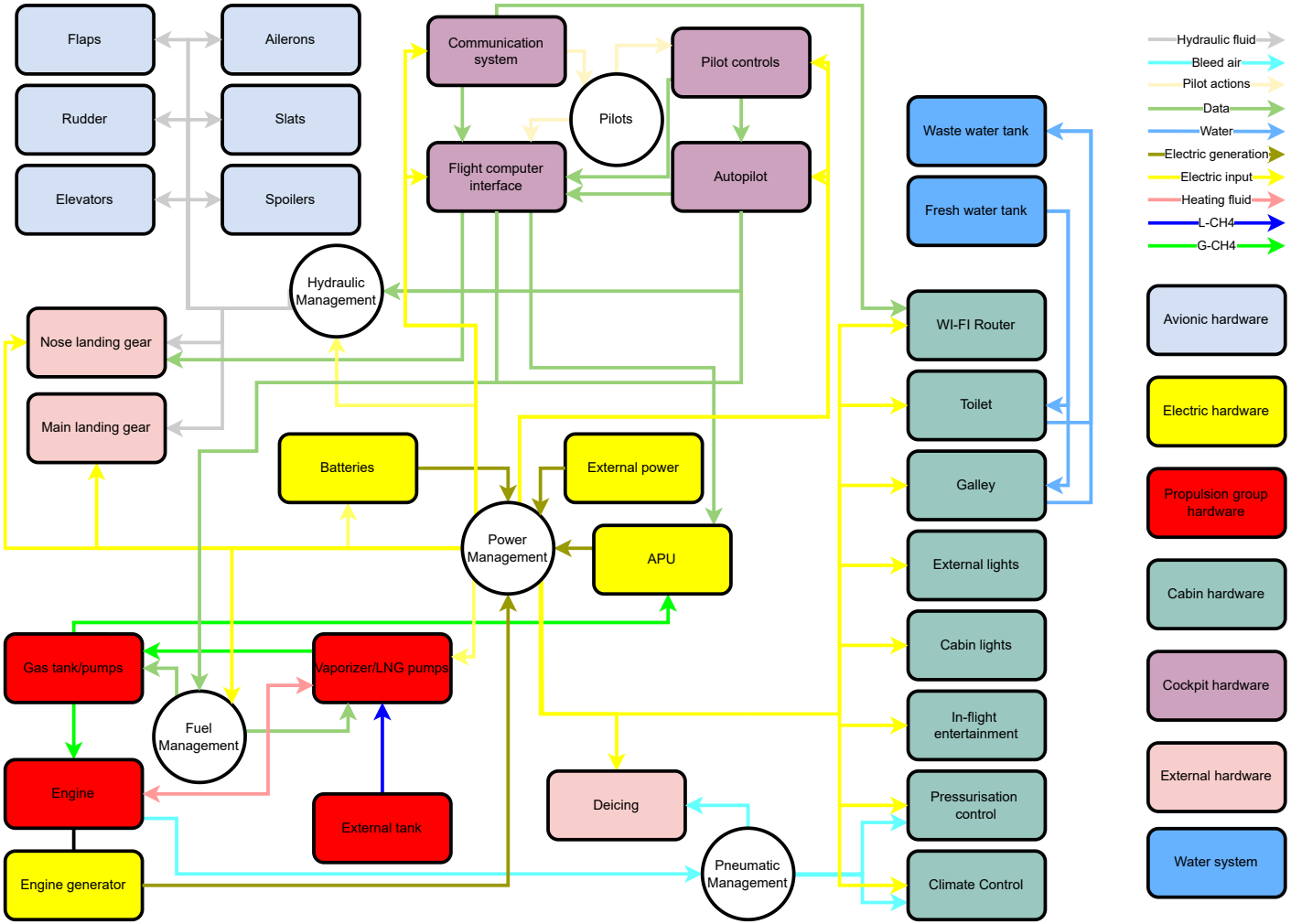

Figure 10.2: Schematic diagram showing the hardware interfaces of the aircraft.

10.2. Electrical System

Regarding the electrical system of the CH4llenger, the systems controlled by the electric power management and their dependencies are depicted in Figure 10.3. Here, the flow between the power generators, the electrical power management system and the equipment on board that makes use of this power is shown. Considering the way these systems receive the power generated by either the external power unit or APU while on the ground or the generators from the engines while in the air, a schematic diagram showing the power distribution through the aircraft and the associated voltages is shown in Figure 10.4.

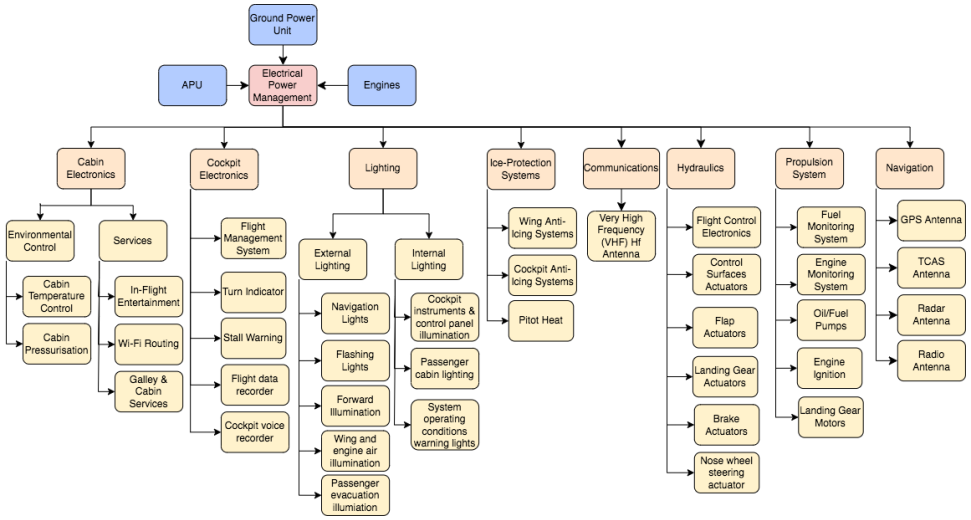

Figure 10.3: Dependencies of the aircraft electrical system.

As can be seen in Figure 10.4, the power is supplied by two engine-driven generators, named Gen 1 and Gen 2, operating in parallel, and additional power generators consisting of the APU generator and external power source [64]. Each generator is connected to its own busbar, where 28 V DC is delivered after conversion by the Transformer Rectifier Unit from the 115 V AC current. To these busbars, the energy consuming services are connected. Furthermore, generator circuit breakers (GCB) and bus tie breakers (BTB) are included in the event the supply from either generator fails, thus ensuring power supply by the interconnected busbars. When external power is connected to the aircraft, it energises both bus tie breakers and the connected bus bar system. Transfer relays ensure the generator busbars and transfer busbars are connected.

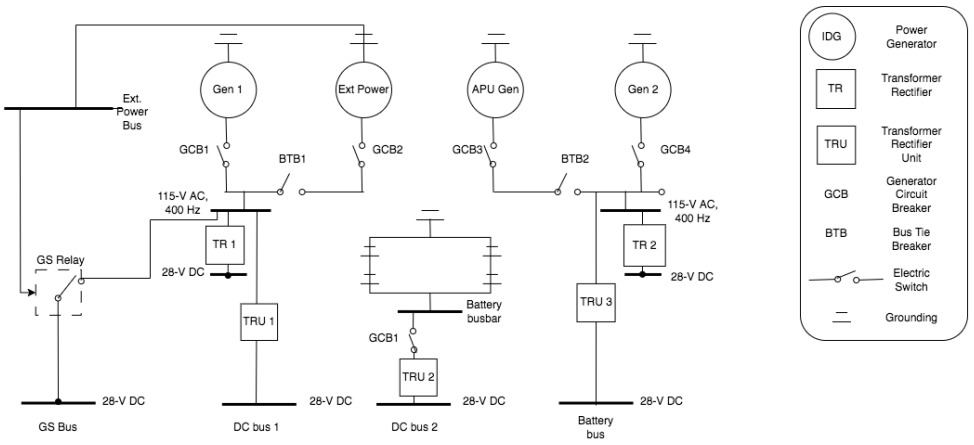

Figure 10.4: Schematic diagram showing the electrical system of the aircraft.

10.3. Hydraulic System Layout

The hydraulic system is responsible for the operation of aircraft mechanical parts, using pressurised fluids. The hydraulic system utilised in the aircraft will resemble that of the Airbus A380 aircraft [65]. Hence, two reservoirs are in place, each with a pathway responsible for different aircraft components. Moreover, an Electric Backup Hydraulic Actuator (EBHA) is also present, placed on the control surfaces of the aircraft. The layout is displayed in Figure 10.5.

It is seen from Figure 10.5 that each reservoir has a valve connected to its designed part. Moreover, the green reservoir is responsible for the left engine, while the yellow reservoir is for the right one. Furthermore, some parts have multiple reservoirs connected to them; this is done as a backup measure in case one pathway is cut off. For certain structures, such as the rudder, not having multiple pathways connected would be catastrophic. Naturally, both pathways are not connected to the actuator at the same time, but rather one acts as a backup [66].

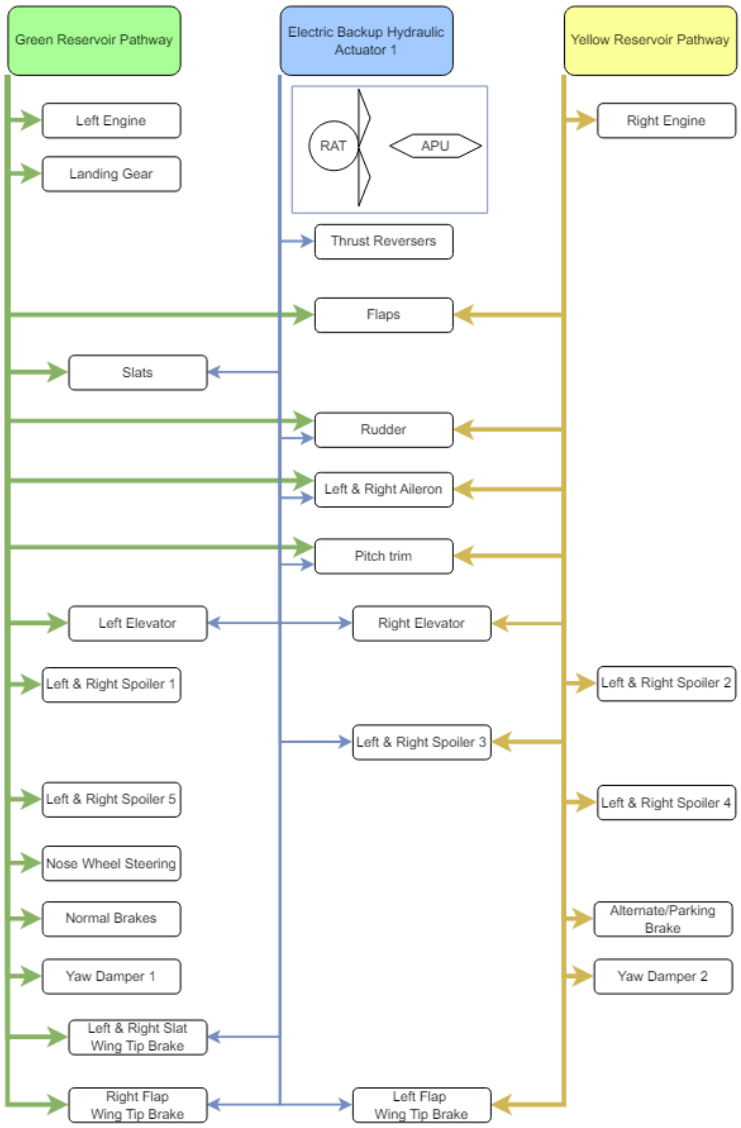

Figure 10.5: Schematic diagram showing the hydraulic system of the aircraft.

10.4. Pneumatic System and Environmental Control

The pneumatic system is required to provide air in order to control the environment in the cabin during flight as can be seen in Figure 10.6. The air is bled from the engines from one of three internal

stages in the jet engine. The low-pressure stage blows bleed air from the fan and is mainly used to cool the bleed air from the later stages. The high-pressure stage is only used when there is not enough air flowing from the intermediate-pressure stage. This occurs when the engines are at low power. After passing through the pre-cooler the air can be used to de-ice the leading edge of the wings. The air is also cross-fed and used in either PACK. During the start, the APU bleed air is fed back into the engines to start up the engines.

The top part of the figure shows how the PACKs, which stands for "Pressurisation & Air Conditioning Kit", mix the bleed air that enters the aircraft with the air in the three parts of the fuselage. The cabin air is also filtered and redistributed in the mixing unit. The ratio in most modern airliners is roughly 50% filtered cabin air and 50% new bleed air. Through the mixing unit, the pilot can control the temperature in the cabin and the ratio of new air to filtered air [67, 68].

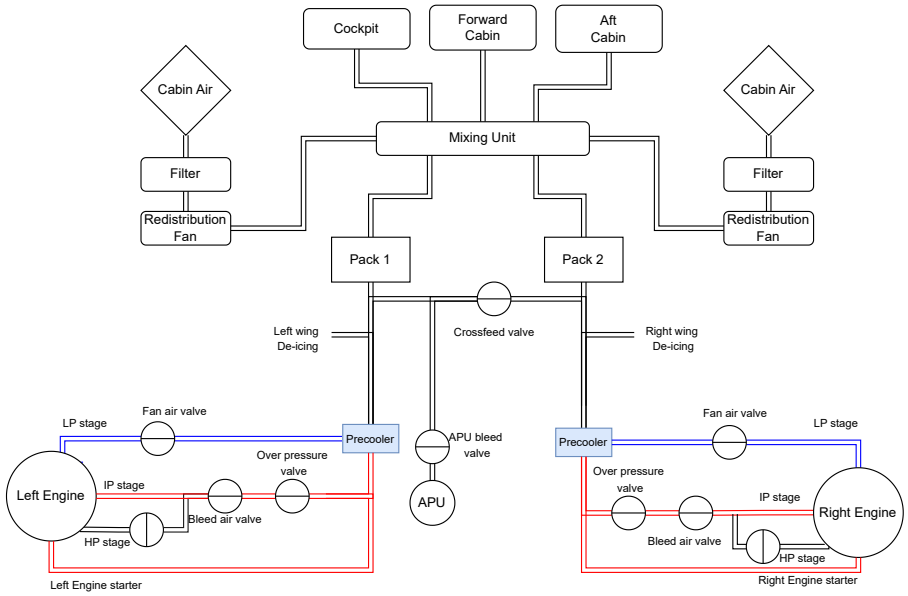

Figure 10.6: Schematic diagram showing the pneumatic and environmental control systems of the aircraft.

10.5. Voice and Data Communications System

The voice and data communications flow is depicted in Figure 10.7. It is inspired by the communications system in the Boeing 737 MAX aircraft, according to chapter 23 of the ATA 100 Specification[1], due to its similar mission characteristics and availability of information about the system elements, and includes the following subsystems:

- High Frequency (HF) Communication System;
- Very High Frequency (VHF) Communication System;
- Satellite Communication (SATCOM) System;
- Emergency Locator Transmitter (ELT);
- Low frequency Underwater Locating Device (ULD);
- Selective Calling System (SELCAL);
- Aircraft Communications Addressing and Reporting System (ACARS);
- Passenger Address (PA) System;
- Service Interphone System;
- Flight Crew Call System;
- Ground Crew Call System;
- Flight Interphone System;
- Static Dischargers;
- Voice Recorder System.

[1] `https://en.wikipedia.org/wiki/ATA_100`, [Cited on 17-June-2024]

HF is reserved for voice and data communication over long distances. It can provide communication both between aircraft as well as ground stations and aircraft and operates in the aeronautical frequency range of 3.0 MHz to 30.0 MHz[2]. The subsystem consists of an antenna, antenna coupler, radio tuning panel (RTP), and transceiver, connected to the rest of the system by the remote electronics unit (REU). VHF is commonly used over line-of-sight distances, either between aircraft or ground stations and aircraft, operating between 118.000 MHz and 136.995 MHz[3]. It consists of an antenna, radio communication panel (RCP), and transceiver, connected to the REU much like HF. Additionally, both subsystems are connected to the proximity switch electronics unit (PSEU) and the selective calling system decoder. The SATCOM system utilises satellites and ground stations to transmit and receive voice and data messages, supplying higher quality data than radio over longer distances[4]. The separate antenna is connected to a satellite data unit and through that to a configuration module.

Moreover, the emergency locator transmitter (ELT) has a separate control panel and antenna, it is also connected to a program switch module. It broadcasts a distress signal automatically when it senses a large change in aircraft's velocity, or it can be started manually with a switch[5]. The underwater locating device (ULD) is also separate, placed in the fuselage, e.g. in the nose[6]. Moreover, static dischargers are placed in several locations on the aircraft in order to decrease receiver interference.

ACARS is a data link communication subsystem, and it relays messages between aircraft and airline ground base. As can be seen from the interfaces in Figure 10.7, the messages can be sent via airband radio; VHF or HF, or alternatively via satellite. A message from the aircraft to the ground base is referred to as a downlink, and the reversed direction of flow is called uplink[7]. The ACARS management unit is connected, among others, to a printer, an ATC transponder and a control display unit.

The selective call system's function is to inform the flight crew about calls coming in from the airline ground stations. It consists of a decoder, a control panel, and a program switch module. The decoder is also connected to the REU through an audio control panel. The passenger address system supplies announcements, chimes, and boarding music to the cabin. Its key elements are the passenger signs panel in the cockpit and the PA amplifier, all connected to the rest of the overall system. The service interphone is used by the ground crew to talk to each other or to the flight crew. Three sub-systems can be identified; flight crew operation, attendant operation, and ground crew operation. The flight crew elements are the ACP, flight interphone, and interphone jack. On the attendant's side, there is an attendant handset and panel, and the ground crew has headsets, jacks, and switches. The flight crew call system notified the flight compartment of calls from the attendants and vice-versa. Similarly, the ground crew call system informs the flight compartment of incoming calls from the ground crew and vice-versa. The flight interphone, as mentioned before, consists of headsets, headphones, and hand mic, among others, indirectly connected to the flight interphone speakers.

Lastly, the voice recorder system consists of a recorder unit connected to the REU, as well as a cockpit voice recorder panel, VR switch, and a clock. It records radio transmissions and sounds inside the cockpit, in order to aid investigators in case of an incident [8]. The schematic diagram in Figure 10.7 is merely a general representation of how the different elements are interconnected, but does not indicate the locations of the elements nor is it all-encompassing.

[2] https://www.nzaviator.co.nz/editorial/exploring-hf-and-vhf-in-aviation, [Cited on 16-June-2024]
[3] https://wiki.ivao.aero/en/home/training/documentation/Frequency, [Cited on 16-June-2024]
[4] https://aea.net/AvionicsNews/ANArchives/SatComDec03.pdf, [Cited on 16-June-2024]
[5] https://skybrary.aero/articles/emergency-locator-transmitter-elt, [Cited on 16-June-2024]
[6] https://skybrary.aero/articles/underwater-locating-device-uld, [Cited on 16-June-2024]
[7] https://www.icao.int/Meetings/a41/Documents/WP/wp_519_en.pdf, [Cited on 16-June-2024]
[8] https://www.ntsb.gov/news/Pages/cvr_fdr.aspx, [Cited on 17-June-2024]

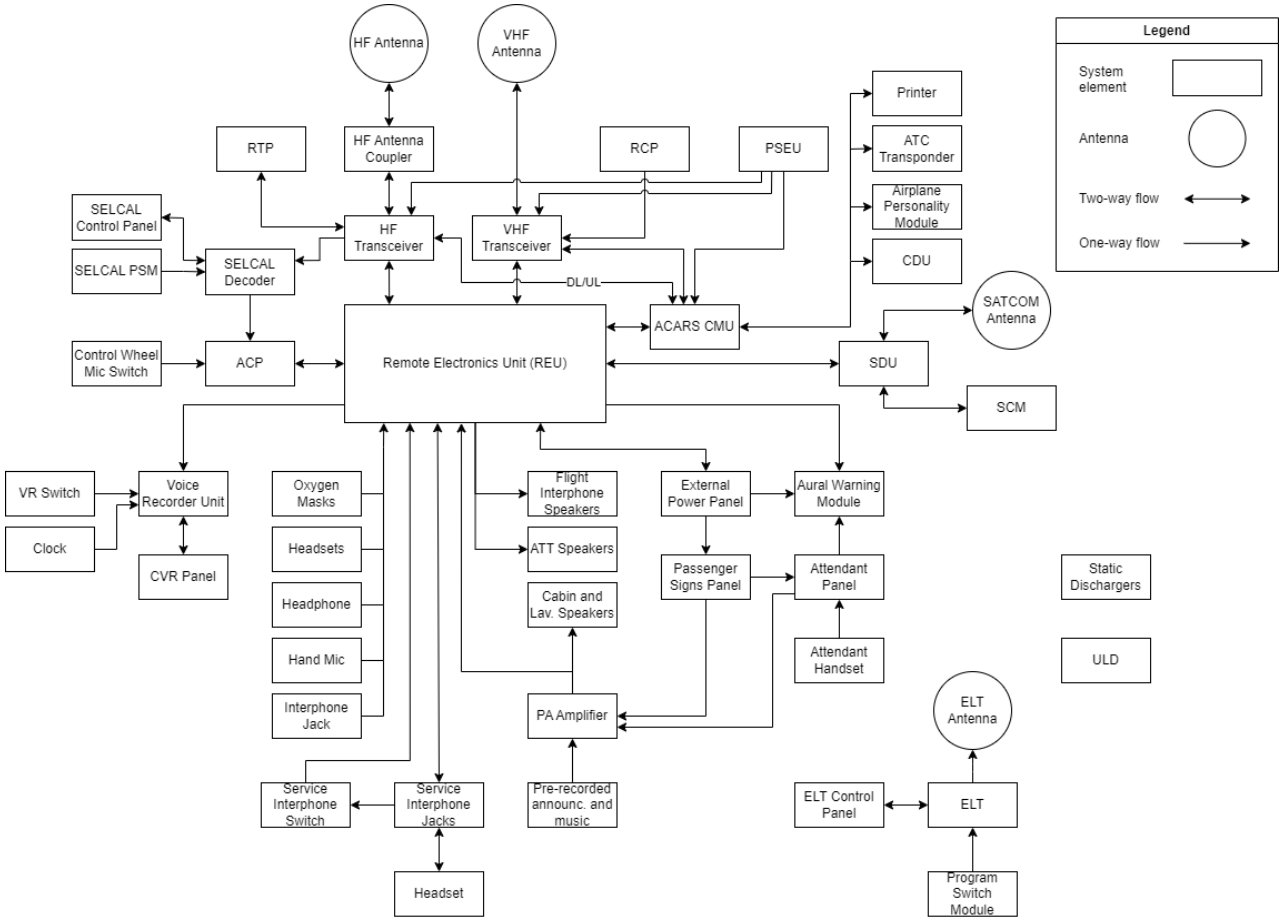

Figure 10.7: Schematic diagram showing the voice and data communications flow of the aircraft.

11. RAMS Characteristics

An additional design aspect that needs to be considered is the Reliability, Availability, Maintainability and Safety (RAMS) Characteristics. Various aircraft (sub)systems can be examined as to how they perform with respect to those criteria. In order to properly examine the different systems, however, the RAMS parameters first need to be properly defined, after which each parameter can be analysed.

- **Reliability** - the ability of the systems to work according to their intended function without failure [1]. Assessed in section 11.1
- **Availability** - the readiness of the systems to operate when needed [1]. Assessed in section 11.1
- **Maintainability** - The ease of servicing and performing potential repairs to the aircraft [1]. Assessed in section 11.2
- **Safety** - the ability of the system to perform within the acceptable level of identified risks [1]. Assessed in section 11.3

At the end in section 11.4 reccomendations on how to continue this are given.

11.1. Reliability and Availability

To examine the reliability and availability of the CH4llenger aircraft, its potential failure modes need to be identified along with their likelihood and potential frequency of occurrence. Given the similarity of the aircraft to the A321neo, the main focus was placed on the novel systems as they shall require more attention and scrutiny. The identified failure mods of the said systems are presented in Table 11.1. Based on these the RAMS characteristics are to be analysed.

Table 11.1: Analysis of the failure modes.

ID	System	Failure Mode	Effect	Likelihood	Mitigation
FAI-01	Propulsion	Engine failure	Yawing moment introduced, necessitating a significant deflection of the rudder, which would, in turn, cause a loss in efficiency and range	Low	During the design of the rudder, this scenario was taken into account, so as to ensure that it can generate sufficient counteracting yawing moment
FAI-02	Fuelling	Leakage of the tank	Quick depletion of fuel prohibiting the aircraft from reaching its destination; fire hazard	Low/Medium	Multiple leak detection sensors installed, along with the frequent maintenance of the tank and the entire fuel system as a whole
FAI-03	Fuelling	Tank burst	Loss of fuel; in the case of burst of one of the two external tanks, a large shift in the lateral position of the C.G. would occur leading to stability issues	Medium	Additional strengthening of the external tanks to prevent the tank bursting during potential strike upon take-off or landing, along with requiring frequent maintenance of the entire system
FAI-04	Undercarriage	Landing gear does not deploy	Inability to land conventionally	Low	Frequent replacement of the landing gear along with its regular maintenance
FAI-05	General	Structural failure of an aircraft component	Loss of performance; potential loss of the aircraft	Low/Medium	Frequent maintenance of the most fragile components that may be subject to the greatest stresses
FAI-06	Propulsion	Propulsion system Failure	Loss of mass flow to gaseous tank; no throttleability	Low/Medium	Frequent maintenance of plumbing

[1] `https://blogs.sw.siemens.com/simcenter/aviation-rams-engineering/`, [Cited on 17-June-2024]

In Table 11.1, several failure modes of the various aircraft systems have been identified. Based on that, it can be observed that FAI-02, FAI-03, FAI-05 and FAI-06 have the highest likelihood of occurring. As a result, in order to ensure that the aircraft performs with sufficient reliability, additional redundancy of the component mechanisms is introduced as in the case of FAI-02, where numerous sensors have been installed. This is done in order to ensure accurate detection of any potential fuel leaks, even if one of the sensors were to fail. Furthermore, in the case of FAI-03, additional strengthening of the fuel tank structure is performed. This is done to ensure the reliability of the aircraft as well as its safety, preventing a potential tank burst if a tank strike were to occur. The FAI-05 failure mode, on the other hand, entails a structural failure of an aircraft component, which could prove detrimental to the performance of the CH4llenger as a whole. To ensure the reliability and the continuous availability of the CH4llenger aircraft its components are to be stringently tested and an additional contingency added. Finally, in order to reduce the chance of any failure mode occurring, frequent maintenance of the aircraft is to be performed as a mitigation strategy.

11.2. Maintainability

To assess the maintainability of the CH4llenger, the systems corresponding to the failure modes identified in Table 11.1 need to be revisited with the analysis of their ease of repair or potential replacement. Based on the table it can be observed that, as a prevention strategy for most failure modes, frequent maintenance of the components has been included. In order to be able to perform it efficiently the components themselves need to be designed in such a way that their repair and potential replacement is not only possible, but also viable. With that in mind, different aircraft maintenance checks were identified, each of which corresponds to a different severity and frequency of the checks. The different maintenance checks are presented in Table 11.2, with their frequency stemming from the maintenance frequency of the A321neo[2].

Table 11.2: Time between maintenance checks.

Check Type	Flight Hours
A	750
C	12 000
D	6 years

At the same time, however, several components of the CH4llenger significantly differ from the A321 neo, requiring their own, separate maintenance/replacement schedule. Given the novel technology being used, it has been decided to implement a more stringent maintenance schedule to prevent any unexpected damages. With that in mind a preliminary schedule has been created, which can be observed in Table 11.3.

[2] https://aviationweek.com/special-topics-pages/crossover-narrowbody-jets/profitability-aim-crossover-jets-better, [Cited on 17-June-2024]

Table 11.3: Maintenance checks of novel components.

Component	Maintenance frequency	Reasoning
Engine	5 000 flight hours	Although some engines can operate longer without the need for maintenance, in the case of CH4llenger aircraft, the permittable number of hours has been limited to 5 000 flight hours[3], given the novel fuel used aboard the aircraft
External CH4 tanks	Visual inspection after every flight, with a tank overhaul every 100 flight cycles	Instead of performing the maintenance of the external tanks as part of the A-check presented in the Table 11.2, it has been determined to maintain the tanks more frequently, given their external location as well as their frequent attachment to/detachment from the aircraft
Fuel system	100 flight cycles that incorporate the detachment of the fuel tank	The fuel system will be the most susceptible to sustaining damage or imperfections upon detachment of the fuel tanks. As a result, just like the external tanks, the system is to undergo detailed maintenance every 100 flight cycles
Internal gas buffer tank	Part of the A-check	To ensure that the internal buffer tanks are checked frequently, it has been decided to incorporate their maintenance into the A-check as presented in the Table 11.2

11.3. Safety

To ensure the safety of the aircraft when a system fails, redundancy is applied during the design process. The flight controls have a layer of redundancy for important control surfaces by controlling them through different hydraulic systems as can be seen in Figure 10.5. The fuel system has a layer of dependency built in as an extra gas line runs from the gas buffer tank to the engine in case the main fuel line fails. This is pictured in Figure 6.1. Moreover, multiple pumps will be placed in parallel to provide the engine with fuel if one pump fails.

Aviation Authorities

Another safety aspect worth considering is the regulations stemming from the aviation authorities such as the Federal Aviation Authority (FAA) and the European Aviation Safety Agency (EASA). These organs have implemented documentation specifying the safety of passenger aircraft such as the CS25 Certification Specifications courtesy of EASA[4]. To ensure a safe design the aircraft is to adhere to these regulations. Although several design considerations are to be regarded as similar to the ones implemented in the case of the A321neo, some of them, notably the fuel system, differ substantially. For this reason, special attention will be dedicated to subpart E of the CS25 document, especially CS25.951-CS25.1001, which relate to the fuel system of the aircraft. One of the design considerations, done to ensure compliance with the regulations, is the installation of the lightning rods at the end of the fuel tanks so that the tanks themselves are protected from lightning strikes, as specified in CS25.954. Furthermore, as mentioned in subsection 6.4.4, the tanks can be jettisoned in case of an emergency. This will improve safety by avoiding the risk of tank explosion during a crash landing or should a swift return to the airport be necessitated as specified in CS25.1001.

11.4. Recommendations

To properly ensure the safety of the CH4llenger aircraft further work will have to be performed. Given that no commercially available methane powered passenger aircraft currently exists, proper certification compliance cannot be performed yet. As a result, more coordination and communication with the responsible authorities will be required. During the certification process, new means of compliance will likely need to be created given the unconventional solutions applied during the design of CH4llenger. For these reasons, and to ensure a smooth certification process, the collaboration with the governing bodies should start at a relatively early phase of the design and involve numerous personnel.

[4] `https://www.easa.europa.eu/sites/default/files/dfu/CS-25_Amdt%203_19.09.07_Consolidated%20version.pdf`, [Cited on 17-June-2024]

12. Operations

The operations and logistics of a novel aircraft are critical to assess in order to evaluate the aircraft's implementation into regular operation. This chapter explores factors pertaining to the implementation of methane in airports around the world. This is done by proposing different sizes of airports, routes that would connect them, how the fuel is generated and how the fuel would be transported. More locally, turn-around operations are investigated, running from fuel storage to how the wing tanks are attached to the aircraft and maintenance aspects.

Firstly, three types of airports are explored in section 12.1, investigating the amount of flights per day they can sustain. Subsequently, routes between the airports are looked into, synthesising a potential market that could grow from utilising methane. From typical hub routes to more exotic options like smaller airports directly connected to each other (section 12.2).

Subsequently, fuel synthesis is discussed in particular detail in section 12.3, as there are caveats to using a green fuel. This process of creating synthetic methane requires recaptured carbon and green hydrogen to be produced. Green hydrogen requires clean water and green electricity. Moreover, the possibility of using biomethane as a supplement is also introduced. This would involve anaerobic digestion but is a lot less efficient and is only a product of waste biomass.

After the synthesis of fuel transportation is regarded in (section 12.4). After obtaining gaseous methane, it is either liquefied and transported in a cryogenic tank or left as a gas and transported through pipelines. The mode of transportation depends on the size of the airport. After transportation the methane may have to be liquefied if transported as gas. Finally, the fuel would have to be stored at the airport.

Following the logistics of the fuels, the specific airport operations are considered in section 12.5. Two main activities are of priority for the use of novel aircraft: the refuelling procedure and the general turn-around procedure. The refuelling procedure shall look into different options for having the novel types of fuels end up in the fuel tanks of the aircraft. The general turn-around procedure investigates the critical flow of activities that could occur from landing to take-off of the aircraft. Additionally, given the prevalent amount of sustainable fuels at the airport, it is recommended that all ground vehicles utilise sustainable fuels as well. Thus, the airport should implement a sustainable ground vehicle infrastructure ahead of the move to fully sustainable aircraft implementation in order to make the change more comfortable.

12.1. Types of Airports

Three sizes of airports are defined, allowing for an insight into potential future airport operations. These are large, medium, and small-sized airports, defined by the amount of traffic they experience. Table 12.1 show airports of each category that have been investigated. Through investigating the size of airports locations and local markets can be investigated to stimulate demand.

Table 12.1: Airports considered as part of operations.

	Option 1	Option 2	Option 3	Option 4
Large	London Heathrow (LHR)	Amsterdam Schiphol (AMS)	New York Kennedy (JFK)	Toronto Pearson (YYZ)
Medium	Toulouse-Blagnac (TLS)	Copenhagen (CPH)	Boston Logan (BOS)	Pittsburgh International (PIT)
Small	Eindhoven (EIN)	Richmond International (RIC)		

Large Airports
Large airports are defined as major existing hubs, with the highest traffic in terms of transatlantic operations. This includes the likes of Heathrow, JFK and LAX. Daily transatlantic operations can reach 119 flights a day. To represent the number of methane flights, 10% of those flights will be considered, these being a maximum of 12 flights per day. With each flight needing 55 000 litres of methane, a total of 660 000 litres of methane is necessary to accommodate all aircraft.

Medium Airports
Medium airports experience lower amounts of traffic and next to no transatlantic activities. Due to the small nature of the aircraft concept being considered and its long-range potential a new market could emerge. Expected traffic of one to three flights per day to other medium-sized airports across the Atlantic could easily be feasible. This would not overburden the medium airport with new infrastructure and excessive logistical operations, such as at the fuel storage or through refuelling procedures. The total daily consumption of fuel would be 165 000 litres per day.

Small Airports
Small airports are those in remote locations or with small volumes of traffic. They would not have a robust liquid methane infrastructure but rather accommodate enough fuel for a flight a week. As such, they would consume 55 000 litres of fuel over a period of a week.

12.2. Types of Routes
With differing sizes of airports and a 3917 nautical mile range on the CH4llenger, the logistics between them are analysed. This section will investigate feasible routes that can operate when the aircraft is introduced to the market. Once established in the industry, the range of airports will expand.

To help realise the possible routes, several example airports were chosen to represent methane hubs for the future, as depicted in Table 12.1. A map with the airports indicated can be seen in Figure 12.1. Four large and four medium-sized airports were chosen, two on either side of the Atlantic Ocean. These represent airports that would be able to sustain methane infrastructure and subsequently be able to expand and support the growth of methane. One small airport was chosen on either side of the Atlantic to represent more isolated and lower-demand areas, to show that methane can be implemented to connect less developed airports.

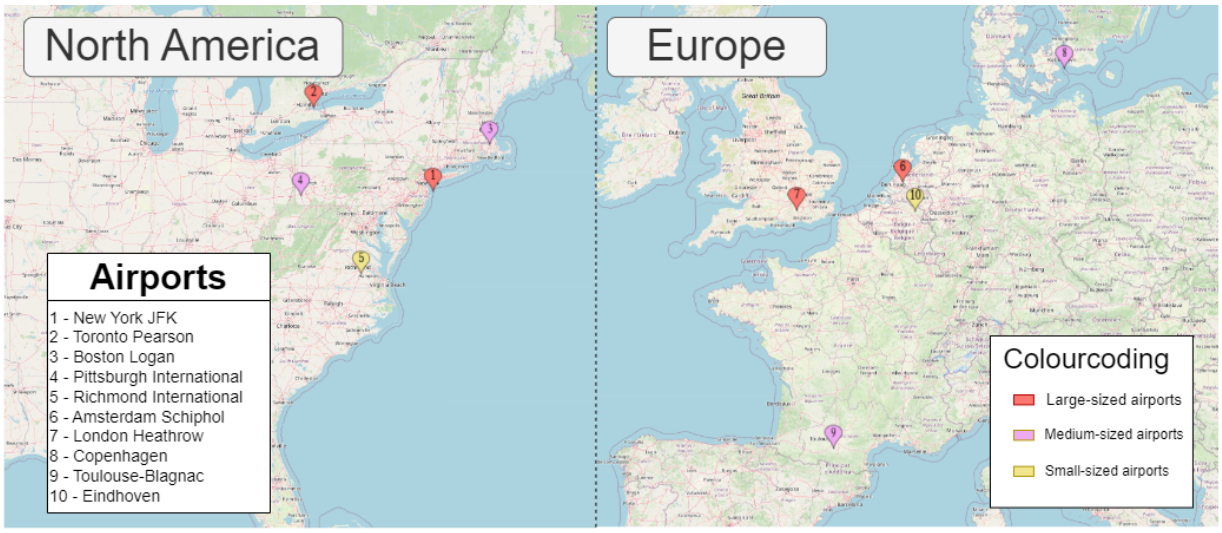

Figure 12.1: Locations of airports to be installed for transatlantic flights.

Based on the selected airports, several route options can be considered:

Large to Large Routes
These routes are between the large hubs, allowing for the most methane-powered flights per day. This makes up the majority of methane traffic and shall be the main focus for improvements on the tank refuelling processes.

Large to Medium Routes
This route allows for routes that typically need a stop through a hub to now be directly connected to the other side of the Atlantic. This represents an emerging market segment that could be very profitable and could relieve pressure from major hubs. Furthermore, at the medium airports 'innovation hubs' could be created, whereby different use-cases of the fuel can be tried and tested alongside operations, thus further reinforcing the need for medium airports.

Large to Small Routes
This route connects more isolated airports with lower capacities to the other side of the Atlantic. This route acts mostly as a proof of concept to show that the proposed Methane aircraft can be used in a versatile set of conditions. Moreover, it allows more direct connection to communities that typically would have to take extended journeys in order to cross the Atlantic. The airports would not have such a robust methane infrastructure, but could still reap the benefits, such as using methane for ground vehicles and heating when aircraft are not in operation. Small to Small routes would be unfeasible in the initial stages of implementation of the aircraft due to the infrastructure not being readily in place, and these routes being hard to economically sustain. After the proof of concept run, this possibility could be expanded upon.

Medium to Medium Routes
This route follows the same idea as the Large to Medium concept, although passengers can fly directly to less populated hubs rather than having to pass through Large hubs. These flights would be the starting point of connecting 'innovation airports' and could create an international community, strengthening the use-case of methane for aviation.

Figure 12.2: The shaded area indicates where the CH4llenger can fly from Schiphol airport.

Once the routes are established and the adoption of methane becomes widespread, expansion plans can be established. The shaded area of Figure 12.2 depicts the range of the aircraft originating

from the hub airport of Schiphol airport. With the primary focus on the East Coast of the USA and Canada. Expansion can grow into rural Canada, potentially connecting isolated locations with Europe. Furthermore, other locations such as Northern Africa and parts of Sub-Saharan Africa can be considered as possible locations to fly to. This includes Addis-Ababa, which can further link routes to Southern Africa and parts of South America. Moreover, hubs in the Middle East could be established, potentially connecting routes to East Asia. In conclusion, growth will be important to the global connection of methane-powered aircraft, starting with a strong initial implementation in the Western hemisphere.

12.3. Fuel Synthesis

With a holistic investigation into the adoption of methane in aircraft utilisation, its conception and impact must be considered. This section looks into ways to produce methane and factors that impact its availability and way of being distributed through local markets.

12.3.1. Synthetic Methane

Synthetic methane production involves a chemical process where hydrogen and carbon dioxide react to produce methane and water. This process, known as methanation, typically occurs in the presence of a catalyst, commonly nickel-based, which facilitates the reaction at lower temperatures and pressures. The catalyst plays a crucial role in the efficiency of the reaction, allowing it to proceed at a practical rate and enhancing the overall yield of methane [69].

The general reaction can be represented by Equation 12.1, known as the Sabatier reaction. This reaction is exothermic, meaning it releases heat, which can be advantageous for maintaining the reaction conditions but may also require careful management to avoid overheating and catalyst deactivation. Managing the thermal dynamics of the reaction is essential to maintain optimal catalyst activity and longevity, ensuring a consistent production rate and quality of the synthetic methane [69].

$$CO_2 + 4H_2 \rightarrow CH_4 + 2H_2O \tag{12.1}$$

The hydrogen used in methanation is usually produced through water electrolysis, a process that splits water into hydrogen and oxygen using electricity. When the electricity used for electrolysis comes from renewable sources, the resulting hydrogen is referred to as green hydrogen. This green hydrogen is then combined with captured carbon dioxide, which can be sourced from industrial emissions or directly from the atmosphere [70]. The integration of these processes not only helps in producing synthetic methane, but also makes the synthetic methane a carbon-neutral fuel [71].

The efficiency of synthetic methane production is composed of the three different processes involved. To begin with, according to TES CTO Jens Schmidt, 83% of the lower heating value that goes into the reactor is recovered; the remaining 17% is high-temperature heat, which could be re-used to generate electricity, increasing the efficiency of the process up to 90% [1]. While this seems high, the efficiency of the production of green hydrogen through hydrolysis must also be considered. According to Pashchenko, industrial production of green hydrogen has achieved up to 85% efficiency [72]. Lastly, the efficiency of the carbon capture method should also be taken into account. According to several sources, carbon capture efficiency is relatively high, being around 90%.Taking everything into account, the overall efficiency (without including high-temperature heat used for electricity) would be around 63.5%. While not ideal, this efficiency is still a lot higher than synthetic kerosene, as the Low-Temperature Fischer-Tropsch process for creating the kerosene has a 66.4% efficiency [73], and in combination with carbon-capture, gives a total production efficiency of 30.5%.

[1] `https://tes-h2.com/blog/molecules-mass-and-finding-the-right-energy-balance-a-deeper-look-into-the-methanation-process`, [Cited on 18-July-2024]

Innovations and advancements in catalyst development, process optimisation, and integration with renewable energy sources continue to enhance the efficiency and viability of synthetic methane production. Researchers are exploring various catalyst materials and reaction conditions to further improve the reaction rates and reduce energy consumption. For instance, there are developments in engaging light to induce catalytic activity in methanation. Additionally, coupling methanation with advanced carbon capture technologies and renewable hydrogen production methods can enhance the overall sustainability and economic feasibility of the process [74].

Additionally, the methanation process contributes to the circular carbon economy, promoting sustainability and helping to mitigate climate change. By capturing and reusing carbon dioxide the process is essentially carbon-neutral, thus playing a significant role in efforts to decarbonise the energy sector. This aspect of methanation aligns with global goals for reducing carbon footprints and advancing towards a more sustainable and resilient energy system [71].

In conclusion, the production of synthetic methane through methanation is a promising pathway for creating a sustainable and carbon-neutral energy carrier. By leveraging renewable energy and CO_2 capture, methanation supports broader climate goals by being carbon-neutral. The transportation of methane will be described in more detail in section 12.4, highlighting the practical aspects and benefits of incorporating synthetic methane into the current energy infrastructure.

12.3.2. Biomethane

In addition to the production of synthetic methane using carbon capture, it would be possible to add the production of biomethane. Biomethane is methane that is derived from biomass, which is essentially waste and residues of biological origin or organic material from agriculture. The end product of the process would be methane and carbon dioxide that could be used for the production of synthetic methane [75].

Primarily, biomethane is best produced using anaerobic digestion. Anaerobic digestion involves the break down organic matter using bacteria or microorganisms; they digest feedstocks in the absence of oxygen, eventually making biogas. Biogas is composed of mostly methane and carbon dioxide, but is not pure enough to be considered biomethane. Hence, the biogas would be scrubbed or purified of the carbon dioxide and the rest of the impurities, resulting in methane of high purity; the removed carbon dioxide could be added to the additional carbon dioxide captured for the purpose of methanation of synthetic kerosene [76].

Biomethane, if used, would be primarily produced as a supplement to synthetic methane. Its existence assumes the presence of waste, which means its benefits stem from negative influences on the environment. Hence, in an ideal world, only synthetic methane is used as a fuel source for the CH4llenger. To add to that, biomethane's production efficiency is low at around 36% [77], essentially matching that of synthetic kerosene. Despite its low efficiency, it already has wide-scale applications in the industry, as will be explained in subsection 12.3.3.

Overall, anaerobic digestion for biogas production and the following upgrading of biogas accounts for 90% of total biomethane production worldwide, according to [78]. If implemented even on a small scale, the technology seems to be feasible for the purposes of the air transport industry.

12.3.3. Biomethane Current Scale and Networks

Biomethane production is currently experiencing high growth rates, with governments putting in place regulations and targets for biomethane produced by the end of the decade. The European Commission for example has put in place the REPowerEU plan with the goal of producing 35 billion cubic metres (bcm) of biomethane by 2030.

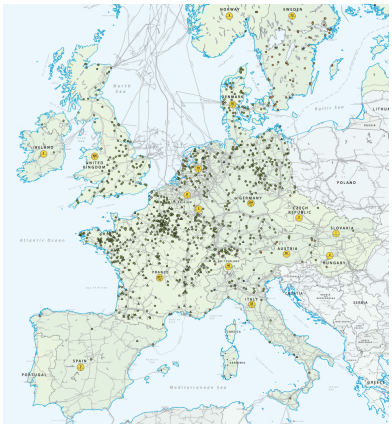

Figure 12.3: Zoomed-in map.

In order to accomplish this goal, biomethane plants have been built and are still being constructed in order to meet this increase in demand. As of 2024, Europe has reached a total of 1322 biomethane production facilities, which implies a growth of 30% in plants with respect to two years prior. The location of these plants within Europe is captured in the "Biomethane Map 2022-2023", as seen in Figure 12.3. With these new plants, Europe is currently already producing over 35 bcm and is expected to scale up production even more in the upcoming years [2].

With the growth of the production facilities, however, there also come challenges regarding the transport of methane for example. It is suggested that the biomethane production plants are built close to existing LNG pipelines and infrastructure in order to allow for efficient transportation. Another important factor to consider in the scaling-up is the plant size, as extensive plants could lead to deforestation[3].

12.3.4. Cost of Synthetic Methane and Biomethane

When it comes to producing synthetic methane by means of carbon capture, Direct Air Capture (DAC) has been extensively investigated as the preferred method to capture these carbon dioxide emissions. The costs involved with this method range between 693 to 1587 euros per ton CO_2 according to [79]. Taking a methanation plant in Abu Dhabi as an example, it turns out the electrolyser constitutes the most costly component, followed by PV field, hydrogen storage tank, and lastly the reactors. Combining these costs then leads to the cost of synthetic methane being around 3 euros per kilogram in present times. In contrast, green hydrogen is deemed to currently still be more expensive per kilogram [79]. Furthermore, looking forward to 2050, [80] predicts synthetic methane to cost 31 cents per kilogram as a lower bound and 2.1 euros as an upper bound. Since this market research does not include the scenario of a revolution in the aviation sector by using methane-fuelled aircraft, likely an economy of scale for synthetic methane will cause the price to be driven down, leading to the estimation of 31 cents per kilogram to be selected for further calculations.

In terms of biomethane, globally the costs of production range between 54-91 euros/MWh, showing large economies of scale [80]. These costs are comprised of capital costs, operational costs and feedstock costs. Of the costs, the production facility is on average the most costly element of the biomethane supply chain [81]. The total feedstock-related costs consist of feedstock, pre-treatment capital & operational as well as compliance costs and show a large range in cost. For the capital cost

[2] https://www.europeanbiogas.eu/strongnew-record-for-biomethane-production-in-europebrshows-eba-gie-biomethane-map-2022-2023-strong/, [Cited on 17-June-2024]

[3] https://www.euractiv.com/section/energy/news/the-future-of-biogas-in-europe-its-a-local-affair/, [Cited on 17-June-2024]

especially, economies of scale have been noted to have the strongest impact on biomethane production cost. However, projections for the upcoming years have shown the costs for biomethane decreasing significantly, with a price of 0.62 euros/kg by 2050 according to CE Delft [82].

12.3.5. Liquefaction

Considering that the airports and aircraft will be utilising liquid methane, the gaseous methane will need to be liquefied at a liquefaction plant. Despite undergoing a purifying process during its production, the methane will still have to be pre-cooled in order to remove any remaining impurities. Then, the methane is further cooled to its boiling point of -160°C at one atmosphere, usually through several layers of refrigerators. This reduces the volume of the methane by a factor of around 600, but of course the storage tanks will have to be insulated to keep the cold temperatures [83].

There are multiple ways that methane is typically liquefied. For large-scale purposes, such as ship tanker transport, it is liquefied near the production plant; these liquefaction plants are most commonly located in onshore methane export terminals with large access points. In certain situations, the gaseous methane is liquefied offshore by floating LNG floats, which would be useful in an area with multiple remote airports, such as in the South Pacific. For smaller airports, it could be liquefied in smaller satellite LNG facilities that are connected to gas transmission or distribution lines or liquefied within the storage facility in the airport [83]. More information on the structure of the transport will be denoted in section 12.4.

12.4. Transportation

With the fuel being sourced and produced away from the places it is used, methods of transporting the fuels must be implemented and robustly set in place in order to allow a healthy methane ecosystem to thrive. Three main methods are considered: trucks, trains and pipelines. These would allow ease of access to methane from hubs such as methane plants or ports.

12.4.1. Small Airports

Considering small airports, they do not have many flights and will likely not be able to have large infrastructural changes. Therefore, having a liquefaction plant on-site may not be feasible, and it is preferred to bring the fuel directly to the airport in its liquid form. This presents the challenge that the further away a methane liquefaction plant/ ship port is located, the greater the transportation challenges. Utilising methane imports at ports will present further challenges. The two transportation modes for methane are generally speaking by trucks or train[84]. Transportation through long-distance cryogenic pipelines seems unfeasible due to its infrastructural challenges and energy requirements. A truck can carry about 34 000 litres [84]. Given that the aircraft will carry 55 000 litres of liquid methane, two trucks will be needed per week. A railway, on the other hand, can carry about 110 000 litres per tank. Reassessing the feasibility of using trains, it seems excessive to adopt a railway system such that a train can pass through it once a week.

12.4.2. Medium Airports

As already stated, medium-sized airports will have to be able to refuel about 3 flights per day. Due to this increase in fuel consumption, transportation modes start to become feasible. This includes the transportation of methane through natural gas pipelines. In this case, a liquefaction plant would need to be set in place at the airport. Such a plant is inspired by an existing design [85], and would provide liquefied methane at the needed scale. In addition to this, the transportation modes of trucks and trains are also considered. With the increase of required fuel volume to 165 000 litres, 5 trucks or 1 train wagon would be required per day. This renders transportation by trucks feasible, but transportation by trains remains an unlikely choice.

12.4.3. Large Airports

For this airport option, the fuel volume requirements are four times larger compared to the previous one, at 660 000 litres. Therefore, a slightly larger liquefaction plant would be required. Looking at the other modes, this time 20 trucks, or 6 train wagons are required per day. While 20 trucks per day does still seem feasible, it is starting to lead to more complicated operations. On the other hand, utilising 6 train wagons seems like a more realistic value to be used. Hence, this airport option is capable of using the most diverse set of transportation modes. Nevertheless, operations may be the easiest by having natural gas pipes and liquefying the fuel.

12.5. Airport Logistics

In order to facilitate the amount of fuel necessary for the continuous functioning of transatlantic, methane-powered aircraft sufficient fuel must be present at the airport. Furthermore, the storage system should be malleable to accommodate varying rates of resupplying in case of logistical delays. Given the three airport sizing possibilities, different operational plans shall be considered. Furthermore, the aircraft design in consideration can fit up to around 206 people, thus is not on par with larger aircraft. As such, liquid methane operations shall not take over the entirety of daily transatlantic activity when the aircraft is introduced to the market.

12.5.1. Large Airports

With twelve flights expected per day, it is important that sufficient amounts of fuel are available, even despite unforeseen circumstances. As such, a multiplication factor of five is imposed. This ensures the airport can run for five days without refuelling. This also represents the maximum time that liquid methane can be stored without dramatic losses. Therefore, 3.3 million litres of liquid methane is to be stored at the airport.

With 3.3 million litres of liquid methane needing to be stored, a three-tank storage system was chosen, with each tank being 1.1 million litres. As such, at least one tank can be continuously used whilst another is being refuelled. Existing methane storage tanks exist such as those supplied by CryoSpain [4]. As such, industry-standard tanks will be bought to store the Liquid Methane on-site at the airport.

The new Liquid Methane storage tanks shall be implemented at the same location as those where kerosene tanks are. However, space must be allowed for the tank exchange centre, where trucks holding the empty external tanks of planes will arrive and have them refuelled with Liquid Methane.

12.5.2. Medium Airports

With 165 000 litres of liquid methane being used per day, a moderate amount of tolerance must be imposed, particularly if transport via trucks/other above-ground options as small delays could spiral into a larger hold-up. Therefore, a three-time multiplier on fuel is imposed, to allow for logistical problems to be mitigated, and sized with respect to the logistical capabilities of the airport. As such, a total of 495 000 litres of liquid methane is to be stored at the airport.
Again, a three-storage tank system shall be implemented, each capable of holding a day's worth of fuel. This follows the same reasoning as the large airport, allowing for logistical flexibility.
Finally, the storage location will follow the same idea as the large airport by being at the same location as the kerosene tanks and allowing space for tank refuelling.

12.5.3. Small Airports

Small airports are interesting due to their ultimately smaller demand due to their limited flight traffic. With one projected flight per week, a limited volume of fuel is stored. With losses, delays or perhaps some overfilling necessary, one and a half times the volume of a standard flight shall be stored, thus

[4] `https://cryospain.com/storing-liquefied-natural-gas`, [Cited on 11-June-2024]

resulting in 82 500 litres of liquid methane.

A single tank shall be used to store the fuel due to the limited amounts of fuel utilised and the lack of operational difficulty. It shall again be located among other fuel tanks, with space for external tank refuelling.

12.6. Refuelling Process

Once at the airport, the distribution of fuel from storage to the aircraft must be adapted to cryogenic means. As such, a new methodology must be implemented to allow for the specific properties of liquid methane, including and not only limited to the cryogenic nature it has. Methods for the different sizes of airports are proposed to optimise operational logistics.

12.6.1. Refuelling at Large and Medium-Sized Airports

Truck operations are already very robustly in place at airports and utilised to transport Jet A-1 fuel. The same methodology could be employed for cryogenic fuels by loading filled external tanks and driving them directly to the aircraft at the stand.
The overall refuelling process is depicted in Figure 12.4, it would commence with two trucks carrying two truck beds one after the other, arriving with empty tanks at the tank refuelling centre, where the tanks will be filled with liquid methane. Subsequently, the truck drives to the aircraft at the gate and proceeds to remove the existing empty tanks onto an empty truck bed. This is facilitated by the truck beds being able to raise to connect with the tanks and being able to lower them on their own accord. Subsequently, the filled tank is attached in place. The same process is repeated on the other side of the aircraft, either by the same truck or another truck, depending on the logistical capabilities of the airport. After which, the tanks are vented of gas (leaving only liquid) or purged (everything removed) at the fuel storage area to recuperate as much methane as possible. The tanks are then either sent to a maintenance centre if they are not to be used for a while, where they are cleaned and monitored or brought back to the tank refuelling centre and the cycle restarts.

In the case of a medium-sized airport, a single truck could be used for refuelling, which has three truck beds: two for the filled tanks and one free to accept an empty tank whilst a filled tank is being loaded. This process is likely to take more time as one tank has to wait for the other to be attached. Thus, work cannot be performed in parallel, but saves on the number of operation personnel.

Moreover, if an incident were to happen with a singular truck, the entire fuel system would not be compromised, thus inherently employing safety in its design. The time for refuelling would be very rapid due to the nature of simply replacing tanks and not waiting for fuel to pour in. So long as the logistical planning of trucks arriving at the aircraft is managed well, particularly at large airports, then the turnaround time can be absolutely minimised. This method also allows for flexibility, for if the aircraft is moved to another gate the trucks can adapt with ease. The operational complexity of a system like this would again be moderate, but it has its own problems. For one, personnel would have to be specially trained to exchange the fuel tanks, be able to analyse specific pipe connections, secure special bolts, and know how to properly vent/clean tanks during maintenance. A simple error could lead to grave safety hazards and environmental consequences, leading to an explosion in the worst-case scenario.

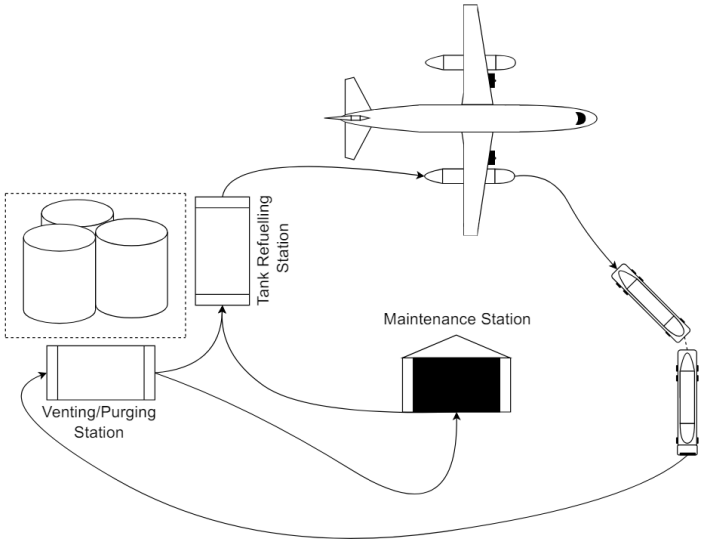

Figure 12.4: Process for refuelling the aircraft.

Furthermore, the necessary upgrades to infrastructure would be minimal, with upgraded trucks being the main difference, yet an increase in operational complexity would result due to more personnel being needed to ensure proper refuelling and safety.

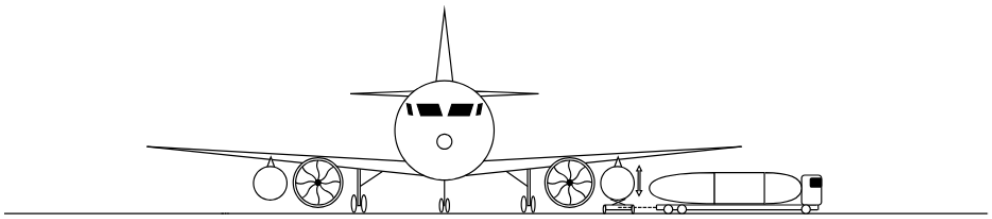

Figure 12.5: Schematic depicting external tank loading concept.

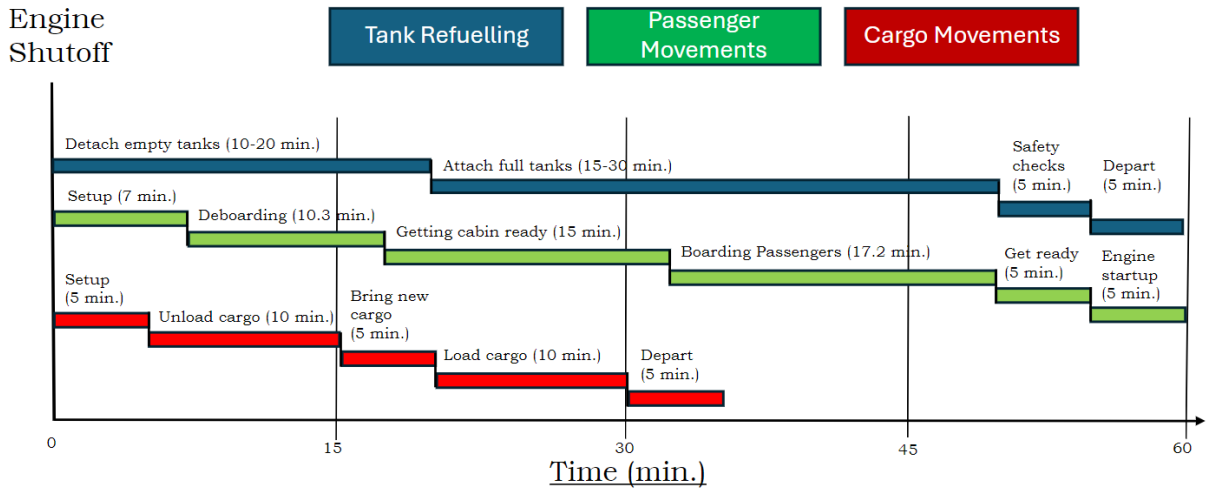

Figure 12.6: Gantt chart of the turnaround procedures.

12.6.2. Recuperation of Gaseous Methane

During the refuelling process of the liquid methane tanks, there will be a substantial amount of methane which has undergone gasification. In airports which have liquefaction plants, this can simply be liquefied along with the incoming gaseous methane. However, in airports which do not have such an infrastructure, this methane needs to be dealt with. Releasing it to the atmosphere will result in large amounts of greenhouse gas emissions. Therefore, an alternative is proposed in which the gaseous methane is temporarily stored in pressurised tanks and then fed through a gas generator to power the airport. While such a concept is not considered in much more detail, the existing Jensen power plant [5] can be used as a point of reference.

12.7. Turn-Around Process

Concluding chapter 12 on operations, a turn-around process is elaborated. This entails the ground operations surrounding the aircraft between landing and take-off, ensuring that all critical activities are performed within an allocated 1-hour window as per requirement **CH4-STK-06**. The process is split into three main streams of activities: refuelling, passenger and cargo movements. The turnaround procedure assumes that all necessary equipment is stationed at the gate ahead of the aircraft's arrival.

12.7.1. Large and Medium Sized Airport Turn-Around Process

The refuelling operation commences by having the trucks carrying full tanks waiting at the gate for the aircraft to arrive. Once engine shut-off has occurred, a safety perimeter is established, denoted with cones. With the area clear, an empty tank is removed. The tank is detached by removing bolts and disconnecting the various cryogenic feed lines. This takes up to 20 minutes, with the time to properly check the system ahead of detaching it, assuring safety and no hazards that could propagate. The second activity is to attach the filled tanks. This is done by the truck bed raising the tank into position and the ground workers attaching feed lines and ensuring that safety checks are performed. This process takes 30 minutes with the time to not rush the process and make sure that the tanks are attached properly and are performing correctly. Subsequently, final safety checks are performed on the aircraft as well as on the truck so that the tanks are considered to be in a 'safe' configuration. Finally, the area is cleared up, and the trucks depart the gate, allowing the aircraft to taxi away.

In the passenger movements, firstly the aircraft has to be set up. That is, the doors have to be connected to a skybridge/ staircase, then the doors are opened, and lastly, the crew has to be in the right position to accommodate the outgoing passengers. An estimate for this is 7 minutes. Afterwards, passengers board the plane. In the A321 manual [15] it is indicated that this should take 20 pax/minutes, corresponding to 10.3 minutes for all passengers. Before passengers can board the plane, the cabin has to be ready. Here, the cabin is cleaned and a toilet service, water service, and security check are performed. Estimates are hard to get, however, it is assumed that this will take about 15 minutes. Again, a value from the A321 manual is used, being about 12 pax/minutes, leading to around 17.2 minutes. Afterwards, the aircraft has to get ready before the engines can start up. This includes getting all the crew members inside and closing the door. Such a procedure should take around 5 minutes. Lastly, the engines are started up before the aircraft departs. Again, this takes about 5 minutes.

As for the cargo movements, the first step is to approach the aircraft with the cargo and set up all the necessary equipment. This includes opening the aircraft cargo hold, setting up the conveyor belts and getting the trucks into position. This takes 5 minutes. Next, all the cargo from the forward, aft, and bulk cargo compartments is unloaded from the plane, taking 10 minutes. Subsequently, the next truck with new luggage and cargo arrives and sets itself into position, taking 5 minutes. This cargo is then loaded into the aircraft, taking 10 minutes. Finally, all the equipment is cleared away and the aircraft is ready for engine start-up.

[5] `https://www.jenbacher.com/en/gas-engines`, [Cited on 17-June-2024]

12.7.2. Small-Sized Airport Turn-Around Process

With the limited operational capabilities of small airports, a different refuelling procedure must be considered. Here, it is considered that the tanks shall not be detached but rather refuelled whilst still being attached to the aircraft. This would be facilitated by refuelling them via the same ports that would be used to refuel them at the tank refuelling centre. This helps smaller-sized airports continue operating without extensive infrastructure. However, as depicted in Figure 12.7, refuelling cannot happen when passengers are boarding/onboard the aircraft, thus the entire process takes longer, with a total turn-around time of 66.7 minutes.

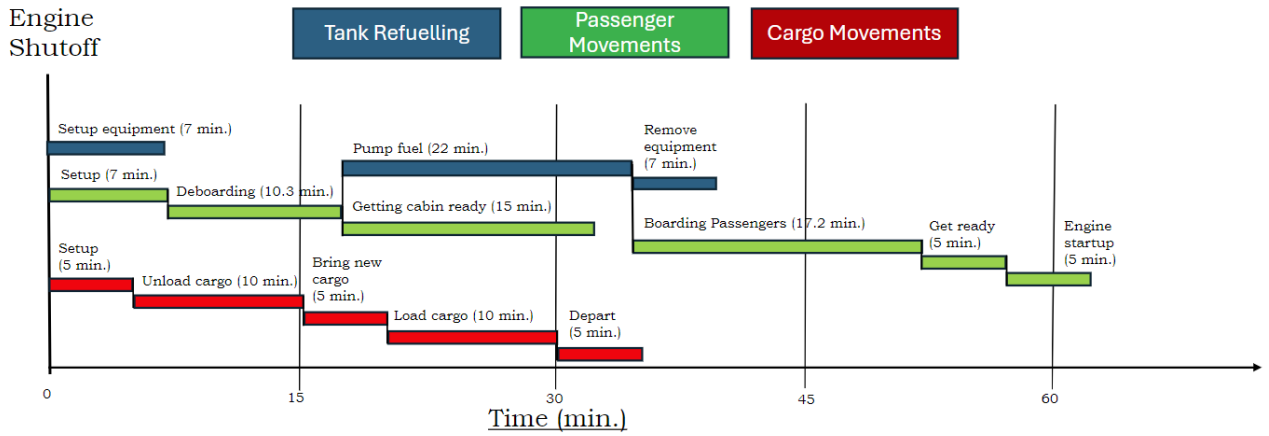

Figure 12.7: Ground operations Gantt chart for small-sized airports.

12.8. Recommendations

With the possible scope to continue innovating past the synthesis of this report, some recommendations for future research have been identified.

Firstly, routes between small airports (small to small) could be investigated further. It was assumed that because of the transatlantic nature of the aircraft, such flights would not be popular and not worth considering in more detail due to limited market attractiveness and not enough small airports willing to make the change to methane. Nevertheless, a limited number of similar routes might be in demand, even if they are not necessarily transatlantic. Hence, in a more advanced future stage, this should be revisited to see how this could be adapted in an emerging market and allow for further connectivity in the world.

Additionally, a primitive fuel tank transport concept was developed utilising trucks with trailers. With further development, it would be beneficial to consider the type and amount of trucks which go to the aircraft, and how many trailers they each carry. Moreover, tracks or guided trailers could be used to make the use of trailers even easier to implement. Notably, more futuristic designs involving fully automated systems could be researched.

Lastly, Figure 12.6 and Figure 12.7 propose a turn-around procedure. With more experience with the nuances of methane and how it is handled in an airport setting, updated ground operations could follow along with a more realistic duration of the respective procedures.

13. Cost Analysis

A cost analysis needs to be performed in order to establish the costs in the different stages of the life cycle and determine the operation costs. With these numbers computed, a return on investment can then be found in order to verify the economical viability of the product. The chapter start with a cost breakdown structure in section 13.1 to investigate the different sources of cost throughout the lifetime of the project. Then the section dives into details by investigating the research and development cost in section 13.2, manufacturing costs in section 13.3, total production costs in section 13.4, capital costs contingency in section 13.5, operational costs in section 13.6, direct operation costs in subsection 13.6.1 and finishes off with return on interest in section 13.7.

13.1. Cost Breakdown Structure

Markish from the Massachusetts Institute of Technology conducted extensive research on the valuation techniques of commercial aircraft [86]. The cost breakdown of a new aircraft was analysed by looking at the operational, development and manufacturing costs of aircraft at the time, as seen in Figure 13.1. According to Markish, those three sections compose 97% of the cost, while the rest do not concern the manufacturers. As a result, those aspects have been omitted from the analysis. Furthermore, tools and jigs required for the final assembly of the systems are considered in the cost of the systems themselves.

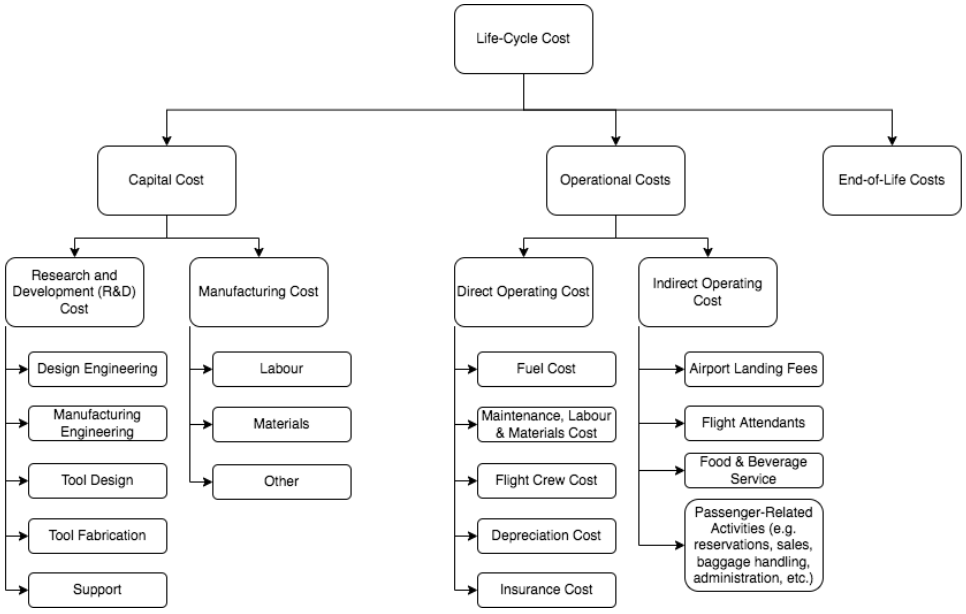

Figure 13.1: Structure showing the breakdown of aircraft costs.

13.2. Research and Development (R&D) Costs

The first part of the capital costs of the aircraft will come from research and development (R&D), which is considered a non-recurring cost; given that the aircraft will be of relatively novel design, much of the cost and time will be allocated towards research. As shown in Figure 13.1, the R&D costs are separated into design engineering, manufacturing engineering, tool design, tool fabrication and support.

Moreover, the aircraft itself is separated into different categories. There are namely the wing, empennage, fuselage, landing gear, propulsion, systems, and payloads, which refers to payload storage.

Table 13.2 contains R&D costs per kilogram of the aircraft part. It is important to note that the propulsion system was originally omitted from the breakdown. The reason for that is that the majority of the system is designed from scratch as it encompasses new unconventional technology.

To estimate how much of the total aircraft cost is to be made up by the propulsion system, further analysis of the market was performed. While Willcox [87] places the estimate of an engine making up approximately 10% of the total cost of the aircraft, looking at the list prices of the A321neo and the LEAP-1A engines installed on it, the cost fraction is significantly larger. The engines of the aircraft, serving as a baseline of the to-be-designed aeroplane, are responsible for 22.4% of the total cost, with LEAP-1A said to be costing $14.5 million each and the A321neo $129.5 million including engines[1] [2].

What needs to be considered as well is that while the A321neo operates using conventional fuels, CH4llenger will not. As a result, it has been assumed that the propulsion system of the new aircraft (excluding any contingencies) will be at least **50%** more expensive. Due to the lack of publicly available data, this number has been assumed to be leading, however, large contingencies shall be taken in further budgeting.

Based on that, the cost of the propulsion system as a fraction of the total aircraft cost can be obtained. Taking the A321neo as an example, the new cost fraction can be calculated as follows:

$$\text{Cost} = \frac{2 \cdot Eng_1}{AC - 2 \cdot Eng_0 + 2 \cdot Eng_1} = \frac{2 \cdot 1.5 \cdot Eng_0}{AC - 2 \cdot Eng_0 + 2 \cdot 1.5 \cdot Eng_0} = \frac{3 \cdot Eng_0}{AC + Eng_0} \tag{13.1}$$

Using the values for the LEAP-1A and the A321neo, the cost of the propulsion system would account for 30.2% of the aircraft, which can be used to obtain a detailed budget breakdown of the aircraft, shown in Table 13.1.

Table 13.1: Cost distribution of the propulsion system [%].

Category	Engineering Design	Material Engineering	Tool Design	Tool Fab	Support	Labour	Materials	Other	Total
Propulsion	38.356	9.586	10.072	33.370	4.501	2.736	1.004	0.397	100.00

Table 13.2 shows the actual value obtained from Markish, who used statistical models based on stochastic differential mathematics [86], in addition to the propulsion system. The numbers have been adjusted to account for inflation, as the report was published in 2002.

Table 13.2: R&D costs of different aircraft components.

USD	Design Engineering	Material Engineering	Tool Design	Tool Fab	Support	Totals /kg
Wing	26490	6621	6954	23046	3111	66222
Empennage	77912	19480	20451	67783	9154	194779
Fuselage	47941	11984	12586	41712	5632	119855
Landing Gear	3731	934	978	3245	437	9325
Propulsion	96766	24184	25409	84186	11355	241900
Systems	51250	12814	13452	44588	6020	128124
Payloads	16078	4018	4220	13990	1890	40196

13.3. Manufacturing Costs

In addition to the research and development costs, there is the actual production cost of the aircraft. This cost mainly consists of labour and the materials needed, as well as other minor costs. Using the

[1] `https://www.geaerospace.com/news/press-releases/joint-ventures/cfm-leap-1a-powers-airbus-a321neo-first-flight`, [Cited on 17-June-2024]

[2] `https://pilotpassion.com/how-much-does-an-airbus-plane-cost/`, [Cited on 02-May-2024]

values from Markish [86], the cost breakdown per kilogram of each subsystem is included in Table 13.3. These were also adjusted for inflation.

Table 13.3: Production costs of different aircraft components [USD/kg].

	Labour	Materials	Other	Totals
Wing	609	204	88	901
Empennage	1614	484	233	2331
Fuselage	679	190	98	967
Landing Gear	107	98	16	221
Propulsion	1574	5778	228	2380
Systems	315	91	46	452
Payloads	405	100	59	564
Final Assembly	58	4	3	65

Table 13.4: Final production cost breakdown per subsystem.

Million USD	Manufacturing	R&D	Total
Wing	5.719	1.008	6.727
Empennage	3.338	0.669	4.007
Fuselage	14.277	4.244	18.521
Landing Gear	0.926	0.094	1.019
Propulsion	36.893	8.994	45.887
Systems	1.617	1.099	2.717
Payloads	27.371	4.678	32.049
Final Assembly	0.539	0.000	0.539
Aircraft	90.141	21.324	**111.465**

13.4. Total Production Cost

Using the weight values from section 8.3, the actual values of the cost per subsystem for both the design as well as the manufacturing can be calculated. The breakdown per subsystem is displayed in Table 13.4. The research and development cost assumes that 417 aircraft will be delivered, and so the total R&D cost is also divided by 417. This number results in the production cost to be around 112 million USD.

13.5. Capital Cost Contingency

With a target of $120 million per unit of the proposed design, contingency must be absolutely implemented in order to account for unpredictable costs/evolved risks that would impact the cost of a particular category and phase. Utilising fractional estimates established in [88], margins of the absolute cost related to each category as shown in Table 13.6. Based on the significance of each phase, a value between the minimum and maximum margin value is utilised to measure contingency. The margin values have been reduced as this report contains the reasoning towards the end of the conceptual design phase. As several of the systems have been designed, the risks involved with their design are lower, which is reflected by the smaller contingencies.

Table 13.5: Contingency margin values for aircraft costs [Million USD].

Category	Manufacturing	R & D	Total
Wing	0.858	0.101	0.959
Empennage	0.501	0.067	0.568
Fuselage	1.428	0.212	1.640
Landing Gear	0.139	0.009	0.148
Propulsion	11.068	1.799	12.867
Systems	0.323	0.165	0.488
Payloads	2.737	0.468	3.205
Final Assembly	0.108	0.000	0.108
Aircraft	17.054	2.929	19.982

Table 13.6: Contingency margin percentages for aircraft costs.

Category	**Contingency Margin** (%)
Wing	10-15
Empennage	10-15
Fuselage	5-10
Landing Gear	10-15
Propulsion	20-30
Systems	15-20
Payloads	10
Final Assembly	20

As stated in Table 13.6, the contingency margin for each system is determined by both the fact that the project is currently in an early design phase as well as an estimation of the size of the changes that will be performed. The wing, empennage, landing gear, and systems categories all have a contingency margin of 10 to 15%, as they will be impacted by the use of the alternative fuel, naturally. The fuselage, however, is given a margin range of 5 to 10%, as it is quite a simple structure, and the basis for it is fairly similar to the Airbus A321neo. Similarly, the payloads are also expected not to differ too much, and so a smaller contingency of 10% is allocated towards it. Of course, due to the nature of the project, meaning the selection and use of an alternative fuel, the development and design of the propulsion system will have larger uncertainties. As a result, a larger contingency margin of 20-30% is allocated

so that any potential inaccuracy of the cost estimate associated with the novel system is also accounted for.

Moreover, each phase of each category is allocated either the lower end or the higher end of the margin, depending on the significance of the phase towards the category. Generally, the design and development are typically given the lower end of the contingency margin. On the other hand, the production and maintenance and are typically given the higher end of the margin. As it can be seen in Table 13.5, the overall contingency allocated per aircraft is around $20 million per unit, which is roughly a quarter of the total cost budget. This would mean that the target cost of the aircraft would be roughly $92 million.

13.6. Operational Costs

As shown in Figure 13.1, the operational cost consists of direct operating costs and indirect operating costs. As for the former, the direct operating cost can be computed by means of empirical relations for each of six components, namely fuel cost, maintenance, labour &materials cost, flight crew cost, depreciation cost and insurance cost as seen in [89]. The indirect operating cost is then also estimated by means of an empirical relation from the same source.

13.6.1. Direct Operating Cost

In order to compute the Direct Operating Cost (DOC), the cost per mile C_{am} for each of the six components needs to be computed and summed in order to find the total DOC. When looking at the first element of the DOC, namely the fuel cost, the total amount of required liquid methane in kilograms was divided by the number of travelled nautical miles (3500 nm according to **CH4-STK-01**) in order to obtain the 6.71 required kilograms of methane per nautical mile travelled. Given the green methane price per kilogram currently is projected to be 31 cents per kilogram, a total C_{am} of 2.22 USD/nm was found subsection 12.3.4.

Now, looking at the second component of the DOC, the maintenance, labour & materials cost, the costs were split up into the costs associated with the airframe and those with the engines, each subsequently subdivided into its labour cost and material cost. The airframe labour C_{am} was then found using the relation [89]:

$$C_{am_{airf_{lab}}} = \frac{L_{mh_f} \cdot t_f + L_{mh_c}}{V_b \cdot t_b} \cdot r_L \cdot \sqrt{M_{cr}} \tag{13.2}$$

From this equation, the number of labour man-hours per flight cycle L_{mh_c} was determined following from $L_{mh_c} = 6 + 0,05 \cdot \frac{W_e}{1000} - \frac{630}{\frac{W_e}{1000}+120}$ and the number of labour man-hours per flight hour L_{mh_f} from $0.56 \cdot L_{mh_c}$. The, t_f is the block time t_b, namely 9.25 h for the mission profile, minus the ground part of 0.25 h [89] [3]. The block speed V_b, following from t_b in combination with the range, was determined to be 378.4 nm/h. Next, the labour rate r_L was based on the one reported in [89] with inflation included, ending up at 54.63 USD/h in 2024. Lastly, the the critical Mach number M_{cr} for subsonic aircraft according to this source should be taken to be the unity. Thus, combining these parameters and computing the C_{am} from the airframe due to labour is 0.78 USD per nautical mile. Secondly, looking at the materials cost for the airframe, the following relation holds [89]:

$$C_{am_{airf_{mat}}} = \frac{(TC - n_e \cdot C_e) \cdot (3.08 t_f + 6.24) \cdot 10^{-6}}{V_b \cdot t_b} \tag{13.3}$$

TC being the total aircraft capital cost, 120 M USD, n_e being the number of engines and C_e being the cost per engine, which for a LEAP-1A is 14.5 M USD [4], the C_{am} for the airframe materials amounts to

[3] `https://www.airwaysmag.com/legacy-posts/longest-narrow-body-flights23`, [Cited on 18-June-2024]

[4] `https://aviationweek.com/air-transport/aircraft-propulsion/lion-group-completes-55-billion-leap-1a-purchase`, [Cited on 18-June-2024]

0.88 USD per nautical mile.

The same procedure can be followed to determine the labour and material costs for the engine. The former is obtained using the relation [89]:

$$C_{am_{eng_{lab}}} = \frac{r_L \cdot n_e}{V_b \cdot t_b} \cdot (0.6 + 0.027 \cdot \frac{F_{to}}{1000} \cdot t_f + 0.065 + 0.03 \cdot \frac{F_{to}}{1000}) \tag{13.4}$$

With the takeoff force of 240.6 kN, the C_{am} for engine labour is 2.27 USD per nautical mile. The materials cost due to the engine is then 2.03 USD per nautical mile found from [89]:

$$C_{am_{eng_{mat}}} = \frac{2 \cdot n_e \cdot \frac{C_e}{10^5} \cdot (1.25 \cdot t_f + 1))}{V_b \cdot t_b} \tag{13.5}$$

Now, moving on to the third of the six criteria, the flight crew cost is found using take-off weight W_{to} of 207969 pounds according to [89]:

$$C_{am_{crew}} = (0.349 \cdot \frac{W_{to}}{1000} + 836.4) \cdot V_b^{-0.1} \tag{13.6}$$

This leads to a C_{am} of 2.23 USD per nautical mile.
The fourth criterion, the depreciation cost, follows from [89]:

$$C_{am_{depr}} = \frac{0.9 \cdot TC - 0.3 \cdot c_e \cdot C_e}{U \cdot V_b \cdot t_{dep}} \tag{13.7}$$

Here, the utilisation factor U and fixed depreciation period t_{dep} follow from the graph in [89] and are defined as 4600 h/year and 12 years respectively. Thus, this leads to a depreciation cost C_{am} of 4.75 USD per nautical mile. Lastly, the insurance cost of the hull can simply be calculated from $C_{am_{hull}} = \frac{r_i \cdot TC}{U \cdot V_b}$ to be 1.38 USD per nautical mile. Now, finally combining all individual C_{am}, a total direct operating cost of $DOC = C_{am_{airf_{lab}}} + C_{am_{airf_{mat}}} + C_{am_{eng_{lab}}} + C_{am_{eng_{mat}}} + C_{am_{crew}} + C_{am_{depr}} + C_{am_{hull}} = 16.54$ USD per nautical mile is found.

13.6.2. Indirect Operating Cost

As for the Indirect Operation Cost (IOC), the IOC consists of costs related to the airport landing fees, flight attendants, food & beverage service and passenger-related costs such as reservations, sales, baggage handling and administrative costs. The relation as given in [89] for the IOC, is as such [89]:

$$IOC = R^{-0.41} \cdot (1.42 \cdot 10^{-4} \cdot W_{to} + (0.13 + 1.4 \cdot LF) \cdot N_p^{-4.4}) \tag{13.8}$$

In this equation, LF represents the Load Factor, namely the fraction of the number of paid passengers to the number of seats available N_p, which is 206. For the characteristics of the flight, the LF is 83 % according to [5]. Thus, the IOC computed is 9.32 USD per nautical mile.

13.7. Return on Investment & Operational Profit

Considering all major airlines will be transitioning to a low-emission fleet over the coming decades and the CH4llenger is the first of its kind on the market, a large market share is expected over time. In the upcoming years however, an aircraft demand of about 417 aircraft was found in subsection 4.1.4. Considering $C_{inv} = 417 * 21.32 = 8892.1$ million USD with 21.32 million USD being the R&D cost and assuming a 20% profit margin, the following Return on Investment is estimated:

$$ROI = \frac{N_s \cdot UC - N_s \cdot TC - C_{inv}}{C_{inv}} = \frac{417 \cdot 133.8 - 417 \cdot 111.47 - 8892.1}{8892.1} = 0.0472 \tag{13.9}$$

Thus, assuming 417 aircraft sold, the Return on Investment is found to be 4.7 %.

[5] `https://www.flyplay.com/en/news/83-load-factor-68-growth-in-passenger-number`, [Cited on 18-June-2024]

14. Sustainable Development Strategy

Aircraft production and operations have a substantial and ever-growing impact on the environment. The main goals of the mission, according to the previously defined mission need statement and project objective statement, are to ensure carbon neutrality during operation and minimal energy usage. To make this possible, sustainability should remain a key element in all stages of the project. Firstly, it is important to differentiate between environmental impact and sustainability, which should not be used interchangeably. Sustainability is a broad concept, which can be subdivided into three pillars; social, environmental, and economic sustainability [90]. The sustainable development strategy described in this chapter addresses both the way sustainability is taken into account in the design and the way the product contributes to sustainable development.

14.1. Social Sustainability

Social sustainability offers a societal viewpoint on sustainability. Typically, five different aspects of social sustainability can be distinguished. These include: social equity and inclusion, democratic participation and empowerment, livelihood security, social well-being, and lastly quality of life. With regards to aviation, the International Federation of Air Line Pilots' Associations (IFALPA) urges "all aviation stakeholders to take an active role in developing a new, socially sustainable aviation industry based upon a principle of creating prosperity within, not just from, the markets it has the privilege of serving"[1]. It places an emphasis on increasing employee and customer well-being by taking into account the costs of lost jobs, maintaining social protections, and accounting for income disparity, as well as being consistent with the overall economic and political landscape and national security when devising aviation regulations and guidelines. Furthermore, to maintain societal sustainability public image, the project shall make an attempt to converse with external NGOs as well as any organisation interested in terms of sustainability.

From the perspective of this project, social sustainability is maintained through a few measures; the work distribution should be fair, equal, and fitting to an individual's skills. Moreover, the UN Sustainable Development goals are kept in mind in order to further the sustainable organisation of the team. Throughout this project, social responsibility will be kept in mind, for example, during design and operation, by determining best practices in refuelling with the least impact on the local population and reducing noise pollution to improve well-being. Other relevant measures pertinent to this project but out of the current scope would be devising a socially just ticket price system that considers the disparity of income inequality.

14.2. Economic Sustainability

Economic sustainability refers to promoting long-term economic growth and encompasses the activities and practices supporting this goal [91]. It should be noted, however, that social, environmental and cultural aspects of the community should not be compromised in the process. More specifically, the International Civil Aviation Organisation (ICAO) calls for an affordable, fair, and efficient air transport system that supports a competitive economy and a balanced development [92]. In the context of this project, some of the anticipated challenges are upfront development costs associated with innovative technologies and profitability. Therefore, a significant amount of time has been dedicated to researching novel fuels as well as careful cost management and market research, including an analysis of current trends and future predictions. Infrastructure constraints are also addressed as part

[1] `https://www.ifalpa.org/media/3536/social-sustainability-11-may-2020.pdf`, [Cited on 25-April-2024]

of the aircraft maintenance analysis. More specifically, incorporating economic sustainability into the aircraft's design entails optimising efficiency and cost-effectiveness at every stage. This involves not only keeping in mind the costs of materials and technologies but also reducing operational expenses over the aircraft's life cycle by factoring in maintenance simplicity and longevity.

14.3. Environmental Sustainability

The environmental impact pillar of sustainability entails the responsible use of natural resources and preserving global ecosystems so that the ability of future generations to meet their needs is not compromised[2]. It has been predicted that, unless the environmental impact of aviation per passenger-kilometre is significantly reduced with respect to today's levels, the development of air travel will be greatly hindered [93].

This project, emphasises the environmental impact aspect of sustainability, which is addressed below in more detail. The organisational approach to environmental sustainability consists of a set of procedures that have been adhered to by all team members throughout the project duration. The person primarily responsible for enforcing the sustainability policy and keeping track of the environmental impact of the design is the Environmental Impact Officer. All engineering departments as named previously should adhere to the following measures:

1. At every stage of the design, the environmental impact should be considered by all departments through a weighted trade-off of the sustainability criteria.
2. The environmental sustainability-related top-level requirements should be complied with at all times.
3. Environmental impact should be a criterion in all design-related trade-offs and decisions.
4. The environmental impact associated with all design decisions should be quantified (or estimated) and documented, adhering to the specified indicators (see: section 14.4).
5. If applicable; the measures taken to minimise the environmental impact and their quantification (estimations) should be reported to the Environmental Impact Officer during the weekly Progress Meetings.

Moreover, several requirements concerning environmental impact and sustainability have been formulated, specifically the stakeholder requirement **CH4-STK-14** and its sub-requirements. Which were of primary importance during the fuel selection process. According to **CH4-STK-14-01**, all fuel options of a non-renewable origin were eliminated in the first stages of the selection. **CH4-STK-14-02** and **CH4-STK-14-02** call for a sustainable production and transport of the fuel, which was addressed in chapter 12.

Moreover, all functions carried out during an aircraft's lifetime should be performed with the least environmental impact possible. In particular, as shown in the functional flow diagram in chapter 5, block 2.0 "Produce aircraft", block 5.0 "Operate aircraft", and block 6.0 "Dispose of aircraft" have the potential to minimise use of natural resources, emissions, pollution, etc.

14.4. Life Cycle Assessment

Life cycle assessment (LCA) is a method of assessing the environmental impact of a commercial product throughout all its life cycle stages. It can be seen as a comprehensive guide for engineers, which helps understand the implications of various design choices [94]. The steps to a life cycle analysis can be summarised as follows:

1. Goal and scope definition,
2. Inventory analysis,

[2] `https://www.un.org/en/academic-impact/sustainability`, [Cited on 03-May-2024]

3. Impact assessment,
4. Interpretation of the results.

In the context of an energy-efficient aircraft development, the goal and scope definition is a comparative analysis of different concepts, comprising both an empty aircraft and the fuel, in terms of their environmental impact "from cradle to grave" [95]. The inventory analysis is based on the European Life Cycle Database (ELCD). Based on the results of the inventory analysis, the environmental impact can be assessed in terms of a single score (SS); point/passenger-kilometre. The score is evaluated on the basis of the so-called "midpoint" and "endpoint" categories [96], which will serve as environmental impact indicators in this project. The flow from inventory analysis to indicators is shown in Figure 14.1.

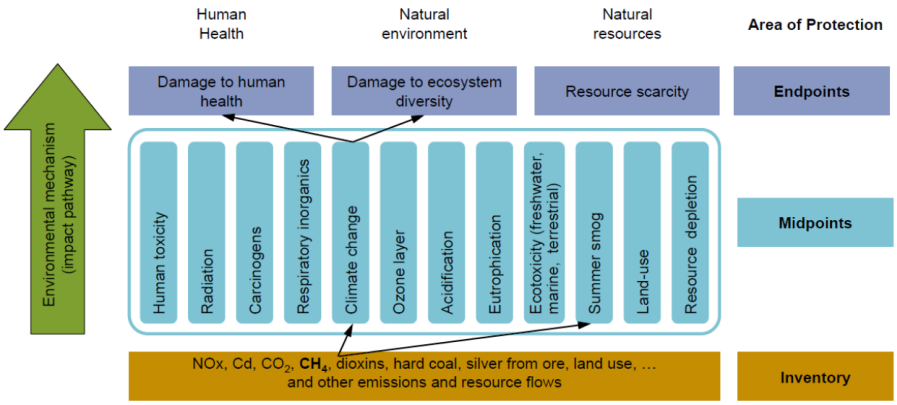

Figure 14.1: "Midpoint" and "endpoint" categories resulting from the inventory analysis [96].

The general stages of the life cycle of the developed aircraft are shown in Figure 14.1, and the stages corresponding to the fuel are included below, highlighting the importance of the fuel selection in the design and for the environmental impact of the product. It should be noted that the sizes of the arrows do not correspond to the actual timeline.

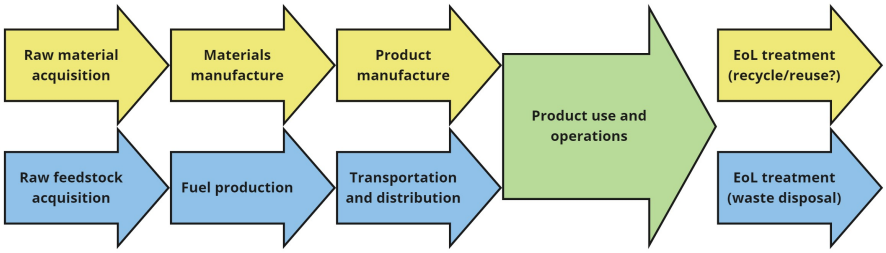

Figure 14.2: Life cycle stages of the aircraft and fuel.

Every stage in Figure 14.2, requires resources and energy, and in turn produces waste, all of which should be estimated and later scaled. There is potential for product reuse or recycling, which is addressed in the recommendations as well as in the future steps as explained in chapter 16.

14.5. Fuel Production Sustainability Aspects

It is of high importance to analyse the sustainability impacts of methane production, specifically regarding the environmental, social and economic repercussions. In this section, firstly the sustainability aspects and local impacts of the production process will be analysed, followed by a discussion on the type of methane to be used in the CH4llenger and the fuel timeline.

14.5.1. Local Community Impacts

A distinction needs to be made between the impact on local communities of the production of synthetic methane compared to that of biomethane. Biomethane has been proven by epidemiological studies

to pose the risk of exposing humans to endotoxins and fungi that can lead to (chronic) respiratory illnesses. Moreover, environmental monitoring has revealed high concentrations of a particular matter, microbial agents and volatile organic compounds (VOCs) due to the production of biomethane [97]. Clearly, in terms of social sustainability, this exposure to chemical and biological pollutants is not a desirable outcome.

When it comes to environmental sustainability, and thus the emissions generated by the methanation process, one notable difference between the synthetic methane and biomethane production is the CO_2 byproduct generated in the anaerobic digestion process as well as small amounts of hydrogen sulphide, siloxanes and moisture particles [3]. Only after this CO_2 has been separated from the produced methane, the "purified" biomethane is obtained. However, this byproduct CO_2 can be reused in multiple ways. One promising option is to recycle the separated "waste" CO_2 and use it together with green hydrogen for synthetic methane production section 12.3. Other uses of the captured CO_2 include among others mineral carbonates, biomass production, fuels, chemicals, PH control and liquefied CO_2 [98]. Thus, this way CO_2 is not released into the atmosphere, improving the environmental sustainability of this process.

In terms of other emissions, a measurement campaign that also measured nitrous oxides and ammonia emitted, found (leaked) methane to be the dominating source of greenhouse gas emitted from these plants [99]. However, these emissions from biogas production plants are extremely hard to quantify. One method explored is the determination of the total emission through remote sensing [99]. Based on the time-dependent behaviour of the emitted gas plume and a meteorological model or use of a tracer gas, the emissions can then be approximated. Following from this research, methane emission rates range roughly between 2 and 10 m^3/h. Since biogas is considered to be climate-neutral fuel since the carbon in the biogas is obtained from the atmospheric CO_2, these emissions are not considered [100]. Synthetic methane generation on the other hand mostly has water as a byproduct, thus no extensive filtering of the methane from the byproducts is required.

14.5.2. Fuel Projections

Combining the considerations regarding the production, emissions and social sustainability aspects of both biomethane and synthetic methane, it is determined that synthetic methane is preferred as the fuel of the future for the CH4llenger. Not only is synthetic methane completely carbon neutral in its production, eliminating all possibilities for carbon leakage in the process, but it also has less harmful health impacts for the workers in terms of social sustainability. Furthermore, the potential for creating an economy of scale for synthetic methane production offers great economic potential, favouring economic sustainability.

Regrettably, the production of synthetic methane will likely not be at a large enough scale required to power all CH4llenger aircraft at the start of service in 2035. Considering the EU's net-zero emissions goal is set for 2050, it is unrealistic for large strides in the scaling up of synthetic methane production to have taken place before that time. That is why, for economic considerations of the customer airlines, the timeline in Figure 14.3 is recommended to be followed if they do not have access/budget to sufficient synthetic methane by the time of purchase/start of service of the methane aircraft fleet.

Over the span of the upcoming decades, the main methane fuel source used by the aircraft will gradually transition from more LNG-based sources to a mix of solely biomethane and synthetic methane by 2050, to eventually only the completely carbon emission-free synthetic methane. This transition process is depicted in Figure 14.3.

[3] `https://www.nationalgrid.com/stories/energy-explained/what-is-biogas`, [Cited on 17-June-2024]

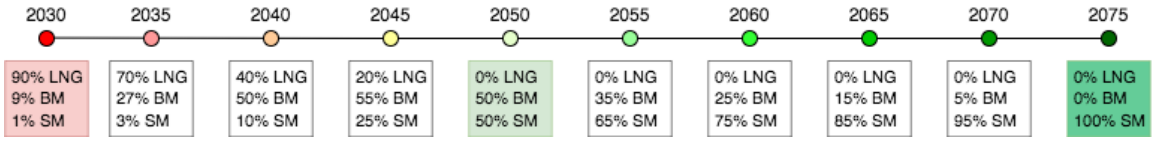

Figure 14.3: Timeline of methane fuel type used to power CH4llenger aircraft in the coming decades.

14.6. Design-Specific Sustainability Aspects

With the CH4llenger aircraft concept finalised, the environmental, social, and economic impact of the design can be revisited and discussed in more detail. This section summarises the synthetic methane-specific considerations, as well as ones arising from the unconventional detachable wing-mounted fuel tanks.

14.6.1. Environmental Impact

The environmental impact is predominantly assessed on the basis of emissions associated with the production and combustion of synthetic methane. Conventional jet fuel is used as a benchmark, and hydrogen is incorporated in the analysis in order to evaluate the methane design against another type of alternative aviation fuel. The pollutants taken into account in this analysis are CO_2, NO_X, which is a major contributor to smog formation[4], H_2O, which has the potential to form contrails, amplifying the greenhouse effect[5], and particular matter (PM), such as dust, dirt, and soot particles, which affect the air quality and contribute to climate change. The fuel masses in Table 14.2 and the heat values are taken from the initial Class I weight estimation [1]. The fuel masses were all obtained for a sample mission of a 3500 nm range.

With the fuel masses and heat values available, the emissions were calculated based on the energy-specific and mass-specific energy indices of the selected fuels[6] [101]. The CO_2 and H_2O indices are expressed in kg/MJ, and the NO_X and PM in g/kg, due to having much smaller magnitudes, summarised in Table 14.1.

Table 14.1: Energy-specific and mass-specific emission indices of selected aviation fuels.

	ESEI CO_2 [kg/MJ]	ESEI H_2O [kg/MJ]	MSEI NO_X [g/kg]	MSEI PM [g/kg]
Jet A/A-1	0.073	0.029	18.000	0.100
CH_4	0.050	0.045	1.800	0.000
H_2	0.000	0.075	0.100	0.000

Subsequently, the emissions in kg are obtained by multiplying the masses or total energies; the products of masses and respective heat values, with the indices. The results are presented in Table 14.2. It should be noted that CH4llenger is considered to be completely CO_2 neutral when operating on synthetic methane, as per the stakeholder requirement **CH4-STK-07**. The CO_2 emitted during operation is offset in the carbon capture process; the captured CO_2 is used for the production of synthetic methane. However, even if a different type of fuel is used, such as biomethane or LNG, the CO_2 emissions would still be $\approx$ 29% lower when compared to jet fuel combustion.

[4] `https://www3.epa.gov/region1/airquality/nox.html`, [Cited on 15-May-2024]

[5] `https://science.nasa.gov/earth/climate-change/steamy-relationships-how-atmospheric-water-vapor-amplifies-earths-greenhouse-effect/`, [Cited on 15-May-2024]

[6] `https://archive.ipcc.ch/ipccreports/sres/aviation/110.htm`, [Cited on 17-June-2024]

Table 14.2: Emissions of different pollutants from the combustion of selected aviation fuels based on estimations of fuel masses for a design range of 3500 nm.

	Fuel mass [kg]	Heat value [MJ/kg]	CO_2 [kg]	H_2O [kg]	NO_X [kg]	PM [kg]
Jet A/A-1	26 371	43.02	82 817	32 900	474.68	2.64
CH_4	23 530	50.00	58 825	52 943	42.35	0.00
H_2	10 547	120.00	0	94 923	1.06	0.00

The H_2O emissions are ≈ 60% greater for methane with respect to jet fuel. In the case of hydrogen, water vapour emissions are ≈ 189% higher than those of Jet A. Notably, H_2O emissions themselves do not guarantee contrail formation. While the phenomenon constitutes up to 35% of aviation's contribution to climate change, only about 2-10% of global flights create about 80% of contrails[7]. Research is being conducted into re-routing certain flights, such as steering under or over areas, where the Schmidt-Appleman criterion is not satisfied, and contrails are not formed. Therefore, H_2O emissions could potentially be mitigated[8]. On the other hand, NO_X emissions are the most favourable for hydrogen, with methane still producing 10 times fewer kilograms of nitrogen oxides than conventional jet fuel. Particular matter emissions are negligible for both hydrogen and methane.

14.6.2. Social Impact

When it comes to social sustainability, the CH4llenger will play a crucial role in connecting the world. With ever more stringent regulations regarding emissions, the only way to keep flying and enable people to stay connected is to bring carbon-neutral aircraft to market. Thus, the CH4llenger will be of key importance to maintaining social sustainability in the aviation sector. One of the factors affecting social sustainability is ticket prices. Considering the projected fuel costs of synthetic methane in 2050, which is about 30 cents/kg compared to 50 cents/kg for kerosene currently is relatively low, and the linear relationship between ticket price and cost, the ticket prices are not expected to rise significantly compared to current prices [102]. Compared to methane, hydrogen not only has a higher fuel cost, but it also requires high investment for the infrastructure and logistical demands it imposes, thus likely driving the ticket price up significantly.

14.6.3. Economic Impact

Regarding the economic sustainability impacts of introducing the methane aircraft, positive impacts on the economy are to be expected. Firstly, the jobs and economic value that a scaled-up synthetic methane fuel industry will generate will likely benefit countries' economies. Moreover, considering the infrastructural modifications required at airports and the operations aspects of for example truck-driven fuel tank transport, new jobs are to be generated on that front too. One of the challenges currently still consists of improving the image of methane as an aviation fuel, especially compared to hydrogen, as it currently does not boast a high spot on the political agenda. A strategy that could be implemented is communicating with the government and authorities early on, such that the methane fuel option gains a positive image in their eyes and is put high on the priority list. Furthermore, marketing campaigns can be set up in order to improve the general public's vision of methane as a promising aviation fuel.

14.7. Recommendations

Combining all considerations regarding the sustainability of both the fuel production process as well as those pertaining to the design itself, several recommendations can be given. Regarding recommendations to scale up fuel production, global solutions are needed. First of all, worldwide synthetic methane production needs to be scaled up as soon as possible if net zero emissions by 2050 are to be achieved. Given the current small scale of synthetic methane production combined with

[7] https://www.technologyreview.com/2024/03/12/1089620, [Cited on 27-May-2024]

[8] https://www.researchgate.net/figure/Schmidt-Appleman-criterion-for-contrail-formation-The-red-line-represents-the-state-of_fig3_244478376, [Cited on 27-May-2024]

its high costs addressed in section 12.3, it poses the risk of being economically unfeasible for airlines to get on board with using this fuel compared to the more financially attractive LNG. Second of all, international markets and partnerships need to be developed such that a global network of (synthetic) methane production and distribution can be established under high standards and fair prices. For example, good working conditions in plants need to be ensured by global quality regulations. Third of all, guidelines need to be set up as to the industry-scale direct carbon capture technology, in order to ensure consistent standards of the CO_2 used in the synthetic methane production. Additionally, these standards should ensure the production of hydrogen used in the methane synthesis process is to be truly green.

The recommendations pertaining to the environmental impact of the aircraft begin with performing a complete life cycle assessment, according to the steps specified in section 14.4. This will give a thorough overview of the impact of all life cycle stages, while the analysis at this stage was limited to quantifying selected emissions during a typical operation. The midpoints and endpoints shown in Figure 14.2 can be addressed in more detail. Additionally, the design itself could benefit from a more efficient, novel combustor. In their emissions analysis of a hydrogen-fuelled and kerosene-fuelled Airbus A320, Khan et al. suggest that there is potential to significantly reduce NO_X emissions by using a more efficient combustor, although more research would have to be done in the area of methane-fuelled aircraft. Lastly, regarding water vapour emissions, it is advised to research contrail-prone areas and explore re-routing flights which would normally pass through those. As mentioned in subsection 14.6.1, 2-10% of global flights contribute to the creation of around 80% of contrails, therefore there is a large potential to mitigate them.

15. Compliance Matrix

The final design of the aircraft has to fulfil the mission need statement set out at the beginning of the project. To do this the design must be compliant with the requirements given to us by the client and those found through stakeholder analysis. These stakeholder requirements flow down from the mission need statement and are the highest level of requirements that need to be fulfilled. Besides the requirements from stakeholders, the aircraft also has to perform a set of functions to fly transatlantically. These functions were explored in the functional flow diagram presented in chapter 3. From these functional flow diagrams, a set of requirements also flowed down. It was chosen to check whether the design fulfilled both of these sets to ensure the design could function within the constraints set by stakeholders.

The requirements are presented in Table 15.1 and the design compliance is evaluated in the same table. For each requirement, it is indicated if it is fulfilled and if this is the case it is indicated in which chapter this is described. If the requirement is not fulfilled it is indicated why this is the case and if necessary what needs to be done to make it comply.

Table 15.1: Compliance matrix for stakeholder and functional requirements.

ID	Requirement	✓	Location
CH4-MNS	To reduce the environmental impact of aviation by designing a novel aircraft that is capable of transatlantic flights by 2030		
CH4-STK-01	The aircraft shall have a range of 3500 nautical miles	✓	section 8.12
CH4-STK-02	The aircraft shall be able to accommodate 206 passengers in a 2-class configuration during transatlantic flight	✓	section 5.4
CH4-STK-02-01	The aircraft shall be able to accommodate 206 passenger seats	✓	section 5.4
CH4-STK-02-02	The aircraft shall be able to carry enough food for 206 passengers during a transatlantic flight	✓	section 5.4
CH4-STK-02-03	The aircraft shall have enough toilets to allow 206 passengers to use the toilets during a transatlantic flight	✓	section 5.4
CH4-STK-03	The aircraft shall have a maximum payload weight of at least 25 tonnes	✓	section 8.4
CH4-STK-04	The aircraft shall be able to operate from a 3000-meter runway at MTOW and 0m ISA	✓	section 8.1
CH4-STK-05	The aircraft shall have a turn-around time of at most one hour	✓	section 12.7
CH4-STK-06	The aircraft shall be able to perform standard turn-around procedures	✓	subsection 6.4.4 and section 12.7
CH4-STK-06-01	The aircraft shall allow for loading and unloading of the cargo	✓	section 12.7
CH4-STK-06-02	The aircraft shall allow for loading and unloading of the passengers	✓	section 5.4
CH4-STK-06-03	The aircraft shall allow for servicing the utilities	✓	section 12.7
CH4-STK-06-04	The aircraft shall allow for it to be refuelled	✓	subsection 6.4.5
CH4-STK-07	The aircraft shall have net zero CO_2 emissions	✓	subsection 14.6.1
CH4-STK-08	The aircraft shall fly with the lowest possible required energy	-	This stakeholder requirement is unverifiable, but its goal was considered at every design stage.
CH4-STK-09	A prototype of the aircraft shall be ready by 2030	✓	subsection 16.2.3
CH4-STK-10	The aircraft shall have a maximum unit cost of $120 million	✓	chapter 13
CH4-STK-11	The aircraft shall be able to operate from remote airports	✓	subsection 12.3.5
CH4-STK-12	The aircraft shall comply with rules from regulating bodies	✓	section 11.3
CH4-STK-13	The aircraft shall help the social sustainability of the aviation industry	✓	section 14.1
CH4-STK-14	The aircraft shall be able to fly on sustainable fuels	✓	chapter 6
CH4-STK-14-01	The aircraft shall be able to fly on a fuel possible to be sustainably produced	✓	section 12.3

Continued on next page

Table 15.1– continued from previous page

ID	Requirement	✓	Location
CH4-STK-14-02	The fuel shall be produced sustainably	-	Airlines may start by using unsustainable methane but will switch to synthetic methane as it becomes more available. This is discussed in subsection 14.5.2
CH4-STK-14-03	The fuel shall be transported sustainably	✓	chapter 12
CH4-FUN-01	The aircraft shall allow the pilots to communicate with ATC	✓	section 10.5
CH4-FUN-02	The aircraft's engines shall be controllable	✓	section 6.1, section 6.5
CH4-FUN-02-01	The aircraft's engines shall be able to be started	✓	section 6.1
CH4-FUN-02-02	The aircraft's engines shall be able to be throttled	✓	section 6.5
CH4-FUN-03	The aircraft shall be controllable during taxi	✓	section 5.5
CH4-FUN-04	The aircraft shall be able to perform take-off	✓	section 8.1
CH4-FUN-05	The aircraft shall be able to climb away from the airport	✓	section 8.1
CH4-FUN-06	The aircraft shall be able to stow its landing gear	✓	section 8.7
CH4-FUN-07	The aircraft shall be controllable in the air	✓	section 8.5
CH4-FUN-07-01	The aircraft shall have roll control	✓	subsection 5.2.3
CH4-FUN-07-02	The aircraft shall have yaw control	✓	section 5.6
CH4-FUN-07-03	The aircraft shall have pitch control	✓	section 8.5
CH4-FUN-08	The aircraft shall be able to enter cruise conditions	✓	section 8.1
CH4-FUN-09	The aircraft shall be able to be trimmed	x	This is not evaluated at this stage
CH4-FUN-10	The aircraft shall not touch the ground with anything other than the landing gear during operations	✓	section 5.5, section 8.7
CH4-FUN-11	The airports shall be able to receive the fuel for the aircraft	✓	subsection 6.4.5
CH4-FUN-12	The airports shall have the infrastructure to store the fuel for the aircraft	✓	section 12.5
CH4-FUN-13	The airports shall have the infrastructure to refuel the aircraft	✓	section 12.6

For this stage of the evaluation only the stakeholder and functional requirements are evaluated. These are the highest level of requirements and thus important, but many are not yet that detailed. For complete compliance of the design with the goal of the project the system and subsystem requirements also need to be evaluated. This will be done in future through similar means and also testing and further analysis. As these requirements are already taken into account in the design steps taken compliance with these requirements is likely to occur.

16. Future Steps

With the closing of this report, the next steps in the creation of CH4llenger are summarised to provide structure and integrity in the development of the aircraft. This chapter oversees the Production Plan and PDDL. The production plan in section 16.1 explains the process necessary to construct the aircraft in an efficient and sustainable manner. This allows the aircraft to be implemented to the market faster and allows for quicker adoption of the technology. section 16.3 discusses the possibilities for creating an aircraft family around the CH4llenger design.

Moreover, the Project Design and Development Logic in section 16.2 plans the next stages of the project, from finalising the design to retiring the aircraft from service. This gives structure as to how to perform the steps following the initial design as presented here. Special attention is given to the tests that will be performed to analyse and optimise the aircraft design. Moreover, it considers relations with the customer and operational aspects to support the aircraft's use.

16.1. Production Plan

The production plan serves as an overview for producing the aircraft, from the part manufacture of key structural components to the sub-assembly of major aircraft components, to the final assembly of the aircraft. The diagrams displayed in the next three pages depict these three steps, respectively.

In the part manufacture, due to the vast amount of individual parts within an aircraft, it has been chosen only to give explanations of certain key structural components. Here, their manufacturing process, starting from a metal sheet/block, is explained. Furthermore, more nuanced parts which are not very relevant, such as the engine pylon and landing gear components, have not been elaborated on.Subsequently, these parts and others are used in the sub-assembly process of major aircraft components. Parts which are not produced locally are bought and imported from other companies all over the world. During sub-assembly, various parts are put together through adhesive bonding, welding, bolts, pins, or nuts. Following, all these major components are stored and transported to the final assembly plant. At the final assembly plant, the entire aircraft is put together. This process has a specific chronological order, with various tests being performed in between. Most of these procedures have been inspired by existing commercial aircraft from Boeing and Airbus [103]. Finally, the aircraft is inspected and shipped out.

This preliminary production plan gives a general overview of the early stage of design. As such, not all components are sized to absolute intricacy, thus production methods cannot be confirmed. As the aircraft approaches the final design, and more detail becomes known on how specific components are manufactured, this plan may be reviewed.

Part manufacture of key structural components

Carbon and Glass fibre composites

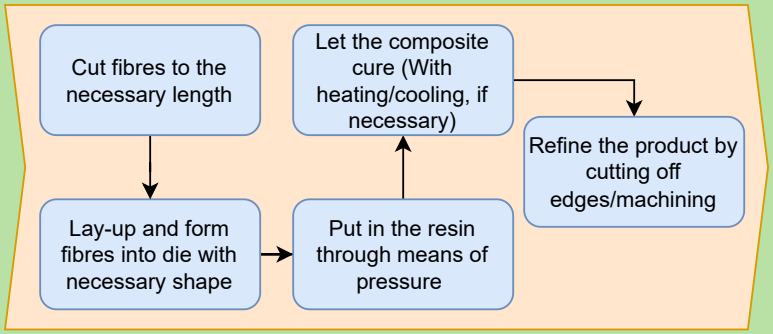

- Liquid methane tank fairing
- Nose cone fairing
- Wing group ribs
- Wing group stringers
- Wing group spars
- Wing group skin
- Fuselage skin

Aluminium-Lithium alloy

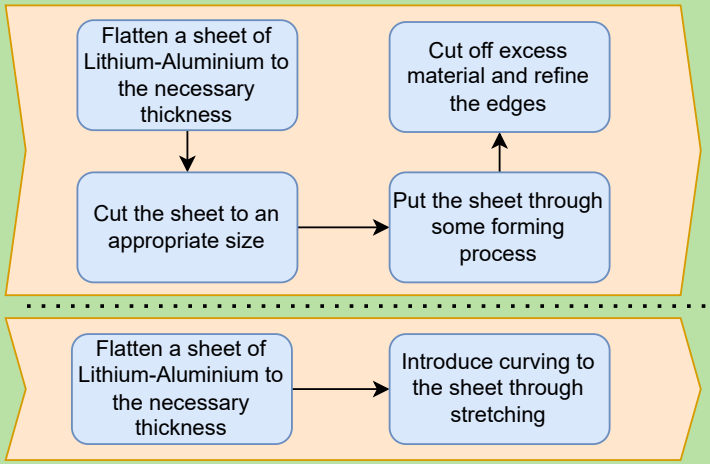

- Fuselage stringers
- Fuselage frames
- Fuselage struts
- Fuselage skin

Aluminium-2219

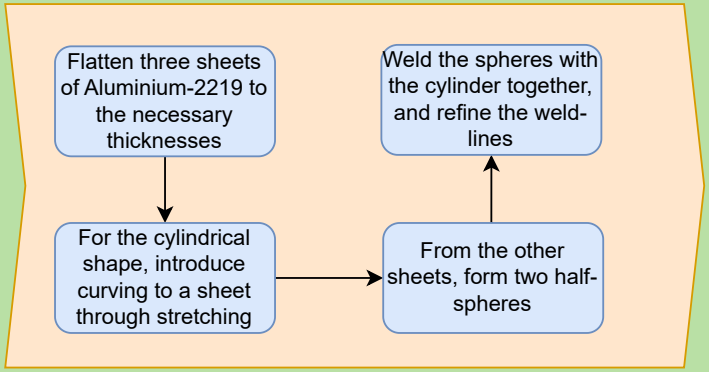

- Gaseous methane tanks
- Liquid methane tank pressure vessel

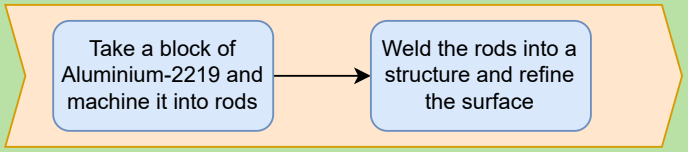

- Liquid methane tank pylon

Aluminium-2024-T3

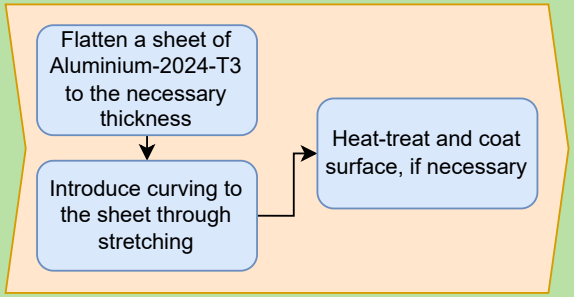

- Wing group leading edges

Steel

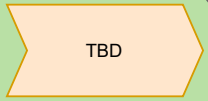

- Landing gear wheels
- Landing gear torque arms
- Landing gear struts

Titanium

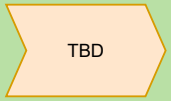

- Engine pylon

Legend

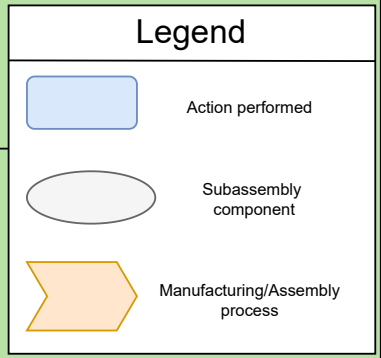

Subassembly of major aircraft components

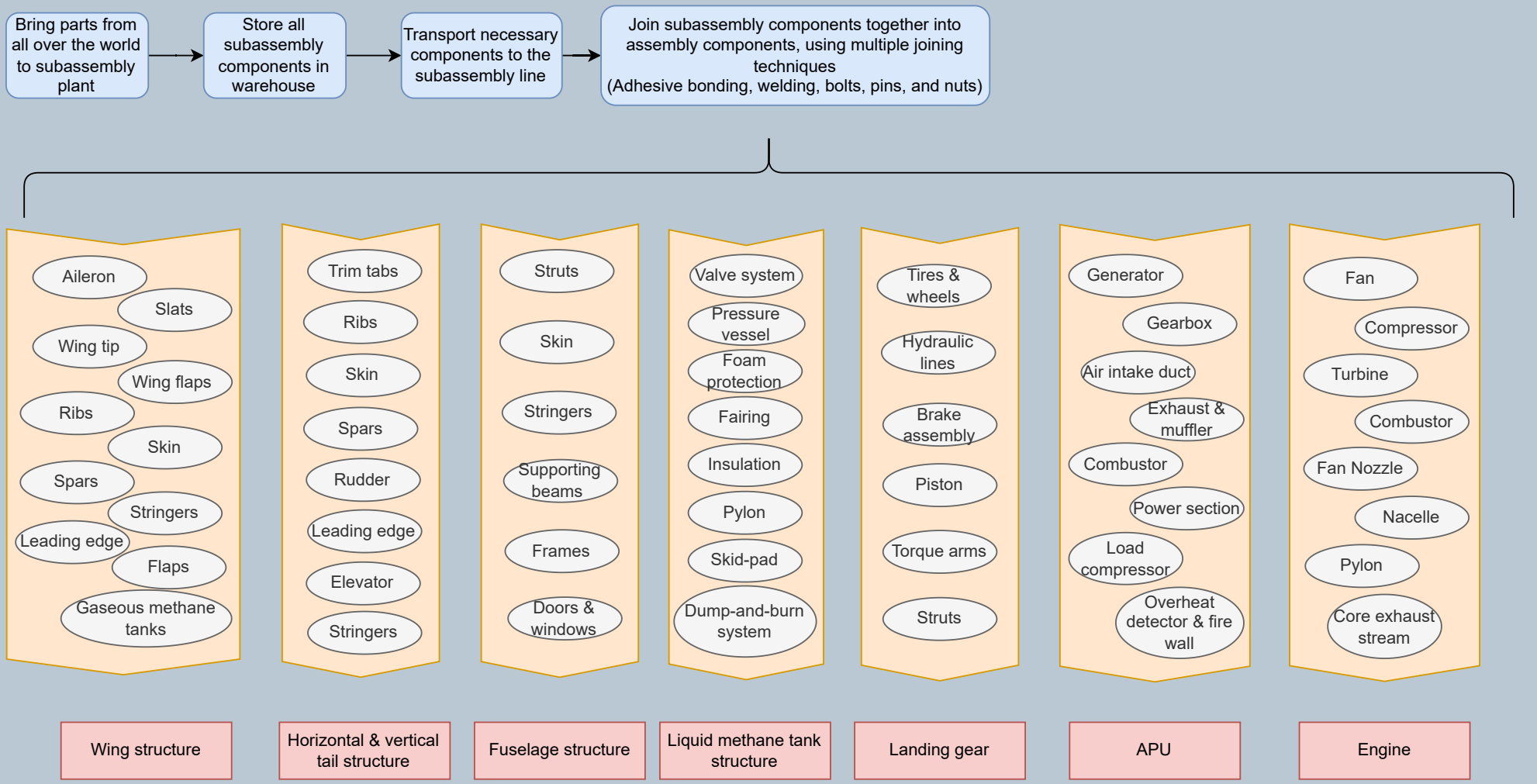

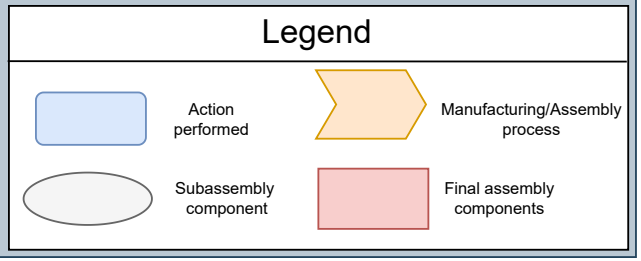

Final assembly of the aircraft

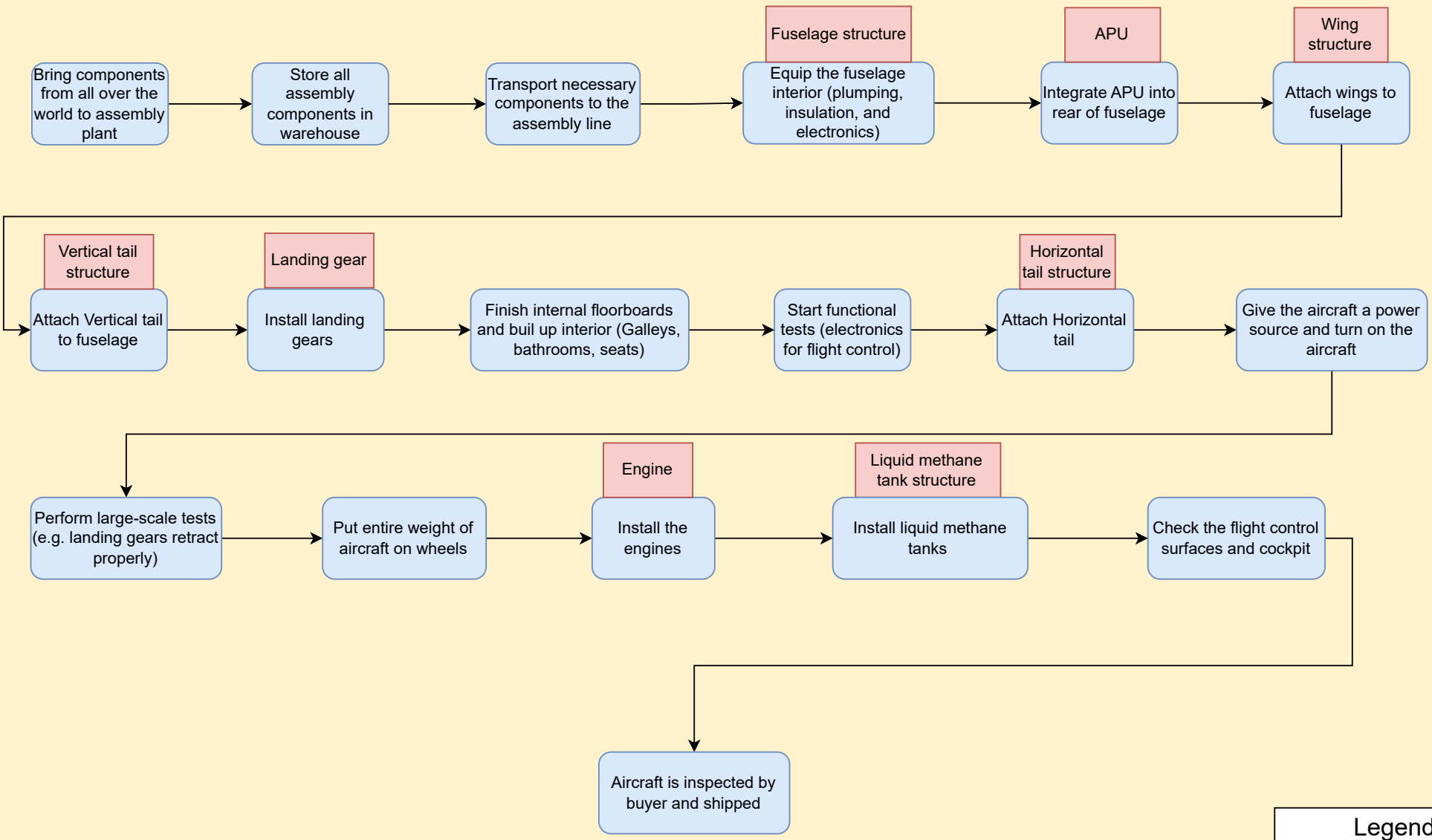

16.2. Project Design and Development Logic

Concluding this report, a preliminary design for the CH4llenger aircraft and an initial idea for the fuel logistics are presented. Post-submission, these will need to be worked out further. To detail the steps and their timeline a project design and development logic was made. This is presented in subsection 16.2.2 giving an idea of the relation between the necessary steps to complete the aircraft design and fuel logistics. In subsection 16.2.3 a Gannt chart is presented, which details all deadlines for after the project. Additionally, it describes the steps taken to prepare for the maintenance of the aircraft and its end of life.

16.2.1. Testing

One of the aspects that is still to be considered is the testing of the aircraft to validate its performance. For that, several tests were proposed, each corresponding to the given system of the aircraft. The overview of the tests has been compiled in Table 16.1.

Table 16.1: Future Tests

ID	Test	Description
PROP-01	Firing Test	Aircraft engine and fuel system is to be suspended from a test set-up to test its firing capability and thrust
PROP-02	Pressure Tests	Fuel line is to be subjected to pressures 1.5 times above maximum operating pressure to ensure it doesn't burst when subjected to possible overpressure
PROP-03	Fluid Line Test	Leak tests are to be performed to ensure that no fluid leakage occurs during flight operations
PROP-04	Environmental Tests	The engine performance is to be analysed to obtain the data corresponding to particulate emissions emitted in-flight
AERO-01	Wind tunnel Tests	The aircraft is to be subjected to wind tunnel testing to test its drag characteristics and aerodynamic performance
STRU-01	Pressurisation Tests	The fuselage is to be subjected to pressurization loads double of what it is to experience during regular operations
STRU-02	Vibration Tests	The aircraft structure is to be subjected to vibrations similar to those found in flight, to ensure that the structure does not get damaged.
STRU-03	Whiffle Tree Test	The wing is to be subject to a distributed load to test the bending of the structure
CONT-01	Operational Load Testing	On-ground load tests are to occur to ensure the proper functioning of the control system
CONT-02	Test Flights	The performance of the control surfaces is to be checked by subjecting it to flight conditions
PAYL-01	Operational Load Testing	On-ground load tests are to occur to ensure the proper functioning of the aircraft with the payload onboard
PAYL-02	Test Flights	Dummy payload is to be loaded onto the aircraft to test the performance of the aircraft

16.2.2. Project block diagram

By the end of the project duration, an aircraft concept will be selected, a preliminary design of this aircraft will be finalised, and a preliminary analysis of the associated logistics of fuel production and transport will be performed. Still, much will need to be done to make sure that the aircraft is fully operational. These steps are detailed in the Project Design and Development Logic (PDDL) diagram presented in Figure 16.1.

Firstly, a detailed design of the entire aircraft has to be made. This design should give the dimensions of all parts and how they need to be put together. This design is then tested through various methods. Firstly, the design can be tested using computer models, like FEM and CFD. After this prototypes can be produced and tested at various scales, from wind tunnel tests to full flight tests, as described in Table 16.1. In the diagram, extra attention is paid to the testing of the fuel system as this is critical to the project and where most of its innovations are implemented. After each test, the design should be iterated upon.

After the design is fully finished final prototypes can be made for a final flight test and certification. Simultaneously a manufacturing plan can be developed and a plan to integrate the logistics of the fuel can also be developed. These logistics are very important to the project and should be considered carefully. Both the way that fuel is to be produced and transported to the airfield and also how the fuel will be loaded onto the aircraft. For this possibly other equipment will need to be developed.

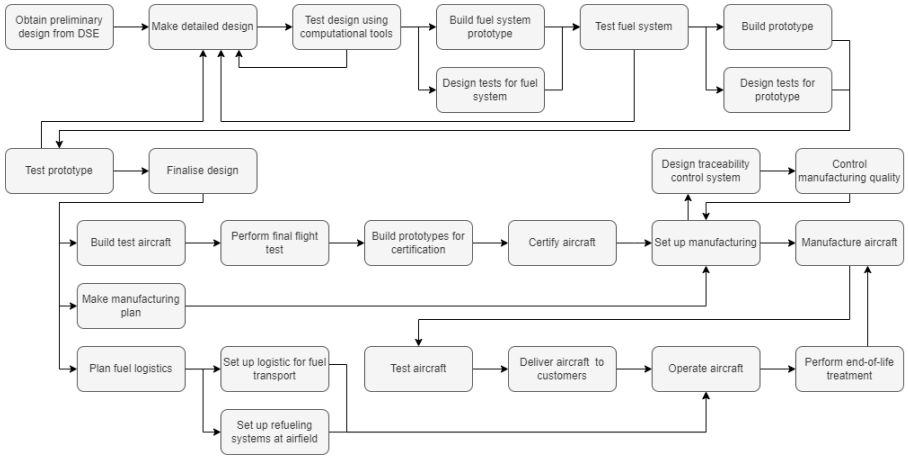

Figure 16.1: PDDL diagram showing the steps to be taken in the aircraft development process.

After the certification of the aircraft is done the mass manufacturing of the aircraft can be prepared. Factories can be prepared as well as tools and manufacturing methods. At the same time, a traceability control system should be set up to ensure the quality of the produced parts and assess the quality of manufacturing. In case manufacturing is found to be insufficient the design of the process should be iterated. The needed infrastructure should also be put in place. When the aircraft is done it should be tested whether it is manufactured correctly. Finally, it can then be delivered to the user.[1]

16.2.3. Gantt chart

These steps detailed in subsection 16.2.2 also need to be completed in a timely manner in order to meet the requirements of the project. For this reason, deadlines have to be set and a timeline was made in order to ensure that the project runs on time and everyone knows the schedule for completion. This timeline is presented in a Gantt chart giving the time it takes to complete each task and when important milestones need to be reached. The Gantt chart is kept general, however, as not much is known about available resources. It mostly indicates the general timeline and completion dates.

The first part of the Gantt chart is based on requirement **CH4-STK-09**. This says that a prototype has to be made and ready to fly by 2030. This is a tight deadline so development will continue immediately after the completion of the DSE. By the end of 2029, the aircraft will need to be finalised, meaning that by 2030 a test flight can be performed.

After this the aircraft will need to be certified, in order to ensure that the aircraft can fly and is allowed by all aircraft authorities. This will take several years as the aircraft incorporates many new technologies. This leads to the aircraft being certified by the middle of 2033.

Once the design starts to be finished a method for manufacturing the aircraft will need to be designed. This will start by the end of 2028, so the production can begin once the aircraft is certified. From this point on production and delivery will begin and is projected to continue until 2047. During this time the production will have to be monitored to ensure product quality.

In order to operate the aircraft the new infrastructure for fuel production and refuelling needs to be in place by the time the aircraft will be delivered to airlines. This means that by half of 2034, these fuel systems need to be in place. In order to make sure that this is done in time a more detailed design of the fuel system needs to start development by 2026.

[1] `https://aertecsolutions.com/en/2024/04/17/aircraft-design-processes-an-exciting-journey-from-conception-to-flight/`, [Cited on 13-June-2024]

Finally, once the aircraft have been manufactured they need to be tested individually and then delivered to the airlines. For as long as the aircraft is then in operation the airlines will have to be supported in their operations and maintenance. At the end of life, the aircraft will be processed and recycled to contribute to a circular economy, thus closing off the sustainability cycle.

16.3. Aircraft Family

The current CH4llenger is designed to bring 25 tonnes of payload, a range of 3900 nmi in order to complete transatlantic flights. To do this the aircraft requires two cryogenic fuel tanks with a volume of 30000 litres each. Should the CH4llenger be used for flights within the United States or Europe, significantly less fuel is required. For flights of 1500 nmi only 9 tonnes of methane is required. This has a volume of 21000 litres of fuel. The fuel tanks for short range flights can therefore be half as large as the current tanks CH4llenger uses. Through using smaller and therefore lighter tanks, even more fuel is saved when flying CH4llenger during short flights.

Therefore, a future step for the CH4llenger project is to size cryogenic tanks for a shorter range. As these tanks can be attached to the CH4llenger similarly, the weight saving will greatly benefit the fuel consumption on flights of less than 1500 nmi.

Another option for short range is to use the same tanks as in the standard CH4llenger, however to fill the tanks with hydrogen rather than methane. When filling the current fuel tanks, roughly 3900 kg of LH_2 is used. With this the CH4llenger has a range of 1370 nmi. The tanks will need to be slightly adjusted, as hydrogen requires significantly more insulation and a slightly different fuel management system. However, this does show that with slight modifications CH4llenger can be used for short range, flying on either methane or liquid hydrogen.

With a future family of aircraft being developed from the CH4llenger, a major step towards green aviation can be made. Both for long transatlantic flights and short intercontinental flights, significant CO_2 reductions can be made with the possibility to fly fully carbon-neutral, when either using synthetic methane or hydrogen. As the tanks are located near the centre of gravity, the flight of the CH4llenger with different tanks will not have a massive impact on how the aircraft flies. This allows for easier pilot certification and the more flexibility for airlines in route selection.

ID	Task Name	Duration	Start	Finish	Predecessors
1	**Make detail design**	**1612 days**	**Mon 1-7-24**	**Wed 4-9-30**	
2	Generate initial aircraft detail design	65 days	Mon 1-7-24	Fri 27-9-24	
3	Test design using computational tools	130 days	Mon 30-9-24	Fri 28-3-25	2
4	Iterate on aircraft design	131 days	Mon 30-9-24	Mon 31-3-25	3SS
5	Make fuel tank prototype	66 days	Tue 1-4-25	Tue 1-7-25	4
6	Design fuel tank tests	75 days	Tue 1-4-25	Mon 14-7-25	4
7	Test fuel system	150 days	Tue 15-7-25	Mon 9-2-26	5;6
8	Iterate fuel system design	180 days	Tue 7-10-25	Mon 15-6-26	7SS+60 days
9	Design aircraft prototype tests	140 days	Tue 16-6-26	Mon 28-12-26	8
10	Build aircraft prototypes	530 days	Tue 16-6-26	Mon 26-6-28	8
11	Test aircraft prototypes	525 days	Tue 29-12-26	Mon 1-1-29	9;10SS
12	Iterate aircraft design	555 days	Tue 10-8-27	Mon 24-9-29	11SS+160 days
13	Finalise design	0 days	Tue 25-9-29	Tue 25-9-29	12
14	Build Test aircraft	246 days	Tue 25-9-29	Tue 3-9-30	13
15	Perform final flight test	0 days	Wed 4-9-30	Wed 4-9-30	14
16	**Certify aircraft**	**655 days**	**Wed 8-1-31**	**Wed 13-7-33**	
17	Build aircraft for certification	250 days	Wed 8-1-31	Tue 23-12-31	15FS+90 days
18	Certify aircraft	535 days	Wed 25-6-31	Tue 12-7-33	17SS+120 days
19	Aircraft certified	0 days	Wed 13-7-33	Wed 13-7-33	18
20	**Prepare fuel logistics**	**2160 days**	**Mon 6-4-26**	**Mon 17-7-34**	
21	Design fuel logistics	970 days	Mon 6-4-26	Fri 21-12-29	
22	Set-up fuel transport logistics	1190 days	Mon 24-12-29	Fri 14-7-34	21
23	Set-up refuelling logistics at airport	1190 days	Mon 24-12-29	Fri 14-7-34	21
24	Airports ready for operations	0 days	Mon 17-7-34	Mon 17-7-34	22;23
25	**Manufacturing**	**4621 days**	**Tue 25-9-29**	**Tue 11-6-47**	
26	Make manufacturing plan	416 days	Tue 25-9-29	Tue 29-4-31	13
27	Set-up manufacturing	911 days	Tue 18-12-29	Tue 14-6-33	26SS+60 days
28	Design traceability control system	715 days	Tue 18-12-29	Mon 13-9-32	26SS+60 days
29	Start manufacturing	0 days	Wed 15-6-33	Wed 15-6-33	27;28
30	Manufacture aircraft	3650 days	Wed 15-6-33	Tue 11-6-47	29
31	Control aircraft manufacturing	3650 days	Wed 15-6-33	Tue 11-6-47	29
32	**Delivery and support**	**14600 days**	**Mon 17-7-34**	**Fri 30-6-90**	
33	Test aircraft	3650 days	Mon 17-7-34	Fri 10-7-48	30SS;24
34	Deliver aircraft	3650 days	Mon 17-7-34	Fri 10-7-48	30SS;24
35	support aircraft operations	14600 days	Mon 17-7-34	Fri 30-6-90	30SS;24
36	Set-up recycling plan	1201 days	Fri 21-12-29	Fri 28-7-34	
37	discussion with potential customers	2338 days	Mon 1-7-24	Wed 15-6-33	

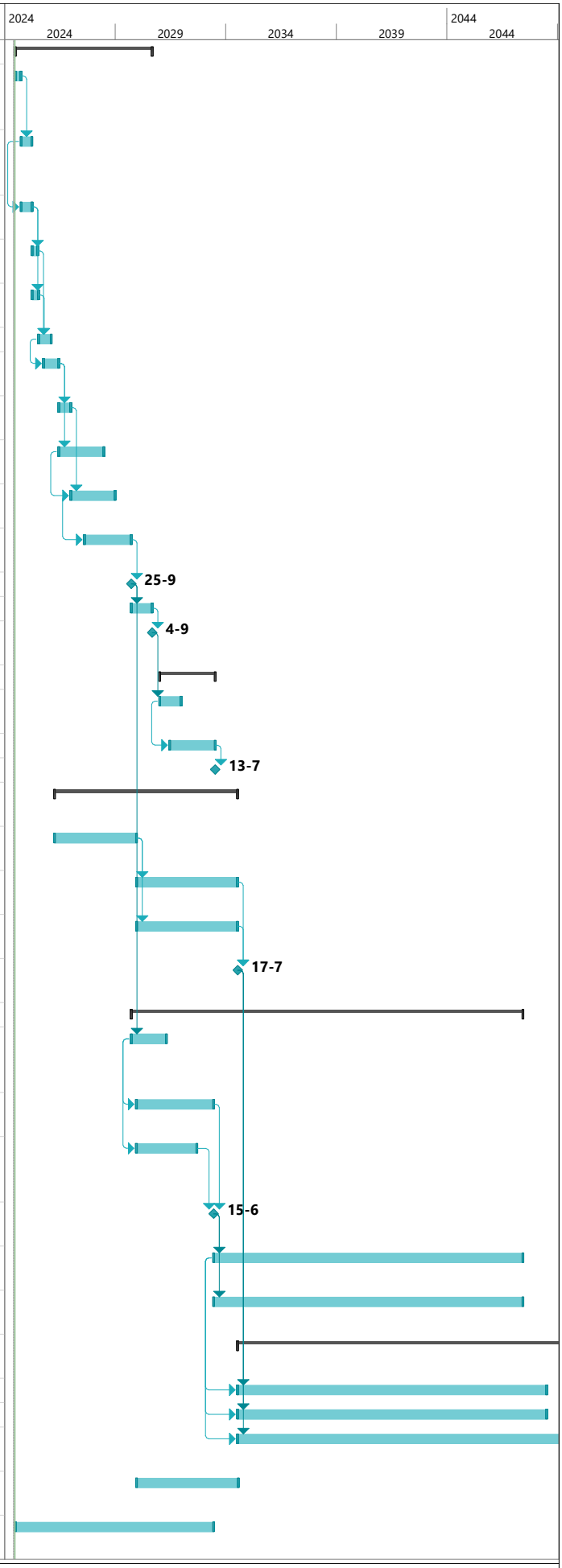

Project: ganttpddl
Date: Mon 17-6-24

Summary | Manual Task | Manual Milestone

17. Conclusion and Recommendations

With all the designs and concepts presented, this chapter acts to bring together all the ideas and represent our findings. This runs from the choice of fuel, to the design of the aircraft, to the operations and logistics that shall be considered once brought to market. Furthermore, discussion of the results is presented, expressing the limitations of the report. These recommendations stemming from the findings could positively impact the commercial aviation industry thereafter.

17.1. Conclusion

With an increasing market in commercial flights coupled with raising concerns regarding the environmental impact of aviation, the industry must evolve. This report set out to address exactly that, by investigating key criteria that can drive a sustainable commercial aircraft industry, from aircraft systems to fuel operations. Driven by the mission need statement: "To reduce the environmental impact of aviation by designing a novel aircraft that is capable of transatlantic flights by 2030", the CH4llenger was conceived. This aircraft was chosen to fly on liquid methane with a novel propulsion system, as in its life-cycle it is CO_2 neutral and can further inspire a sustainable fuel ecosystem. Moreover, a 'whole-image' philosophy was employed throughout the report, considering sustainability from the earliest stages of the fuel's synthesis to aircraft end-of-life operations.

Summarising Main Research Findings

The report commenced by investigating crucial risks, requirements and functions that the aircraft and operations must address. With this form of guidance in place, the aircraft design process starts with a Class I investigation being performed. This resulted in an initial C.G. estimate for the aircraft, already considering the external wing tanks, by having the OEW and fuel approximated using statistical data from literature by Roskam. Subsequently, the wings, tail, landing gear, empennage and fuselage of the aircraft were sized and a Class II weight estimation was performed, resulting in a fuel and payload diagram and thus a scissor plot. Then the process was iterated and new weights and C.G.s were conceived. This continued until the iterations converged to an ideal range. Finally, materials were decided for the varying systems and finally, structural tests were performed, all proving the capabilities of the aircraft.

With an estimated aircraft sizing, the focus turned to the propulsion system; the most innovative system of the aircraft. Here, the engine, propulsion system infrastructure, and wing tanks were sized. LEAP-1A engines, adapted to have a higher combustion chamber temperature, would necessitate a 0.53 kg/s mass flow of fuel to sustain cruise at 38 000 ft. Furthermore, a two-tank system would be implemented to feed the engine. Here, firstly liquid methane is vaporised into a gas and either fed into the engine or into high-pressure tanks. These tanks store the methane such that it can be fed into the engines at a later stage, allowing for contingency and faster throttle responses. With the mass flow known, the external fuel tanks were accurately constructed such that 30 seconds of maximum thrust is provided. Regarding the storage of the liquid methane, these need to hold 55.000 litres of liquid methane. Hence, two fuel tanks of 30.000 litres capacity were placed on each wing, spanning a length of 10.17 m. Designing these tanks to hold a pressure of 3 bars, an inner lining of Al-2219 was used, with an insulation layer of Polyvinylchloride. Additionally, an aerodynamic and impact-resistant cowling was installed. This was constructed from CFRP on the surface, and polyurethane foam within the nose-cone, able to absorb the force of impacts of similar magnitudes to a bird strike. Given that it was decided to make these tanks removable, a novel rail/hook system was developed. Here, three

Al-2219 rods tanks slide and lock on a railing system attached to the wings.

The other critical aspect of this report is the operations and logistics part. This is involved in bringing a methane powered aircraft to market, looking at the necessary infrastructure and turnaround needed. When looking at the airports which could house such infrastructure, three types of airports were identified. These are large, medium, and small-sized airports with 12 daily, 4 daily and 1 weekly transatlantic flight(s) respectively. As a starting point in adopting methane-fueled commercial aviation, six hubs on either side of the Atlantic were chosen. Notably, a new market in flights between medium-sized airports was possible due to the small size of the CH4llenger aircraft. Having assessed the airport sizes and locations, the sustainable generation of methane through methanation and biomethane was analysed. Here, it was found that methanation is preferable due to its cleaner and scalable production, but biomethane is a good alternative in the short term. Looking at the transportation of the fuel to the airport, LNG trucks, LNG trains, and gas pipelines were chosen as viable options. Depending on the airport size and location, the preferable of the three would be selected. At the airport, a storage system was designed to maintain operations without restocking for multiple days. Finally, to transport the fuel to the aircraft, trucks were chosen. Here, medium and large airports would refuel the aircraft by attaching/detaching the fuel tanks, while small sized airports would simply refuel tanks directly at the aircraft.

With a firm proposition in place, the various future markets were assessed. It was found that the commercial aviation market is expected to have a Compound Annual Growth Rate (CAGR) of 3.5% between 2023 and 2032. The LNG market has shown large growth in the past years, but seems to come to a point of saturation. Nevertheless, the production of sustainable methane is expected to have a lot of potential for future growth, and thus high CAGR. This is evident through alternative sustainable fuels having high expected growth in the near future. For example, SAF is predicted to experience a 47.7 % CAGR until 2030. Moreover, between 420 and 750 CH4llenger aircraft are expected to be brought into service to replace existing fossil-fuelled aircraft, providing a market demand immediately when brought to market. Finally, with costs and revenue investigated, a 20% return on investment is expected on the first set of aircraft delivered.

Suggesting Implications for the Field of Knowledge
Overall, this study strengthens the idea that sustainable disruptive change in the world of commercial aviation is feasible. This report had the goal to design a novel aircraft that can cross the Atlantic with least emissions possible. Stemming from the operations research of the designed aircraft, it was established that the implementation of methane can lead to an exponentially growing and self-supporting industry. In order to maintain the CO_2 neutral goal, operational procedures such as the production and transportation of methane can utilise sustainable methane. This additionally increases the demand for sustainable methane, further driving the market, and securing its implementation in industry. Moreover, it was seen that methane can be quite easily substituted into existing aircraft engines, thus the investment would not be that significant to modify an already very meticulous system. Furthermore, considering connecting smaller airports could generate additional demand, decentralising methane demand from large hubs. Finally, the goal of being CO_2 neutral can be realised, and along the way, other sustainable industries such as the one for green hydrogen and carbon capture can profit from investments in the CH4llenger project.

Significance of the Findings of the Study
This thesis has provided a deeper insight into the benefits sustainable methane has over conventional alternatives. Reductions of 30% of CO_2 emissions and ten times reduction of NO_x have been calculated when using methane fuel in the CH4llenger in comparison to the conventional kerosene. Since the CH4llenger will eventually operate solely on synthetic methane produced by carbon capture, this offers a great promise/perspective for environmental sustainability in meeting the 2050 net-zero goals.

Moreover, social sustainability and economical sustainability have been optimised too, with low ticket prices enabled through reduced fuel costs. This is a result of an economy of scale effect from growing demand for synthetic methane production, thus also boosting the economy and creating new jobs in the process.

Limitations of the Current Study
Despite the intricate depth the report has explained, the CH4llenger design has some limitations due to the scarcity of technical details pertaining to a methane propulsion system and a significantly shortened research and development schedule. Generally, a preliminary design has been performed on novel systems, yet they mostly use conventional data and empirical equations which relate mostly to conventional aircraft. For example, in wing sizing, as the fuel is stored in the external fuel tanks, the loading, structure and shape are completely different to the norm. This was addressed, yet in the next more detailed steps of the design, this could be proven to be significantly wrong. The same could be said for the propulsion system, where conventional methods mixed with first-principles were used to size the system.

Other considerations include the wing drop tank not being designed for recovery, for example by using parachutes after being jettisoned. Furthermore, the 2030 timeline and 120 million dollar budget are very ambitious given the high level of new technological development required for the aircraft compared to the A321neo with the same resource constraints. The uncertainty of predicting the synthetic methane market creates a huge limitation too, as it is difficult to estimate the market share the CH4llenger will be able to gain. This is true given the major EOMs already planning to implement alternative sustainable aircraft in the same time period, and how the CH4allenger will play into this. Moreover, the local or European Governments, and potentially private companies, would need to help incentivise the growth of the sustainable methane market. Currently, this market it is not a leading political topic, and it might find more resistance than necessary to be implemented. Lastly, the public might be quite sceptical about flying in a plane powered by cryogenic methane, especially with the imposing-looking external wing tank system. Hence, the psychological impact of the novel aircraft have not been analysed.

17.2. Recommendations

The CH4llenger offers a promising solution to the net-zero emissions target, enabling the world to stay connected whilst not harming the environment or the economy. Of course, next steps and iterations still need to be taken in order to refine the final design and ensure optimal performance and efficiency. Further developments are in the propulsion system of the aircraft, making it possible to carry hydrogen in short-haul flights, designing a (e.g. parachute) system to recover the fuel tank after emergency jettison, and developing a family of aircraft for different ranges to be able to sustainably reach even the most remote locations.

On a bigger scale, speeding up the transition to synthetic methane by boosting worldwide production and establishing global partnerships and guidelines to ensure consistent standards and prices, is critical. This includes the development of airworthiness standards, which propose standards to ensure the safe running of the aircraft. Moreover, guidelines need to be put into place regarding the industry-scale carbon capture technology and the green hydrogen used in the production process. This way, the challenge of net-zero civil aviation will be truly met.

References

[1] DSE Group 27. "DSE Midterm Report Group 27". In: *Midterm Review* 1 (2024).

[2] DSE Group 27. "DSE Baseline Report Group 27". In: *Baseline Review* 1 (2024).

[3] P. Roling. *Project Guide Design/Synthesis Exercise: Ultimate Energy Efficient Transatlantic Aircraft*. TU Delft, 2024.

[4] J. Hoelzen et al. "H2-powered aviation at airports – Design and economics of LH2 refueling systems". In: *Energy Conversion and Management: X* 14 (2022), p. 100206.

[5] R. Vos. *Lecture 7 - Empennage and Undercarriage Design*. Tech. rep. TU Delft, 2022.

[6] J. Roskam. *Airplane Design: Part I: Preliminary Sizing of Airplanes*. Lawrence, Kansas: DARcorporation, 1985.

[7] C. Karunakaran. "Study of flow field over fabricated airfoil models of NACA 23015 with its kline-fogleman variant". In: *Advances in Aerospace Science and Applications* 3.2 (2013), pp. 95–100.

[8] R. Vos. *Lecture 6 - Wing and Propulsion System Design*. Tech. rep. TU Delft, 2022.

[9] W.H. Mason. "Transonic aerodynamics of airfoils and wings". In: *Notes in Configuration Aerodynamics, Virginia Tech* 4.4 (2006).

[10] F. Oliviero. *Lecture 1 - Fundamentals on Aircraft aerodynamic designs*. Tech. rep. TU Delft, 2022.

[11] F. Oliviero. *Lecture 2 - Aircraft aerodynamic analysis: Estimation of Lift and Drag*. Tech. rep. TU Delft, 2022.

[12] O. Gur, W.H. Mason, and J.A. Schetz. "Full-Configuration Drag Estimation". In: *Journal of Aircraft* 47.4 (2010), pp. 1356–1367.

[13] F. Oliviero. *Lecture 3 - Aircraft aerodynamic analysis: Mobile surfaces of the wing*. Tech. rep. TU Delft, 2022.

[14] L.W. Traub and M.P. Kaula. "Effect of leading-edge slats at low Reynolds numbers". In: *Aerospace* 3.4 (2016), p. 39.

[15] Airbus S.A.S. *Aircraft Characteristics Airport and Maintenance Planning*. 2020. URL: https://www.airbus.com/sites/g/files/jlcbta136/files/2022-02/Airbus-techdata-AC_A321_0322.pdf (visited on 05/28/2024).

[16] Boeing. *Boeing 717 Airport Compatibility Planning Document*. 2024. URL: https://www.boeing.com/content/dam/boeing/boeingdotcom/commercial/airports/acaps/717.pdf (visited on 06/11/2024).

[17] R. Vos. *Lecture 5 - Fuselage Design*. Tech. rep. TU Delft, 2022.

[18] E. Torenbeek. *Advanced Aircraft Design: Conceptual Design, Technology and Optimization of Subsonic Civil Airplanes*. John Wiley & Sons, 2013.

[19] NeoNickel. *Nickel Alloys for Aerospace Applications*. 2024. URL: https://www.neonickel.com/nickel-alloys-for-aerospace-applications (visited on 05/28/2024).

[20] D. Samudrapom. *The Best High-Temperature Alloys for Aerospace Applications*. 2023. URL: https://www.azom.com/article.aspx?ArticleID=22897 (visited on 05/28/2024).

[21] American Elements. *Melting Point of Common Metals, Alloys, and Other Materials*. 2024. URL: https://www.americanelements.com/meltingpoint.html (visited on 05/28/2024).

[22] S. Sampath et al. "Processing science of advanced thermal-barrier systems". In: *MRSBulletin* 37.10 (2012).

[23] D. R. Clarke and S. R. Phillpot. "Thermal barrier coating materials". In: *Materials Today* 8 (2005).

[24] ThoughtCo. *Flame Temperatures Table for Different Fuels*. 2024. URL: https://www.thoughtco.com/flame-temperatures-table-607307 (visited on 06/06/2024).

[25] M. Yahyaoui, A. Anantha-Subramanian, and I. Lombaërt-Valot. *The Use of LNG as Aviation Fuel: Combustion and Emissions*. 2024. URL: https://arc.aiaa.org/doi/epdf/10.2514/6.2015-3730 (visited on 05/30/2024).

[26] A. Cervone. *AE2230-II, Formula Sheet for Exam - RP+EPS*. Tech. rep. TU Delft, 2023.

[27] J.D. Mattingly and K. M. Boyer. *Elements of Propulsion: Gas Turbines and Rockets, Second Edition*. Cambridge University Press, 2016.

[28] A. Cervone. *AE2230-II, Lecture-5 AeroEngines - 2021*. Tech. rep. TU Delft, 2023.

[29] T. Wlodek. "Analysis of boil-off rate problem in Liquefied Natural Gas (LNG) receiving terminals." In: *IOP Conference Series: Earth and Environmental Science* (2019).

[30] Vahterus. *Fact Sheet: Fully Welded Plate Heat Exchanger Partial 2 Phase*. Mar. 27, 2015.

[31] G. D. Brewer, R. E. Morris, and J. W. Moore R. H. Lange. *Study of the application of hydrogen fuel to long-range subsonic transport aircraft*. Tech. rep. NASA, 1975.

[32] G.D. Brewer. *Hydrogen Aircraft Technology*. New York: CRC Press, 1991.

[33] C. Winnefeld et al. "Modelling and Designing Cryogenic Hydrogen Tanks for Future Aircraft Applications". In: *Energies* 11.1 (2018).

[34] P. Rompokos et al. "Liquefied Natural Gas for Civil Aviation". In: *Energies* 13.22 (2020).

[35] E. Torenbeek. *The computation of characteristic areas and volumes of major aircraft components in project design*. Tech. rep. TU Delft, 1973.

[36] E. Zaretsky et al. "Impact response of high density flexible polyurethane foam". In: *International Journal of Impact Engineering* 39.1 (2012), pp. 1–7.

[37] H.S. Fowler. "Tests on the bird impact resistance of polyurethane foam". In: *Canadian Aeronautics and Space Journal* 15.6 (1969), pp. 221–224.

[38] Ir. B.T.C. Zandbergen. *Lecture 3 - Generation of Wing and Thrust/Power Loading Diagrams*. Tech. rep. TU Delft, 2023.

[39] D.M.J. Peeters. *AE1108-II Formula Sheet*. Tech. rep. TU Delft, 2022.

[40] US Air Force. *North American F-86 Sabre Pilot's Flight Operating Instructing*. S.F. Hoerner, 1965.

[41] T. Kandasamy, S. Rakheja, and A. Ahmed. "An analysis of baffles designs for limiting fluid slosh in partly filled tank trucks". In: *The Open Transportation Journal* 4.1 (2010).

[42] M. Naveen and M. Kumar. "Conceptual Design of Fuel Dumping System in Aircraft". In: *International Journal of Aviation, Aeronautics, and Aerospace* 9.2 (2022), pp. 1–5.

[43] S.T. de Paula Andrade et al. *Fuel Cells as APU in Aircrafts*. Springer International Publishing, 2022, pp. 147–169.

[44] O.Z. Sharaf and M.F. Orhan. "An overview of fuel cell technology: Fundamentals and applications". In: *Renewable and Sustainable Energy Reviews* 32 (2014), pp. 810–853.

[45] William J. Hughes. *Energy Supply Device Aviation Rulemaking Committee*. Federal Aviation Administration. 2019. URL: `https://www.faa.gov/regulations_policies/rulemaking/committees/documents/media/Energy%20Supply%20Device%20ARC%20Recommendation%20Report.pdf` (visited on 06/01/2024).

[46] B.C. Castro Pereira Araújo and F.M. Ribeiro Proença Brojo. "Substitution of a Conventional Gas Turbine By a HT-PEMFC APU: Feasibility Study". In: *KnE Engineering* 5.6 (2020).

[47] J Hale. "Boeing 787, From the ground up". In: *Aero* (2006).

[48] T.S. Srivatsan et al. *Aluminum-Lithium Alloys*. Elsevier Inc, 2014.

[49] Y. Atescan-Yuksek et al. "Comparative life cycle assessment of aluminium and CFRP composites: the case of aerospace manufacturing". In: *The International Journal of Advanced Manufacturing Technology* (2024).

[50] K. Stonaker et al. *Material characterization of aluminium lithium alloys used in aerospace applications*. Federal Aviation Administration, 2020.

[51] Hexcel. *AS4 Product Sheet*. 2023.

[52] D. P. Wells and B. L. Horvath. *The Flight Optimization System Weights Estimation Method*. Tech. rep. NASA, 2017.

[53] D.P. Raymer. *Aircraft Design: A Conceptual Approach*. AIAA education series. American Institute of Aeronautics and Astronautics, Incorporated, 2018.

[54] F. Oliviero. *Lecture 6 - Weight and Balance in Aircraft Design*. Tech. rep. TU Delft, 2024.

[55] F. Oliviero. *Lecture 7 - Requirement Analysis and Design principles for A/C stability and control (Part 1)*. Tech. rep. TU Delft, 2024.

[56] F. Oliviero. *Lecture 8 - Requirement Analysis and Design principles for A/C stability and control (Part 2)*. Tech. rep. TU Delft, 2024.

[57] H.V. Borst S.F. Hoerner. *Fluid-Dynamic Lift*. Mrs. Liselotte A. Hoerner, 1985.

[58] S.F.Hoerner. *Fluid-Dynamic Drag*. S.F. Hoerner, 1965.

[59] F. Nicolosi, D. Ciliberti, and P. Della Vecchia. "Aerodynamic design guidelines of aircraft dorsal fin". In: *34th AIAA Applied Aerodynamics Conference*. 2016, p. 4330.

[60] W.A. Timmer and S.J. van Elsloo. *AE2111-I: System Design – Project Reader*. Tech. rep. TU Delft, 2022.

[61] T.H.C. Megson. *Aircraft Structures for Engineering Students*. Butterworth-Heinemann, 2016.

[62] Boeing Commercial Airplanes. *737NG Quick Reference Handbook*. Flight Crew Operating Manual. Boeing. 2009.

[63] F. Carta and A. Pirondi. "Damage tolerance analysis of aircraft reinforced panels". In: *Frattura ed Integrit'a Strutturale* 5.16 (2011), pp. 34–42.

[64] EHJ Pallett. *Aircraft Electrical Systems*. Pearson, 1987.

[65] M. Palomeque. *A320 - Dual hydraulic loss*. Tech. rep. Airbus, 2017.

[66] Airbus SAS. *A350-900 Flight Deck and Systems Briefing for Pilots*. 2011. URL: https://www.smartcockpit.com/docs/a350-900-flight-deck-and-systems-briefing-for-pilots.pdf (visited on 05/29/2024).

[67] T. Kruckenberg. *International Filtration News*. 2021. URL: https://www.filtnews.com/aviation-is-opening-up-again-how-can-filtration-help-re-start-the-industry-while-continuing-to-protect-the-environment/ (visited on 06/03/2024).

[68] Canadair Regional Jet. *Environmental Control System*. 2003. URL: https://www.smartcockpit.com/docs/Bombardier_CRJ_00-Environmental_Control_System.pdf (visited on 06/03/2024).

[69] S. Rönsch et al. "Review on methanation – From fundamentals to current projects". In: *Fuel* 166 (2016), pp. 276–296.

[70] A. R. Razmi et al. *Future Grid-Scale Energy Storage Solutions*. 1st ed. Academic Press, 2023.

[71] M. Fonder et al. "Synthetic methane for closing the carbon loop: Comparative study of three carbon sources for remote carbon-neutral fuel synthetization". In: *Applied Energy* 358 (2024).

[72] D. Pashchenko. "Green hydrogen as a power plant fuel: What is energy efficiency from production to utilization?" In: *Renewable Energy* 223 (2024), p. 120033.

[73] K. Atsonios, J. Li, and V.J. Inglezakis. "Process analysis and comparative assessment of advanced thermochemical pathways for e-kerosene production". In: *Energy* 278 (2023), p. 127868.

[74] Y. Zhu et al. "Making light work: Designing plasmonic structures for the selective photothermal methanation of carbon dioxide". In: *EES Catalysis* 2 (2024).

[75] storengy. *Methanation: Biomethane's natural complement. An innovative solution to valorize the CO2 of biogas*. 2022. URL: https://www.storengy.com/sites/default/files/mediateque/pdf/2023-01/PLAQUETTE%20METHANATION%20WEB_EN_1.pdf (visited on 06/06/2024).

[76] M.J.B. Kabeyi and O.A. Olanrewaju. "Biomethane Production and Applications". In: *Anaerobic Digestion-Biotechnology for Environmental Sustainability*. IntechOpen, 2023.

[77] A. I. Adnan et al. "Technologies for Biogas Upgrading to Biomethane: A Review". In: *Bioengineering* 6 (2019), p. 92.

[78] ETIP Bioenergy. *Biomethane*. 2020. URL: https://www.etipbioenergy.eu/images/ETIP_B_Factsheet_Biomethane.pdf (visited on 06/06/2024).

[79] C. Tregambi et al. "Techno-economic assessment of a synthetic methane production process by hydrogenation of carbon dioxide from direct air capture". In: *International Journal of Hydrogen Energy* 48.96 (2023), pp. 37594–37606.

[80] C. Wouters et al. *Market state and trends in renewable and low carbon gases in Europe*. 2020. URL: https://www.europeanbiogas.eu/wp-content/uploads/2020/12/GfC_MSTReport_2020_final.pdf (visited on 05/29/2024).

[81] Biomethane Industrial Partnership Task Force 4.2. *Insights into the current cost of biomethane production from real industry data*. Tech. rep. 2023.

[82] D. Nelissen et al. *Availability and costs of liquefied bio- and synthetic methane*. 2020. URL: https://cedelft.eu/wp-content/uploads/sites/2/2021/03/CE_Delft_190236_Availability_and_costs_of_liquefied_bio-_and_synthetic_methane_Def (visited on 05/27/2024).

[83] Energy KnowledgeBase. *Liquefaction*. 2024. URL: https://energyknowledgebase.com/topics/liquefaction.asp (visited on 06/05/2024).

[84] Cambridge Systematics. "Risk assessment of surface transport of liquid natural gas". In: *Cambridge Systematics* (2019), pp. 1–167.

[85] Wärtsilä. *LNG plants – mini and small scale liquefaction technology*. Tech. rep. Wärtsilä, 2016.

[86] J. Markish. *Valuation techniques for commercial aircraft program design*. Tech. rep. Massachusetts Institute of Technology, 2002.

[87] K. Willcox. *Optimization in Aerospace Engineering*. 2003. URL: https://dspace.mit.edu/bitstream/handle/1721.1/36378/16-885JFall2003/NR/rdonlyres/Aeronautics-and-Astronautics/16-885JFall2003/8CACE2FE-A136-4B03-93B6-08F81FC911BB/0/pres%5C_willcox.pdf (visited on 06/11/2024).

[88] E. Gill. *Lecture 3 - Risk Management & Concurrent Engineering*. Tech. rep. TU Delft, 2024.

[89] P. Sforza. "Chapter 11 - Aircraft Pricing and Economic Analysis". In: *Commercial Airplane Design Principles*. Boston, United States: Butterworth-Heinemann, 2014, pp. 453–475.

[90] N. Duic, K. Urbaniec, and D. Huisingh. "Components and structures of the pillars of sustainability". In: *Journal of Cleaner Production* 88 (2015), pp. 1–12.

[91] C. Ruggerio. "Sustainability and sustainable development: A review of principles and definitions". In: *Science of The Total Environment* 786 (2021), pp. 147–481.

[92] ICAO. “Sustainability and Economic Development of Air Transport”. In: *Proceedings of the Worldwide Air Transport Conference (ATCONF)*. Montréal, Canada: ACM Press, 2013.

[93] J. Green. “Civil aviation and the environmental challenge”. In: *The Aeronautical Journal* 107.1072 (2003), pp. 281–299.

[94] K. Simonen. *Life Cycle Assessment*. 1st ed. London, United Kingdom: Routledge, 2014.

[95] K. Kossarev, A. Scholz, and M. Hornung. “Comparative environmental life cycle assessment and operating cost analysis of long-range hydrogen and biofuel fueled transport aircraft”. In: *CEAS Aeronautical Journal* 14 (2022), pp. 3–18.

[96] D. Melideo, E. Ortiz Cebolla, and E. Weidner. *Life Cycle Assessment of Hydrogen and Fuel Cell Technologies*. Tech. rep. European Comission, 2020.

[97] M. Tamburini et al. “Analysing the Impact on Health and Environment from Biogas Production Process and Biomass Combustion: A Scoping Review”. In: *International Journal of Environmental Research and Public Health* 20.7 (2023).

[98] S. S. Cordova et al. “What should we do with CO2 from biogas upgrading?” In: *Journal of CO2 Utilization* 77 (2023), p. 102607.

[99] J. Liebetrau et al. *Methane Emissions from biogas plants. Methods for measurement, results and effect on greenhouse gas balance of electricity produced*. Tech. rep. 2017.

[100] M.A. Holmgren et al. “Measurements of methane emissions from biogas production - Data collection and comparison of measurement methods”. In: (2015).

[101] U.S. Environmental Protection Agency. *AP 42, Fifth Edition, Volume I: External Combustion Sources*. Technology Transfer Network, Clearinghouse for Emission Inventories and Emissions Factors, 1995.

[102] D. Pal and S. K. Mitra. “Do airfares respond asymmetrically to fuel price changes? A multiple threshold nonlinear ARDL model”. In: *Energy Economics* (2022), pp. 106–113.

[103] Ir. J. Sinke. *AE3211-II Production of Aerospace Systems Lecture*. Tech. rep. TU Delft, 2024.